Karlsruhe Institute of Technology

Annual Report 2018/19

Institute for Nuclear Waste Disposal

By H. Geckeis, M. Altmaier, S. Fanghänel (Eds.)

INE SCIENTIFIC WORKING DOCUMENTS 01

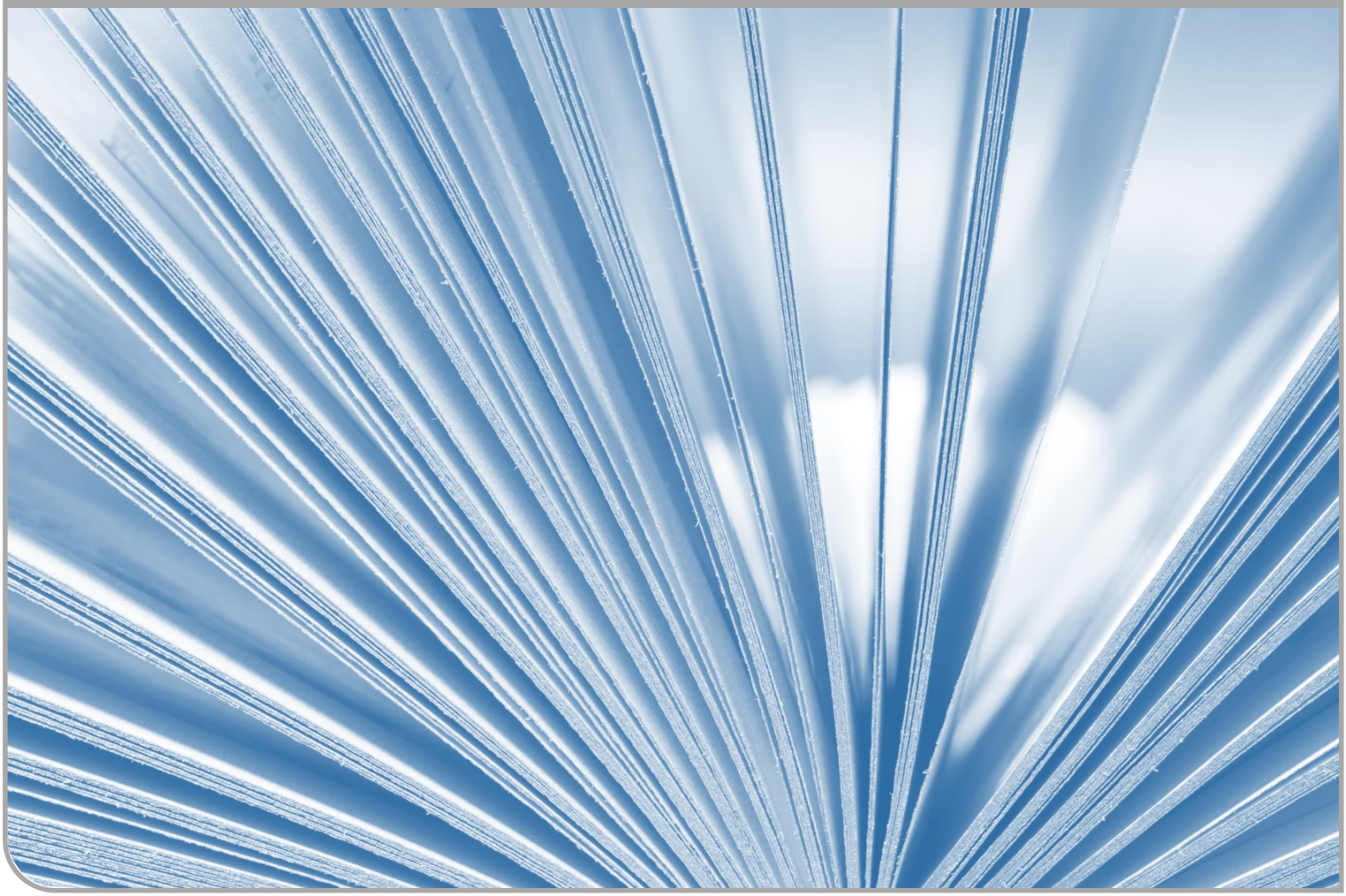

Institut für Nukleare Entsorgung (INE)

Hermann-von-Helmholtz-Platz 1
76344 Eggenstein-Leopoldshafen
www.ine.kit.edu

Impressum

Karlsruher Institut für Technologie (KIT)
www.kit.edu

2020

URL: http://www.ine.kit.edu/53.php
ISSN: 2701-262X
DOI: 10.5445/IR/1000120630

Obituary for the death of Dr. Bernd Schimmelpfenning

Our institute was struck in 2019 by the sudden and unexpected death of Dr. Bernd Schimmelpfennig, who had been since 2003 the head of the computational chemistry group at INE. Dr. Schimmelpfennig was an internationally renowned expert for the development and application of quantum chemistry codes tailored to solve electronic structures and bonding properties of the heavy '5f' or 'actinide' elements, requiring, i.a., the explicit treatment of relativistic effects to describe their electronic states. As one of the few specialists of actinide quantum chemistry worldwide, Dr. Schimmelpfennig has given numerous impulses in this field, allowing the refinement of our molecular scale understanding of nuclear materials in the context of geological repository concepts.

Table of contents

1 Introduction to the Institute for Nuclear Waste Disposal (INE)

The **Institute for Nuclear Waste Disposal** (INE), at the Karlsruhe Institute of Technology **KIT** performs R&D focusing on

(i) Long-term safety research for nuclear waste disposal (key focus of INE research),
(ii) Radiation protection
(iii) Decommissioning of nuclear facilities
(iv) Geoenergy.

All R&D activities of INE are integrated into the program Nuclear Safety Research within the KIT-Energy Center and the program Nuclear Waste Management, Safety and Radiation Research (NUSAFE) within the Helmholtz Association. INE contributes to German provident research for the safety of nuclear waste disposal, which is the responsibility of the Federal Government.

Following the decision taken by Germany to phase out the use of nuclear energy, the safe disposal of long-lived nuclear waste remains as a key topic of highest priority. Projections based on scheduled operation times for nuclear power plants (Amendment to German Atomic Energy Act, August 2011) in Germany indicate that about a total of 17,770 tons of spent nuclear fuel will be generated. About 6,670 tons have been shipped to France and the UK until 2005 for reprocessing, to recover plutonium and uranium. Consequently, two types of high level, heat producing radioactive waste (HLW) have to be disposed of safely: spent nuclear fuel and vitrified high level waste from reprocessing (HLW glass). The disposal of low- and intermediate level waste present in much larger quantities likewise needs to be addressed.

Over the last decades, a consensus within the international scientific/technical community was established, clearly emphasizing that disposal in deep geological formations is the safest way to dispose of high level, heat producing radioactive waste. Disposal concepts with strong inherent passive safety features ensure the effective protection of the population and the biosphere against radiation exposure over very long periods of time. The isolation and immobilization of nuclear waste in a repository is ensured by the appropriate combination of redundant barriers (multi-barrier system).

Long term safety research for nuclear waste disposal at INE develops geochemical expertise and models to be used in the nuclear waste disposal Safety Case, focusing primarily on the detailed scientific description of aquatic radionuclide chemistry in the geochemical environment of a repository. Work concentrates on the disposal of spent nuclear fuel and HLW-glass in the relevant potential host rock formations currently considered: rock salt, clay and crystalline rock formations. Actinides and long-lived fission and activation products play a central role, as they dominate HLW radiotoxicity and risks over long periods of time. Long-lived anionic fission and activation products are likewise investigated as significant contributors to the maximum radiation dose projected for relevant scenarios.

Relevant long-term scenarios for nuclear repositories in deep geological formations have to take into account possible radionuclide transport via the groundwater pathway. Possible groundwater intrusion into emplacement caverns may cause waste form corrosion and eventually radionuclide release. Radionuclide mobility is then determined by the various geochemical reactions in complex aquatic systems: i.e. dissolution of the nuclear waste form (HLW glass, spent nuclear fuel), radiolysis phenomena, redox reactions, complexation with inorganic and organic ligands, colloid formation, surface reactions at mineral surfaces, precipitation of solid phases and solid solutions.

Prediction and quantification of all these processes require fundamental thermodynamic data and comprehensive process understanding at the molecular scale. Radionuclide concentrations in relevant aqueous systems typically lie in the nano-molar range, which is exceedingly small in relation to main groundwater components. Quantification of chemical reactions occurring in these systems require the application and development of advanced tools and experimental approaches, to provide insight into the chemical speciation of radionuclides at trace concentrations. Innovative laser and X-ray spectroscopic techniques are continuously developed and applied to this end. A specialized working group performing state-of-art ~~theoretical~~ quantum chemical calculations for radionuclide ~~actinide~~ chemistry supports both interpretation of experimental results and optimized experiment design.

The long-term safety of a nuclear waste repository must be demonstrated by application of modelling tools on real natural systems over geological time scales. Geochemical models and thermodynamic databases are developed at INE as basis for the description of radionuclide geochemical behavior in complex natural aquatic systems. The prediction of radionuclide migration in the geosphere necessitates coupled modelling of geochemistry and transport. Transferability and applicability of model predictions are examined by designing dedicated laboratory experiments, field studies in underground laboratories and by studying natural analog systems. This strategy allows to identify and analyze key uncertainties and continuously optimize the developed models.

The R&D topic **radiation protection** at INE focuses on the assessment of radiation exposures of

humans by estimating doses from external radiation fields. The strategy driving this work is to provide techniques and models for an individualized dosimetry, which goes beyond the current approach of applying reference models in dose assessment. Both the specific anatomical and physiological features of the exposed individual and the specific effective radiation fields are considered in the frame of an individualized dosimetry. Work is performed in close cooperation with the KIT safety management SUM.

The R&D topic **decommissioning of nuclear and conventional facilities** at INE expands the existing activities at the Institute of Technology and Management in Construction (KIT-TMB). Research in this field is focusing on a better understanding of the complete decommissioning process in Germany as well as on a global level.

The topic **geoenergy** is mainly focusing on geothermal energy research in fractured reservoir systems with special focus on Enhanced Geothermal Systems (EGS).

INE laboratories are equipped with all necessary infrastructures to perform radionuclide/actinide research, including a shielded box line enabling the investigation of spent nuclear fuel and nuclear waste glass, alpha glove boxes, inert gas alpha glove boxes and radionuclide laboratories. State-of-the-art analytical instruments and methods are applied for analysis and speciation of radionuclides and radioactive materials. Advanced spectroscopic tools exist for the sensitive detection and analysis of radionuclides. Trace element and isotope analysis is made by instrumental analytical techniques such as atomic absorption spectroscopy (AAS), ICP-atomic emission spectroscopy (ICP-AES) and ICP-mass spectrometry (Quadrupole-ICP-MS and high resolution ICP-MS). Methods available for surface sensitive analysis and characterization of solid samples include X-ray diffraction (XRD), atomic force microscopy (AFM) and laser-ablation coupled with ICP-MS. A modern X-ray photoelectron spectrometer (XPS) and an environmental scanning electron microscope (ESEM) are installed. Laser spectroscopic techniques are developed and applied for sensitive actinide and fission product speciation such as time-resolved laser fluorescence spectroscopy (TRLFS), laser-induced breakdown detection (LIBD) and Raman spectroscopy. Insight into structural and electronic properties of radionuclide species is obtained by X-ray absorption fine structure (XAFS) spectroscopy and related techniques available at the INE-Beamline and the ACT experimental station at the KIT synchrotron source KARA. INE's beamlines, in close proximity to INE controlled area laboratories, represent in combination with the other analytical methods a unique experimental infrastructure, which both profits from and contributes to INE's leading expertise in the field of actinide chemistry and spectroscopy. A 400 MHz-NMR spectrometer adapted to measuring radioactive liquid samples adds to the analytical and speciation portfolio of INE. Quantum chemical calculations are performed on INE's computing cluster, which is equipped with 17 nodes and 76 processors. The INE CAD workstations enable construction and planning of hardware components, process layout and flow sheets. The institute workshop is equipped with modern machine tools to manufacture components for specific experimental and analytical devices in hot laboratories.

In 2018 and 2019, the **Institute for Nuclear Waste Disposal** had around **90 employees** working in the five departments and two clusters, which reflect the R&D and organizational tasks of the institute (Fig. 1).

Fig. 1: *Organizational chart of the Institute for Nuclear Waste Disposal (INE)*

2 Education and training

Teaching of students and promotion of young scientists is of fundamental importance to ensure high-level competence and to maintain a leading international position in the fields of nuclear and radiochemistry. INE scientists are strongly involved in teaching at KIT Campus South and the Universities of Heidelberg, Jena and Strasbourg as well as the TU Darmstadt.

Prof. Dr. **Horst Geckeis**, director of INE, holds a professorship for radiochemistry at KIT Campus South, Department of Chemistry and Biosciences. He teaches fundamental and applied radiochemistry for chemistry students in bachelor and master courses. A radiochemistry module consisting of basic and advanced lectures on nuclear chemistry topics and laboratory courses has been set up for master students in Karlsruhe. In addition, Dr. **Marcus Altmaier**, head of the department radiochemistry, gives a lecture concerning the chemistry of f-elements.

Prof. Dr. **Sascha Gentes** head of the department decommissioning of nuclear and conventional facilities holds a professorship at the Institute for Technology and Management in Construction at the KIT-Department of Civil Engineering, Geo and Environmental Sciences and gives lectures in the field of decommissioning of nuclear facilities, environmentally-friendly Recycling and Disassembly of Buildings, Machinery and Process Engineering as well as construction technology.

Prof. Dr. **Petra Panak**, heading a working group on actinide speciation at INE, holds a professorship of radiochemistry at the Heidelberg University. A basic course in radiochemistry is offered for bachelor and/or master students. An advanced course comprised of the chemistry of f-elements and medical applications of radionuclides is also offered. The advanced radiochemistry lectures are supplemented by scientific internships at the INE radioactive laboratories.

Around 30 students from Karlsruhe and Heidelberg participated in two 3-week radiochemistry laboratory courses in 2018 and 2019 held at KIT Campus North in the FTU radiochemistry and hot laboratories at INE. Some students are intensifying their knowledge in nuclear/radiochemistry topics during scientific internships at INE. Obviously, students are very interested in nuclear chemistry topics and appreciate the various semester courses.

Dr. **Tonya Vitova** gives lectures at the KIT Campus South, Department of Chemistry and Biosciences, in the field of instrumental analytics and Prof. Dr. **Eva Schill** at the Department of Civil Engineering, Geo and Environmental Sciences in the field of geothermal energy as well as at the university of Darmstadt. Dr. **Volker Metz** gives lectures at the Department of Mechanical Engineering in the field of nuclear fuel cycle. Lectures and practical units are taught by Dr. **Frank Heberling** and Dr. **Volker Metz** at KIT Campus South, Department of Civil Engineering, Geo and Environmental Sciences, focused in 2018 and 2019 on "environmental geology: radio- and chemotoxic elements".

Dr. **Andreas Bauer** is lecturing Clay Mineralogy at the University of Jena. His lecture deals with the mineralogical characterization of these fine materials and the importance of quantifying surface reactions. In the second part of the lectures sound, practical advice on powder X-ray diffraction in general is provided, as well as a useful set of step-by step instructions for the novice.

Dr. **Andreas Geist** gives lectures at the École européenne de chimie, polymères et matériaux in Strasbourg concerning the Solvent Extraction of Metal Ions.

Moreover, INE was involved in many schools and workshops concerning the education and teaching of students and young scientists.

Through this close cooperation with universities, students are educated in the field of nuclear and actinide chemistry, which most universities can no longer offer. Hence, INE makes a vital contribution to the intermediate and long perspective of maintaining nuclear science competence. Moreover, INE is involved in the education of trainees (chemical lab technicians, industrial mechanics and product designers) as well as student internships like BORS and BOGY.

PhD students

In 2018 and 2019, 18 doctoral students worked at INE on their dissertations; five doctoral students were awarded their doctorate in 2018 and one in 2019. Topics of the doctoral students are:

1. Influence of carbonate on the radium uptake by barite
2. Application of high-resolution x-ray absorption (HR-XAS) spectroscopy for the investigation of the release and solubility of radionuclide species originating from highly radioactive waste in aquatic media
3. Determination of geothermal relevant parameters in high temperature and superheated reservoirs with gravimetric and magnetotelluric methods
4. Aqueous chemistry of technetium in the presence of inorganic and organic ligands
5. In-situ structural studies of uranium during interaction with magnetite
6. Investigation of the diffusion of U(IV), Np(IV), Pu(IV), and Am(III) at ultra-trace levels through natural clay with accelerator mass spectrometry
7. Electromagnetical und Eigenpotential monitoring of fluid injections in crystalline rock
8. Investigation of the radionuclide inventory and chemical interactions at the interface between

nuclear fuel and zircaloy cladding of irradiated light water reactor fuel rod samples

9. Potential Influence of oxygenated Glacial Meltwater on Radionuclide (re)mobilization in fractured rock
10. Steel corrosion and actinides sorption by iron corrosion products under saline conditions
11. Joint inversion of magnetotelluric and gravity data from Mt. Viilarica area (S-Chile)
12. Retention of Iodine by secondary phases in the near field of a radioactive waste repository
13. Behavior of natural radionuclides in soil/groundwater systems
14. Investigations of Np, Tc, and Se structural properties applying in situ high-energy resolution X-ray emission/absorption spectroscopy
15. Studies on the complexation of actinide and lanthanide ions with N,O-donor ligands
16. Impact of the degradation products of an ion exchange resin (UP2) on the uptake of radionuclides by cement
17. Fundamental research to the optimization of the EU-RO-GANEX process
18. Accurate neutron scattering based Monte Carlo Simulations of Radiation Fields and Dosimetry imposed by stored High-Level Nuclear Fuel Waste

3 National and international cooperation, conferences and workshops

3.1 National and international cooperation

INE R&D involves numerous national and international collaborations and projects. These are described in the following.

National

INE is involved in various bi- and multilateral collaborations with national research centers, universities and industrial partners on different topics. The projects are partly supported by the German Federal Ministry for Economics and Technology (BMWi), the Federal Ministry for Education and Research (BMBF), the Federal Ministry for the Environment, Nature Conservation, Building and Nuclear Safety (BMU), the Federal Company for Radioactive Waste Disposal (BGE), the German Research Foundation (DFG) and the Helmholtz Association (HGF).

The **ThermAc** project aims at extending the chemical understanding and available thermodynamic database for actinides, long-lived fission products and relevant matrix elements in aquatic systems at elevated temperatures. To this end, a systematic use of estimation methods, new experimental investigations and quantum-chemistry-based information is intended. ThermAc has started in March 2015 and is projected for three years with an additional 1.5 year extension phase. The project is funded by the German Federal Ministry for Education and Research (BMBF) and is coordinated by KIT-INE. The ThermAc project is developed in order to improve the scientific basis for assessing nuclear waste disposal scenarios at elevated temperature conditions.

The work of KIT-INE within **VESPA II** (initiated in September 2017) is highlighting the key relevance of geochemical research for evaluating radionuclide retention and mobilization in the frame of nuclear waste disposal. Based upon new systematic experimental studies, a significant increase of understanding regarding the behavior of long-lived fission and activation products, i.e. ^{99}Tc, ^{79}Se and ^{129}I, has been obtained. Fundamental site- and host-rock independent thermodynamic data derived within VESPA allow a better modeling and prediction of radionuclide chemistry in aquatic systems. The retention of radionuclides on several relevant mineral phases is analyzed and quantified. As a result of the work performed by KIT-INE within VESPA II, the long-term safety of different repository concepts and scenarios can be assessed on a decisively improved scientific level.

Within the **THEREDA** project, KIT-INE provides thermodynamic data – complex formation constants, solubility data – for selected radionuclides from experiments and literature. The data are incorporated into a centrally managed and administered database of evaluated thermodynamic parameters after passing an evaluation process. This database is open for registered user. Thermodynamic data are required for environmental applications in general and radiochemical issues in particular. THEREDA, funded by the the Federal Company for Radioactive Waste Disposal (BGE), is developed as a national (reference) standard and basis for future Safety Assessments for a national nuclear waste repository.

The **GRaZ** project deals with the migration of radionuclides in the near field of a repository for radioactive waste in clay formations with focus on the hyper-alkaline water-cement-system. KIT-INE investigates the retention of actinides and lanthanides by clay minerals in presence of relevant inorganic and organic ligands. The project focusses on carbonate, and cement additives (e.g. plasticizer and superplasticizer) like gluconate and citrate. The impact of these ligands on the sorption and solubility of actinides is studied in a wide pH range up to hyperalkaline pH values. One important aim of the project is the consistent thermodynamic modelling of experimental solubility, complexation, and sorption data. The project provides basic knowledge and thermodynamic data needed in the frame of a long-term safety analysis of different repository concepts.

The **KOLLORADO-e3** project focuses on the erosion stability of compacted bentonite (geotechnical barrier) as a function of the contact water chemistry/hydraulics and the formation of near-field colloids/nanoparticles as potential carriers for actinides/radionuclides. The project activities include a detailed experimental program quantifying the bentonite erosion and the reversibility of actinide bentonite nanoparticle sorption reversibility (including AMS method development).

The mechanical and chemical stability of steel containers containing nuclear waste play an important role in performance assessment of disposal sites. The project **KORSO** aims at improving the understanding of steel corrosion in saline environments under conditions representative of disposal sites for heat generating waste. Microscopic and spectroscopic techniques are applied to identify the underlying corrosion mechanisms and their kinetics in dedicated experiments in saline, anoxic and elevated temperature conditions. The second aim is to investigate the retention of radionuclides by secondary phases identified in corrosion experiments by applying spectroscopic and chemical methods. The ultimate goal is to reduce uncertainties concerning interaction mechanisms between radionuclides and corrosion products, and thereby improve confidence in the long-term prediction of radionuclide mobility.

The Helmholtz young investigators group (HYIG) **"Advanced synchrotron-based systematic investigations of actinide (An) and lanthanide (Ln) systems to understand and predict their reactivity"** systematically investigates the electronic and coordination

structures of actinide (An) and chemical homologue lanthanide (Ln) systems with novel synchrotron-based high energy resolution X-ray emission/absorption/inelastic scattering techniques. The experimental results are supported by theoretical calculations and simulations with quantum chemical codes. These investigations improve the understanding of An/Ln reactivity in repository systems and waste matrices on a molecular scale and thereby support the reliability of safety case evaluation of the repository long term safety. The elucidation of electronic and coordination structures of An/Ln systems provide basic insight into relationships between structure and reactivity of actinide elements, which is a present scientific frontier.

SMILE is a project dealing with reactive transport modeling (Smart-Kd in long term safety-assement – applications). The main goals of SMILE are the extension of the concept developed up till now towards inclusion of redox-reaction, to corroborate the chemical description of interfacial reactions via more fundamental insight in structure, stoichiometry and thermodynamic parameters of relevant surface complexes, to compare state of the art surface complexation in the evaluation of available experimental data, to extend the experimental data basis via batch- and column experiments on laboratory systems, to calculate smart Kd-martrices for selected redox-systems, and to apply the concept and verify the concept via experiments and modeling for systems that are closer to environmental systems in a critical manner. This is supposed to pave a fundamental basis allowing to transfer the smart-Kd-concept to various geological settings. Additionally, this will allow for the coupling of the concept to geochemical reactive transport codes to be initiated.

In the framework of measures for retrieval of radioactive waste and decommissioning of the **Asse II salt mine**, provisions for emergency preparedness are taken. Therefore, the operator of Asse II, the Federal Company for Radioactive Waste Disposal (BGE), performed an exploration drilling in the overlaying sedimentary rocks of the salt diapir and coordinates studies with respect to the near-field of the radioactive waste. INE contributes both to the studies on radionuclide retention by rocks of the overlaying sediments as well as to studies on the geochemical milieu and radionuclide solubility in the near-field of the radioactive waste. Drill cores and a pore water sample of the exploration borehole, comprising Triassic shell limestone (Muschelkalk) and Bunter sandstone (Buntsandstein) were used in sorption experiments with several radionuclides. Based on the experimental results, sorption coefficients are derived, which are important input parameters for the assessment of the radionuclide retention capability of the sedimentary rocks overlaying the Asse II salt mine. With respect to the near field of the waste within Asse II, INE compiles the present state of knowledge on geochemical processes in the waste emplacement rooms. Experimental studies performed by INE provide the basis for improved radionuclide source terms.

The collaborative project **iCross** is jointly funded by HGF and BMBF. Goal of the project is to progress towards a more realistic description of waste disposal systems, i.e. to reduce the need for conservative assumptions in model predictions of radionuclide migration through the near- and far field around nuclear waste repositories. In order to demonstrate significant progress within the three years funding period, the **iCross** consortium agreed to focus on two aspects of this very general task: 1) radionuclide migration through the evolving near-field (i.e. multi-barrier system), with a special focus on the canister-bentonite interface, and 2) the influence of heterogeneities in the host rock on radionuclide migration, from the micro- to the regional scale. Investigations involve laboratory- as well as underground research laboratory experiments (mainly in Mt. Terri, Switzerland), and modelling exercises from quantum chemical simulations through pore-scale modelling, continuum-scale modelling to regional scale THMC models. The **iCross** consortium combines competences from the HGF program NUSAFE / research field "Energy", with the HGF research field "Earth and Environment", with the goal to become the cornerstone for a "Helmholtz Competence Centre for Nuclear Waste Reposity Research".

The collaborative project **TRANSENS** is the first large scale project in Germany to conduct transdisciplinary research on management of spent nuclear fuel and vitrified high level waste. TRANSENS aims at evaluating technical, safety related and procedural aspects of disposal strategies for highly radioactive waste from the view-point of all involved academic disciplines such as natural sciences, engineering, law and social science. A major goal of this transdisciplinary research project is the interaction between scientists of various disciplines and citizen scientists. Thereby, members of the public, actors from practice and other non-academic stakeholders will be involved in the research process. Within the project, KIT-INE is responsible for a work package on developing criteria for decisions at critical points or "switch points" for recertifications on the route from interim storage to deep geological disposal of highly radioactive waste.

Geothermal energy will be a crucial element of the German *Energiewende*, in particular of the heat transition. The geothermal development faces a number of drawbacks resulting from immature technological development in early prototypes. Although major technological developments have been made, the related major setback, the low acceptability of deep geothermal technology by the society, remains. This is where the inter- and transdisciplinary project **GECKO** comes in. GECKO aims at involving the public in a co-design process that is linked to the establishment of deep geothermal infrastructures for heat production and storage at the KIT Campus North. The campus is located on the largest known thermal anomaly in Germany with approx. 170 ° C at a depth of 3 km. At INE, different scenarios of utilization and their respective consequences will be established using numerical modelling to provide the co-design process with the consequences of criteria decisions and alternatives in the design.

The **Helmholtz Climate Initiative** involves research on climate mitigation and adaptation. In the *ZeroNet-Zero-2050* Cluster, strategies and new approaches to achieve rapid and far-reaching reductions in emissions from all greenhouse gases including removal from the atmosphere and permanent storage or turning into high energy-density chemical energy carriers by renewable energy are scientifically examined and evaluated in four projects with regard to the German framework. In addition, two case studies are carried out with external stakeholders. The *Climate Neutral City*, is placed at the city of Karlsruhe. In the project *Potential and Integration of Subsurface Storage Solutions*, INE contributes to the topic of high-temperature heat storage. Forecasting chemical processes and related changes in reservoir condition over the operation time is carried out using thermo-hydraulic-chemical (THC) that are coupled to the district heating models or even including sector coupling.

International

The international Colloid Formation and Migration (**CFM**) project focuses on the stability of the bentonite buffer/backfill in contact with water conducting features and the influence of colloids on radionuclide migration in crystalline host rocks coordinated by NAGRA (National Cooperative for the Disposal of Radioactive Waste, Switzerland). The project uses the experimental set-up in the controlled zone at the Grimsel Test Site (Switzerland). Additional partners involved are from Japan (JAEA, NUMO, CRIEPI), South Korea (KAERI), Finland (POSIVA Oy and Helsinki University), Switzerland (NAGRA, PSI-LES), Spain (CIEMAT), Sweden (SKB, KTH), United Kingdom (NDA RWMD) and United States (LANL). INE plays a decisive role in the laboratory program and is mainly carries out the field activities

EURATOM FP7, Horizon 2020 and EJP

European Joint Programme on Radioactive Waste Management (**EURAD**) is a large scale integrated research programme dealing with various aspects of safe management of nuclear waste (www.ejp-eurad.eu/). Within EURAD, INE is stongly involed in EURAD and contributes to four workpackages: Cement-Organic-Radionuclide-Interactions (CORI), Fundamental understanding of radionuclide retention (FUTuRE), Spent Fuel Characterisation and Evolution Until Disposal (SFC) and Uncertainty Management multi-Actor Network (UMAN).

INE is coordinating the WP CORI. CORI aims to develop an in-depth understanding of the interaction of cementitious materials with organic matter and radionuclides. Organic materials are present in some nuclear waste and as admixtures in cement-based materials and can potentially influence the performance of a geological disposal system, especially in the context of low and intermediate level waste disposal. The potential effect of organic molecules on radionuclide migration is related to the formation of complexes in solution with some radionuclides of interest (actinides and lanthanides) which can increase the radionuclide solubility and decrease the radionuclide sorption. INE is active in all WPs of CORI, performing two separate studies in cooperation with EMPA (Switzerland) and with SKB (Sweden).

FUTURE aims at realizing a step change in quantitative mechanistic understanding of radionuclide retention in the repository barrier system. Work in FUTURE concerns the identification of constraints and the increase in predictability of radionuclie migration properties in “real” clay and crystalline rocks, quantifying the influence of key parameters of the heterogeneous rock/water system such a rock structure, redox interfaces, water saturation, reversibility etc.. Work of INE focusses on the investigation of radionuclide retention processes on clay materials, using a large set of modern analytical tools.

The SFC workpackage aims mainly to establish beyond state-of-the-art quantification of the characteristics and chemical processes of spent nuclear fuel assemblies from discharge of nuclear reactors, during interim storage until (pre-)disposal activities. Within SFC, INE contributes with experimental and numerical studies to improve determination of radionuclide inventories of spent nuclear fuel rods and to assess chemical interaction between spent nuclear fuel pellets and cladding within the fuel rods**.**

A follow-up of the FP7 project SACSESS, **GENIORS** focuses on actinide separations related to future multiple recycling strategies. GENIORS is expected to provide the EU with science-based strategies for nuclear fuel management and contribute significantly to its energy independence. In the longer term, the project’s results will facilitate radioactive waste management by reducing its volume and radiotoxicity, and support a more efficient utilization of natural resources. 24 Partners from 10 countries contribute to GENIORS; a formal collaboration with US-DOE is established. The project is coordinated by CEA; KIT is in charge of the hydrometallurgy domain.

The overall objective of the Horizon 2020 project **BEACON** is to develop and test the tools necessary for the assessment of the mechanical evolution of an installed bentonite barrier and the resulting performance of the barrier. This will be achieved by cooperation between design and engineering, science and performance assessment. The evolution from an installed engineered system to a fully functioning barrier will be assessed. This will require a more detailed understanding of material properties, of the fundamental processes that lead to homogenization via water saturation, of the role of scale effects and improved capabilities for numerical modelling. The goal is to verify the performance of current designs for buffers, backfills, seals and plugs. For some repository designs mainly in crystalline host rock, the results can also be used for the assessment of consequences of mass loss from a bentonite barrier in long-term perspective.

Within the European Commission Horizon 2020 frame, the study of modern spent nuclear fuel dissolution and chemistry in failed container conditions is included in the **DISCO** collaborative project. The aims of this project are, first, to enhance the understanding of

spent fuel matrix dissolution under conditions representative of failed containers in reducing repository environments and, second, to assess whether novel types of fuel (MOX, UO_2 doped with additives such as Cr, Gd) behave like the conventional ones (UO_2). INE provides results on the dissolution of MOX fuel under reducing conditions and, in addition, is the leader of work package 3 "Spent fuel dissolution experiment" supervising the spent nuclear fuel dissolution experiments that will be performed by the different partners within the project. INE also contributes to work package 2 "Preparation and characterization of samples and experimental systems".

INE contributes actively to international organizations, such as the Thermodynamic Database Project of the Nuclear Energy Agency (NEA).

CEBAMA is a collaborative project investigating cement-based materials, properties, evolution and barrier functions within the European Commission Horizon 2020 frame (www.cebama.eu). Scientific and technical research in CEBAMA is largely independent of specific disposal concepts and addresses different types of host rocks, as well as bentonite. CEBAMA is not focusing on one specific cementitious material, but aims at studying a variety of important cement-based materials in order to provide insight on general processes and phenomena. CEBAMA is coordinated by INE and was finalized in 2019.

The goal of the H2020 project **DEEPEGS** is to demonstrate the feasibility of enhanced geothermal systems (EGS) for delivering energy from renewable resources in Europe. Testing of stimulating technologies for EGS in deep wells in different geologies will deliver new innovative solutions and models for wider deployments of EGS reservoirs across Europe. DEEPEGS will demonstrate advanced technologies for widespread exploitation of high enthalpy heat (i) beneath existing hydrothermal field at Reykjanes (volcanic environment) with temperature up to 550°C and (ii) very deep hydrothermal reservoirs in France with temperatures up to 220°C. The focus on business cases will demonstrate advances in bringing EGS derived energy (TRL6-7) to market exploitation. We seek to understand and address social concerns about EGS deployments. We will through risk analysis and hazard mitigation plans ensure that relevant understanding and minimization of the risks will be implemented as part of the RTD business case development.

The **GEMex** project is a EU-Mexico joint effort in development of Enhanced Geothermal Systems (EGS) and Superhot Geothermal Systems (SHGS) at Acoculco and Los Humeros that bases on three pillars:

1 – Resource assessment of these geothermal sites by understanding the tectonic evolution, fracture distribution and hydrogeology and predicting in-situ stresses and temperatures at depth.

2 – Reservoir characterization including novel geophysical and geological methods to be advanced for the specific condition. Accompanying high-pressure/ high-temperature laboratory experiments will provide the input parameters.

3 – Concepts for site development will include definition of drill paths, a design for well completion including suitable material selection, and optimum stimulation and operation procedures for safe and economic exploitation. In these steps, we will address issues of public acceptance and outreach as well as the monitoring and control of environmental impact.

3.2 Migration'19 conference

The 17th International Conference on Chemistry and Migration Behaviour of Actinides and Fission Products in the Geosphere (Migration Conference) was held on September 15–20 2019 at the Uji Campus of Kyoto University in Kyoto (Japan). The conference was co-organized by Kyoto University and KIT–INE, and addressed topics related with (i) Aquatic chemistry of actinides and fission products, (ii) Migration behaviour of radionuclides, (iii) Geochemical and transport modelling, and (iv) Application to Case Studies. A special session with invited contributions was dedicated to the „Research activities towards HLW disposal in Japan and remediation of the Fukushima Daiichi NPS site". More than 260 participants (> 60 students) from 19 different countries attended the conference in Kyoto, bringing together world leading experts, junior scientists and students from different branches of the Migration research community. Among more than 220 poster contributions, three poster prizes were awarded to the students E. Gerber (France), N. Moore (USA) and A. Yamaguchi (Japan) (in alphabetical order). The dates and venue of Migration 2021 were announced during the conference banquet: the 18th Migration conference will be held on September 12–17 2021 in Nantes (France).

3.3 ABC-Salt (VI) and HiTAC (III) Workshop in Karlsruhe

On the 25th and 26th of June 2019 the 6th workshop on "Actinide Brine Chemistry in a Salt-based Repository - ABC-Salt (VI)" was held at the ACHAT Plaza Hotel in Karlsruhe, Germany. Organized by INE in collaboration with the Los Alamos National Laboratory (LANL), the workshop addressed topics such as ongoing repository projects in salt rock, the geochemistry in salt formations, the influence of microbial effects, modern experimental techniques, actinide chemistry in highly saline solutions, and thermodynamic modeling or corresponding database projects. Approximately 50 participants from 10 different nations (USA, Australia, Korea, Japan, Canada, Russia, Spain, Switzerland, France and Germany) met in Karlsruhe. The aim of the workshop was to present recent work and latest scientific results to the international community of specialists and to conceive concepts for future developments in the context of aquatic geochemistry and radiochemistry in highly saline solutions. The 3rd Workshop on "High Temperature Aqueous Chemistry - HiTAC (III)" took place on June 27, 2019, immediately following the ABC-Salt meeting.

Repositories designed for the final disposal of high-level radioactive waste will experience significantly higher temperatures over hundreds of years after waste emplacement due to the ongoing release of decay heat. Therefore, the correct assessment of the influence of higher temperatures on the geo- and actinide chemistry in repository-relevant aquatic systems is of great importance.

During the HiTAC workshop about 40 participants from 9 different countries met in Karlsruhe to present and discuss the current knowledge in this field. The focus of the workshop was on the aquatic geochemistry and the chemical behavior of radionuclides in repository-relevant systems at higher temperatures.

3.4 International Workshop "Mechanisms and Modelling of Waste / Cement Interactions 2019" and "CEBAMA Final Workshop"

In March 2019, INE was organizing two international workshops in Karlsruhe, both related to the use and performance of cementitious materials in nuclear waste disposal.

The International Workshop "Mechanisms and Modelling of Waste/ Cement Interactions" focused on the chemical understanding and the thermodynamic modelling of the processes responsible for the stabilization of hazardous and radioactive wastes in cementitious systems. Like the earlier meetings in this series of workshops (Meiringen, 2005; Le Croisic, 2008; Ghent 2013; Murten, 2016), the 5th workshop was successfully bringing together world-leading and junior scientists from the different branches of the research communities. The workshop was held from March 25th – 27th and was attended by 115 scientists from 15 different countries. Although many research activities related to cement chemistry take place in the waste management field, there is an ongoing need for close scientific contact to fundamental research on cement chemistry to assure state-of-the-art research and to continue to promote national and international collaboration.

Topics of the International Workshop "Mechanisms and Modelling of Waste / Cement Interactions 2019" covered a variety of relevant topics, including:

- Cement Chemistry & Microstructure (modelling, multiscale-approaches, alternative cements)
- Cement/Rock/Soil Interfaces and Transport (cement/host rock, transport processes and modelling)
- Interaction of Cement with Waste Constituents (radioactive waste, toxic waste, metal binding mechanisms, organic compounds)

- Nanoscale Characterization & Molecular Dynamics (methods at large scale facilities, advanced methods)
- Deterioration and Leaching (alkali-aggregate reaction, carbonation, sulfate interaction, ageing process, natural analogues).

In close connection to the above International Workshop, the Final Workshop of the Collaborative Project Cebama was held in Karlsruhe, on the 28th to 29th March 2019, hosted by KIT-INE.

The EC funded Cebama project (www.cebama.eu) addressed key issues relevant for the use of cement-based materials in nuclear waste disposal applications. The Final CEBAMA workshop was successfully providing a forum for the discussion of scientific and technical project results.

Nearly 70 attendees from 13 countries attended the meeting. The CEBAMA Project Workshop thus contributed to the dissemination of project results and communication with a broader interested community.

4. Fundamental studies: Process understanding on a molecular scale

In order to develop fundamental scientific understanding on a molecular scale and ensure the reliable quantitative prediction of key processes in aquatic chemistry, several R&D studies on radionuclide chemistry and geochemistry are performed at KIT-INE. Aiming at a comprehensive assessment of radionuclide behavior and mobility in aquatic systems relevant for nuclear waste disposal, experimental studies with actinides, long-lived fission and activation products and selected non-radioactive elements of interest are performed. The investigated aqueous systems cover from dilute solutions to highly saline salt brine systems and establish essential site-independent data and process understanding. Work is focusing both on detailed experimental investigations using the unique facilities available at KIT-INE, and subsequently developing reliable chemical models and consistent thermodynamic data. This combined approach allows a systematic and reliable evaluation of key processes such as radionuclide solubility, radionuclide speciation, radionuclide retention and transport processes in relevant near- and far-field scenarios.

The fundamental studies summarized in this section is related to the (i) chemistry and thermodynamics of actinides and fission products in aqueous solution, (ii) radionuclide sorption on mineral phases, and (iii) retention of radionuclides by secondary phase formation. The studies aim at identifying relevant radionuclide retention/retardation mechanisms on a molecular level and their robust thermodynamic quantification in support of the Nuclear Waste Disposal Safety Case. The fundamental studies on aqueous radionuclide chemistry described in Chapter 4 are supporting the applied studies (see Chapter 5) performed at KIT-INE.

4.1 Chemistry and thermodynamics of actinides and fission products in aqueous solution

N. Adam, M. Altmaier, A. Baumann, M. Böttle, N. Cevirim-Papaioannou, K. Dardenne, S. Duckworth, F. Endrizzi, D. Fellhauer, X. Gaona, J.-Y. Lee, M. Maiwald, P.J. Panak, J. Rothe, A. Skerencak-Frech, A. Tasi

Introduction

The aquatic chemistry of actinides and fission products is largely controlled by solubility phenomena, redox processes and hydrolysis / complexation behaviour. An accurate knowledge of the fundamental properties controlling these processes is very important in the context of nuclear waste disposal. Source term estimations and geochemical calculations require complete and correct chemical, thermodynamic and activity models, which need to be based on precise and systematic experimental observations. This section highlights some recent examples of the research performed at KIT–INE within this field in 2018.

The leading role of KIT–INE in the field of aquatic chemistry and thermodynamics is internationally acknowledged in key contributions to highly relevant projects, such as the OECD NEA–TDB thermodynamic series, the Plutonium Handbook edited by the American Nuclear Society, or the IUPAC Subcommittee on Solubility and Equilibrium Data, among others.

Solubility of Tc(IV) in reducing chloride-sulfate systems

Technetium-99 is a fission product relevant in the safety case of repositories for radioactive waste disposal due to its abundance in spent nuclear fuel and its long half-life ($2.1 \cdot 10^5$ a). Technetium can exist in different oxidation states, which accordingly show a very different chemical behaviour. Tc(VII) is the prevailing oxidation state under oxidizing and redox-neutral conditions and exists as soluble and mobile TcO_4^-. Tc(IV) forms sparingly soluble hydrous oxides ($TcO_2 \cdot xH_2O$(am)) under reducing conditions as those expected in deep underground repositories as a result of the anoxic corrosion of iron and steel. Sulfate is an abundant component in different types of groundwater, but can be of particular relevance in the context of salt-rock formations where concentrations of up to 0.2 M can be expected [1-2]. Corrosion of cementitious materials in $MgCl_2$-dominated brines may lead to high $CaCl_2$ concentrations ($\geq$ 2 M) and highly alkaline pH_m ($\approx$ 12, with $pH_m = -\log [H^+]$) conditions [3]. In such systems, sulfate concentration in solution is mostly controlled by the solubility of gypsum ($CaSO_4 \cdot 2H_2O$), which defines significantly lower sulfate concentrations ($\leq$ 0.001 M) [3]. Although Tc(IV) is expected to form weaker complexes with sulfate than with hydroxide, the presence of high concentrations of the former ligand may outcompete hydrolysis and result in the increase of $TcO_2 \cdot xH_2O$(am) solubility under conditions relevant in the context of nuclear waste disposal.

The solubility of Tc(IV) was investigated from undersaturation conditions in 0.3, 1.0 and 5.0 M NaCl–Na_2SO_4–NaOH, 4.5 M $MgCl_2$–$MgSO_4$, and 4.5 M $CaCl_2$–$CaSO_4$ solutions with $[SO_4^{2-}]$ = 0.001–1.0 M and $4.0 \leq pH_m \leq 12.5$. Reducing conditions were retained throughout the experiments with Sn(II) and Fe(0) controlling redox. pH_m, E_h and [Tc] (after 10 kD ultrafiltration) were monitored for up to 60 days. pH_m values were determined according to $pH_m = pH_{exp} +$

A_m, where A_m are empiric correction factors determined in this work for the investigated binary and ternary systems. Solid Tc phases were characterized after attaining equilibrium conditions using XRD, SEM–EDS and quantitative chemical analysis.

Experimental (pe + pH_m) values (with pe = –log a_{e^-} = 16.9 E_h (V)) are well below the Tc(VII)/Tc(IV) redox borderline in all solubility samples, indicating the predominance of Tc(IV) in the investigated chloride-sulfate systems in the presence of Sn(II) or Fe(0). Solid phase characterization indicates that $TcO_2{\cdot}xH_2O$(am) is the solid phase controlling the solubility of Tc(IV) in the presence of up to $[SO_4^{2-}]_{tot}$ = 1.0 M. Solubility results are exemplarily shown in Figure 1 a and b for 5.0 M NaCl–Na_2SO_4 and 4.5 M $CaCl_2$–$CaSO_4$, respectively

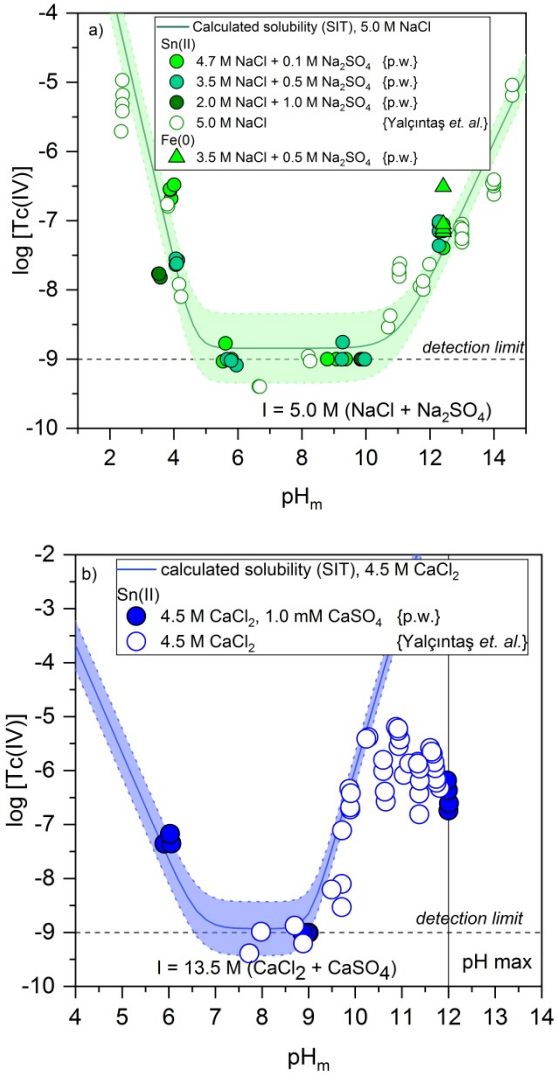

Fig. 1: Experimental solubility data of Tc(IV) measured in the presence of Sn(II) and Fe(0): (a) in 5.0 M NaCl–Na_2SO_4 (filled symbols); (b) in 4.5 M $CaCl_2$–$CaSO_4$ (filled symbols). Empty symbols in Figures (a) and (b) correspond to solubility of Tc(IV) reported in [4] under analogous conditions but in absence of sulfate. Solid lines correspond to modelled solubility of Tc(IV) in absence of sulfate calculated with the thermodynamic models reported in [4] and [5].

Solubility data determined in this work are in good agreement with Tc(IV) solubility data reported in previous studies conducted under analogous conditions but in the absence of sulfate [4], thus indicating that sulfate has a minor impact on the solubility of $TcO_2{\cdot}xH_2O$(am) in the investigated pH_m-range and salt concentrations. Although the formation of Tc(IV)–SO_4 complexes under very acidic conditions has been previously described in the literature [6], our study indicates that sulfate can hardly outcompete hydrolysis in the pH_m conditions investigated in this work and thus it is expected to play a minor role in the solution chemistry of Tc under repository-relevant conditions.

Impact of organic cement additives on the solubility of Th(IV) and U(VI) in intermediate ionic strength conditions

Concrete and cementitious materials are used in repositories for radioactive waste disposal for construction purposes and for the stabilization of the waste. Such materials will buffer the pH in the alkaline range ($9 \leq pH \leq 13.3$) over a long time–scale. Several organic additives are used to modify the physical and chemical properties of the cement, *e.g.* superplasticizers, accelerators, etc.. These additives can be leached from cement upon solution contact (eventually undergoing degradation) and potentially impact the solubility and sorption properties of radionuclides in the repository. The complexation behavior of some model compounds representing organic cement additives or degradation products (*e.g.* gluconate) was previously investigated, showing that especially poly-hydroxocarboxylic acids form strong complexes with actinides under hyperalkaline pH conditions representative of cementitious systems [7-12]. However, most of these studies focus on low ionic strength conditions and cannot be directly extrapolated to intermediate or high ionic strength systems such as those potentially expected in rock-salt formations or specific clay systems with elevated ionic strength porewater.

The solubility of Th(IV) and U(VI) was studied in the presence of selected organic cement additives and model compounds: adipic acid, methyl acrylate, citric acid (Cit), melamine, ethylene glycol, phthalic acid and gluconic acid (GLU). Experiments were performed under Ar atmosphere in NaCl (2.5/5.0 M), $CaCl_2$ (1.0/3.5 M) and $MgCl_2$ (1.0/3.5 M) solutions with $9 \leq pH_m \leq 13$. Independent batch samples were prepared from undersaturation conditions with well-defined solid phases: $Th(OH)_4$(am), $Na_2U_2O_7{\cdot}H_2O$(cr) (equilibrated in NaCl systems), $CaU_2O_7{\cdot}3H_2O$(cr) (equilibrated in $CaCl_2$ systems) and $UO_3{\cdot}2H_2O$(cr) (equilibrated in $MgCl_2$ systems). The initial concentration of organic ligands in solution was set constant in all systems to $[L]_0$ = 0.025 M, except in specific cases where the ligand concentration in the matrix solutions was controlled by solubility. The total concentration of Th and U in the aqueous phase was quantified by ICP–MS after 10 kD (2-3 nm) ultrafiltration.

Solubility data determined in this work are exemplarily shown for Th(IV) (1.0 M $CaCl_2$) and U(VI) (2.5 M NaCl) in Figures 2 a and b, respectively. In all investigated salt systems, the solubility of Th(IV) and U(VI) remains unaffected in the presence of adipic acid, methyl acrylate, melamine, ethylene glycol and phtalic acid.

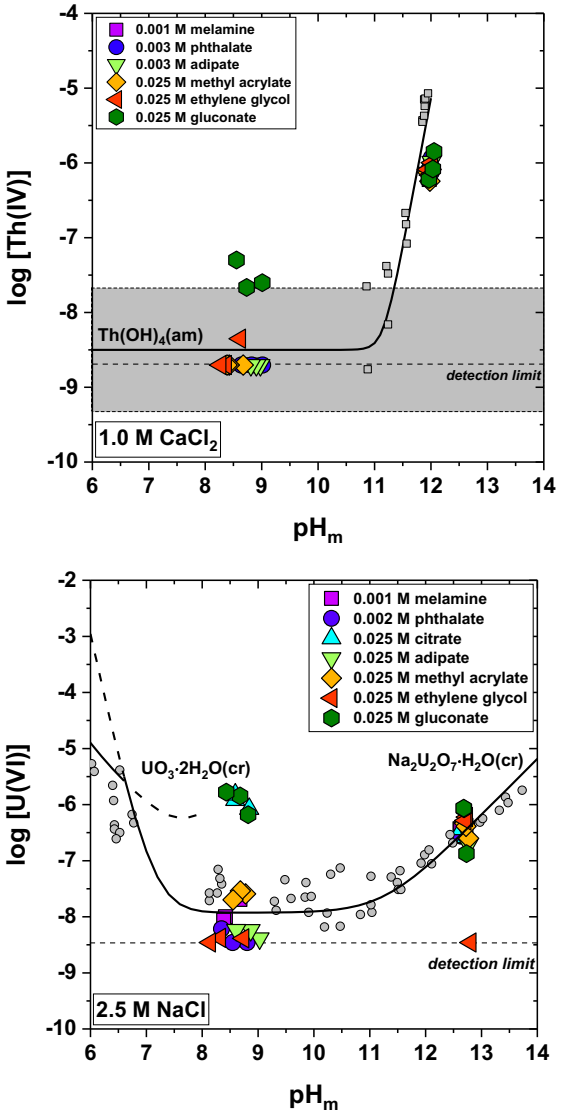

Fig. 2: (a) Experimental solubility data of Th(IV) in the presence of melamine, phthalate, adipate, methyl acrylate, ethylene glycol and gluconate in 1.0 M $CaCl_2$ solutions. Grey symbols represent experimental data for the solubility of $Th(OH)_4(am)$ in the ligand-free system [14]. Solid lines refer to the calculated solubility of $Th(OH)_4(am)$ in $CaCl_2$ solutions in the absence of any ligand as calculated by SIT using thermodynamic data in [14]; (b) Experimental solubility data of U(VI) in the presence of melamine, phthalate, citrate, adipate, methyl acrylate, ethylene glycol and gluconate in 2.5 M NaCl solutions. Grey symbols represent experimental data for the solubility of $UO_3·2H_2O(cr)$ and $Na_2U_2O_7·H_2O(cr)$ in 2.5 and 5.0 M NaCl in the ligand-free system [15]. Solid lines refer to the calculated solubility of $UO_3·2H_2O(cr)$ and $Na_2U_2O_7·H_2O(cr)$ in the absence of any ligand as calculated by SIT using thermodynamic data in [15].

Gluconate and citrate importantly enhance the solubility of Th(IV) and U(VI) in NaCl and $MgCl_2$ solutions, although the overall impact strongly depends on the pH_m and salt concentration. These results underline the important role of (α-) alcohol groups in (poly-) hydroxocarboxylic acids (*e.g.* GLU and Cit) in the complexation of actinides under hyperalkaline pH conditions, where a strong competition with hydrolysis is to be expected. In contrast to experimental results at low ionic strength, the impact of gluconate and citrate on the solubility of Th(IV) and U(VI) is importantly decreased in solutions with $[CaCl_2] \geq 1.0$ M as a background electrolyte. This is expectedly due to the formation of stable binary Ca–GLU and Ca–Cit aqueous complexes and, in the case of citrate, to the low solubility of $Ca_3Cit_2(s)$ that further decreases the total ligand concentration in solution [13]. Furthermore, in the case of Th(IV), the very stable ternary complex forming in alkaline $CaCl_2$ solutions ($Ca_4Th(OH)_8^{4+}$) outcompetes the complexation of organic ligands with Th(IV) under these conditions (Figure 2 a).

The screening experiments conducted within this study contribute to the identification of organic cement additives and model compounds potentially impacting the solution chemistry of An(IV) and An(VI) under intermediate and high ionic strength conditions ($I \approx 2.5 - 5.0$ M). This shows evident differences with respect to investigations conducted under low ionic strength conditions, and thus represents a very relevant input in the safety case of repositories for radioactive waste disposal where such elevated ionic strength conditions are expected. Further systematic solubility studies of Th(IV) and U(VI) in the presence of citrate and gluconate are on-going and will lead to the development of comprehensive chemical, thermodynamic and activity models for these systems.

Solubility of $Ca_2UO_2(CO_3)_3·10H_2O(cr)$ in dilute to concentrated NaCl solutions at $T = 22 - 80$°C

Ternary Ca-U(VI)-CO_3 aqueous species are known to play a relevant role in the solution chemistry of U(VI) in natural environments. The formation of these aqueous complexes is also foreseen in certain repository concepts for nuclear waste disposal, potentially impacting the U(VI)/U(IV) redox borderline under near-neutral pH conditions. Although a large body of experimental studies dealing with Ca-U(VI)-CO_3 aqueous species can be found in the literature [16-19, among others], very limited information is available for the solid phase counterparts [20]. Considering the widespread formation of the mineral liebigite $Ca_2UO_2(CO_3)_3·10H_2O(cr)$ in nature, such ternary solid phases may also play a role in controlling the solubility of U(VI) under those boundary conditions where ternary Ca-U(VI)-CO_3 aqueous species dominate the aqueous speciation of U(VI).

In this context, series of solubility experiments with a well-defined $Ca_2UO_2(CO_3)_3·10H_2O(cr)$ solid phase

were conducted in ≈ 0.02, 0.51 and 5.61 m NaCl solutions with initial pH_m = 7.9 – 8.2. Experiments were performed under air atmosphere at T = 22 and 80 °C. Concentrations of U, Ca and pH_m were monitored for up to 132 days. The starting solid material as well as all solid phases after terminating the solubility experiments were characterized by XRD, SEM–EDS and quantitative chemical analysis (ICP–MS/OES).

XRD patterns and quantitative chemical analysis confirm that $Ca_2UO_2(CO_3)_3 \cdot 10H_2O$(cr) is the solid phase controlling the solubility of U(VI) in ≈ 0.02 and 0.51 m NaCl solutions at T = 22 °C. The U(VI) solid phase equilibrated in 5.61 m NaCl at T = 22 °C shows distinct XRD patterns that match well those available for andersonite, $Na_2CaUO_2(CO_3)_3 \cdot 6H_2O$(cr). Remarkable changes are observed in the XRD patterns of U(VI) solid phases equilibrated at T = 80 °C. In combination with quantitative chemical analysis, XRD data supports the complete transformation of the starting U(VI) solid phase to Ca- and Na-uranates ($CaU_2O_7 \cdot 3H_2O$(cr), $Na_2U_2O_7 \cdot H_2O$(cr) and possibly sub-stoichiometric Na-phases).

Figure 3 shows solubility data (as log [U] *vs.* pH_m) for all investigated systems at T = 22 and 80 °C. Remarkably high concentrations of U (Figure 3) and Ca (data not shown) are determined for the systems equilibrated in [NaCl] ≤ 0.51 m at T = 22 °C. The ratio Ca : U in the aqueous phase after attaining equilibrium conditions is ≈ 2 : 1, indicating a congruent dissolution of $Ca_2UO_2(CO_3)_3 \cdot 10H_2O$(cr). Significantly lower concentrations of uranium are measured for the sample equilibrated in 5.61 m NaCl at T = 22 °C, in line with the formation of $Na_2CaUO_2(CO_3)_3 \cdot 6H_2O$(cr) confirmed by solid phase characterization.

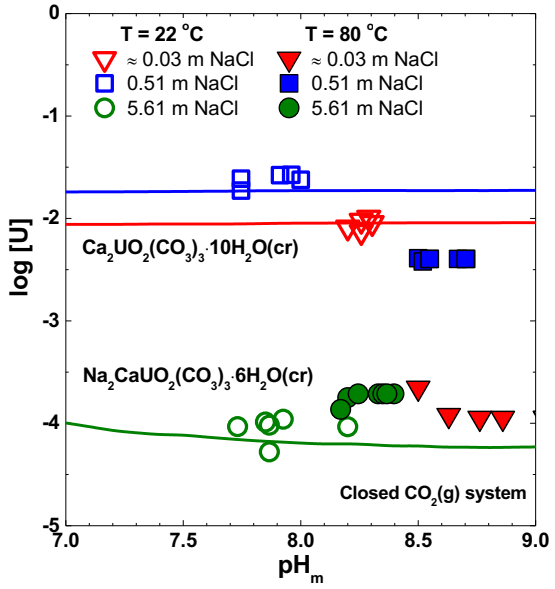

Fig. 3: Solubility of U(VI) at T = 22 and 80 °C under air atmosphere, with $Ca_2UO_2(CO_3)_3 \cdot 10H_2O$(cr) used as starting solid material. Solid and dashed lines represent the calculated solubility of U(VI) and corresponding uncertainty, using thermodynamic data derived in this work and reported in the literature [18, 21].

Solubility samples equilibrated at T = 80 °C show a significant shift of pH_m towards more alkaline conditions. This is related with the less favored dissolution of CO_2(g) with increasing temperature, which results in the degassing of CO_2(g) and consequent proton consumption. Significantly lower concentrations of U are measured for samples equilibrated at T = 80 °C in ≈ 0.02 and 0.51 m NaCl solutions, compared to analogous systems equilibrated at T = 22 °C. This observation is in line with the solid phase transformation confirmed by XRD and quantitative chemical analysis.

Solubility data determined in this work at T = 22 °C, in combination with solid phase characterization and thermodynamic data reported in [18] for the formation of ternary Ca-U(VI)-CO_3 aqueous complexes are used to derive log $K°_{s,0}\{Ca_2UO_2(CO_3)_3 \cdot 10H_2O(cr)\}$ and log $K°_{s,0}\{Na_2CaUO_2(CO_3)_3 \cdot 6H_2O(cr)\}$.

These results complement previously reported thermodynamic data, and allow complete thermodynamic and geochemical calculations for the system UO_2^{2+}–Na^+–Ca^{2+}–H^+–CO_2(g)–HCO_3^-–CO_3^{2-}–H_2O(l), including U(VI) aqueous species and solid compounds of relevance in the context of repositories for nuclear waste disposal.

Thermodynamics of the NpO_2^+ complexation with acetate at elevated temperatures

The present work focuses on the complexation of NpO_2^+ with acetate OAc^- [22]. The complexation is studied in $NaClO_4$ and NaCl solutions by absorption spectroscopy in the near-IR region as a function of the total ligand concentration $[OAc^-]_{total}$, ionic strength (I_m = 0.5 – 4.0 m) and temperature (T = 20 – 85 °C).

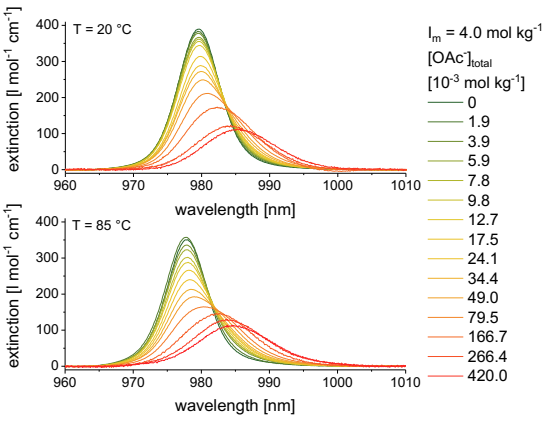

Fig. 4: Absorption spectra of Np(V) as a function of $[OAc^-]_{total}$ at $I_m(NaClO_4)$ = 4.0 m and T = 20, 85 °C [22].

In Figure 4 the absorption spectra of Np(V) at T = 20 and 85 °C, and I_m = 4.0 m $NaClO_4$ are displayed as a function of the total ligand concentration. At 20 °C the absorption maximum of the solvated Np(V) aquo ion is at λ = 979.5 nm. With increasing $[OAc^-]_{total}$, the absorption maximum of Np(V) is bathochromically shifted, and two isosbestic points at 983.7 and 986.0 nm are observed. Furthermore, the Full Width at Half Maximum (FWHM) of the absorption band increases with $[OAc^-]_{total}$. These observations clearly indicate

the formation of two different (innersphere) Np(V) acetate complexes. At T = 85 °C the changes of the spectral features are more pronounced as the bathochromic shift and the increase of the FWHM are larger. These observations confirm that the formation of the Np(V) acetate complexes is fostered at increased temperature indicating an endothermic complexation behavior.

Evaluation of the spectra by principle component analysis reveals the formation of two Np(V) acetate complexes with a stoichiometry of $NpO_2(OAc)_n^{1-n}$ (n = 1,2). With increasing $[OAc^-]_{eq}$ the chemical equilibrium is shifted towards the complexed species (see Figure 5). The comparison of the species distributions at T = 20 and 85 °C clearly shows that at equal ligand concentrations the molar fractions of $NpO_2(OAc)_n^{1-n}$ are increased at higher temperature.

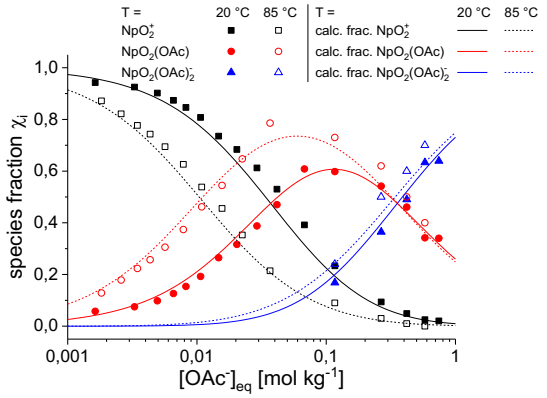

Fig. 5: Species distribution of Np(V) as a function of the equilibrium (free) acetate concentration. (I_m = 4.0 m $NaClO_4$; T = 20, 85 °C) [22].

The log β^0_n(T) values for the formation of $NpO_2(OAc)$(aq) and $NpO_2(OAc)_2^-$ are calculated according to the law of mass action using the determined speciation and the equilibrium acetate concentrations. The conditional stability constants are extrapolated to I = 0 with the specific ion interaction theory (SIT) for both background electrolytes ($NaClO_4$, NaCl).

The log β^0_n(T) values obtained in NaCl and $NaClO_4$ media are in excellent agreement and thus, averaged values are calculated. In the temperature range of 20 to 85 °C the stability constant log β^0_1(T) of $NpO_2(OAc)$(aq) increases from (1.31 ± 0.18) to (1.80 ± 0.16). The stability constant log β^0_2(T) of $NpO_2(OAc)_2^-$ increases from (1.35 ± 0.17) to (1.96 ± 0.21).

The obtained log β^0_n(T) correlate linearly with the reciprocal temperature T^{-1} (see Figure 6). Thus, the temperature dependence is well described by the integrated Van't Hoff equation. Linear regression yields the thermodynamic functions $\Delta_r H^0$ and $\Delta_r S^0$ of the complexation reactions. Both reactions are endothermic ($\Delta_r H^0_{m,1}$ = (14.8 ± 1.6) kJ mol^{-1}, $\Delta_r H^0_{m,2}$ = (19.0 ± 2.1) kJ mol^{-1}) and driven by the gain of entropy ($\Delta_r S^0_{m,1}$ = (74 ± 10) J mol^{-1} K^{-1}, $\Delta_r S^0_{m,2}$ = (89 ± 16) J mol^{-1} K^{-1}). Furthermore, the SIT specific binary ion-ion interaction coefficients between the Np(V) acetate complexes and Na^+/ClO_4^- and Na^+/Cl^- (ε_T(i,k)) are determined as a function of temperature. The obtained values show no significant temperature dependence indicating that the effect of temperature on $\Delta\varepsilon_{i,k}$ is rather small and therefore negligible in the temperature range of 20 to 85 °C. Thus, temperature-independent binary ion-ion interaction coefficients for both complexes are evaluated: ε(NaCl, $NpO_2(OAc)$(aq)) = (0.02 ± 0.06) kg·mol^{-1}, ε($NaClO_4$, $NpO_2(OAc)$(aq)) = (0.15 ± 0.06) kg·mol^{-1} and ε(Na^+, $NpO_2(OAc)_2^-$) = –(0.01 ± 0.06) kg·mol^{-1}.

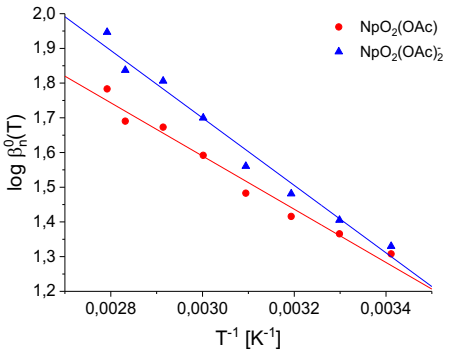

Fig. 6: Plot of log β^0_n(T) (n = 1, 2) as a function of the reciprocal temperature and fitting according to the integrated Van't Hoff equation [22].

References

[1] Schuessler, W., et al., Mater. Res. Soc. Symp. Proc., 663, 791, (2001).

[2] Lucchini, J. F., et al., Radiochim. Acta, 101, 391–398, (2013).

[3] Bube, C., et al., Physics and Chemistry of the Earth, 64, 87–94, (2013).

[4] Yalcintas, E., et al., Dalton Trans., 45, 8916–8936, (2016).

[5] Baumann, A., et al., New J. Chem., 41, 9077-9086, (2017).

[6] Vichot, L, et al., Radiochim. Acta 91, 263–271, (2003).

[7] Warwick, P., et al., Radiochim. Acta 92, 897–902, (2004).

[8] Tits, J., et al., Applied Geochemistry, 20, 2082–2096, (2005).

[9] Gaona, X., et al., Journal of Contaminant Hydrology, 102, 217–227, (2008).

[10] Felmy, A. R., et al., Radiochim. Acta, 94, 205-212, (2006).

[11] Colàs, et. al., Radiochim. Acta, 99, 269-273, (2011).

[12] Felipe-Sotelo, M., et al., Journal of Hazardous Materials, 300, 553–560, (2015).

[13] Hummel, W., et al., NEA OECD, Elsevier, (2005).

[14] Altmaier, M., et al., Radiochim. Acta, 96, 541-550, (2008).

[15] Altmaier, M., et al., Journal of Chemical Thermodynamics, 114, 2-13, (2017).

[16] Bernhard, G., et al., Radiochim. Acta, 89, 511-518, (2001).

[17] Kalmykov, S. N. and Choppin, G. R., Radiochim. Acta, 88, 603-606, (2000)

[18] Lee, J.-Y. and Yun, J.-I., Dalton Trans., 42, 9862-9869, (2013).
[19] Endrizzi, F. and Rao, L., Chem. Eur. J., 20, 14499-14506, (2014).
[20] Alwan, A. K. and Williams, P. A., Mineral Mag., 43, 665-667, (1980).
[21] Guillaumont, R., et al., Chemical Thermodynamics Vol. 5: Update on the Chemical Thermodynamics of Uranium, Neptunium, Plutonium, Americium and Technetium, OECD-NEA, (2003)
[22] Maiwald, M. M., et al., New J. Chem., 42, 7796, (2018).

4.2 Sorption on mineral surfaces

4.2.1 The use of second harmonic generation to study adsorption kinetics in ternary systems and adhesion processes

J. Lützenkirchen

In co-operation with:

A. Abdelmonem[a], E. Redel[b]

[a] Institute of Meteorology and Climate Research (IMK), Karlsruhe Institute of Technology (KIT) , Hermann-von-Helmholtz-Platz 1, 76344 Eggenstein-Leopoldshafen, Germany

[b] Institute of Functional Interfaces (IFG), Karlsruhe Institute of Technology (KIT) , Hermann-von-Helmholtz-Platz 1, 76344 Eggenstein-Leopoldshafen, Germany

Introduction

In the context of reactive transport the time frames and residence times of aqueous solutes are usually sufficiently long to assume local equilibria. However, in the context of ion adsorption, it has been observed in some cases that desorption can be very slow and sometimes even so slow that ion binding to mineral surfaces has been considered irreversible. Time dependent studies might therefore gain importance in defining desorption rates as a first step, and subsequently understanding in why desorption is so slow.

At present, most published studies dealing with the adsorption of solutes on mineral surfaces involve or assume equilibrium conditions. The study of the adsorption kinetics is difficult due to the fast initial solute uptake that has been usually observed. Since separation steps that are required to analyse the solute concentration remaining in solution require a certain time, the use of such approaches in kinetic studies (i) limits the time frame to the time required for separation and consequently and (ii) does not allow to establish the initial rate of adsorption. Instead in-situ methods are required, which may involve amongst others the use of ion-specific electrodes [1], the pressure-jump-technique [2] or time-resolved spectroscopic methods [3]. In the present case we have tested a non-linear optical technique (second harmonic generation, SHG) to indirectly study adsorption kinetics in binary and ternary systems. The set-up has been previously described in much detail [4-5], and applied to the surface (sapphire-c) used here [6-8]. While we cannot directly observe ion uptake with this technique, it is possible to follow the SHG signal from a constant initial value to a constant final value after addition of a solute. For the binary systems tested it was found that the time resolution is probably insufficient to derive uptake rates. However, in ternary systems, and using the comparison to the concomitant binary systems, it was clearly possible to observe a time dependent equilibration. In these first experiments we used a sapphire (0001) surface as a mineral template and Ca^{2+} and SO_4^{2-} as solutes in NaCl electrolytes and at neutral pH. The rather weakly adsorbing solutes were chosen to avoid irreversible adsorption that would limit the amount of experiments that can be carried out with the rather expensive sapphire substrate

Measurements in the binary system

The equilibrium (or steady-state) uptake established after a few seconds on addition causes an increase in SHG signal for Na_2SO_4 solutions and a decrease for NaCl and $CaCl_2$ solutions. A decrease in the signal due to Ca-addition which is arising from a change in the ordering of the interfacial dipoles (that contribute to the non-linear optical response of the interface) here corresponds to an increase in fundamental positive charge, which is found for pH titrations at constant salt level. Thus the addition of sulphate would be equivalent to decreasing positive charge or increasing negative charge, which is expected for the adsorption of an anion. The addition of NaCl in turn corresponds to the non-specific adsorption of the electrolyte ions and has been interpreted in terms of bare surface charge shielding. In the general model, with increasing NaCl concentration such shielding would result in enhanced protonation for a positive surface and enhanced deprotonation for a negative surface. The two effects can only be disentangled with a comprehensive model, but in most cases in the literature only the shielding effect has been involved in quantitative interpretations.

The scaled SHG signals on addition of 20 mM Cl or Na solutions at constant pH (pH 5.8) are 1.06 for Na_2SO_4, 0.95 for NaCl, and 0.60 for $CaCl_2$. The numbers indicate the SHG signal relative to the absence of solutes (i.e. the signal in MilliQ water). As discussed the anion increases the signal, which must mean specific adsorption of sulphate, since bare shielding as in the case of NaCl decreases the signal. Compared to NaCl for constant chloride concentration, the calcium solution decreases the signal by roughly 40 percent, which suggests interactions beyond bare shielding. Unlike the sodium and calcium chloride systems, the concentration curve for sodium sulphate shows a non-monotonic behaviour. Following an initial increase in the signal the response hits a maximum with subsequent decrease. This can be interpreted by initial spe-

cific adsorption of the sulphate ion dominating followed by subsequent shielding for example once the maximum sulphate uptake has occurred (or when the effect of sulphate uptake is outweighed by the shielding effect. In the studied concentration range the signal did not shift below the water reference signal, suggesting that the sulphate persisted at the interface.

Measurements in the ternary system

Figure 1 shows the results of the experiments, where either $CaSO_4$ (to yield a final concentration below the precipitation threshold of gypsum) is added to the sapphire surface at fixed NaCl concentration or $CaCl_2$ is added to a solution of Na_2SO_4 that had reached a steady state with the sapphire surface. The final concentrations of all ions were identical for the two cases.
When $CaSO_4$ was added to the system, the SHG signal decreased within a few seconds to the steady state that had been observed in the independent experiments for bare $CaCl_2$ solutions of comparable concentrations. This result would suggest that sulphate does not play any significant role in the ternary system.

However, the kinetics observed in the system with pre-adsorbed sulphate is much slower when $CaCl_2$ is

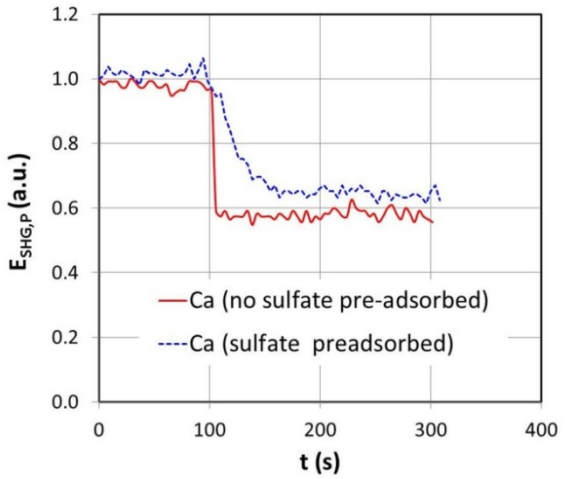

Fig. 1: SHG signal as a function of time for the NaCl /$CaSO_4$, and Na_2SO_4/$CaCl_2$, systems. The final concentrations of all ions were identical for both experiments. For the systems where no sulphate was pre-adsorbed, $CaSO_4$ was added to a NaCl solution. For the system where sulphate was pre-adsorbed, a $CaCl_2$ solution was added to a Na_2SO_4 solution.

added. It takes about 50 to 60 seconds until the SHG signal achieves a constant value. Note that steady-state values for both cases (at $t > 200$ s) are indistinguishable and appear higher in the sulphate system only because no attempt was made to shift the average signals at $t <$ 100 s to the same levels.

The data in Figure 1 suggest that sulphate is not able to affect Ca uptake on sapphire-c when both are simultaneously added to the solution. In the absence of calcium, as discussed above sulphate is adsorbed, but is then gradually desorbed by the adsorbing calcium. The adsorption of calcium (or desorption of the sulphate) is a comparatively slow process.

In summary we have shown that the non-linear optical technique of second harmonic generation allows the study of transient adsorption processes at interfaces. By keeping the ion-concentrations in all systems equal the approach can be used to initially test the occurrence of ternary surface complexes and competitive equilibria. Ideally desorption rates can be obtained.

Extension of the kinetic studies to other phenomena

It has been previously shown that transient studies involving non-linear optical techniques involving Sum Frequency Generation (SFG) might shed new insight in dissolution processes [9]. These measurements have been more recently repeated and the results were reproduced using SHG [5]. Another topic where these transient investigations could be interest is the interaction of particles with surfaces.

In the remainder of this chapter we show some initial results concerning the interaction of nano-particles with mica-surfaces.

Figure 2 shows the results of experiments where TiO_2 nano-particles have been added to a mica surface at pH 9. Although these are unfavorable conditions for interaction (both surfaces have a net negative electrokinetic charge), the SHG signal as shown in Figure 2a

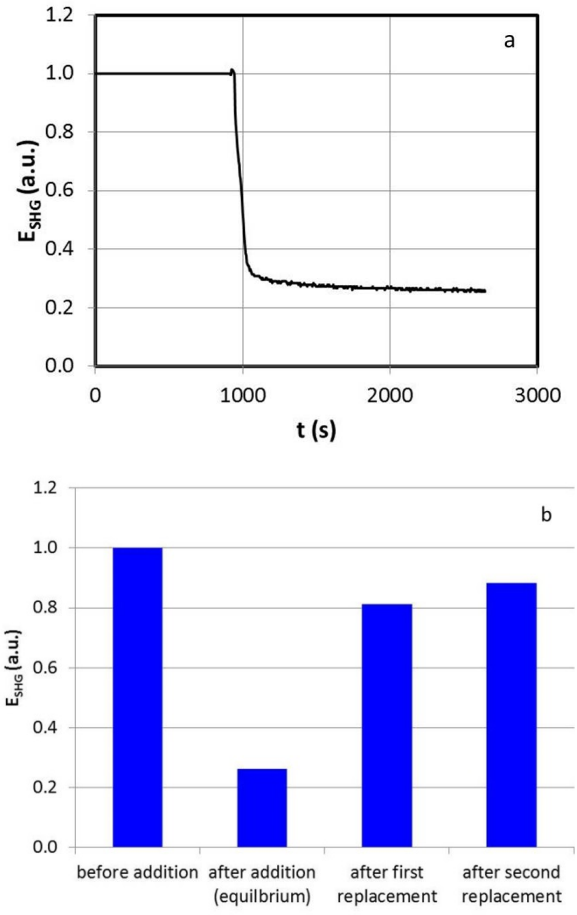

Fig. 2: Interaction of TiO_2 nano-particles with mica at pH 9 as studied by SHG. a) addition of particles b) reversibility study.

decreases indicating the perturbation of the interfacial dipoles by the nano-particles. The precise interaction cannot be inferred from this kind of data. The added nano-particles, however, must come sufficiently close to the surface to perturb the ordering of the interfacial dipoles. We observe an initial fast decrease where within about a minute the signal decreases by about 70 percent. This is followed by a much slower step, which might be due additional particles adhering or ordering of the particles already present at the interface. The experimental data suggest that the kinetics of interaction can be measured in this way conveniently. Maybe even more interestingly the reversibility of the interaction can be investigated. Figure 2b shows to what extent the interaction can be reversed by adding solution of the same composition except for nano-particles. The data show that with the first replacement the signal recovers to about 80 percent of the initial value, meaning that part of the nano-particles is removed. A second solution replacement increases this to about 85 % which suggests that part of the particles is irreversibly bound at the mica surface.

This second part corroborates the feasibility of kinetic studies involving second harmonic generation. The advantage is the in-situ nature of the measurement and lack of any restriction with respect to salt levels. The disadvantage is that the method is limited to systems involving one flat surface which in general has to be suitable for non-linear optical measurements. An alternative option would be applying scattering SHG, which although a challenge for non-spherical particles, will be considered in our future work.

References

[1] R.A. Durst, B.T. Duhart, Analytical Chemistry, 42, 1002-1004, (1970).

[2] N. Mikami et al., Journal of Physical Chemistry, 87, 1454-1458, (1983).

[3] C. Luengo et al., Journal of Colloid and Interface Science, 300, 511-518, (2006).

[4] A. Abdelmonem et al. Atmospheric Measurement Techniques, 8, 3519-3526, (2015).

[5] J. Lützenkirchen et al., Journal of Colloid and Interface Science 529, 294-305, (2018).

[6] J. Lützenkirchen et al., Geochemical Transactions, 15, 1-14, (2014).

[7] A. Abdelmonem et al., Atmospheric Chemical Physics, 17, 7827-7837, (2017).

[8] J. Lützenkirchen et al., Advances in Colloid and Interface Science, 251, 1-25, (2018).

[9] D. Lis et al., Science, 344, 1138-1142, (2014).

4.2.2 Sorption of europium onto montmorillonite in the presence of gluconate

F. Rieder, T. Rabung

Introduction

The interaction of trivalent actinides with clay mineral surfaces shows in general strong uptake [1]. Such strong retention was demonstrated recently also for highly saline conditions [2]. A significant decline in sorption is, however, to be expected in presence of organic complexing ligands. These ligands may either be naturally occurring compounds (e.g. humic acids [3]) or originating from the waste form or the concrete used. Among other relevant complexing ligands, gluconate is a representative of α–hydroxo carboxylic acids and an analogue to isosaccharinic acid, which is the main product of cellulose degradation as well as an important cement additive. The complexation of trivalent actinides with gluconate might significantly decrease their sorption to mineral surfaces. As gluconate is known to be complexing metal ions, the formation of ternary complexes between ligand, actinide and electrolyte cations is possible. A sound mechanistic understanding and a reliable prediction of the metal ion sorption under relevant conditions requires experimental data with a variation of sensitive system parameters (e.g. pH_m, ligand concentration, background electrolyte concentration and composition etc.). By combining all available information reliable thermodynamic models can be derived and validated.

Results and discussion

No published data are available dealing with the sorption of trivalent lanthanides and actinides onto montmorillonite in presence of gluconate at different ionic strength. In order to assess the strong radionuclide retention capacity of clay minerals either in bentonite barriers or claystone host rocks, the potential impact of strong complexing ligands on the sorption of these nuclides must be quantified. In the present work batch sorption experiments with Eu(III) on montmorillonite (Na-SWy-2) in presence of gluconate were performed, using a solid to liquid ratio of 1 g/L, different NaCl (0.1, 1, 3 M) and $CaCl_2$ (0.06, 0.6, 2 M) background electrolytes concentrations and a constant ligand concentration of 0.01 M gluconate. In addition a second batch sorption series at fixed pH_m-values (pH_m= 9, 10.5, 12) was performed as a function of the ligand concentration ([gluconate] = $5 \cdot 10^{-3}$ - $1 \cdot 10^{-4}$ M). The total radionuclide concentration was limited to $2 \cdot 10^{-8}$ M ^{152}Eu (carrier free) for each batch. All experiments were performed under argon atmosphere with an equilibration time of 3-4 day. To avoid precipitation of binary salts including electrolyte compounds and the organic ligand, every system was simulated as a function of pH_m (using the geochemical code PHREEQC and the database THEREDA or the PSI/Nagra Chemical Thermodynamic Database). Based on the simulation results the uptake experiments were set up below the solubility level of the binary phases. To eliminate effects of microbial degradation every solution containing organic ligands was freshly prepared and used directly.

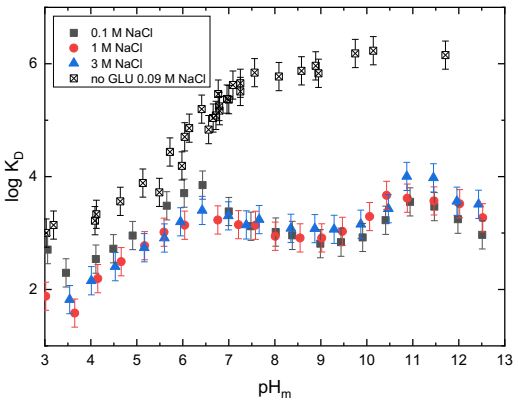

Fig. 1: Eu(III) sorption onto montmorillonite in presence of 0.01 M Na-Gluconate in different NaCl electrolytes solutions (0.1 M black, 1 M blue, 3 M red) shown as logarithmic distribution coefficient log K_D vs. pH_m. To estimate the effect of gluconate, an experimental series from Schnurr et al. [4] in absence of any competing ligand was added (open symbols, 0.09 M NaCl).

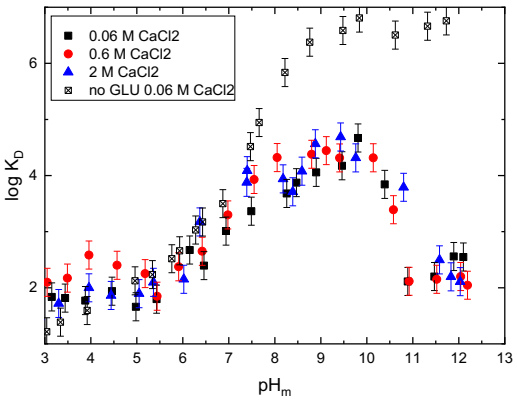

Fig. 2: Eu(III) sorption onto montmorillonite in presence of 0.01 M Ca-Gluconate in different $CaCl_2$ electrolytes solutions (0.06 M black, 0,6 M blue, 2 M red) shown as logarithmic distribution coefficient log K_D as a function of pH_m. To estimate the effect of gluconate, an experimental series from Schnurr et al. [4] in absence of any competing ligand was added (open symbols, 0.06 M $CaCl_2$).

In the presence of gluconate, a reduction of Eu(III) retention is observed over the pH_m-range from pH_m= 3-12.5. In the low pH_m region (pH_m = 3-7) the retention increases from log K_D = 2 to 3.5. No impact of the ionic strength in NaCl background electrolyte solutions is observed (Fig. *1*).

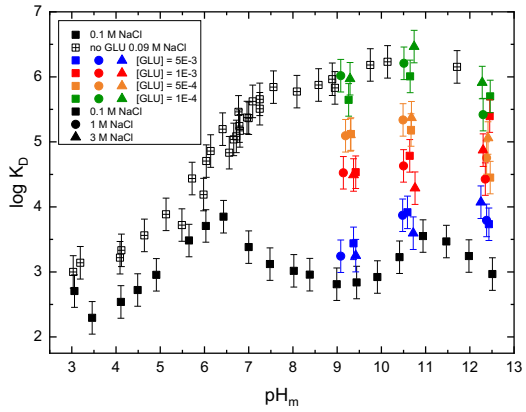

Fig. 3: Eu(III) sorption onto montmorillonite at different gluconate concentrations in 0.1, 1, 3 M NaCl. To estimate the effect of the gluconate concentration, an experimental series from Schnurr et al. [4] in absence of any competing ligand (open symbols, 0.09 M NaCl) and an experimental series in presence of 0.01 M Na-gluconate (black squares, 0.01 M gluconate) was added.

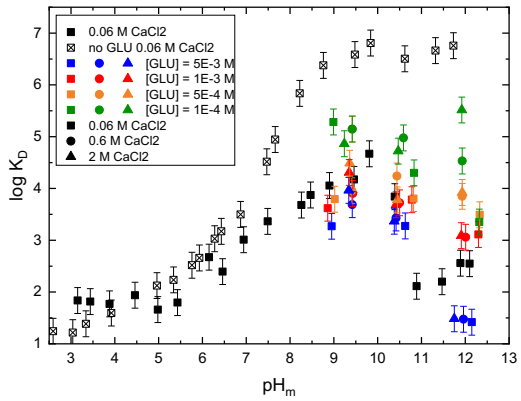

Fig. 4: Eu(III) sorption onto montmorillonite at different gluconate concentrations in 0.06, 0.6, 2 M $CaCl_2$. To estimate the effect of the gluconate concentration, an experimental series from Schnurr et al. [4] in absence of any competing ligand (open symbols, 0.09 M NaCl) and an experimental series in presence of 0.01 M Na-gluconate (black squares, 0.01 M gluconate) was added.

Above pH_m = 7 the logarithmic distribution coefficient remains constant between log K_D = 3-4. This is by 1-2 orders of magnitude lower compared to the data of Schnurr *et al.* where no competing ligand is present. Experimental data derived from the $CaCl_2$ containing system show no effect of gluconate in the lower pH_m region (pH_m < 7) (Fig. *2*). A behavior similar to the NaCl system is observed between pH_m = 7-10.5, where the log K_D remains constant around 4. However, at pH_m above 10 the distribution coefficient decreases again. This second decrease may be attributed to the formation of ternary Ca-Eu(III)-GLU or quaternary Ca-Eu(III)-GLU-OH complexes. A remarkable finding is the absence of any dependency on the ionic strength in both electrolyte solutions.

The sorption of Eu(III) on montmorillonite at different gluconate concentrations and different background electrolyte solutions is shown as a function of the pH_m in Figure 3 (NaCl) and Figure 4 ($CaCl_2$). The results are compared with data in absence (open symbols, black, same ionic strength) and presence of gluconate (0.01 M, closed symbols, black). In NaCl solutions a decrease in retention takes place with increasing gluconate concentration, resulting in a log K_D = 3-4 at $5 \cdot 10^{-3}$ M gluconate. This is in good agreement with the previously determined values at $1 \cdot 10^{-2}$ M gluconate.

These results allow the definition of a lower limit of $1 \cdot 10^{-4}$ M gluconate, under which no effect on the sorption of An(III) and Ln(III) occurs. Also, an upper limit of about $5 \cdot 10^{-3}$ M gluconate is determined, above which higher ligand concentrations have no additional impact on the sorption. A similar trend is observed in $CaCl_2$ containing systems. Due to the higher complexity of this system caused by the interaction of Ca and gluconate, the determined data show a greater scattering.

Conclusions

The presence of competing ligands like gluconate shows a major effect on the sorption behavior of trivalent lanthanides and actinides. Batch sorption experiments in presence of gluconate show, depending on the gluconate concentration, a significant reduction of the sorption of Eu(III) onto montmorillonite over the whole pH_m-range covered in this study.

References

[1] M.H., Bradbury, B., Baeyens, H., Geckeis, , T. Rabung, Geochimica Et Cosmochimica Acta, 69, 5403-5412, (2005).

[2] A. Schnurr, et al., Geochimica et Cosmochimica Acta, 151, 192-202, (2015).

[3] T. Rabung, et al., Radiochim. Acta, 82, 243, (1998).

[4] A., Schnurr, *Institut für Nukleare Entsorgung (INE)*. 2015, Karlsruher Institut für Technologie (KIT): Karlsruhe. P. XIV, 147 Seiten.

4.3. Retention of radionuclides by secondary phase formation

N. Vozárová, T. Platte, F. Duske, N. Finck, F. Heberling, V. Montoya, D. Schild, E. Soballa, S. Kraft, N. Ait Mouheb, J. Rothe, K. Dardenne, T. Schäfer

Introduction

The final disposal in deep geological formations is considered as prime option for the safe disposal of high-level nuclear waste. During the (geo)chemical evolution of the repository system, ground water may migrate through the barriers and ultimately reach the canisters. In aqueous environment, constituents of the multi-barrier system will start corroding or altering and secondary phases will form. For example, various Fe secondary phases, such as Fe (hydr)oxides, silicate or carbonates, may form upon corrosion of steel canisters. Accurate determination of the corrosion mechanism will not only provide information on the nature and amounts of corrosion products, but also on canister lifetime. Similarly, cementitious materials used to construct the repository will undergo alteration upon contact with ground water. Thorough understanding of corrosion/alteration processes is key information for the Safety Case.

Secondary phases represent a chemical barrier, which may significantly delay the migration of radionuclide released from the waste matrix to the far field. Various molecular scale processes can result in radionuclide immobilization, from surface retention to structural entrapment. Among them, structural incorporation, with formation of solid solutions, has a large potential for efficient long-term immobilization. However, though the formation of solid solutions is common in nature, kinetic and thermodynamic models relevant for the Safety Case are only available for a few selected systems. Such models can be developed by combining experimental information obtained by applying advanced microscopic, spectroscopic and diffraction techniques, with complementary computational studies. This strategy is applied at KIT-INE where models are developed for the structural incorporation of key radionuclides into relevant secondary phases. Examples of ongoing studies performed within national and international projects are presented below.

Corrosion of carbon steel in various brines at elevated temperature

In deep geological disposal facilities, nuclear waste is foreseen to be encapsulated in thick-walled steel containers. Intrusion of water will lead to container corrosion and limit container integrity. For safety assessment and the Safety Case, knowledge of corrosion rates and corrosion mechanisms are important information as the corrosion products potentially provide an additional barrier hindering radionuclide (RN) migration to the far field. Steel corrosion under conditions representative of disposal in clay-based repositories (e.g., under consideration in France and Belgium) has been reported [1,2] but knowledge of detailed corrosion mechanisms under saline conditions (e.g., possible geologic formation in Germany and United States) combined with careful analysis of corrosion product formation and their role for RN retention, is still limited.

The corrosion studies performed here focus on the detailed investigation of the carbon steel-spheroidal graphite iron, which is used as a canister material for spent fuel. The experiments are performed in airtight autoclaves. The defined conditions are anoxic (closed in an argon filled glovebox), saline and at elevated temperature of 90 °C. The brines used for the corrosion experiments were taken from the literature describing the Asse salt dome brine composition [3]. These correspond to saturated NaCl and $MgCl_2$ with addition of respective salts as follows: (Solution 3) NaCl with additions of 0.02 M $CaCl_2$, 0.02 M Na_2SO_4, 0.015 M K_2SO_4 and 0.015 $MgSO_4$ and (Solution 1) saturated $MgCl_2$ with additions of 0.3 M NaCl, 0.8 M KCl and 0.15 M $MgSO_4$. The experiments ran for 3 and 6 months either in saturated brines w.r.t NaCl and $MgCl_2$ or in the respective solutions 1 and 3. At the end of the experiments, the pH and Eh were measured after cooling the autoclaves down to room temperature. Then, the formed secondary phases were characterized using the XPS, SEM-(EDX), XRD and Raman techniques under anoxic conditions. Subsequently the weight loss was determined and the corrosion rate in µm/a was calculated.

The carbon steel samples were prone to the graphitic corrosion regardless of the brine. This process takes place when the iron around the inclusion is preferentially corroded due to the positioning of anode (iron) and cathode (graphite). This then causes the peeling/abrasion of graphite and significantly contributes to the corrosion rate. In brines rich in NaCl, sheet silicate phases were present, such as greenalite $Fe_3Si_2O_5(OH)_4$ and cronstedtite $Fe_{2-3}(Si,Fe)_2O_5(OH)_4$ while in competition with chloride phase β-$Fe_2(OH)_3Cl$. The addition of sulfate compounds (solution 3) decreased the corrosion rate by hindering the formation of the secondary phases, however, the formed phases remained the same. In saturated $MgCl_2$ brine, single Cl phase β-$Fe_2(OH)_3Cl$ was formed with significant coverage (Fig. 1). β-$Fe_2(OH)_3Cl$ is a metastable phase and is prone to transforming with time into green rust chloride/sulfate depending on the presence of sulfate in the brine. Overall, magnesium presence seems to be inhibiting the formation of silicate phases. Addition of sulfates (solution 1) hindered also in this case the formation of secondary phases and the corrosion rate decreased.

The pH evolution showed small increases except for cronstedtite formation in solution 3 at 90 °C where pH

decrease was observed. For all samples, the pH maintained at near neutral values. The Eh decreased in all samples. In the literature [4], in solution 1 the lowest corrosion rate was observed, 50 µm/a at 150 °C. We have observed lower corrosion rate of 20 ± 2 µm/a at 90 °C, but 4 ± 0.5 µm/a at 25 °C showing its strong dependence on the temperature. For solution 3, the corrosion rate in literature was 25 µm/a at 150°C, while we have observed much lower rate of 7 ± 1 µm/a at 90 °C. These corrosion rates are so far based on the single experiment and further longer running experiments will give better insights as well as show whether the corrosion rate progresses linearly or not.

Retention of iodine by Fe secondary phases

^{129}I is produced by fission of ^{235}U with a yield of 0.7 %. With its long half-life of 15.7 million years, it plays an important role for the safety case of repositories [5]. Iodide (I^-) is the most thermodynamically stable species in the near-field under repository relevant conditions [6]. In contrast to cationic species such as actinides (e.g. Cm^{3+}, Am^{3+}, Pu^{4+},…), anionic species like iodide might be retained more likely at positively charged surfaces, such as e.g., layered double hydroxides (LDH). LDHs occur in iron hydroxide or Green Rust (GR) by oxidation of the steel containers for example. Because of their positively charged surfaces, Fe-corrosion products may represent an important sink for anionic radionuclide species like iodide.

The structure of GR can be described as octahedral $Fe(OH)_6$ units that share edges to build brucite-like layers. The iron in these units appears as Fe(II) and Fe(III) and the layers are therefore positively charged. To achieve charge balancing, anionic species and water molecules are positioned between the layers. Bernal et al. divided the GR family into two groups based on their X-ray diffraction data (XRD) [7]: GR type 1 with a rhombohedral crystal structure and type 2 with a hexagonal crystal structure. The most common anions for GR type 1 is Cl^- and CO_3^{2-}; for GR type 2 it's SO_4^{2-}.

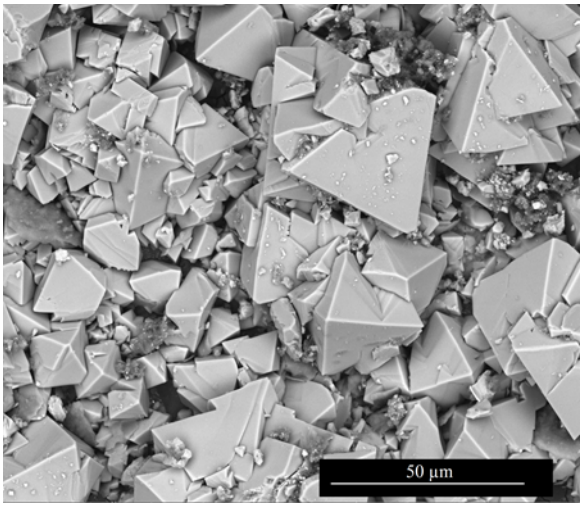

Fig. 1: SEM picture of carbon steel in 3.4 M $MgCl_2$ after 3 months at 90 °C showing visible β-$Fe_2(OH)_3Cl$ crystals noting the high surface coverage.

As a representative of GR type 1 family, GR-Cl was synthesised and characterised. It crystallizes in small plates that are shown in Fig. 2. The synthesis was performed by direct precipitation from a solution containing $Fe^{(II)}Cl_2$ and $Fe^{(III)}Cl_3$ with an adjusted pH of 7 by NaOH. X-ray powder diffraction pattern shows intense peaks at 11.5 °2θ (d_{003} = 7.7 Å) and 22.9 °2θ (d_{006}) (Fig. 2).

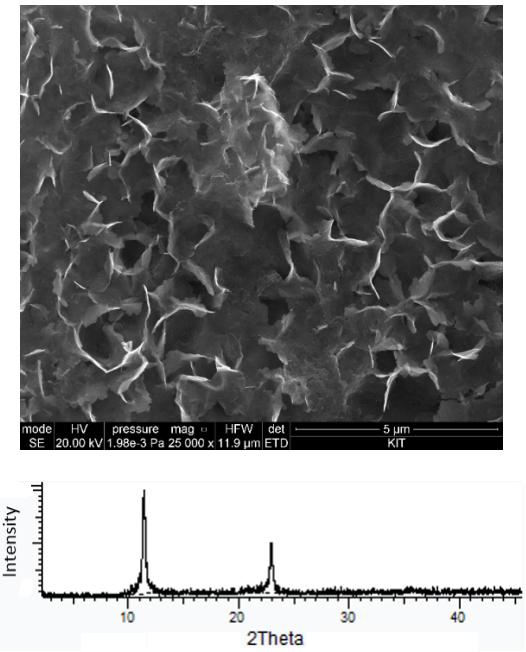

Fig. 2: SEM picture (top) and X-ray diffractogram (Cu Kα, bottom) of chloride green rust.

After the GR syntheses iodine with a concentration of 16 µmol*L^{-1} was added to different experiments. We performed an adsorption experiment where NaI was added to a GR-Cl suspension with a concentration of 2 g/L. Not only was the pH varied between 6.0 and 8.5 but also the ionic strength between 0.05 M and 5 M NaCl and the contact time from 1 to 7 days. At the end of the experiment, the solid was separated from the liquid by centrifugation to determine the amount of retention. First results show no significant sorption of iodine at GR-Cl.

Separately, coprecipitation experiments have been performed. In this experiment, iodide was present during the GR-Cl synthesis. The diffractogram shows the formation of GR and is similar to that of GR-Cl but the peaks are shifted to lower angles (d_{003} = 8.0 Å). This proves an increase of the interlayer spacing which may be attributed to a Cl^- substitution by the larger I^- ($r(Cl^-)$ = 1.81 Å; $r(I^-)$ = 2.20 Å) [8]. Furthermore, the diffractogram shows only a shift of the diffraction peaks, suggesting a homogeneous I^- distribution within the interlayer.

Additionally a GR-I synthesis via $Fe(OH)_2$ as a precursor was tested. The $Fe(OH)_2$ was synthesized by precipitation from a $FeCl_2$ solution. After centrifugation, a NaI solution was added and after a few hours, the oxidized suspension was separated and analyzed. The XRD diffractogram shows no $Fe(OH)_2$ but GR that is in agreement with the GR-I structure of Vins J. et al

[9]. Compared to GR-Cl the peaks shift to lower angles (d_{003} = 8.3 Å).

Summarizing iodine shows low interaction with GR but it can be substituted for Cl^- within the interlayer of LDH. Further adsorption experiments with a lower concentration of iodine are planned. In addition, a solid solution series between the end members GR-Cl and GR-I is intended. There are also transformation reactions from GR-Cl/I structures to magnetite by increasing the pH planned.

Speciation of iron in cementitious materials

Clay minerals and cement-based materials are typically used as confinement barriers in many concepts of deep disposal facilities. Depending on the design, cement and clay minerals may be in contact or be sufficiently close so that the pore-water from both materials interact, and thereby affect (in time and space) their physico-chemical properties. Because the pore-water of "classical" ordinary Portland cement materials is very alkaline (pH ≥ 13), "low"-pH cements have been developed to reduce the interaction between cement and clay. In their synthesis, the clinker content is partly substituted by silica fume or fly ashes [11]. Main differences with Portland cements are the presence of C-S-H phases with a Ca/Si ratio <1 and the absence of portlandite in low pH cements. The initial microstructure and the chemical composition are among the most important information needed to understand and model the degradation of these materials in contact with clay minerals.

Within a PhD thesis performed at KIT-INE within CEBAMA, hydrated low pH cements have been prepared and characterized using various analytical techniques in the laboratory [12]. Yet, uncertainties remain concerning the speciation of structural Fe, making good prediction of Fe behaviour very challenging. Because of overlapping signals from Fe- and Al-containing samples the identification of Fe-containing hydrate phases using standard techniques available in the laboratory is very complicated. This limitation can be overcome by applying X-ray absorption spectroscopy (XAS) at the Fe *K*-edge. XAS has already shown to be a complementary technique providing molecular-scale information for classical cements [13], but not for low pH cementitious materials so far.

Fe *K*-edge X-ray absorption spectra were recorded at the BM26A beamline at the ESRF (Grenoble, France) and at the BL22 beamline at ALBA (Barcelona, Spain). Spectra recorded for low-pH hydrated cement pastes synthesized using either silica fume (MIX 3C, 3D, 3E) or a combination of silica fume and blast furnace slag to form a cement (CEB paste) and a low-pH concrete (CEB concrete) were compared to several reference compounds. Reference substances include among others, the starting clinker and silica fume, the ferrites C2F ($Ca_2Fe_2O_5$) and C4AF ($Ca_2(Al,Fe)_2O_5$), a calcium silicate phase with Ca:Si = 1.0 (CSH 1.0) and Fe-ettringite [14].

XANES of all samples and reference compounds are located at similar energy position, except magnetite ($Fe^{II}Fe^{III}_2O_4$), indicating that Fe is present only in trivalent state in the samples (Fig. 3). All low-pH cement samples prepared with silica fume have very similar structure of the main absorption edge, hinting at very comparable binding environment. This structure is also similar to that of cement prepared with a mixture of silica fume and blast furnace slag. Interestingly, the XANES of Portland cement paste (Fig. 3) is comparable to that of the low pH counterparts, whereas that of the concrete significantly differs.

Quantitative information was obtained by linear combination analysis (LCA). Fit results indicate that Fe speciation in samples MIX 3C, 3D and 3E is very similar, with half of Fe located in ettringite and the other half in CSH 1.0 and unreacted clinker. In the clinker, Fe is present mostly as C4AF, with low amounts of C2F and ferrihydrite. Results also suggest that Fe environment in CEB paste is a mixture of C2F (~50 %), ettringite (~30 %) and hematite (~20 %). The Fe speciation in Portland cement slightly differs: Fe is mostly located in ettringite (~75 %) and a lower proportion in C4AF (~25 %). XANES results show that the Fe speciation in cementitious materials is significantly influenced by the nature of the starting materials. In the concrete, Fe is located in an environment differing from that of the cement pastes. Analysis of EXAFS data are in progress and corroborate LCA data. This study provides valuable information, which is required for robust predictive geochemical and reactive transport modelling.

Characterization of (As, Sb) in geothermal scalings

One of the activities of the secondary phases group besides studies on radionuclide retention in the context of nuclear waste disposal, is the investigation of secondary phases formed in the thermal water circuit of geothermal power plants, so called scalings. Since the application of phosphonic acid based inhibitors, efficiently preventing formation of Ra-containing $(Ba,Sr)SO_4$ scalings, scalings in geothermal plants in the Upper Rhine Graben are dominated by a mixture of PbS, As, and Sb. While PbS could be satisfactorily characterized as galena by a combination of XRD and SEM-EDX, the nature of the X-ray amorphous As and Sb containing phase remained an open question [15]. Now, using X-ray absorption spectroscopy, we were able to characterize this material as an inhomogeneous amorphous alloy of elemental As, and Sb, with a local structure corresponding to the rhombohedral metal phases As(0) and Sb(0).

Three scaling samples were investigated. These were dried and stored under inert gas conditions (Ar-glovebox). SEM-EDX showed that they were dominated by the above mentioned mix of PbS, As and Sb. As K-edge EXAFS was measured up to k = 13.5 $Å^{-1}$, and Sb K-edge EXAFS was measured up to k = 16 $Å^{-1}$, at the INE-Beamline and the ACT-station of the CAT-ACT-Beamline, respectively.

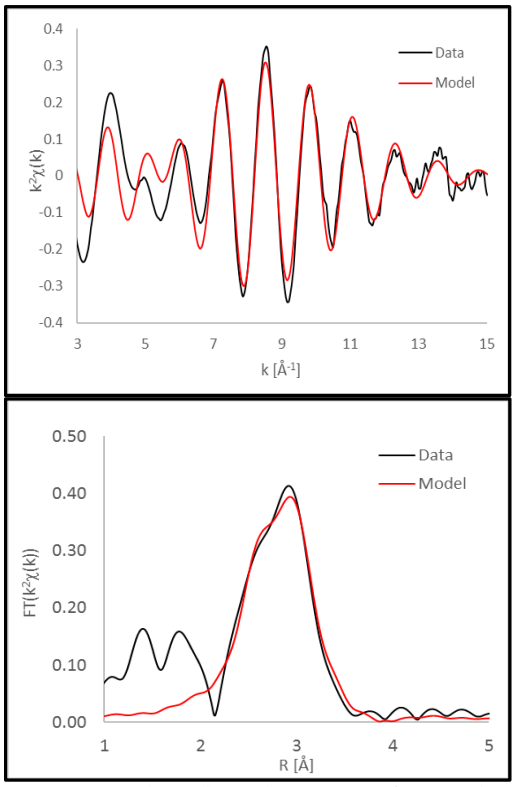

Fig. 4: Exemplary Sb K-edge EXAFS of one scaling sample and corresponding model spectrum (top), and the corresponding Fourier Transform spectrum + model (bottom).

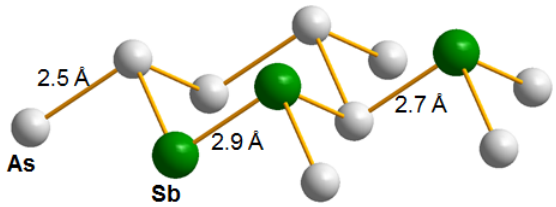

Fig. 5: Ball and Stick representation of the suggested local structure of (As,Sb).

Comparing the absorption edge positions with reference compounds clearly demonstrated that As and Sb in the scaling samples are present in elementary form. Models to the EXAFS data (exemplary Sb-data are shown in Fig. 5) demonstrated that As is coordinated by As (R = 2.45 ± 0.02 Å, N= 1.9± 0.3) and Sb (R = 2.65 ± 0.01 Å, N= 0.7 ± 0.3), similarly to Sb, which is coordinated by As (R = 2.68 ± 0.01 Å, N= 1.4 ± 0.3) and Sb (R = 2.87 ± 0.01 Å, N= 1.4 ± 0.3). It is interesting to note that the bond distance of As-Sb matches perfectly no matter whether derived from Sb- or As-data, and it is quite exactly the average of the bond distances As-As and Sb-Sb.

Coordination numbers of these coordination shells sum up to about three, as expected on the basis of the As(0) and Sb(0) structures. Concerning the As/Sb ratio, SEM-EDX results show varying ratios with an average close to 2:1. Coordination numbers determined by EXAFS, thus suggest a tendency towards demixing of the alloy with a preference of As to be coordinated by As (As/Sb ~2.7:1), and a preference of Sb to be coordinated by Sb (As/Sb ~1:1). Bond distances and coordination numbers suggest that the local structure around As and Sb corresponds to the rhombohedral metal phases. Absence of further coordination shells in the EXAFS signal demonstrates only local ordering and may thus explain the amorphous appearance of the material in XRD. A ball and stick representation of the local (As,Sb) structure is depicted in Fig. 5. These findings lead us to the conclusion that (As, Sb) in the investigated geothermal scalings is an inhomogeneous amorphous alloy of elemental As and Sb.

Acknowledgements. We thank E. Wieland (PSI, Switzerland) for providing the Fe-ettringite spectrum. We thank B. Lothenbach (EMPA, Switzerland) for providing the reference materials C2F and C4AF, S. Gaboreau (BRGM, France) for providing the C-S-H phases and T. Vehmas (VTT, Finland) for providing the CEB paste and CEB concrete samples. The ESRF and ALBA are acknowledged for provision of synchrotron radiation beam time, as well as the INE-Beamline and the ACT-station of the CAT-ACT-Beamline at the Karlsruhe Synchrotron Light Source.

References

[1] Y. El Mendili, et al., *Corros. Sci.*, **88**, 56-65 (2014).
[2] M. Schlegel et al., *Corros. Sci.*, **136**, 70-90 (2018).
[3] B. Kienzler, A. Loida, *Endlagerrelevante Eigenschaften von hochradioaktiven Abfallprodukten. Charakterisierung und Bewertung. Empfehlung des Arbeitskreises HAW Produkte*. Wissenschaftliche Berichte FZKA 6651, Forschungszentrum Karlsruhe (2001).
[4] E. Smailos, and B. Fiehn, *In-situ Corrosion Testing of Selected HlW Container Materials under the Conditions of the HLW Test Disposal in the Asse Salt Mine.* Wissenschaftliche Berichte FZKA 5508. Forschungszentrum Karlsruhe (1995).
[5] X. Hou et al. *Anal. Chim. Acta* **632**, 181-196 (2009).
[6] E. C .Gaucher et al. *C. R. Geoscience* **338**, 917-930 (2006).
[7] J. D. Bernal et al. *Clay Miner. Bull.*, **4**, 15-30 (1959).
[8] R. D. Shannon, *Acta Cryst.*, **A32**, 751-767 (1976).
[9] J. Vins et al., *Collection Czechoslovak Chem.Commun.* **52**, 93-102 (1987)
[10] W. Hummel et al., *C. R. Chimie*, **10**, 948-958 (2007).
[11] C. Cau dit Coumes et al., *Cem. Concr. Res.*, **36**, 2152-2163 (2006).
[12] N. Ait Mouheb et al. In. Altmaier et al. Proceedings of the 1st annual workshop of CEBAMA Project, KIT Scientific Report 7734, Karlsruhe, Germany (2017).
[13] B. Z. Dilnesa et al., *Cem. Concr. Res.*, **58**, 45-55 (2014).
[14] G. Möschner et al., *Geochim. Cosmochim. Acta*, **72**, 1-18 (2008).
[15] R. Haas-Nüesch et al., *Geotherm.*, **71**, 264-273 (2018).

5 Applied studies: radionuclide retention in the multi-barrier system

Long-term safety of a deep geological repository for nuclear waste depends on a multi-barrier system which consists of technical and geo-technical barriers such as the waste form, the canister, backfilling and sealing of the mined openings as well as on the natural barrier function of the host rock. A series of applied studies on subsystems of various multi-barrier systems are performed, which cover a variety of components with specific characteristics and properties. Investigations presented in the first sub-chapter cover the experimental quantification of radionuclide release from spent nuclear fuel under strongly reducing conditions. In the following, experimental studies on diffusion of Np(V) in compacted illite under aerobic conditions are described. The third subchapter deals with the occurrence and stability of colloids, and their impact on radionuclide migration.

5.1 Higly radioactive waste forms

E. Bohnert, M. Böttle, E. González-Robles[1], M. Herm, L. Iglesias Pérez, T. König, V. Metz, N. Müller, A. Walschburger

[1]present address: Palma, Illes Balears, Spain

Radionuclide Release from Spent Nuclear Fuel Samples in High pH Solution under Anoxic / Reducing Atmosphere

Introduction

Assessing the performance of spent nuclear fuel (SNF) in a geological disposal system requires the understanding and quantification of the radionuclide release into the aqueous as well as gaseous phase. The release of the radionuclides into water will be constituted by two main processes:

i. Short-term release of the so-called instant release fraction (IRF).
ii. Long-term release dominated by the dissolution of the UO_2 grains, which is referred to as matrix contribution.

In Belgium, for SNF and vitrified high active waste disposal, a specific engineered barrier system, the so-called "Supercontainer" concept, was developed. With respect to SNF disposal, the "Supercontainer" comprises fuel assembly canisters in carbon steel over packs, which are surrounded by an over pack of a Portland cement, concrete buffer, and an outer stainless steel envelope [1-3].

After re-saturation of the engineered barriers, the pore water composition will be altered by interactions with concrete. The altered pore water can be simulated by a "young cement water with calcium (YCWCa)" solution (pH ~13.5) that represents a certain degree of concrete alteration. The YCWCa is composed mainly by KOH and NaOH, and in a minor concentration by Na_2SO_4, $Ca(OH)_2$, and $CaCO_3$.

Due to the slow corrosion rate of the canister material under highly alkaline conditions [4], the SNF could come in contact with the evolved highly alkaline solution. In parallel, a certain H_2 partial pressure will built-up due to steel corrosion processes. Consequently, the aim of the experimental work is to study the corrosion behaviour of the UO_2 matrix of SNF in YCWCa in presence of H_2 overpressure.

The aim of this work is to study the corrosion behaviour of the UO_2 matrix and the fast/instant release fraction of spent nuclear fuel (SNF) in high alkaline pH solutions under anoxic/reducing atmosphere.

Overall, three leaching experiments are performed with the following specifications:

- 40 bar of a H_2/Ar gas mixture with a H_2 partial pressure of 3.2 bar.
- 3.75 bar of a H_2/Ar gas mixture with a H_2 partial pressure of 0.3 bar.
- 1 bar Ar atmosphere (in absence of H_2).

In this communication, the results obtained from four out of seven planned samplings regarding the release of radionuclides into the gaseous and aqueous phase are shown.

Spent nuclear fuel samples

The studied SNF specimens were sampled from fuel rod segment N0204 of fuel rod SBS1108. The fuel rod was irradiated during four cycles in the pressurize water reactor Gösgen (KKG, Switzerland) and discharged in May 1989 after 1226 effective full power days. During reactor operation, an average burn-up of 50.4 GWd/t_{HM} as well as average linear power of 260 W/cm was achieved.

The fuel rod segment was stored gas-tight until 2012 which implies a cooling time of almost 24 years before characterisation and cutting of the segment.

Characteristic data of the studied SBS1108-N0204 fuel rod segment are given in [3,4]. Based on results of a puncturing test of the fuel rod segment, the fission gas release into the plenum of the segment was previously calculated to be 8.35% [4,5].

Sample preparation

A total of three SNF samples with Zircaloy cladding were cut from the fuel rod segment. The fuel rod segment was placed in a hot cell under N_2 atmosphere (with an O_2 content <1%) and cut by means of a diamond wafering blade (Buehler Isomet® series 15HC)

installed on a cutting machine. Considering that the cutting process was performed in the absence of cooling liquid, it was performed slowly to limit any heating as a result of friction between the blade and the pellets.

The cutting was performed from mid to mid pellet positions in order to obtain 20 mm length samples, which includes a complete pellet plus two half pellets (thereby including two inter-pellet gaps).

The samples were stored in a tightly closed steel container flushed continuously with Ar, to avoid any potential oxidation of the surfaces, prior to the start of the leaching experiments.

Before the start of the leaching experiments, the samples were characterized by means of an optical microscope and the samples masses as well as dimensions were determined (see table 1).

Tab. 1: Masses and dimensions of the SNF specimens used in the experiments.

Sample	1	2	3
weight (g)	18.6	18.1	18.6
lenght (mm)	23.4	22.6	23.3
diameter (mm)	10.7	10.8	10.8

Autoclaves

The leaching / corrosion experiments were carried out in Ti-lined autoclaves (Berghof) with a volume of 250 mL. The autoclaves were equipped with two valves in the Ti-lid to allow sampling of gaseous and aqueous aliquots.

The autoclaves were modified to enable remote handling by manipulators in the shielded box-line of KIT-INE. Before using the autoclaves in the experiments, they were cleaned to remove potentially wall-adhering impurities of the fabrication process. In an ultrasonic bath the autoclaves were subsequently immersed in:

- RBS-solution (Roth chemicals), which is a cleaning solution for non-corrosive materials, containing mainly NaOH, hypochloride and tensides,
- 1 M HNO_3,
- Milli-Q-water.

After the cleaning process the autoclaves were submitted to a leak tightness test to ensure a constant pressure during the leaching / corrosion experiments. In each tightness test an overpressure of 40 bar Ar was applied during five days. At the end of the test no evidence of pressure loss were observed in any of the autoclave.

Leaching experiments

Three leaching experiments were performed under anoxic/reducing conditions. As leachant, a solution of YCWCa was prepared in a glove-box under argon atmosphere, using ultrapure water (Merck Millipore) and analysis grade chemicals (Merck), following the instructions given in [5]. The only modification with respect to the original preparation instruction was the decrease of Ca concentration in solution from (7.0×10^{-4}) M to (4.8×10^{-4}) M in order to avoid a possible precipitation of secondary phase due to the high concentration of Ca. A summary of the composition of the YCWCa is given in table 2.

Tab. 2: Theoretical and experimental composition of the YCWCa.

YCWCa	[Na] (M)	[K] (M)	[Ca] (M)	[Al] (M)	[Si] (M)
theoretical	1.4×10^{-1}	3.7×10^{-1}	4.8×10^{-4}	6.1×10^{-4}	3×10^{-4}
experimental	1.4×10^{-1}	3.4×10^{-1}	3.8×10^{-4}	b.d.l*	b.d.l*

*b.d.l: below detecton limit.

The samples were mounted in a titanium sample holder to ensure the contact of both pellet surfaces with the solution.Once the SNF samples were placed inside the autoclaves, these were closed and purged with Ar, to avoid air intrusion, and filled with (220 ± 5) mL of the YCWCa solution. Finally, the total pressure was adjusted by an Ar/H_2 gas mixture (with volume fractions of 92% Ar and 8% H_2; provided by Basi and Schöberl GmbH) or pure Ar in order to create anoxic/reducing conditions:

- To (40 ± 1) bar with a H_2 partial pressure of (3.2 ± 0.1) bar.
- To (3.7 ± 0.1) bar with a H_2 partial pressure of (0.4 ± 0.1) bar.
- In the case of the experiment with Ar the autoclave was purged with Ar and the pressure was set to (1 ± 0.1) bar.

After one day of exposure, the first gaseous and liquid samples were taken and analysed (washing step). The solution was completely renewed, in order to reduce the amount of ^{135}Cs and ^{137}Cs in solution. Replenishment was done using (220 ± 5) mL of fresh YCWCa solution and the Ar/H_2 or pure Ar gas atmosphere was re-established, following the procedure previously described.

During the leaching experiments, a series of gaseous (50.0 ± 2.5) mL and liquid (15 ± 1) mL samples were taken from each autoclave. After each sampling, the gas volume of the autoclaves was purged with Ar, and the initial conditions were again established. Except the first sampling (washing step), the solution was not replenished after the samplings.

Gas sampling from leaching experiments

Each autoclave of the leaching experiments was connected by stainless steel tubing to a pump with an Ar supply within the shielded box-line. The steel tubing continued to the same type of stainless steel sampling cylinder as used for the puncturing test. The sampling cylinder was placed outside the shielded box.

At first the tubing was evacuated and subsequently purged with Ar five times. During the last evacuation step, the overpressure in the autoclave was reduced to approximately 1 bar in a controlled way. Once the overpressure was reduced, the gas sampling was started by opening the valve of the autoclave and, at the same time, the valve of the sampling cylinder. The gas sample was released from the autoclave to the sampling cylinder within two minutes.

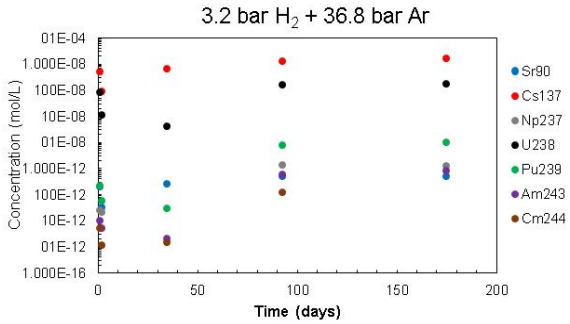

Fig. 1: Concentrations as a function of leaching time for the experiment performed in 3.2 bar H_2 and 36.8 bar Ar atmosphere.

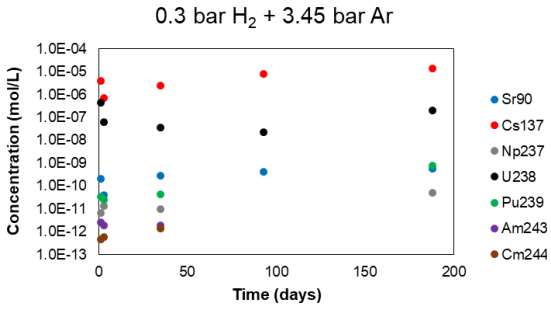

Fig. 2: Concentrations as a function of leaching time for the experiment performed in 0.3 bar H_2 and 3.45 bar Ar atmosphere.

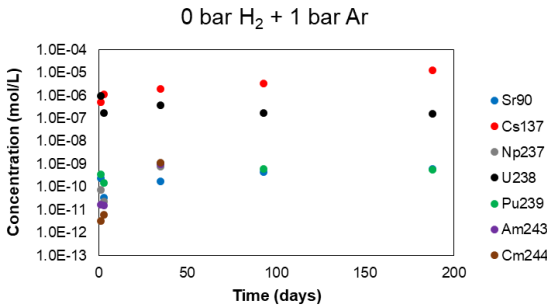

Fig. 3: Concentrations as a function of leaching time for the experiment performed in pure 1 bar Ar atmosphere.

In the case of the experiments carried out with 1bar of Ar, a reduction of the pressure was not needed, therefore the sampling started immediately after purging and evacuating of the connections five times.

Gas mass-spectrometry

Gas samples collected during the puncturing test and the leaching experiments were analysed by a multipurpose mass spectrometer with customized gas inlet system (GAM 400, InProcess Instruments). The system was equipped with a quadrupole mass analyzer and Faraday as well as secondary electron multiplier (SEM) detector.

The batch-type gas inlet system was optimized for low gas sample consumption. The total gas pressure was controlled at four successive positions within the gas dosage and inlet system. Three different expansion-volumes to charge relatively low gas contents in the desired pressure range were applied. Ten scans of each gas sample were measured, using the SEM-detector, and the mean value was taken. Calibration of the gas mass spectrometer was performed in the same pressure range as the respective range for analyses of the sample aliquots. For calibration, standard gases containing He, N_2, O_2, Ne, Ar, Kr, Xe, and CO_2, with compositions similar to those of the samples, were used.

The isotopic composition of the Ar/H_2 mixture used in the leaching experiments was determined and taken into account as background. The contribution of naturally occurring Kr and Xe isotopes in this so-called "blank gas" was subtracted from the isotopic compositions of the samples. The detection limit of Kr and Xe is 8 and 2 ppm, respectively.

Results and Discussion

The concentrations of ^{90}Sr, ^{137}Cs, ^{237}Np, ^{238}U, ^{239}Pu, ^{243}Am, and ^{244}Cm released into the aqueous phase are shown in figures 1-3 for non-filtered samples.

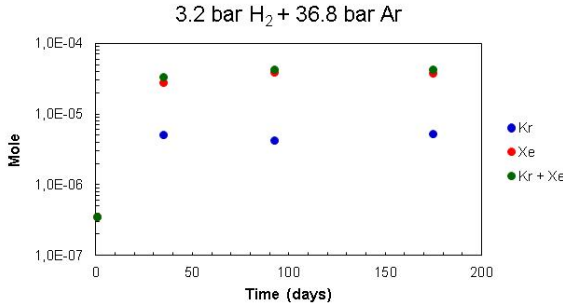

Fig. 4: Measured moles of Kr, Xe and (Kr + Xe) at each sampling for the experiment performed in 3.2 bar H_2 and 36.8 bar Ar atmosphere.

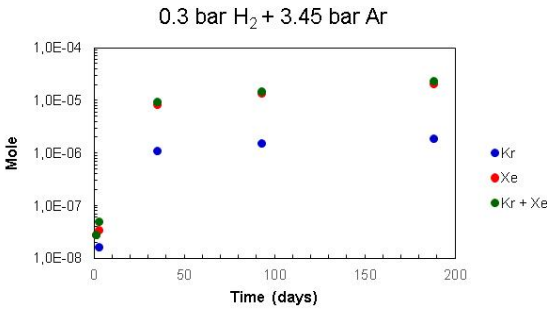

Fig. 5: Measured moles of Kr, Xe and (Kr + Xe) at each sampling for the experiment performed in 0.3 bar H_2 and 3.45 bar Ar atmosphere.

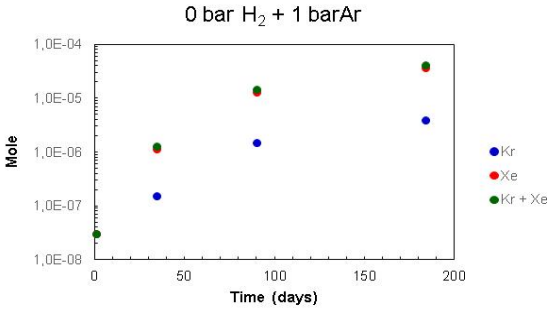

Fig. 6: Measured moles of Kr, Xe and (Kr + Xe) at each sampling for the experiment performed in in pure 1 bar Ar atmosphere.

Within the scatter of the data the release of actinides and ^{90}Sr approaches a steady state. In the case of ^{137}Cs a continuous release is observed.

Regarding the influence of hydrogen pressure on the SNF matrix dissolution, no clear trend can be seen. Within the scatter of the data the concentrations for actinides and fission products released into aqueous solution are very similar in all three experiments.

The moles of Kr and Xe released into the gas phase during each leaching experiment were measured by gas mass spectrometry and are shown in figures 4-6.

As previously explained, the measured moles amount of Kr and Xe were corrected for naturally occurring Kr and Xe isotopes in the Ar or Ar/H_2 "blank gas".

The amount of Kr released during the washing step was under the detection limit in the three experiments. In the first sample after the washing step solely Xe was detected in the experiment performed in 0.3 bar H_2 and 3.45 bar Ar atmosphere. In the case of the other two experiments, 3.2 bar H_2 and 36.8 bar Ar atmosphere and pure 1 bar Ar atmosphere, the amount of moles released of both Kr and Xe were below the detection limit.

The experiments performed in 3.2 bar H_2 and 36.8 bar Ar atmosphere and in 0.3 bar H_2 and 3.45 bar Ar atmosphere show a constant mole release after 200 days of leaching. On the other hand the experiment performed in pure 1 bar Ar atmosphere shows still an increase in the moles of fission gases released after 200 days of leaching.

References

[1] J. Bel et al., *Proceedings - 10th International Conference on Environmental Remediation and Radioactive Waste Management ICEM'05*, Glasgow (UK), 1690-1696, (2005).

[2] R. Gens et al., *Proceedings NUCPERF 2006, Cadarache, France, 27–30 March, 2006, Journal de Physique IV*, **136**, 13–23, (2006).

[3] D. G. Bennett and R. Gens, *J. Nucl. Mater*, **379**, 1-8, (2008).

[4] B. Kursten, et al., *Proceedings of 6th European commission conference on the Management and Disposal of Radioactive Waste, Luxembourg,* (2004).

[5] C. Cachoir, et al., *SCK•CEN Work Instruction IW.W&D.0009*, (2007).

[6] Fanghänel, Th. et al., *J. Sol. Chem.*, **28**: 447 (1999)

[7] Vercouter, Th. et al., *Inorg. Chem.*, **44**: 5833 (2005)

[8] Janicki, R. et al., *Eur. J. Inorg. Chem.*, 3601 (2011)

[9] Fanghänel, Th. et al., *Radiochim. Acta.*, **82**: 47 (1998)

[10] W. Hummel, et.al., *Comptes Rendus Chimie*, **10**, 948-958, (2007).

5.2 Diffusion

A. Beck, E. Bohnert, D. Fellhauer, K. Hardock, C. Joseph, V. Krepper, C. Marquardt, F. Rieder, J. Rothe, B. Schacherl, T. Vitova

In co-operation with:

T. Kupcik[a]

[a] Hessian Ministry of the Environment, Climate Protection, Agriculture and Consumer Protection, Wiesbaden, Germany

Introduction

In the context of the safe disposal of nuclear waste in deep geological formations, the scenario of the migration of waste-released radionuclides through the installed multiple barrier system is an important research topic for safety assessment. Potential geotechnical or geological barriers, which should hinder or retard the migrating radionuclides, can consist of compacted porous materials used as buffers (such as bentonite for repositories in crystalline and argillaceous rocks), sedimentary rocks, or manufactured concretes based on Portland cement, Sorel cement or similar materials. In the absence of fractures and cracks, molecular diffusion is the main transport process for contaminants in such matters.

In the laboratories of INE, radionuclide diffusion experiments with compacted clay minerals and natural clay rocks are conducted. One of the main objectives is the determination of diffusion parameters of repository-relevant radionuclides under a wide range of conditions. This applied research delivers transport parameters which contribute to safety and performance assessment models of nuclear waste repositories. Additionally, fundamental processes underlying the interaction of ions with the porous material during diffusion are investigated such as the accessibility of interlayer space for the migrating species.

Since July 2018, the Helmholtz Association is full partner of the Opalinus Clay underground rock laboratory in Mont Terri, Switzerland. In connection with the *iCROSS* joint project, INE collaborates with international partners at Mont Terri and participates in ongoing diffusion experiments.

Np(V) diffusion through compacted illite

Illite is a clay mineral which can be found in many natural clay rocks investigated as potential host rock for nuclear waste repositories, for instance, in Jurrasic Opalinus Clay from Switzerland (15–40 % [1]) or in Jurrassic Callovo-Oxfordian Clay from Eastern France (5–23 % [2]). As part of the geological barrier, it is therefore essential to know the retention capability of illite in particular regarding to radionuclides with long half-lives such as ^{237}Np ($T_{1/2} = 2.144 \cdot 10^6$ a). Under reducing conditions as to be expected in a nuclear waste repository, Np(IV), which forms mainly less soluble and, as a consequence, less mobile species, will be the dominant oxidation state. Since radiolytic enhanced oxidation and dissolution of spent nuclear fuel has to be taken into account in safety assessments, formation of oxidized radionuclide species like Np(V) is considered for certain release scenarios. Therefore, it is reasonable to study the interaction behaviour of more soluble and more mobile Np(V) species with illite.

Recently, Np(V) sorption on illite was investigated as a function of pH and initial Np(V) concentration in 0.1 mol·L^{-1} NaCl under anaerobic conditions [3]. The authors observed a partial reduction of Np(V) to Np(IV) on the illite surface and could confirm this finding also by analysis with X-ray absorption near-edge structure (XANES) spectroscopy. It was suggested that the Np(V) reduction to Np(IV) in the presence of a sorbing mineral phase is thermodynamically favoured.

The focus of the present study was to investigate the system Np(V) / illite by the means of diffusion experiments under aerobic conditions. The study was aimed to clarify if and to which extent the migrating Np(V) will be reduced to Np(IV). To characterize the Np oxidation states in the illite diffusion samples, solvent extraction and Np M_5 edge high energy-resolution (HR) XANES spectroscopy were applied. Since here, the initial Np concentration was one order of magnitude smaller than in the previous XANES experiment [3], the question was also if XANES spectroscopy is applicable on samples with an environmentally relevant Np load (≈ 20 ppm).

Illite du Puy (Massif Central in Le Puy-en-Velay, Haute Loire, France) was transformed into a homoionic Na-form according to the procedure described in Glaus et al. [4]. X-ray fluorescence (XRF) results of the purified illite are shown in Tab. 1.

Tab. 1: *Chemical composition of illite used in this study determined by XRF (L.O.I.: loss of ignition) [5].*

Compound	wt.%	Compound	wt.%
Na_2O	0.59	CaO	0.41
MgO	3.52	TiO_2	0.73
Al_2O_3	20.80	MnO	0.05
SiO_2	50.80	Fe_2O_3	6.94
P_2O_5	0.29	*L.O.I.*	*7.54*
K_2O	7.82		

With this clay mineral, two Np through-diffusion experiments (Np-1 and Np-2) were started in June 2015 according to the procedure described in Van Loon et al. [6]. The illite was compacted in polyether ether ketone diffusion cells to a dry density, ρ_d, of about 1.6 g·cm^{-3}, a thickness of about 1 cm, and a diameter of about 2.54 cm. Each cell was connected to a high concentration reservoir (HCR) and a low concentration reservoir (LCR) containing 0.1 mol·L^{-1} NaCl at pH 4.7±0.2 and

E_H = 360±20 mV, respectively, which was pumped through the respective end plates of each diffusion cell. To each HCR, $[^{237}Np(V)]_0$ = $1.5 \cdot 10^{-5}$ mol·L^{-1} was added. Each LCR was initially tracer-free.

At distinct time steps, the HCR solution was sampled and the LCR was exchanged and the Np activity and diffusive flux, J [mol·m^{-2}·s^{-1}], were determined. The evolution of the Np concentration in each HCR and the diffusive flux measured in each LCR for the first 230 days of the experiment are shown in Fig. 1.

Based on the experimental conditions and Fick's laws, a 1-dimensional single porosity model was set up

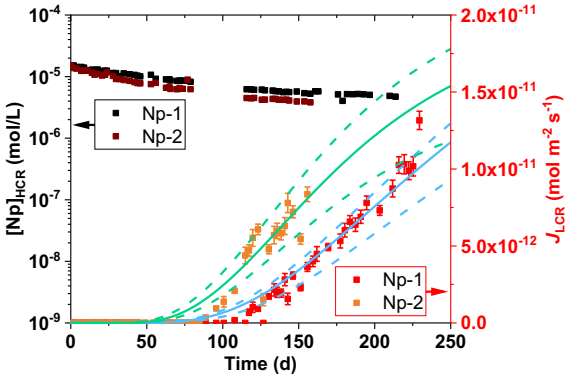

Fig. 1: *Evolution of the Np concentration in HCR and diffusive fluxes for Np in LCR for samples Np-1 and Np-2 (straight lines: COMSOL fit; broken lines: uncertainty).*

using COMSOL Multiphysics® [7]. Fick's first law describes the diffusion process in porous media as follows:

$$J = -D_e \cdot \frac{\partial c}{\partial x} \quad (1)$$

where D_e [m^2·s^{-1}] is the effective diffusion coefficient, c [mol·m^{-3}] is the tracer concentration in the mobile phase, and x [m] is the spatial coordinate. Diffusion is influenced by sorption of the diffusing species on the porous material expressed here as sorption distribution coefficient, K_d [m^3·kg^{-1}]. This diffusion retarding effect is considered in the rock capacity factor α [–].

$$\alpha = \varepsilon_{acc} + \rho_d \cdot K_d \quad (2)$$

The inclusion of α in Fick's law leads to the apparent diffusion coefficient D_a [m^2·s^{-1}]:

$$D_a = \frac{D_e}{\alpha} \quad (3)$$

Fick's second law, where the change of concentration with time, t [s], is considered, is then expressed by:

$$\frac{\partial c}{\partial t} = D_a \cdot \frac{\partial^2 c}{\partial x^2} \quad (4)$$

Fits of the experimental diffusion data with this model are shown in Fig. 1. The corresponding diffusion and sorption parameter values are given in Tab. 2.

Obviously, the Np diffusion in these two cells, although set up in the same way, behaved differently. It seems, that Np is stronger retarded by sorption in cell Np-1 than in cell Np-2. Consequently, a later breakthrough of Np is observed in the LCR of cell Np-1.

Tab. 2: *Best-fit parameter values for Np diffusion in illite (pH 5, I = 0.1 mol·L^{-1} NaCl, ρ_d = 1.6 g·cm^{-3}).*

Sample	D_e [10^{-10} m^2·s^{-1}]	K_d [m^3·kg^{-1}]	D_a [10^{-13} m^2·s^{-1}]
Np-1	1.20±0.35	0.10±0.02	7.3±2.6
Np-2	1.0±0.2	0.060±0.005	10±2

The K_d values obtained with the diffusion experiments are up to one order of magnitude larger than the K_d values obtained by batch sorption experiments with illite at pH 5 under aerobic conditions (0.011±0.008 m^3·kg^{-1} [8]). Notably, the value of Np-2 equals the K_d value for the Np batch sorption on illite under anaerobic conditions (0.057±0.007 m^3·kg^{-1} [8]). This indicates an influence of oxygen-free conditions on the Np-sorption. Wu et al. [9] investigated the Np(V) diffusion in Opalinus Clay at pH 7.6 and found also a one order of magnitude larger K_d in diffusion experiments than in batch sorption experiments. This was attributed to a partial reduction of Np(V) to Np(IV) inside the diffusion cell and consequently, to a stronger retardation of Np in the clay. Their D_e and D_a values amounted to $(6.9\pm1.1)\cdot10^{-12}$ m^2·s^{-1} and $(2.8\pm0.4)\cdot10^{-14}$ m^2·s^{-1}, respectively. Staunton et al. [10] studied the Np(V) diffusion in Fithian illite in 0.01 mol·L^{-1} $NaClO_4$ at pH 6 and found a K_d value of 0.064±0.015 m^3·kg^{-1}, which is in agreement with the Np-2 K_d value of this study. They determined a D_a value of $(3.3\pm0.5)\cdot10^{-11}$ m^2·s^{-1} in their system. The dry densities of the solids investigated in both literature studies are much higher (Opalinus Clay, ρ_d = 2.4 g·cm^{-3}) or much lower (Fithian illite, ρ_d = 0.41 g·cm^{-3}) than in this study providing less or more pore space for the diffusing Np species. This, in addition with the different present chemical conditions (pH, salinity), which affect the type of migrating Np species, determines the diffusion behavior. Therefore, the literature data cannot be directly compared to diffusion parameter values obtained in this study.

After about 230 days, the LCR in both diffusion experiments were no longer replaced in regular time steps. The relatively long duration of the experiment and the large exchange intervals led to the formation of biofilms in the reservoirs. The biofilms caused heavy clocking of the tubing. In the case of Np-1, this led to a stop of solution circulation through the end plates of the diffusion cell. In May 2018, after about 1050 days, both diffusion experiments were stopped and the diffusion cells were dissembled. A significant amount of organic matter was found on the HCR side of cell Np-1 (Fig. 2a). The amount of organic matter in the cell of Np-2 was much lower (Fig. 2b). In a recent study, it was shown that biofilms can interact strongly with radionuclides [11]. This could be a reason for the stronger retardation of Np diffusion in cell Np-1 compared to Np-2. Organic matter can also cause changes in the pH and redox conditions. In the HCR solution of diffusion cell Np-1, the pH increased to 6.5, which not only leads to better growth conditions for most of the

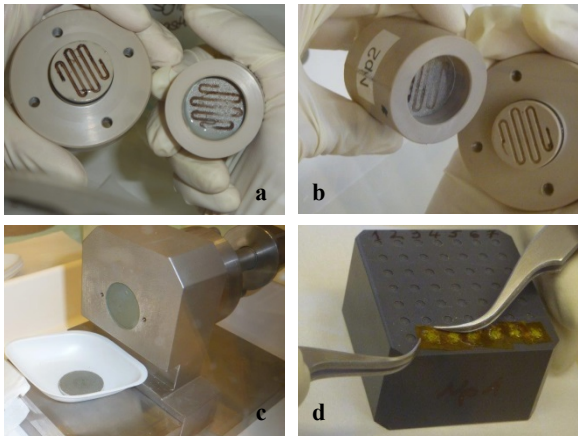

Fig. 2: *a) End plate HCR of Np-1, b) end plate HCR of Np-2, c) segmentation, and d) sample preparation for XANES.*

microorganisms but also may enhance the extent of Np sorption on illite (pH 7, anaerobic conditions, K_d = 0.44±0.14 $m^3 \cdot kg^{-1}$ [8]). In contrast, for cell Np-2, the final pH was 5.0. The final E_H amounted to 434±50 mV for Np-1 and 502±50 mV for Np-2, respectively.

The diffusion cylinders containing the illite samples were introduced into an argon glove-box and segmented in 100-µm-steps into numerous segments (Fig. 2c). Since cell Np-2 was less biased by organic matter, one of its segments (segment 4 ≈ 400 µm diffusion depth) was chosen for Np oxidation state determination by solvent extraction [12]. On this segment about 18±4 ppm Np were sorbed. About 66±6 % of Np could be removed during solvent extraction. About 34±6 % of Np remained on illite. From the desorbed fraction, about 24±3 % were found in the organic phase and attributed to Np(IV). The majority of Np was found in the aquatic phase and attributed to Np(V). This means, the conditions close to the illite sample HCR edge enable Np(IV) formation. This is in agreement with the findings of Wu et al. [9] for Opalinus Clay.

The oxidation state of Np on illite segments was also analysed by Np M_5 edge HR-XANES spectroscopy. For this, fractions of about 2 mg of selected illite segments were filled in the respective indentations of a special sample holder (Fig. 2d) and covered with Kapton foil and Kapton tape. To prevent re-oxidation of potential Np(IV) and to minimize the intensity loss of X-ray radiation by argon, the sample holder was kept under nitrogen atmosphere in a second containment. The measurement was performed under helium atmosphere. As qualitative Np(V) and Np(IV) references, Np solutions prepared by potentiostatic electrolysis were used ([Np] = 0.02 $mol \cdot L^{-1}$ in 1.5 $mol \cdot L^{-1}$ HCl).

The obtained HR-XANES spectra for segments 10 (≈ 1 mm diffusion depth) and 54 (≈ 5.4 mm) of cell Np-2 as well as for the references are shown in Fig. 3. The spectra of the two segments imply a shoulder which is characteristic for Np(V). This shoulder is not very pronounced (smaller in the spectrum of segment 54 than in the spectrum of segment 10) indicating a mixture of Np(IV) and Np(V) present in the samples. Due to the low concentration of Np on the illite and the resulting noise in the spectra, a quantitative determination of Np(V) and Np(IV) is not possible for these samples. However, these results are consistent with the results observed by solvent extraction and by Wu et al. [9].

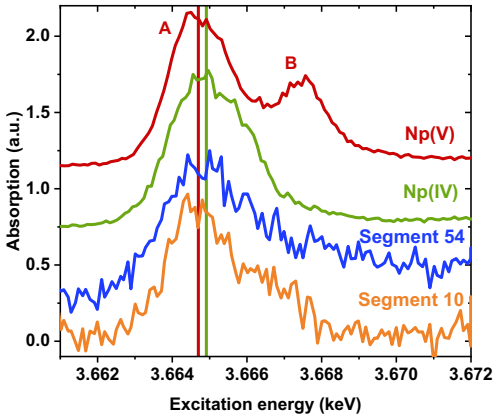

Fig. 3: *Normalized and vertically shifted HR-XANES spectra of two diffusion illite segments of cell Np-2 in comparison with liquid reference spectra of Np(V) and Np(IV).*

References

[1] F.J. Pearson et al. (2003) *Reports of the Federal Office for Water and Geology, Geology Series No. 5,* Federal Office for Water and Geology, Bern.

[2] F. Claret et al., *Clays Clay Miner.*, **50**, 5, 633-646, (2002).

[3] R. Marsac et al., *Geochim. Cosmochim. Acta*, **152**, 39-51, (2015).

[4] M.A. Glaus et al., *Geochim. Cosmochim. Acta*, **165**, 376-388, (2015).

[5] V. Montoya et al., *Geochim. Cosmochim. Acta*, **223**, 1-20, (2018).

[6] L.R. Van Loon et al., *J. Contam. Hydrol.*, **61**, 1-4, 73-83, (2003).

[7] *COMSOL Multiphysics®*, **5.2a**, COMSOL AB, Stockholm, (2016).

[8] B. Schacherl (2018) Master Thesis, Karlsruhe Institute of Technology, Karlsruhe.

[9] T. Wu et al., *Environ. Sci. Technol.*, **43**, 17, 6567-6571, (2009).

[10] S. Staunton et al., *Radiochim. Acta*, **49**, 3, 147-153, (1990).

[11] E. Krawczyk-Bärsch et al., *Geochim. Cosmochim. Acta*, **96**, 94-104, (2012).

[12] P.A. Bertrand and G.R. Choppin, *Radiochim. Acta*, **31**, 3-4, 135-137, (1982).

5.3 Colloid impact on radionuclide migration

M. Bouby, F. Geyer, S. Kraft, S. Kuschel, F. Quinto, F. Rinderknecht[1], Th. Schäfer, A. Schnurr, M. Stoll[2]

[1]present address: Karlsruher Institut für Technologie, Fortbildungszentrum für Technik und Umwelt (KIT-FTU); [2]present address: Berthold Technologies, Bad Wildbad, Germany

In co-operation with:

I. Blechschmidt[a], J. Eikenberg[b], A. Martin[a]

[a] NAGRA Natl. Cooperat. Disposal Radioact. Waste, Wettingen, Switzerland, [b] Paul Scherrer Institut (PSI-LES), Villigen, Switzerland

Introduction

The influence of colloidal/nano-scale phases on the solubility and migration behavior of radionuclides is one of the uncertainties of the repository safety assessment [1, 2]. In our work, we aim to 1) identify the presence and the formation of relevant colloids in repository specific areas, 2) determine their stability as a function of geochemical parameters, 3) elucidate the thermodynamics and kinetics of the colloid interaction with radionuclides, 4) perform laboratory and field experiments to quantify the colloid mobility and their interaction with surfaces. The final goal is to state on the relevance of the nanoparticles (NPs) / colloids for the radionuclides migration in natural geochemical conditions. Laboratory and in-situ migration experiments are required which need the use and development of highly sensitive and sophisticated analytical techniques [3, 4].

Our present activities are conducted with the support and in close collaboration with international nuclear waste management agencies (ONDRAF / NIRAS, Belgium; NAGRA, Switzerland) and in the framework of projects like the BMWi project KOLLRADO-e2. The collaboration with the ONDRAF/NIRAS agency is related to the characterization of natural organic matter derived from different layers within the Belgian Boom Clay formation and their radionuclide interaction.

Experiments performed in the framework of the KOLLORADO-e2 (duration 2017-2019) are closely related to the international CFM (Colloid Formation and Migration) project performed in the Grimsel Test Site. Research on the stability of the geotechnical barrier under glacial melt water conditions and the potential release of bentonite colloids constitutes the scientific goal of the CFM project. In 2009, a tunnel mega-packer system was constructed (Fig.1), minimizing the gradient and groundwater flow in the MI shear zone intersecting the tunnel and enables the work under near natural hydraulic conditions similar to the post-closure situation of a deep geological repository. Migration processes are investigated in the laboratory by looking at the deposition of colloids onto mineral surfaces or in-situ at the Grimsel Test Site. Here the release of colloidal material and radionuclides from a compacted bentonite source is investigated over a long time period in the so-called Long-term In-situ Test (LIT).

Fig. 1: The mega-packer system of the CFM experiment at the Grimsel Test Site. The shear zone is sealed with resin layer and surface packers are installed at outflow points on shear zone intersection. Pressurised water in annulus provides mechanical support to resin layer to counteract hydraulic head in the shear zone.

Colloid mobility controlling processes in single fractures

Rock fractures presenting large apertures enabling high flow velocities can serve as water conducting structures for fluid flow and mass transport within the Earth's crust. As the rock matrix presents a permeability several orders of magnitude lower, those structures serve as preferential conduits for solutes and colloids. The mechanistic understanding of fundamental transport and retention processes is essential to make reliable predictions of the fate of solutes and colloids in the subsurface. This comprehensive topic is of paramount importance in many areas of geo-engineering, for example enhanced geothermal systems, CO_2 sequestration, gas and oil industry, contaminant transport in groundwater systems and especially disposal of nuclear waste in deep geological formations.

In this context, the impact of the flow channel geometry on solute and colloid transport through natural rough fractures was examined. A bottom-up approach was followed. The mechanisms and the processes on mass transport (solute and colloids) were investigated separately in four detailed steps. All experiments were conducted under hydraulic and chemical settings establishing laminar flow and overall unfavorable colloid attachment conditions [5].

In the first step (Fig.2), the interaction of monodisperse fluorescent carboxylated polystyrene colloids (25 nm and 1000 nm diameter) with a plain cut granodiorite surface (Grimsel granodiorite, Aar Massif, Switzerland) or with acrylic glass was investigated experimentally and numerically. Colloid transport experiments in

a synthetic parallel-plate fracture flow cell (simulating a simplified fracture) revealed a dependence of colloid retention on surface roughness, fracture orientation, residence time in the fracture and colloid size. It was shown that the colloid mobility of 25 nm colloids, which is purely diffusion driven, is affected by surface roughness and surface inhomogeneities, while fracture orientation does not affect the colloid retention behavior under the experimental conditions chosen. However, despite the low density, 1000 nm colloids show a gravity dependent residence time behavior, which results in significant sedimentation effects in horizontal orientated fractures, due to the shorter sedimentation length to the bottom fracture wall. Fracture surface roughness, however, does not affect the colloid mobility. Those observations were verified by additional atomic force microscopy measurements using the so-called colloid probe technique, and by 2-D numerical simulations [6].

Moreover, using fluorescent microscopy and surface roughness measurements of different regions of interest on the granodiorite surface, it was shown that the 1000 nm colloids deposited homogeneously on the fracture surface and are therefore independent of mineralogy and surface roughness [7].

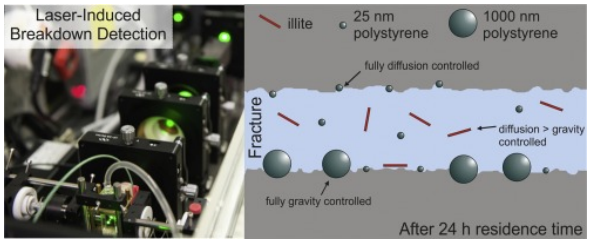

Fig. 2: Parallel-plate fracture transport experiments of nanoparticulate illite in the ultra-trace concentration range investigated by Laser-Induced Breakdown Detection (LIBD) (reprinted from [8]).

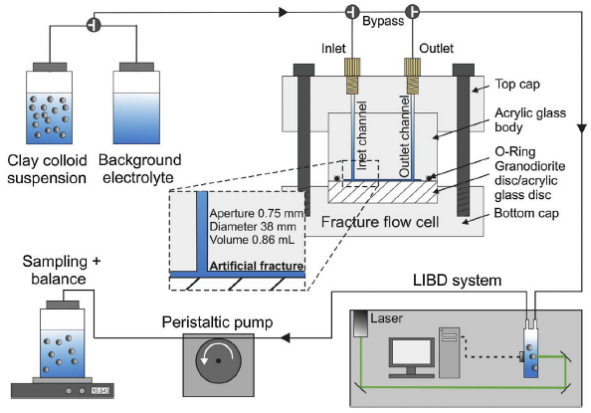

Fig. 3: Scheme of the experimental setup (horizontal fracture orientation). The exchangeable disc in the synthetic fracture flow cell has a hatched marking (reprinted from [8]).

In the second step, the colloid material was changed from synthetic monodisperse microspheres to polydisperse Na-illite colloids (Figs. 2 and 3). Similar transport experiments were conducted using nanoparticulate Na-illite in the ultra-trace concentration range and laser-induced breakdown detection (LIBD) as monitoring technique. Despite the higher density, the experiments indicate that the illite colloids experienced less retention than the monodisperse polystyrene colloids used in step one, which was attributed to the difference in shape, surface charge distribution and colloid size distribution. Therefore, it was shown that polystyrene colloids, which are frequently used in comparable experiments, are non-ideal analogues for polydisperse clay colloids, in order to predict the residence time behavior [8].

In the third step, the impact of flow channel geometry on fluid flow and non-reactive solute transport was investigated experimentally and numerically on two differently altered naturally fractured granite cores. Tomographic imaging and surface roughness measurements illustrated that both fractures are significantly different in terms of spatial heterogeneities and aperture distribution. Based on the 3-D digital data obtained by computed tomography 2.5-D numerical models were generated for both fractures by interpolating the measured aperture distributions onto the 2-D fracture geometries. Via three in- and three outlets at top and bottom of the fractures, different dipole flow fields were examined. The differences between both fractures were clearly reflected by the fluid flow and the solute transport behavior. It was shown in both experiments and simulations that fluid flow and solute transport in the altered fracture are dominated by the fracture geometry, while, in case of the unaltered fracture, the aperture distribution is the dominating parameter. In the presented case, the pronounced tailings can be attributed to complex internal heterogeneities and simple parallel-plate models fail to describe the experimental findings. Those observations demonstrate that the geometry and internal heterogeneities of fractures need to be implemented in numerical simulations in order to model precisely fluid flow and solute transport [9].

In the last step, colloid transport through the same natural granite fractures was investigated for the Na-illite colloids in the ultra-trace concentration range using LIBD as monitoring technique, as introduced in the second step. The flow rates applied and the geochemical unfavorable attachment conditions caused an almost total recovery of the colloids for both fractures. Retardation factors < 1 were obtained in all experimental cases, indicating faster colloid transport in contrast to the solute tracer. It was shown that the retardation factors of the experiments through the altered fracture are considerably smaller, compared to the ones in the unaltered fracture, which breakthrough curves show significant tailing. Moreover, a positive correlation between applied flow rate and acceleration of the colloid was found, which was more pronounced in case of the unaltered fracture. It was assumed that the retardation factors depend on an interaction between internal composition and geometry of the fractures and the sum of exclusion mechanisms and Taylor dispersion. However, based on the experimental and numerical data, a clear discrimination of the dominating process leading to the observed colloid acceleration is not unambiguously possible and needs further investigations.

Update on the Colloid Formation and Migration Project at the Grimsel Test Site

In the course of the Long-term In-situ Test experiment started in May 2014 within the Colloid Formation and Migration project at the Grimsel Test Site, a bentonite source was emplaced in a water conducting feature via a packer system (see Fig. 4). The bentonite plug consists in total of 16 compacted bentonite rings. 12 rings are composed of pure Febex bentonite and 4 rings in contact with the shear zone were produced with a 10% admixture of synthetic Zn-labeled montmorillonite [10]. In all four Zn-/Febex bentonite rings glass vials were emplaced with a Ni- montmorillonite [11] slurry doped with a cocktail of radionuclides (^{45}Ca, ^{75}Se, ^{99}Tc, ^{137}Cs, ^{233}U, ^{237}Np, ^{241}Am, ^{242}Pu) and a conservative tracer (Amino G).

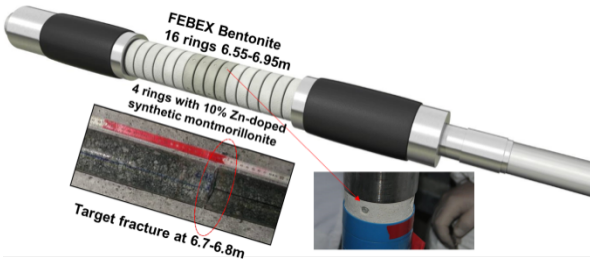

Fig.4: Schematic overview of the LIT packer system emplaced in the MI shear zone showing the compacted bentonite ring set-up and the glass vials emplaced with the radionuclide/Amino-G doped slurry.

This experiment combines for the first time in-situ colloid generation with radionuclide interaction and migration in an advection dominated natural shear zone over a potential migration length of ~6m under well-controlled low flow groundwater conditions mimicking post-closure repository conditions.

Geochemical and hydro-mechanical parameters are monitored continuously on-site with the digital acquisition system (DAS) as volumetric flow velocity, pH, E_h, specific conductivity, fluorescence signal of the effluent (conservative tracer) and swelling pressure of the bentonite source at different locations within the packer system. Samples are taken from the surface packer at the tunnel wall (Pinkel) and from an observation borehole close to the bentonite source (distance: ~10 cm). The later samples are taken at a flow rate of 50µL/min with a fraction collector in head-space vials emplaced inside an Argon glovebox to keep Eh/pH conditions constant. All samples taken are transferred to KIT/INE and analyzed off-site to monitor in addition to the DAS data potential changes in pH, conductivity and fluorescence signal during transfer. The main objective of the sample analysis was however the measurements of the mean colloid size and concentration via LIBD (laser induced breakdown detection), of the colloid size distribution (s-curve LIBD), of the water chemistry analysis (ICP-MS, IC) and radionuclide analysis (ICP-MS, SF-ICP-MS, AMS, LSC and γ-spectroscopy).

After 100 days, the conservative tracer (Amino-G) was detectable by fluorescence measurements and its concentration steadily increased to reach a plateau after 500 d (see Fig. 5). After 720 d the extraction rate was increased from 20 to 50 µL/min followed by a change of the extraction borehole (from CFM11.002 to CFM11.003) which explains the Amino G concentration drop. By increasing the extraction rate, more water was pulled from the surrounding shear zone and diluted the samples. When changing the extraction borehole after 840 days, the first samples show high concentration of Amino G. This is because the water in the packer intervals and the lines was stagnant since installation of the experiment and the conservative tracer diffused and enriched into this volume. However, the high concentrations decreased within the next sample extractions as once again fresh water was pulled from the shear zone rather than the bentonite source. The total mass of conservative tracer released corresponds to approx. 3.5% of the total source term mass.

Radiochemical investigations only found ^{99}Tc in the effluent samples. Technetium was introduced as Tc(VII) in the source and it is not expected to have changed oxidation state which is in line with the Eh values measured in the near-field (around 0 to 200 mV). ICP-MS overestimated the Tc concentrations (5 to 12 ppt) due to isobaric interferences with Ru-99. A newly developed measurement method for AMS, especially designed for analyzing Tc, found significantly lower Tc concentrations in selected samples. Analysis of

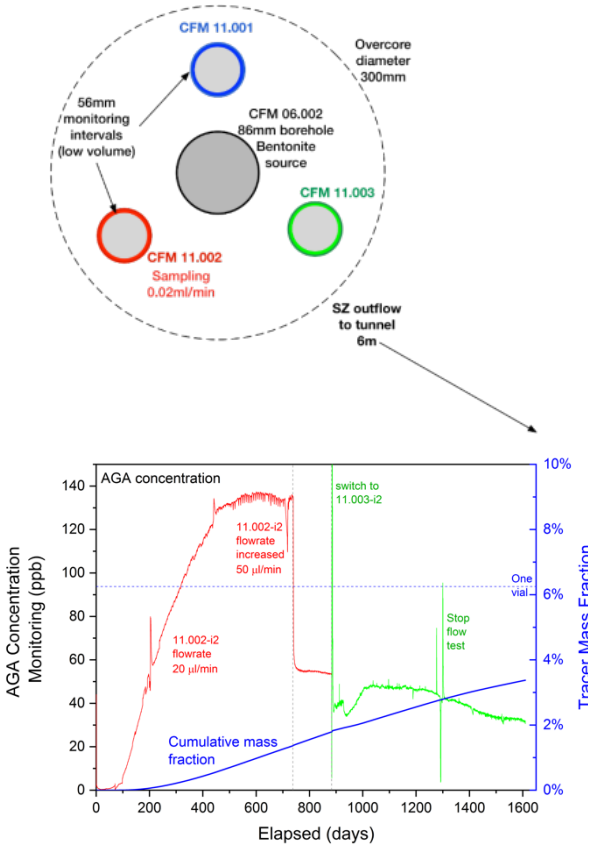

Fig.5: Top: Scheme of LIT borehole symmetry. The bentonite source is located in the central borehole surrounded by three monitoring boreholes. Bottom: Time dependent conservative tracer Amino-G (AGA) concentration evolution and total mass released from source.

additional samples is still ongoing. ICP-MS found neither Np, Am, U nor Pu originating from the LIT tracer cocktail. Measurements with AMS of such actinide nuclides are going to be performed.

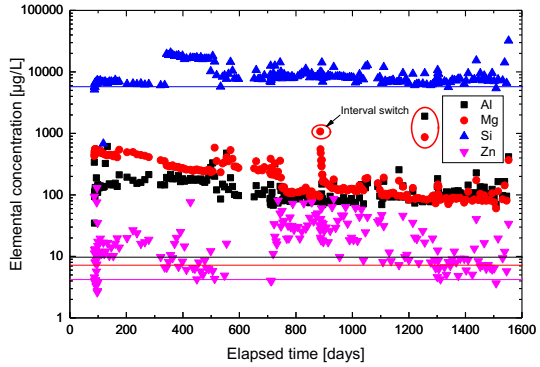

Fig.6: Elemental composition evolution of the samples taken from the observation boreholes close to the bentonite source. Background concentrations are presented as solid lines in the color of the respective element.

Assuming that the Zn and Al concentrations above the background level are directly originating from bentonite colloids (Fig.6), colloid concentrations are calculated to 0.8 mg/L colloids (acc. to the median Al signal) and 0.1 mg/L colloids (acc. to the median Zn signal) in the effluent samples. The mean LIBD determined colloid size is 71 ± 29 nm and colloid median concentration around 0.02 mg/L. There is clearly a discrepancy in colloid concentration calculated by ICP-MS data and derived by LIBD. Bentonite dissolution could explain the discrepancy but uneven distribution of Febex and Zn-montmorillonite has also to be taken into account. More information is needed for a concluding statement and will be accessible after post-mortem analysis of LIT and the mock-up experiments.

Mg concentrations around 380 ± 120 µg/L during the first 700 days of the experiment and 150 ± 130 µg/L during the following time are significantly above the natural concentration of only 7.2 µg/L that can be found within the groundwater. In addition, reversed Mg/Al-ratios in the effluent samples compared to the background level along with decreasing Ca concentrations suggests cation exchange reactions taking place beside gypsum dissolution.

LIT online-monitoring and sample collecting ended in October 2018. Epoxy resin was injected into the monitoring boreholes to stabilize the gel and to isolate it from the surrounding shear zone. In order to retrieve and dismantle the bentonite source for post-mortem analysis, the whole experiment is over-cored with a 360 mm diameter core drill.

References

[1] Honeyman, B.D., *Nature*, **397**, 23-24, (1999).

[2] Schäfer, Th. et al., *Appl.Geochem*, **27**, 390-403, (2012).

[3] Quinto, F. et al., *Anal. Chem*, **87**, 5766-5773, (2015).

[4] Quinto, F. et al., *Anal. Chem,* **89**, 7182-7189, (2017).

[5] Stoll, M., *Colloid mobility controlling processes in single fractures: a bottom-up approach*, PhD thesis, Jena (2018).

[6] Stoll, M. et al., *J. Coll. Int. Sci*, **475**, 171-183, (2016).

[7] Meller, C. et al., *Energy technology*, **5,** 965-1006 (2017).

[8] Stoll, M. et al., *Coll. Surf. A: Physicochem. Eng. Aspects*, **529**, 222-230, (2017).

[9] Stoll, M. et al., *J. Contam. Hydrol.,* **221,** 82–97 (2019).

[10] Reinholdt, M., et al., *Eur. J. Inorg. Chem*., **2001**, 2831-2841 (2001).

[11] Reinholdt, M., et al., *Nanomaterials*, **3,** 48-69 (2013).

6 Coordination chemistry

Coordination chemistry studies in solution are performed related to actinide separations by solvent extraction. These studies address the interactions and the speciation between actinide ions (and other ions) and ligands potentially useful for separating actinides. The focus is on nitrogen donor ligands and on the subtle differences in their interactions between actinide and lanthanide ions of the same charge.
2,6-Bis(1,2,4-triazin-3-yl) pyridines (BTP) and 6,6'- bis(1,2,4-triazin-3-yl)-2,2'-bipyridines (BTBP) have been developed and studied as highly selective lipophilic extracting agents and water-soluble complexing agents for separating trivalent actinides from lanthanides [1]. To overcome some drawbacks such as kinetics and solubility issues [2] or the presence of sulphur atoms [3–4], 2,6-bis(1,2,3-triazol-4-yl) pyridines have been developed, to be used as water soluble complexing agents [5] or lipophilic extracting agents [6].

6.1 Hydrophilic 2,6-bis(1,2,3-triazol-4-yl) pyridine ligands: tuning properties via basicity

P. Weßling, C. Adam, A. Geist, P. J. Panak

In co-operation with:

E. Macerata,[a] E. Mossini,[a] M. Mariani,[a] M. C. Gullo,[b] A. Arduini,[b] A. Casnati,[b]

[a] Politecnico di Milano, Department of Energy, Nuclear Engineering Division, Milano, Italy; [b] Università di Parma, Dipartimento di Scienze Chimiche, della Vita e della Sostenibilità Ambientale, Parma, Italy

Introduction

The water-soluble ligand SO_3-Ph-BTP [3] (Scheme 1) has been used to selectively back extract trivalent actinides, An(III), from loaded organic phases containing both An(III) and lanthanide ions, Ln(III) [7–8]. Nitric acid at a suitable concentration (typically in the range of 0.5 mol/L) is used to keep Ln(III) in the organic phase. However, the sulphur atoms present in the molecule cause problems with waste management.

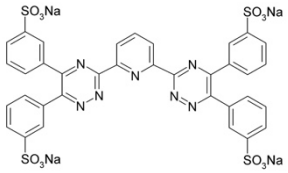

Scheme 1. SO_3-Ph-BTP.

Consequently, the water-soluble ligand PTD (Scheme 2) was developed [5], consisting only of C, H, O and N atoms. Stability constants of the Cm(III)-PTD complexes [9] were found to be rather low compared to SO_3-Ph-BTP complexes [11–12], Table 1. To increase the complexing properties of PTD a modified molecule, OMe-PTD (Scheme 2), was synthesised. The methoxy group activates the aromatic system, expected to result in improved metal ion complexation.

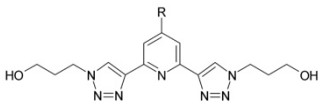

Scheme 2. PTD (R = H) and OMe-PTD (R = -OMe).

Unfortunately, OMe-PTD proved to be less efficient in solvent extraction experiments in which the aqueous phase contained 0.44 mol/L HNO_3. To achieve a performance close to that of PTD in 0.44 mol/L HNO_3 [5], OMe-PTD required different experimental conditions: HNO_3 concentration had to be reduced to 0.1 mol/L and nitrate concentration increased to 1 mol/L by addition of NH_4NO_3.

To understand this behaviour the complexation of Cm(III) with OMe-PTD in 10^{-3} mol/L $HClO_4$ and in 0.44 mol/L HNO_3 was studied using time-resolved laser fluorescence spectroscopy (TRLFS), and its pK_a value was determined by NMR.

Results

Cm(III) complex stability constants

Figure 1 shows the normalised Cm(III) fluorescence spectra in 10^{-3} mol/L $HClO_4$ at varied OMe-PTD concentration.

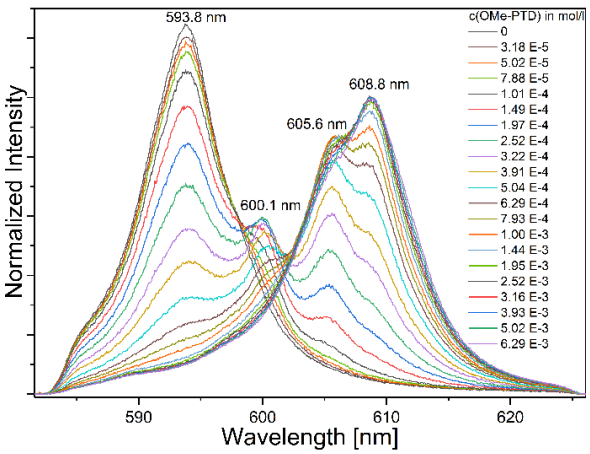

Figure 1. Normalised Cm(III) fluorescence spectra in 10^{-3} mol/L $HClO_4$ at increasing OMe-PTD concentrations.

The emission band at 593.8 nm corresponds to the Cm(III) aqua ion. With increasing ligand concentration, three new emission bands (600.1 nm, 605.6 nm and 608.8 nm) were found. Following peak deconvolution and slope analysis, they were attributed to the

$[Cm(OMe\text{-}PTD)_n]^{3+}$ complexes (n = 1–3). The 1:3 complex had a lifetime of τ = (495 ± 20) µs, indicating the absence of quenching water molecules in the inner coordination sphere [10]. The conditional stability constants for the formation of the 1:1, 1:2 and 1:3 complexes were determined to $\lg \beta'_1 = 3.3 \pm 0.2$; $\lg \beta'_2 = 6.8 \pm 0.2$ and $\log \lg \beta'_3 = 10.3 \pm 0.3$ (Table 1).

Significantly lower conditional stability constants were found in 0.44 mol/L HNO_3, having values of $\lg \beta'_1 = 0.7 \pm 0.2$; $\lg \beta'_2 = 2.0 \pm 0.2$ and $\lg \beta'_3 = 3.0 \pm 0.3$.

pKa value

The pK_a value of OMe-PTD was determined by evaluating the shifts of its ^{1}H signals as a function of pH_c.

With decreasing pH_c a downfield shift of the aromatic protons was observed. No shifts were observed for pH_c values > 4.39 or < 0.96, indicating the existence of only the deprotonated or protonated ligand at these pH values. In the pH_c range between 4.39 and 0.96 only one signal was observed, indicating a fast proton exchange. By analysing the peak shifts relative to the shift of the deprotonated species, a pK_a value of 2.54 ± 0.08 was determined.

Discussion

Conditional stability constants and pKa values for OMe-PTD are reported in Table 1 and compared with the respective values for PTD [9] and SO_3-Ph-BTP [11–12].

Comparing $\lg \beta'_3$ values in 10^{-3} mol/L $HClO_4$, it is evident that OMe-PTD is a stronger complexing agent for Cm(III) compared to PTD. The stability constants (corrected for ligand protonation) differ by almost one order of magnitude in favour of OMe-PTD.

In contrast, the conditional stability constants in 0.44 mol/L HNO_3 show the reverse trend, with the value for MeO-PTD being lower by almost three orders of magnitude. This behaviour is caused by differences in ligand basicity, the pK_a value for MeO-PTD being larger by almost 0.5 units.

The smaller β'_3 value in 0.44 mol/L HNO_3 for OMe-PTD explains why this ligand is less efficient than PTD in solvent extraction experiments.

Finally, SO_3-Ph-BTP forms a much stronger complex with Cm(III), the β'_3 value being larger by 1–2 orders of magnitude than the respective β'_3 values for OMe-PTD and PTD. In addition, SO_3-Ph-BTP is much less prone to protonation.

Due to these differences in complexation and protonation, (OMe-)PTD has to be used at significantly larger concentrations (80 mmol/L) [5] than SO_3-Ph-BTP (10–20 mmol/L) [3].

Conclusions

In conclusion, addition of a methoxy group improves the complexation properties of PTD. However, for conditions relevant to an application as a selective stripping agent for actinides, i.e. approximately 0.5 mol/L HNO_3, ligand protonation overcompensates what is gained by stronger metal ion complexation, in fact making OMe-PTD a less useful compound for the intended application.

Table 1. Cm(III) complex stability constants and pK_a values of OMe-PTD, PTD and SO_3-Ph-BTP in 10^{-3} mol/L $HClO_4$ and 0.44 mol/L HNO_3.

		OMe-PTD		**PTD** [9]		**SO_3-Ph-BTP** [11–12]
		$\lg \beta'_n$	$\lg \beta'_n$*	$lg\ \beta'n$	$lg\ \beta'n$*	$\lg \beta'_n$
Stability constants (in 10^{-3} mol/L $HClO_4$)	n = 1	3.3 ± 0.2	3.4 ± 0.3	3.2 ± 0.2	–	5.4 ± 0.1
	n = 2	6.8 ± 0.3	7.0 ± 0.4	6.6 ± 0.2	–	9.3 ± 0.2
	n = 3	10.3 ± 0.3	10.8 ± 0.4	9.7 ± 0.3	9.9 ± 0.5	12.2 ± 0.3
Stability constants (in 0.44 mol/L HNO_3)	n = 1	0.7 ± 0.2	–	1.7 ± 0.1	–	–
	n = 2	2.0 ± 0.2	–	4.0 ± 0.1	–	–
	n = 3	3.0 ± 0.3	–	5.7 ± 0.2	–	10.6 ± 0.3**
pK_a		2.54		2.1		0.5

* corrected for protonation

** (in 0.5 mol/L HNO_3)

6.2 2,6-Bis(1-(2-ethylhexyl)-1H-1,2,3-triazol-4-yl) pyridine

P. Weßling, C. Adam, A. Geist, P. J. Panak

In co-operation with:

E. Macerata,[a] F. Galluccio,[a] E. Mossini,[a] M. Mariani,[a] M. C. Gullo,[b] F. Sansone,[b] A. Casnati,[b]

[a] Politecnico di Milano, Department of Energy, Nuclear Engineering Division, Milano, Italy; [b] Università di Parma, Dipartimento di Scienze Chimiche, della Vita e della Sostenibilità Ambientale, Parma, Italy

Introduction

CyMe$_4$-BTBP (Scheme 3 top), the current European reference extracting agent for separating An(III) from Ln(III), suffers from drawbacks such as slow kinetics and limited solubility [2, 13–14]. The promising properties of the water-soluble PTD ligand [5] (see also section 6.1) prompted the development of lipophilic extracting agents based on the 2,6-bis(1,2,3-triazol-4-yl) pyridine core [6]. One representative of this family, 2,6-bis(1-(2-ethylhexyl)-1H-1,2,3-triazol-4-yl) pyridine (PTEH, Scheme 3 bottom), has promising properties for separating An(III) from Ln(III) [6], surpassing those of CyMe$_4$-BTBP.

Its complexation properties for An(III) were studied by NMR and TRLFS. For results of the NMR study, see the contribution to the NMR section of the Annual Report. TRLFS was applied to determine stability constants of the Cm(III)-PTEH complexes and to identify the Cm(III) complex formed in the organic phase of a solvent extraction experiment.

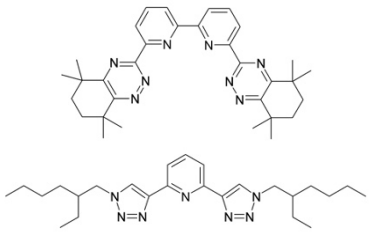

Scheme 3. CyMe$_4$-BTBP (top) and PTEH (bottom).

Results and Discussion

Cm(III) complex stability constants

Figure 2 shows the normalised Cm(III) fluorescence spectra at varied PTEH concentration in methanol containing 5 vol.% water.

The emission bands at 595.1 nm and 598.3 nm correspond to Cm(III) solvated with water and methanol [15]. With increasing PTEH concentration, emission bands at 600.3 nm, 605.8 nm and 608.4 nm were found. These emission bands were attributed to the $[Cm(PTEH)_n]^{3+}$ (n = 1–3) complexes by slope analysis.

The lifetime of the 1:3 complex was τ = (585 ± 12) µs, indicating the absence of quenching methanol or water molecules.

The conditional stability constants for the formation of the 1:1, 1:2 and 1:3 complexes in methanol containing 5 vol.% water were determined to lg β'_1 = 5.2 ± 0.1, lg β'_2 = 10.7 ± 0.1 and lg β'_3 = 16.2 ± 0.2. The stability constant of the 1:3 complex is approximately one order of magnitude lower than the stability constant of the $[Cm(nPr\text{-}BTP)_3]^{3+}$ 1:3 complex (lg β'_3 = 17.4 ± 0.4) in the same solvent [15].

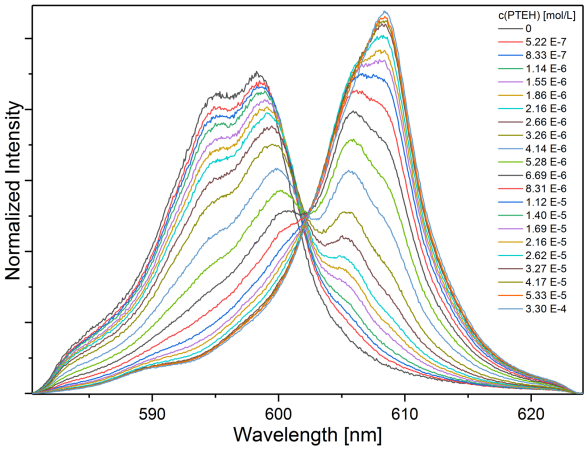

Figure 2. Normalised Cm(III) fluorescence spectra in MeOH + 5 vol.% H_2O at increasing PTEH concentrations.

Figure 3 shows the Cm(III) species distribution as a function of PTEH concentration. Both the 1:1 and 1:2 complexes had a maximum share of approximately 25% at a PTEH concentrations of 2.6 × 10^{-6} mol/L and 6 × 10^{-6} mol/L, respectively. The 1:3 complex became the prevailing species at 4 × 10^{-6} mol/L PTEH.

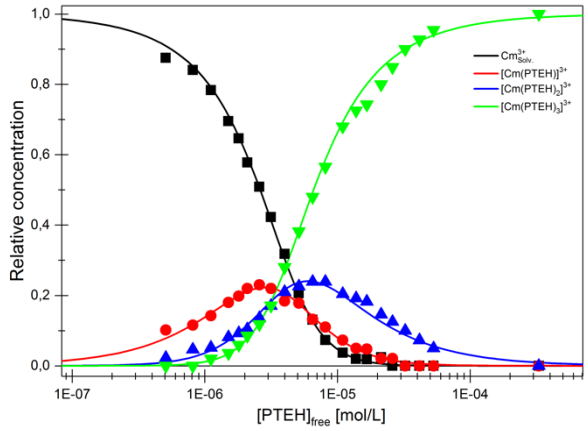

Figure 3. Cm(III) species distribution as a function of the PTEH concentration in MeOH + 5 vol.% H_2O. Lines calculated with lg β'_1 = 5.2, lg β'_2 = 10.7 and lg β'_3 = 16.2.

Identification of the extracted Cm(III) complex

Cm(III) was extracted from 3 mol/L HNO_3 into an organic phase containing 0.2 mol/L PTEH in kerosene/1-octanol (9:1). To identify the complex formed upon extraction the organic phase was investigated using TRLFS.

Comparison of the emission band from the organic phase sample with that of the 1:3 complex from the monophasic titration experiment revealed perfect agreement regarding position of the emission band (608.4 nm) and peak shape. Thus Cm(III) is extracted as the 1:3 complex $[Cm(PTEH)_3]^{3+}$, in agreement with findings for other tridentate *N* donor ligands such as BTP [15–16].

References

[1] P. J. Panak, A. Geist, *Chem. Rev.* **2013,** *113,* 1199.

[2] A. Geist et al., *Solvent Extr. Ion Exch.* **2006,** *24,* 463.

[3] A. Geist et al., *Solvent Extr. Ion Exch.* **2012,** *30,* 433.

[4] C. Wagner et al., *Solvent Extr. Ion Exch.* **2016,** *34,* 103.

[5] E. Macerata et al., *J. Am. Chem. Soc.* **2016,** *138,* 7232.

[6] A. Ossola et al., *J. Radioanal. Nucl. Chem.* **2018.**

[7] A. Wilden et al., *Solvent Extr. Ion Exch.* **2015,** *33,* 91.

[8] R. Malmbeck et al., *Radiochim. Acta* **2018,** *(submitted).*

[9] C. Wagner et al., *Inorg. Chem.* **2017,** *56,* 2135.

[10] T. Kimura et al., *Radiochim. Acta* **1996,** *72,* 61.

[11] C. M. Ruff et al., *Dalton Trans.* **2012,** *41*, 14594.

[12] C. M. Ruff, dissertation, Universität Heidelberg: 2013.

[13] A. Geist et al., In *12th Information Exchange Meeting. Prague (CZ), 24–27 September 2012*, OECD-NEA: 2013.

[14] C. Ekberg et al., *J. Chem. Eng. Data* **2010,** *55,* 5133.

[15] A. Bremer et al., *New J. Chem.* **2015,** *39,* 1330.

[16] S. Trumm et al., *Eur. J. Inorg. Chem.* **2010,** 3022.

7 Development of actinide speciation methods

Developing and maintaining a state-of-the-art portfolio of radionuclide speciation tools encompassing surface science and spectroscopy methods is an important R&D activity at INE, as these methods are indispensable for advancing our understanding of actinide and radionuclide (geo)chemistry or the behavior of nuclear waste forms during interim storage. Radionuclide speciation methods available at INE's controlled area laboratories and the ACT and INE-Beamline stations at the nearby KARA research accelerator are continuously adapted to serve the requirements of in house R&D programs. Access to this unique instrumentation is as well provided to national and international partners in the frame of cooperation agreements or joint research projects. The high-resolution (HR) X-ray emission spectrometer at the ACT station has been repeatedly shown to provide unprecedented insight into electronic and bonding characteristics of actinyl moieties when excited at the actinide 3d core levels. In 2018, the outstanding spectral resolution of the HR-XANES technique implemented at ACT has been for the first time applied to study the subtle "pre-edge" features at the iron K-edge measured for Fe(II)/Fe(III) containing model compounds with tetrahedral and/or octahedral Fe coordination. One of the key challenges in this context is the detailed characterization of Fe in possible HLW canister corrosion products (or other Fe bearing mineral phases such as clays) and the geochemical reactions of such phases with actinides and long-lived fission products released from breached HLW canisters. Co-precipitation of dissolved radionuclides and corrosion products and the following redox reactions may contribute to radionuclide retention in the repository near field. This has been demonstrated by X-ray photoelectron spectroscopy, studying selenium speciation after selenite and selenate co-precipitation with Fe(II)- and Fe(III)-cations under anoxic and oxic conditions, respectively. Conventional fluorescence mode XAFS measurements have been proven to serve as invaluable tool for addressing the speciation of the radionuclide inventory in highly radioactive fragments sampled from spent nuclear fuel. The portfolio of laser based speciation techniques at INE currently comprises TRLFS, LIBD and LIBS. A focus in 2018 has been placed on the investigation of the complexation of trivalent actinide cations by human serum transferrin. Using a combination of TRLFS for Cm(III) speciation, molecular dynamics simulations and density functional theory calculations, detailed insight into the 3D structure of Fe(III)/Cm(III) binding sites of the protein molecule was gained. The coordinating functional groups were identified based on their vibrational modes applying vibronic sideband spectroscopy. The focus of NMR spectroscopy at INE has been traditionally placed on metal-ligand bonding phenomena in the context of f-element coordination chemistry. However, capabilities of solid state MAS NMR spectroscopy are currently gaining more attention, as shown in a recent study to characterize the local chemical environment of iron in naturally occurring and synthetic smectites with different Fe(II)/Fe(III) ratios. Accelerator mass spectrometry (AMS) – more recently established at INE – has been applied in the past two years to analyze the long-term migration behavior of actinides and ^{99}Tc employed in radionuclide tracer tests as well as to observe the behavior of actinides from global fallout in environmental compartments representative for the conditions of a deep geological HLW repository. Many in house research activities at INE benefit from the strong support by computational chemistry methods, providing, e.g., detailed structures of actinides incorporated into HLW canister corrosion products or electron transition probabilities which allow the sound interpretation of experimental UV/Vis/NIR or X-ray absorption/emission spectroscopy data.

7.1 R&D projects conducted at the INE-Beamline and at CAT-ACT at the KIT synchrotron source

A. Beck, R. Dagan, K. Dardenne, N. Finck, E. González-Robles, F. Heberling, M. Herm, S. Kumar, V. Metz, N. Müller, Z. Nie, J. Rothe, T. Vitova

Introduction

Synchrotron radiation (SR) based speciation techniques have become key methods in basic and applied radionuclide research. This development is primarily driven by the need to secure molecular-scale understanding of (geo-)chemical processes determining the mobility of safety relevant radionuclides (i.e., long-lived actinides, fission and activation products generated during nuclear reactor operation), possibly released from a projected repository for highly active, heat-producing nuclear waste. Presently, final disposal in deep bedrock formation is deemed as the preferred option worldwide for the management of spent nuclear fuel (SNF) and high-level waste (HLW) glass used for conditioning of highly radioactive residues from nuclear fuel reprocessing. Speciation techniques like XAS (X-ray Absorption Spectroscopy) provide necessary input parameters (i.e., the physicochemical state of radionuclides under given chemical and thermodynamic boundary conditions such as E_h, pH, ionic strength, presence of complexation agents or adsorbing surfaces etc.) to model long-term evolution scenarios of a projected underground repository for nuclear waste. All countries currently utilizing nuclear fission as energy source - regardless of their concepts for a sustainable future energy mix - are facing additional challenges imposed by the foreseeable prolongation of SNF and HLW-glass interim storage until the availability of a societally accepted, fully licensed and technically functional final repository. Thus, in addition, attempts

to directly characterize SNF and HLW-glass matrices by XAFS (X-ray Absorption Fine Structure, i.e., XANES and EXAFS) are gaining importance in order to address the actual speciation of the radionuclide inventory as well as the possible impact of prolonged dry storage on SNF integrity and future transportability.

The INE-Beamline for radionuclide science [1] at the electron storage ring KARA (KArlsruhe Research Accelerator) became fully operational in 2005 as a flexible experimental station for X-ray based radionuclide speciation investigations. The new hard X-ray beamline 'CAT-ACT' for CATalysis and ACTinide research was commissioned at an adjacent beam port in 2016 [2]. Both the INE-Beamline and the ACT laboratory for synchrotron based radionuclide studies are licensed to handle radioisotopes with activities up to one million times the (isotope specific) exemption limits, including 200 mg each of the fissile isotopes 235-U and 239-Pu. Both experimental stations are the only facilities of their kind in Europe offering direct access to radiochemistry laboratories operating a shielded box-line in close proximity to the synchrotron light source on the same research campus.

INE-Beamline and CAT-ACT operation in 2018/19

After conversion of the KIT synchrotron radiation source from a national user facility to a KIT internal research infrastructure, user operation at the KARA storage ring had to be rearranged to suit new boundary conditions, resulting in a reduced availability of SR beamtime (up to 100 operation days per calendar year). Moreover, since 2016 SR beamtime distribution is no longer based on a peer review proposal process, but on in-house needs within the KIT and HGF research programs and individual agreements between beamline-operating KIT-institutes and external cooperation partners. Cooperation between KIT-IBPT and Helmholtz-Zentrum Dresden-Rossendorf (HZDR) enabled 20 additional days of KARA SR operation in 2019, partially compensating for beamtime losses at the Rossendorf Beamline (ROBL) due to the ESRF (the European Synchrotron Radiation Facility at Grenoble, France) upgrade in 2019/20. In this context, 12 selected projects of IRE scientists (HZDR Institute of Resource Ecology) were carried out at the ACT and INE-Beamline stations, which have provided 20 beamtime days each in 2019 for this cooperation. A total of 33 (in-house & external) projects received beamtime in 2018 at the INE-Beamline and ACT experimental stations, followed by 51 projects in 2019 (excluding HZDR special operation). Ongoing efforts to refurbish the storage ring in the report period enabled a significant gain of the electron beam lifetime and, thus, the permanent transition to a single-injection mode (one daily injection between 8 and ~9 am).

As in the previous years, INE in-house projects in 2018 and 2019 covered the investigation of a broad range of materials containing actinides (*An*) or their chemical homologues (e.g., lanthanides (*Ln*)) and possible fission products in the context of nuclear waste

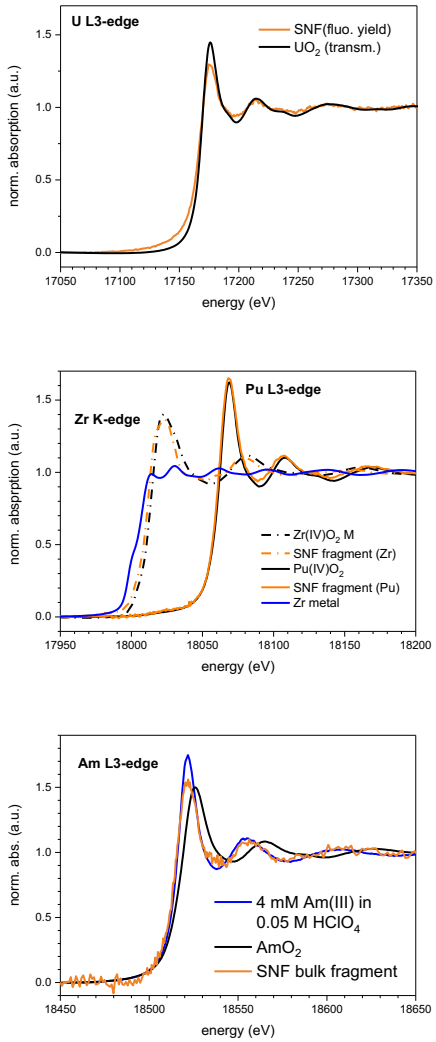

Fig. 1: Normalized XANES spectra obtained for the Gösgen fuel fragment (orange traces) together with spectra of reference compounds recorded at the (top) U L_3-edge, (centre) Zr K- and Pu L_3-edges and (bottom) Am L_3-edge [5].

disposal safety research or basic actinide and radionuclide science. Besides others, studies scheduled for 2018 comprised the Mo speciation in the $CaMoO_4$ – $Na_{0.5}Ln_{0.5}MoO_4$ solid solution series (*Ln*: La, Eu, Yb), XAFS, HR-XANES and µ-XRF investigations of highly radioactive nuclear waste samples (SNF, HLW glass and zircaloy cladding fragments), the investigation of ionic strength effects on americium retention at the magnetite surface, interaction of Np with Fe(II,III)-oxides or Fe-containing clay minerals, the investigation of radioactive scalings sampled from a geothermal pilot power plant, combined Pu M_5 HR-XANES/RIXS and Pu L_3-EXAFS studies of solid and colloidal PuO_2 in aqueous media, the investigation of the ligand configuration in $Th(nPr\text{-}BTP)_3(OTf)_4$ depending on the solvent polarity and the speciation of Th in natural soil samples from Sri Lanka. Some of these studies are presented in more detail elsewhere in this annual report. Studies focussing on the *An* speciation in an original SNF fragment and on Fe-speciation applying Fe K-

edge HR-XANES and RIXS will be presented in more detail below.

Researchers and cooperation partners from the following German and international research institutions conducted research at the INE-Beamline and ACT station in 2018/19:

- CEA Marcoule/Cadarache, France
- SCK-CEN, Belgium
- University of Heidelberg, Germany
- Joint Research Centre Karlsruhe, European Commission
- University of Copenhagen, Denmark
- EPFL Lausanne, Switzerland
- University of Manchester, United Kingdom
- Los Alamos National Laboratory, USA
- HZ Dresden-Rossendorf / IRE, Germany
- Technical University of Delft, The Netherlands
- University of Jena, Germany
- University of Mainz, Germany
- University of Köln, Germany
- Sorbonne Université, Paris, France
- Forschungszentrum Jülich, IEK-6, Germany

As in the preceding years, a considerable share of in-house beamtime was spent for experiments conducted by master and graduate students in the frame of their thesis projects. Beamtime at both lines was as well awarded to S. Kumar (Bhabha Atomic Research Centre, India) to conduct research in the frame of his successful Humboldt Fellowship application at KIT.

Speciation of actinides in a SNF bulk fragment

Work at KIT-INE currently focuses on direct XAFS/HR-XANES speciation investigations of SNF bulk fragments and cladding ring segments (both from the plenum and the central section, where the Zircaloy had been in contact with the fuel during irradiation), originating from a test fuel rod irradiated at Gösgen PWR, Switzerland (238-UO_2 fuel with an initial enrichment of 3.8% 235-U, burn-up ~50.4 GWd/tHM) [3], cf. chapter 5.1. Sample preparation for experiments at the INE-Beamline and ACT station follows the procedure described by Dardenne et al. [4] for the investigation of borosilicate HLW glass fragments. The dose rate of the encapsulated sample (a mm-sized fragment taken near the centre of a fuel pellet) was determined to be 3.45 mSv/h in contact and ~2 µSv/h at 1 m distance, i.e., at the edge of the beamline experimental tables. XAFS data were recorded in total fluorescence yield mode at the U L_3- (17.166 keV), Pu L_3- (18.057 keV), Am L_3-(18.510 keV) and Zr K-edge (17.998 keV), using a Ge solid state detector and an Ar-filled ionization chamber as I_0-monitor (cf. [5] for experimental details).

Figure 1 (top) depicts the fluorescence mode U L_3-XANES spectra obtained for the SNF fragment compared to a reference spectrum taken from an UO_2 pellet (uraninite dispersed in polyethylene powder and pressed to a disk) with an ideal "edge-jump" for transmission measurements. The spectrum of the SNF fragment strongly resembles that of U(IV) in the fluorite type UO_2 reference. The position of the white line (WL) maximum (17.176 keV) and the first inflection point (17.170 keV) clearly point to the prevailing tetravalent oxidation state of uranium in the SNF fragment, while WL broadening and damping as well as EXAFS amplitude losses have to be attributed to a marked "self-absorption" effect, i.e., the expected non-linearity when detecting XAFS of a concentrated element in a "thick" sample in total fluorescence yield mode.

Pu adopts the same fluorite-type crystal structure of a tetravalent cation in the SNF matrix as its U mother, as obvious from the fluorescence mode Pu L_3-XANES shown in Fig. 1 (centre) and comparison to a PuO_2 reference sample. The spectrum of the SNF fragment is unaffected by "self-absorption" compared to that obtained for U. WL and edge positions recorded at the Zr K-edge for the SNF fragment and the monoclinic Zr(IV)O_2 reference sample (in the same graph in Fig. 1, centre) are in agreement with the presence of Zr as a tetravalent fission product cation. The Zr-spectrum of the SNF fragment exhibits a narrower, more symmetric WL, and a reduced energy distance between the WL maximum and the first "shape resonance" compared to monoclinic ZrO_2. These small, but significant differences might indicate more symmetric oxygen coordination in the fuel compared to the reference oxide expected if Zr(IV) remains predominantly incorporated at U(IV) sites in the UO_2 fluorite type lattice.

Finally, Fig. 1 (bottom) depicts the Am L_3-edge XANES obtained for the SNF fragment, a solid Am(IV)O_2 and an aqueous Am(III) reference sample ([Am] = 4 mM in 0.05 M $HClO_4$). Comparing these XANES spectra, we can conclude that – in contrast to U and Pu, which are incorporated as tetravalent cations in the SNF matrix – Am retains its favoured trivalent oxidation state. Am isotopes are generated during fuel irradiation through β-decay of 241-Pu and consecutive neutron capture. Since recoil-induced Am-cation displacement in the UO_2 lattice is not to be expected, the necessary charge balance might occur via formation of Am(III)O_7^{11-} moieties with oxygen vacancies in the cubic, eight-fold coordinated cation site of the fluorite structure. Alternatively, UO_2 can act as redox buffer: Am(IV)→Am(III)/UO_2→UO_{2+x}. This process has been observed by D. Prieur et al. in their study on Am/U oxide solid solution formation [6]. The possibly resulting minor UO_{2+x} fraction has not been detectable in the present study and might require a combination of spatially resolved and high (energy) resolution XAS techniques (i.e., U M-edge HR-XANES) in future experiments.

Iron-speciation with HR-XANES, RIXS and fluorescence emission spectroscopy

As already highlighted in chapter 4.3, one of the foci of the secondary phases group at INE is the investigation of iron corrosion products and other iron bearing secondary phases (e.g., green-rust, magnetite, iron bearing

clays etc.) and their interactions with actinides and fission products. One of the key challenges in this context is the detailed characterization of Fe in the corresponding solids with respect to redox state and coordination environment. Here we present a selection of results from an experiment, in which the high-resolution (HR) X-ray emission spectrometer at the ACT station was equipped with Ge(620) crystals. These crystals allow to record the Fe-K$\beta_{1,3}$ fluorescence emission with HR (~1.9 eV FWHM, Bragg angle ≈ 79°). Goal of the investigation was to test the possibilities of the setup to characterize the electronic structure of Fe(III) and Fe(II) in tetrahedral and/or octahedral oxygen coordination in model compounds. Model compounds and their most important characteristics are summarized below (superscript "VI" stands for octahedral-, and "IV" for tetrahedral coordination):

- hematite (α-Fe_2O_3): ^{VI}Fe(III)
- goethite (α-FeOOH): ^{VI}Fe(III)
- maghemite (γ-Fe_2O_3): ^{VI}Fe(III) + ^{IV}Fe(III)
- magnetite (Fe_3O_4): ^{VI}Fe(II) + ^{VI}Fe(III) + ^{IV}Fe(III)
- iron phosphate ($FePO_4$): ^{IV}Fe(III)
- wuestite (FeO): ^{VI}Fe(II).

The upper image in Fig. 2 shows a sketch of the electron orbitals in Fe(II) and Fe(III) and the electronic transitions relevant for our study. The lower graph displays HR-XANES data measured on the model compounds. Arrows highlight the features of main interest in the present report, namely the excitation energy position of the main absorption edge (transition "a") and the excitation energy position of the pre-edge feature (transition "b"). Of further interest are the energy positions of the maxima of the emission lines (transition "c") measured at excitation energies above the absorption edge ("c/a") and at the pre-edge ("c/b"). For Fe(II) or (III) in octahedral coordination environments with preserved inversion symmetry, transition "b" is dipole forbidden. Thus, only relatively weak quadrupole transitions occur. The pre-edge represents transitions to the $3d_{5/2}$ orbital, which is split into two sublevels (e_g and t_{2g}). For Fe(III) in tetrahedral coordination, Fe d and p valence states mix and as a consequence transition "b" is dipole allowed. In this case, the $3d_{5/2}$ orbital splits in two sublevels with similar energy (t_2 and e).

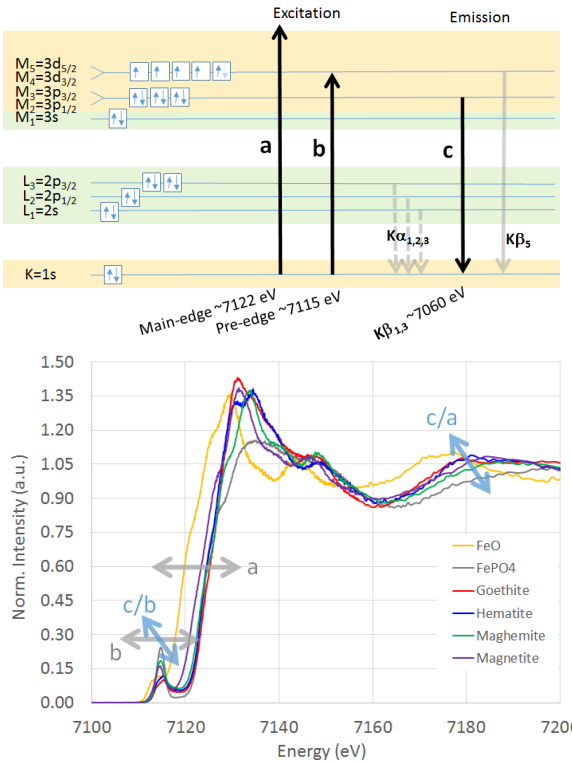

Fig. 2: The upper image shows a sketch of the electronic structure of Fe(II) and Fe(III). The lower graph shows HR-XANES data measured on the model compounds. Arrows indicate the features of main interest in the HR-XANES, RIXS, and fluorescence emission measurements.

The excitation energy position of the main edge ("a") is obtained from HR-XANES data, the emission energy peak above the absorption edge ("c/a") is obtained from fluorescence emission scans, recorded at an excitation energy of 7180 eV. The position of the pre-edge feature with respect to excitation ("b") and emission energy ("c/b") is determined from so called RIXS maps (mesh scans in excitation and emission energy at the pre-edge position). RIXS maps are evaluated using a Phyton script. The pre-edge peaks are fitted with either a single 2D Gaussian, in order to obtain the center of mass of the pre-edge peak (full circles in Fig. 3), or with two 2D Gaussians, in order to determine individual peak positions within split double peaks (open circles in Fig. 3).

The brownish frame in Fig. 3 shows how the average energy of transition "c/b" increases with increasing energy of transition "b" for the model compounds. For Fe in octahedral coordination peaks are split as expected. Splitting in excitation energy direction correlates with a splitting in emission energy direction. This is similar for Fe(II) (yellow frame in Fig. 3) and Fe(III) (blue frame in Fig. 3). Fe(III) in tetrahedral coordination shows, as expected, no significant splitting (grey frame). The mixed structure, magnetite (^{VI}Fe(II & III),

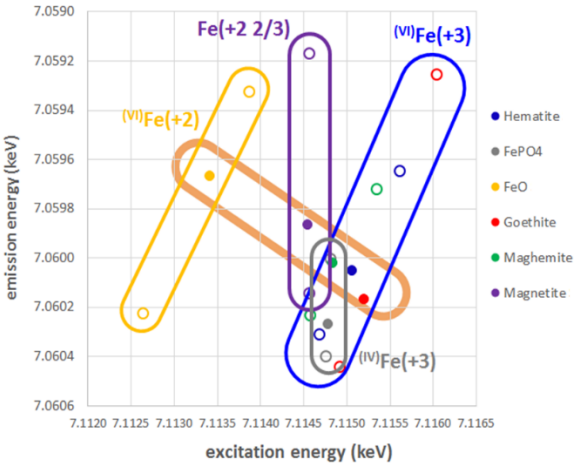

Fig. 3: Pre-edge peak positions determined from RIXS maps.

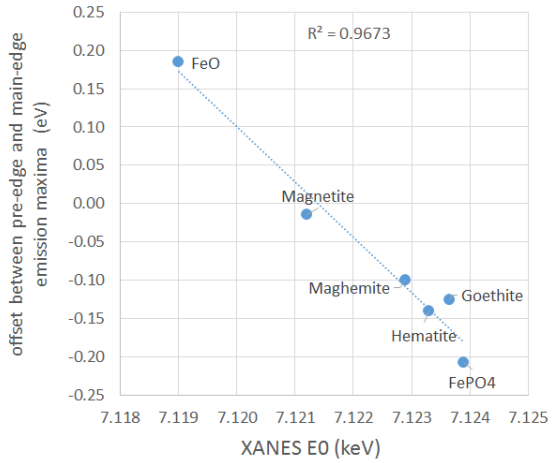

Fig. 4: Energy shift caused by exchange interaction plotted against the position of the main absorption edge.

^{IV}Fe(III)), shows no splitting in excitation energy direction, but significant splitting in emission energy direction.

By comparing the emission energy maxima at the pre-edge ("c/b") with emission energy maxima at the main edge ("c/a", data not shown) we get insight in the so called exchange interaction, i.e. in how far the energy level of the 3p orbitals (transition "c") is sensitive to the presence of an excited electron in the 3d orbital. Values obtained for Fe in our model compounds are plotted in Fig. 4 as a function of the main absorption edge position. The effect observed for Fe is tiny compared to other 3d transition metals (e.g., Ti [7]). It is interesting to note that the energy shift caused by exchange interaction changes sign with changing oxidation state, i.e. ~0.2 eV for Fe(II), ~0 eV for magnetite, and ~-0.1 − -0.2 eV for Fe(III).

As shown here, HR X-ray spectroscopic investigations offer detailed information on the electronic structure of Fe in solids. Fe-Kβ fluorescence has high chemical sensitivity and enables studies of subtle effects like exchange interaction or spin dependent spectroscopy (not shown). Most useful for the characterization of unknown iron phases, however, (tests were performed on leached magnetite, not shown here) is the HR-XANES signal. With respect to HR-XANES we need to mention that this signal can be obtained with higher resolution and flux by recording Fe-Kα fluorescence.

References

[1] Rothe, J. et al., *Rev. Sci. Instrum.*, **83**: 043105 (2012).
[2] Zimina, A. et al., *Rev. Sci. Instrum.*, **88**: 113113 (2017).
[3] Dagan, R. et al., *ATW Int. J. Nucl. Power*, **63**: 526–528 (2018).
[4] Dardenne, K. et al, *J. Nucl. Mater.*, **460**: 209–215 (2015).
[5] Rothe, J. et al., *Geosciences*, **9**: 91 (2019).
[6] Prieur, D. et al., *J. Chem. Thermodyn.*, **97**: 244–252 (2016).
[7] Kas, J. et al., *Phys. Rev. B*, **83**: 235114 (2011).

7.2 Laser spectroscopy

N. Adam, M. Trumm, B. Schimmelpfennig, P. J. Panak

in cooperation with

V. C. Smith,[a] *R. T. A. MacGillivray*[a]

[a] University of British Columbia, Department of Biochemistry and Molecular Biology and Centre for Blood Research, 2350 Health Sciences Mall, Vancouver, British Columbia V6 T 1Z3, Canada

Introduction

If radionuclides are accidentally released to the environment, actinides in particular can cause a serious health risk due to their high radiological and chemical toxicity. However, little is known about the chemical behaviour and potential toxic effects of actinides when incorporated in the human body. For the development of potential decontamination therapies a detailed understanding of the mechanisms of relevant biochemical reactions is urgently required.[1]

A potential reaction that incorporated actinides might undergo is the coordination to human serum transferrin (hTf), the Fe(III) carrier protein in human blood. The complexation of Cm(III) as a representative of trivalent actinides with human serum transferrin and the recombinant N-lobe of human serum transferrin hTf/2N was investigated in previous studies using time-resolved laser fluorescence spectroscopy (TRLFS), extended X-ray absorption fine structure (EXAFS) and UV/Vis spectroscopy.[2-5] The results indicate that Cm(III) coordinates at the Fe(III) binding sites of transferrin under physiologically relevant conditions. Consequently, complexation to transferrin might be a relevant reaction for the distribution of trivalent actinides in the human body. However, no information on the structure of Cm(III) bound at the N- and C-terminal binding sites of transferrin is available yet. Hence, the complexation of Cm(III) with two single point mutants H249A (His → Ala) and Y95F (Tyr → Phe) of the recombinant N-lobe of human serum transferrin hTf/2N was studied using TRLFS. Both mutants are characterized by a substitution of amino acid residues involved in Fe(III) complexation at the N-terminal binding site by non-complexing residues. The experimental results are complemented by molecular modelling. Molecular dynamics (MD) simulations together with DFT (Density Functional Theory) calculations give insights into the three-dimensional structure of Cm(III) bound at the transferrin binding sites. Furthermore, the synergy between vibronic sideband spectroscopy and quantum-chemical computations of vibrational modes allows the identification of the coordinating groups.

Complexation of Cm(III) with the H249A and Y95F mutants

The complexation of Cm(III) with the hTf/2N single-point mutants Y95F (Tyr → Phe) and H249A (His → Ala) was investigated in the pH range from 3.5 to 11.0. The spectra are compared to those of Cm(III) with the native transferrin obtained in previous studies. The latter are characterized by a sharp emission band at $\lambda_{max} = 620$ nm representing the complexation of Cm(III) at the C- and N-terminal binding sites. In case of the Y95F mutant this emission band is missing in the pH dependent spectra (Fig. 1, top) indicating that no complexation of Cm(III) occurs at the binding site. Hence, Tyr 95 plays a key role for the Cm(III) binding at the N-terminal binding site of transferrin. The substitution of Tyr 95 by the non-complexing amino acid

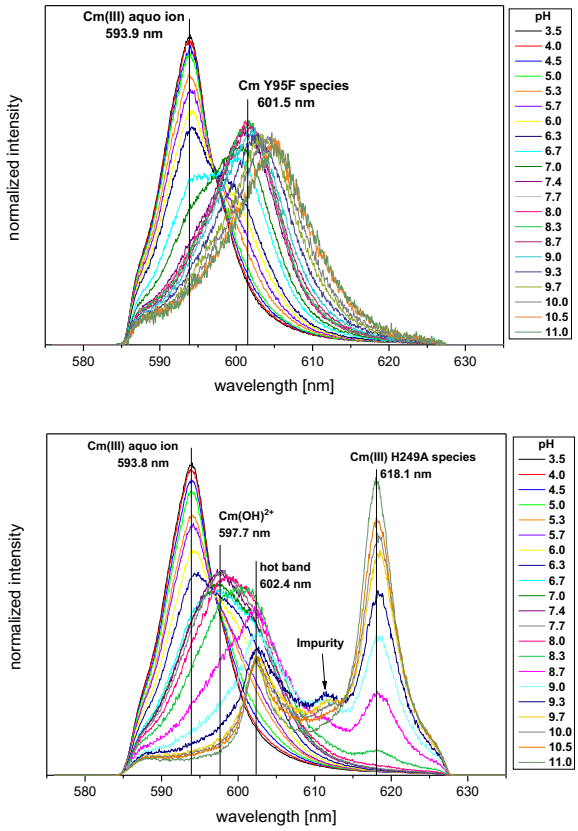

Fig. 1: Normalized fluorescence spectra of the Cm(III) Y95F (top) and H249A (bottom) complexation in the pH range between 3.5 and 11.0; c(Cm) = 1.0·10^{-7} M, c(H249A) = c(Y95F) = 5.0·10^{-6} M, TRIS 10 mM, NaCl 150 mM, T = 296 K.

Phe prevents Cm(III) from forming a strong, multidentate complex at the binding site of the mutant.
In case of the H249A mutant (Fig. 1, bottom) shape and position of the emission band at λ_{max} = 618 nm is comparable to those of Cm(III) coordinated at the C- and N-terminal binding sites of transferrin.[2, 6] The slight blue shift of the emission band is attributed to small variations in the ligand field upon mutation of the His 249 residue. Replacement of His by the non-complexing ligand Ala introduces a slight change to the protein structure and the coordination environment of Cm(III) at the binding site. Furthermore, a significantly higher pH is required to obtain Cm(III) complexation at the binding site of the H249A mutant. The Cm(III) H249A species is formed above pH 8.0 which is 0.6 pH units higher compared to the intact transferrin N-lobe. Nevertheless, Cm(III) complexation at the binding site still occurs which proves that His 249 is not a key ligand like Tyr 95. This is in agreement with the chemical properties of Cm(III) as actinides prefer complexation with hard O donor atoms.

MD simulation of Cm(III) bound at the transferrin binding site

Further structural information was obtained using quantum chemical calculations of Cm(III) complexed at the N-terminal binding site. After the initial equilibration period, the Cm(III) hTf/2N species is formed owing to an applied force. For the subsequent equilibration of the entire protein, another 50 ns were required. As the ionic radii of Fe(III) and Cm(III) show significant differences, we expected different coordination forms accordingly.[7] Analyzing the latter 100 ns of the MD trajectory, all coordinating groups present in the Fe(III) complex are also found for Cm(III), i.e. Asp 63, Tyr 95, Tyr 188 and His 249 in addition to two water molecules, one monodentate and one bidentate carbonate ion. The coordination number of the carboxylic group in Asp 63 is determined to CN_{Asp63} = 1.2 (cf. Table 1) which is in agreement to previous studies also confirming monodentate complexation for the Fe(III) transferrin complex.[8, 9] Furthermore, we determined different bond-lengths for the two tyrosine groups (even after DFT optimization) highlighting their different roles within the complex formation as proposed by He *et al.*[8]

Table 1: Coordination numbers (CN) and bond distances from DFT optimizations (Tyr 95 and Tyr 188 deprotonated, coordination of OH^- instead of H_2O is assumed).

	CN (MD)	CN (DFT)	bond length [Å]
COO^- Asp 63	1.2	1	2.52
C-O^- Tyr 95	1.0	1	2.43
C-O^- Tyr 188	0.9	1	2.51
N-C His 249	0.9	1	2.91
OH^-	-	2	2.07
CO_3^{2-} (bidentate)	1.8	2	2.44
CO_3^{2-} (monodentate)	1.1	1	2.31

Vibronic Sideband Spectroscopy (VSB)

Vibronic sideband spectroscopy (VSBS) is a versatile technique that is used to identify the direct coordination environment of luminescent ions.[3, 10-14] Vibronic sidebands originate from the coupling of electronic transitions from the metal ion with vibrational modes from the coordinating ligands.[15, 16] For the measurement of vibronic sidebands, conditions need to be selected at which the species investigated is present as a pure component. Therefore, the vibronic sidebands of Cm(III) H249A were measured at pH 11.0 in the wavelength range from 620 to 850 nm. The corresponding vibrational energies were calculated from the positions of the vibronic sidebands relative to the zero phonon line (ZPL), which is the Cm(III) H249A emission band at λ_{max} = 618.1 nm. The spectra showed three broad main sidebands at 778 cm^{-1}, 1258 cm^{-1} and 1543 cm^{-1} (Fig. 2).

The vibronic sidebands of the Cm(III) H249A species were compared to those of the Cm(III) bound at the C-terminal binding site of transferrin determined at pH 11.0 (Fig. 2). The spectra are in good agreement indicating the similarity of the coordination environment of Cm(III) at the C-terminal binding site of transferrin and at the binding site of the H249A mutant confirming the minor role of His in Cm(III) complexation at the binding sites. These results are in excellent agreement with those obtained from the pH dependent Cm(III) transferrin and H249A emission spectra described in the previous sections.

The assignment of the measured vibronic sidebands to vibrational modes of the coordinating ligands in the Cm(III) complexes with transferrin and H249A has not been possible to date. Unfortunately, there are no literature data on vibrational energies of different amino acid residues of the proteins available. Therefore, MD+DFT simulations were performed to calculate the vibrational modes of Asp 63, Tyr 95, Tyr 188 and His

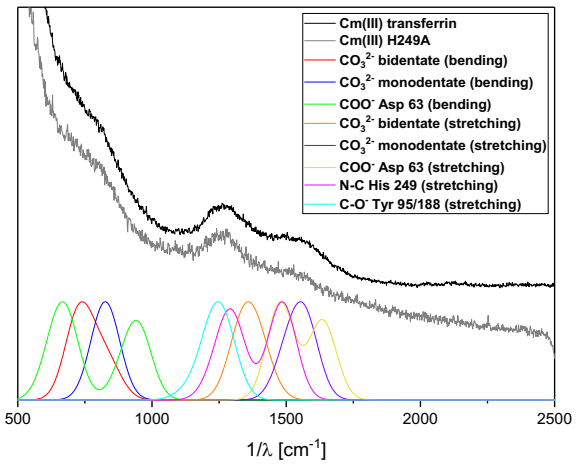

Fig. 2: Comparison of the measured VSB spectra of Cm(III) transferrin and Cm(III) H249A with calculated vibrational frequencies from DFT optimizations (Tyr 95 and Tyr 188 deprotonated, coordination of OH^- instead of H_2O is assumed).

249 as well as of H_2O and CO_3^{2-}. These studies have the potential to identify the coordinating ligands of Cm(III) at the transferrin binding sites.

Calculation of vibrational modes

For the calculation of the structure and the vibrational modes of hTf/2N the protonation/deprotonation of the functional groups was taken into account. Based on the pK_a values of the different amino acid residues we assumed His to be neutral and Asp as well as both Tyr residues to be deprotonated under the given experimental conditions (pH 11). Furthermore, OH^- is taken into account as a potential binding partner for Cm(III).

Based on geometry optimizations, the average bond distances were obtained as summarized in Table 1. The His 249 bond is very weak compared to those of the other coordinating amino acid residues. Computed vibrational modes agree very well with the measured VSB spectra of Cm(III) transferrin and Cm(III) H249A (Fig. 2). However, since several modes overlap it is not possible to make a definite assignment of the measured frequencies. It should be noted that calculated intensities are solely determined by relative abundances of the vibrational modes and are not as reliable as the band positions.

Considering the first vibronic sideband, bending modes of both carbonates and Asp 63 correspond well to the broad shoulder at 778 cm^{-1}. Theoretical results hence suggest the band at 1258 cm^{-1} to be composed of deprotonated tyrosine C-O stretching, His 249 N-$C^{(2)}$ stretching and bidentate carbonate stretching modes (see Fig. 2). Excluding water bending modes, the results indicate that the band at 1543 cm^{-1} envelopes His 249 N-$C^{(1)}$ stretching, monodentate carbonate stretching and Asp 63 stretching modes.

In the present study, the coordination environment of Cm(III) bound at the Fe(III) binding sites of transferrin was investigated using a combined experimental and theoretical approach. The combination of time-resolved laser fluorescence spectroscopy and theoretical modelling provides detailed information on the structure of Cm(III) transferrin for the first time. These results contribute to a better understanding of actinide - protein interaction mechanisms and are therefore of major importance for the identification of relevant transport mechanisms of incorporated radionuclides in the human body.

References

[1] A. E. V. Gorden, et al., *Chem Rev*, **103**, 4207-4282 (2003).
[2] N. Bauer, et al., *Dalton T*, **43**, 6689-6700 (2014).
[3] N. Bauer, Dissertation thesis, Ruprecht-Karls-Universität Heidelberg (2015).
[4] M. Sturzbecher-Hoehne, et al., *J Am Chem Soc*, **135**, 2676-2683 (2013).
[5] N. Bauer, et al., *New J Chem*, **39**, 1375-1381 (2015).
[6] N. Bauer, et al., *Dalton T*, **44**, 1850-1857 (2015).
[7] R. D. Shannon, *Acta Crystallogr., Sect. A: Found. Crystallogr.*, **32**, 751-767 (1976).
[8] Q. Y. He, et al., *Biochemistry*, **36**, 14853-14860 (1997).
[9] H. Abdizadeh, et al., *J Biol Inorg Chem*, **20**, 705-718 (2015).
[10] S. L. Chodos, et al., *J Chem Phys*, **62**, 2411-2417 (1975).
[11] H. Ewald, *Ann. Phys.*, **426**, 209-236 (1939).
[12] S. Freed, *Rev. Mod. Phys.*, **14**, 105-111 (1942).
[13] I. E. T. Iben, et al., *Biophys J*, **59**, 1040-1049 (1991).
[14] M. Trumm, et al., *Dalton T*, **45**, 12308-12311 (2016).
[15] G. Blasse, *Inorg Chim Acta*, **167**, 33-37 (1990).
[16] G. Blasse, *Int Rev Phys Chem*, **11**, 71-100 (1992).

7.3 Microscopy and surface analytics

D. Schild, E. Soballa, N. Ait Mouheb

In co-operation with:

N. Börsig

Karlsruhe Institute of Technology (KIT), Institute of Applied Geosciences, Adenauerring 20b, 76131 Karlsruhe, Germany

Introduction

Corrosion of steel containers in a nuclear repository after a potential ingress of aqueous solution is a source of dissolved iron species, radionuclides, and corrosion products. Co-precipitation of dissolved radionuclides, e.g. ^{79}Se, with steel corrosion products in combination with redox reactions can result in less soluble solid radionuclide forms in the near field. In the far field and under more oxic conditions, Fe(III)-minerals are able to attenuate migration of radionuclides by adsorption and incorporation.

The engineered barrier around nuclear waste containers may consist of cement and surrounding bentonite. Interaction of cement with bentonite pore water can affect the integrity of the barrier.

Retention of selenium oxyanions during the transformation of iron minerals

In this study, we investigated the retention of the aqueous selenium oxyanions selenite $Se^{(IV)}O_3^{2-}$ and selenate $Se^{(VI)}O_4^{2-}$ during the formation of magnetite via $Fe(OH)_2$ and green rust. In addition, the retention of selenium oxyanions by the ferrihydrite-hematite recrystallization is investigated which are typical corrosion products and minerals under oxic conditions.

^{79}Se with a half-life of about 0.327 Ma is one of only seven long-lived fission products and thus relevant in the context of nuclear waste repositories. ^{79}Se decays via β^- (151 keV) without γ-emission and can have a major impact on the total dose rate in the aquifer in the period of 5E+3 to 5E+5 years after nuclear waste disposal. In nature, Se occurs with valences –II, -I, 0, IV, or VI. Se(-II), Se(-I), and Se(0) form less soluble metal selenides or elemental Se. In spent nuclear fuel, Se(-II) is detected, whereas in vitrified highly active waste Se is present in the tetravalent state. Dissolution of waste forms and oxidizing radiolysis products can result in its oxidation to Se(VI). In aqueous systems at high redox potential and neutral to alkaline pH values, selenium is highly mobile in form of the oxyanions selenite and selenate. The Se oxyanions are not sorbing onto kaolinite and montmorillonite at pH > 8, with selenate being the most mobile species.

In a nuclear repository, neutral to alkaline pH values and anoxic conditions are expected to prevail. Anoxic corrosion of steel containers in aqueous solution results in the formation of $Fe(OH)_2$ and H_2. At T > 50°C, $Fe(OH)_2$ transforms to magnetite, water, and hydrogen (Schikorr reaction). At lower temperatures, $Fe(OH)_2$ transforms to intermediate, instable green rust and finally to magnetite, water, and hydrogen.

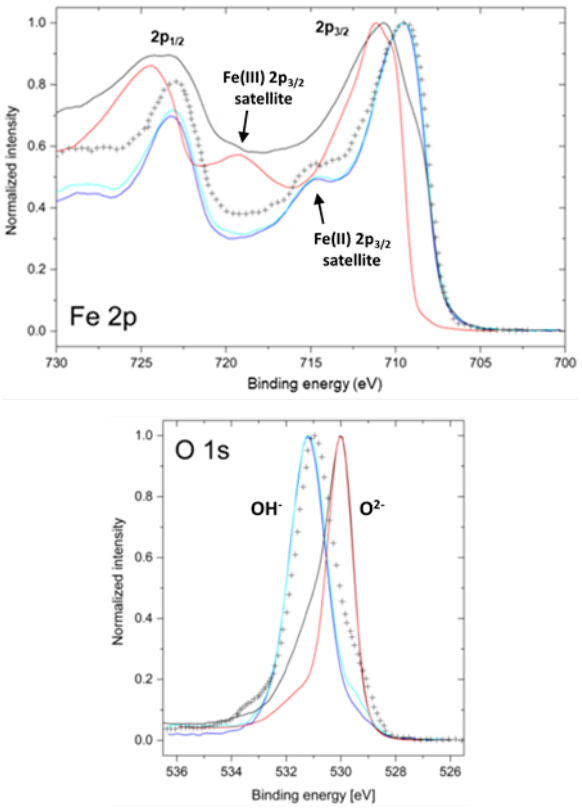

Fig. 1: Narrow scans of Fe 2p and O 1s elemental lines of selenite (blue curve) or selenate (cyan curve) co-precipitated with Fe^{2+}. Comparison with α-Fe_2O_3 [3] (red curve), Fe_3O_4 [3] (black curve), and green rust carbonate [2] (cross symbols).

To simulate the characteristics of Se oxyanions in presence of corroding steel, non-radioactive Se oxyanions were co-precipitated with Fe^{2+} under anoxic conditions. Progressive mild oxidation yielded a final pH of 9.2. More than 99% of selenite and selenate were removed from solution of initial concentrations tested in the range of 0.1 to of 5 mM. The time-dependent reaction was investigated by aliquots taken after 30 minutes and 2 days of reaction and analysed by various techniques [1].

XPS was performed by a ULVAC-PHI VersaProbe II spectrometer by use of monochromatic Al K_α (1486.7 eV) X-ray excitation. Survey spectra and narrow scans of elemental lines were acquired to characterize element composition and bonding state of the elements. The O 1s elemental lines of hydroxide at 531.2 eV or Fe_3O_4 at 530.0 eV were used as charge references

Se lines:	*3s*	*$L_3M_{45}M_{45}$*	*$3p_{3/2}$*	*$L_2M_{45}M_{45}$*	*Valence*
A*)	228.2	178.6	159.9	137.6	Se(-II)
B*)	228.3	178.8	159.8	137.6	Se(-II)
A**)	229.8	179.2	161.2	137.9	Se(0)
B**)	230.0	179.0	161.1	137.9	Se(0)
Se [5]	n/a	n/a	161.2	n/a	Se(0)
Na_2SeO_3 [5]	n/a	n/a	164.1	n/a	Se(IV)
Na_2SeO_4 [5]	n/a	n/a	165.8	n/a	Se(VI)

*Tab. 1: Binding energies of Se elemental lines and valence of Se after co-precipitation of selenite (A) or selenate (B) with Fe^{2+}; *) after 30 min., **) after 2 days of reaction. Reference binding energies of Se(0) as well as Se(IV) and Se(VI) compounds are given for comparison.*

at the samples [2], which is equivalent to charge referencing to the C 1s elemental line of adventitious hydrocarbon at 284.8 eV. The error of binding energies of elemental lines was estimated to ± 0.2 eV. After 30 minutes of reaction, XPS surveys of the precipitates detected selenium in the concentration range of (0.3-0.7) at%, indicating that most of the initial selenium oxyanions were removed from solution. Narrow scans of Fe 2p and O 1s elemental lines are similar in both cases of initial addition of selenite or selenate, as depicted in Figure 1. The Fe $2p_{3/2}$ elemental lines show a maximum intensity at a binding energy of around 709.5 eV and a satellite spacing of 4.7 eV to the main line, characteristic of Fe(II). The O 1s spectra exhibit intense lines at 531.2 eV typical of hydroxide. The Fe 2p and O 1s spectra are similar to those of green rust carbonate [3] but differ clearly from those of α-Fe_2O_3 and Fe_3O_4 samples [4]. Compared to Fe(II), the Fe 2p component of Fe(III) has a higher binding energy and a characteristic satellite with around 8.2 eV distance from the main line.

The Fe 3p elemental line superposes the Se 3d lines commonly used for speciation of selenium. Therefore, binding energies of the photoelectron lines Se 3s and Se $3p_{3/2}$ as well as the Auger lines Se $L_3M_{45}M_{45}$ and Se $L_2M_{45}M_{45}$ were measured and compared to references [5], compiled in Table 1. After 30 minutes of reaction the elemental lines of Se were assigned to Se(-II), regardless if selenite or selenate oxyanions are initially used for co-precipitation with Fe^{2+}. The reduction of selenium oxyanions and formation of nano-particulate iron selenide (< 100 nm) with low solubility is enabled by oxidation and transformation of instable $Fe(OH)_2$ to green rust, in line with findings by XAS [1]. Since the concentrations of chloride and carbonate in solution is higher than that of selenium oxyanions, green rust is present in the chloride and carbonate form and appearance of selenite or selenate green rust can be excluded.

After 2 days of reaction and mild oxidation, the green rust transforms into magnetite. FeSe is oxidized and selenium becomes zero-valent as detected by XPS (Table 1). The binding energies of the photoelectron lines Se 3s and Se $3p_{3/2}$ are more sensitive to the valence state than the Auger lines. Micrometer sized trigonal selenium crystals are identified by SEM-EDX and XRD [1]. In this form, the selenium is preserved, although Se(0) is not thermodynamically stable under alkaline, oxic conditions. The selenium crystals formed during co-precipitation are more stable against re-dissolution than adsorbed selenite or selenate oxyanions. Adsorption of selenate onto magnetite is low and no reduction is detected at hydrochemical conditions similar to the co-precipitation experiments performed, i.e. pH 9.2. At lower pH values under anoxic conditions, e.g. pH 5.3, selenite is readily reduced by magnetite to Se(-II) and subsequently precipitated to FeSe with solubility lower than 6.3E-8 M [6].

Under oxic conditions, co-precipitation of selenium oxyanions with dissolved Fe^{3+} results in adsorption of selenium oxyanions onto ferrihydrite, which is the first precipitated iron phase [7]. During transformation of the amorphous ferrihydrite to crystalline hematite the selenium oxyanions are incorporated and immobilized (pH 7.5, 50° C). The initial valence state of selenium is maintained as indicated by XPS. Selenite at initial concentrations of 0.01 to 1 mM is retained by more than 99%, whereas selenate uptake from solution is only in the range of 10-15%. Selenite uptake during transformation of ferrihydrite to hematite is still higher than pure adsorption to hematite. Desorption experiments indicate higher selenite desorption in case of previous adsorption than for co-precipitation [7].

The results of these studies demonstrate that reduction of selenium oxyanions during co-precipitation with Fe^{2+} or incorporation by hematite can attenuate migration of mobile selenium oxyanions under alkaline condition more effectively than adsorption onto mineral surfaces.

Interaction of low pH cement with bentonite pore water

In most of the concepts developed internationally, concrete and clay materials are used as confinement barriers for radioactive waste. Both materials are chemically very different and their interactions might alter their chemical and physical characteristics. In order to increase the durability of these barriers, low pH cements were developed within the nuclear waste disposal context. Understanding of the interactions occurring between low pH cement materials and clay is of high importance in order to simulate the engineered barrier alteration. In the framework of the HORIZON 2020 “Cement-based materials, properties, evolution, barrier functions (Cebama) Project”, the characterization of the alteration process occurring at the low pH cement / clay pore water interface (MX-80 bentonite) has been performed by using SEM-EDX.

The sample selected for this study is the hydrated low pH cement paste, which was manufactured within the project by the Technical Research Centre of Finland (VTT). The hydrates and raw materials identified in this low pH cement paste (pH 11.7) are described in [8]. Initially, the sample is mainly composed of C-(A)-S-H phases with Ca/Si ratios between 0.6 - 1.1 and an Al/Si ratio of 0.05. Unreacted silica fume is also present, while ettringite is identified as a minor hydrated

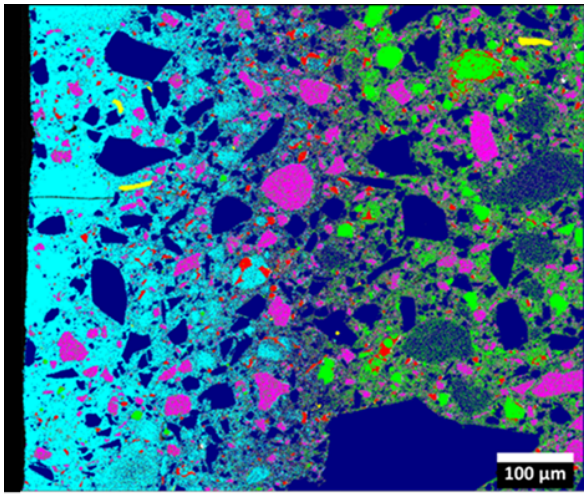

Fig. 2: Phase distributions in false colours overlaid on the electron image of a cross-section of low pH cement (Cebama type) after contact with bentonite pore water. Left side: surface of cement, Mg-exchanged C-S-H (cyan, C/S=0.17), quartz filler (blue), $MgAlCa_4Si_3O_xH_y$ (pink), belite (green), tetracalcium aluminoferrite (red), muscovite (yellow).

solid phase. Unreacted clinker (alite and belite), blast furnace slag, and quartz filler were identified as well in the sample. No portlandite or Friedel's salt are present.

The experimental set-up consists of batch experiments, where fully saturated low pH cement samples with a dimension of 10×10×10 mm^3 are placed in polyethylene containers filled with a volume of 40 ml of bentonite pore water. In order to study alteration in one dimension, the sample is sealed with an epoxy resin, except to one side kept in contact with bentonite pore water (pH 8). Since calcium-silicate-hydrates (C-S-H) with C/S ratio of 0.8 are unstable below pH 10 [9], their decalcification is expected.

After 6 months of reaction under anoxic condition at room temperature, the low pH cement is immersed in isopropanol in order to stop the reaction. To characterize the alteration zone, and to identify qualitatively the chemical perturbation of the low pH cement, SEM-EDX mapping was applied to polished cross-sections. Multivariate analysis is used to explore the full spectral

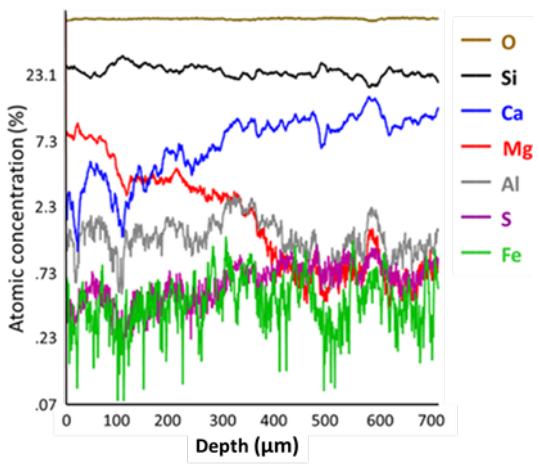

Fig. 3: Elemental depth profile extracted from the data of the map depicted in Figure 2.

data stored at every pixel of the map (Thermo Scientific Pathfinder software, ver. 1.3). A phase is defined if a certain amount of similar spectra is present in the dataset. The phases differ in their elemental compositions and are not necessarily crystalline. A result of such a procedure is depicted in Figure 2. However, the phases originally containing hydrates or hydroxides were transformed to oxides by the heat generated by the impinging electron beam. For this reason, only the elemental ratios are given except for oxygen and hydrogen. Magnesium ($9.65 \cdot 10^{-3}$ M) contained in bentonite pore water reacts with the cement by exchange with calcium. Particles of $MgAlCa_4Si_3O_xH_y$ (attributed to blast furnace slag not reacted) and belite (Ca_2SiO_4) are transformed at the magnesium exchanged zone to magnesium containing phases with C/S = 0.17 and M/S = 0.4. The abundance of tetracalcium aluminoferrite ($4CaO \cdot Al_2O_3 \cdot Fe_2O_3$) particles is also diminished in the magnesium exchanged zone. Quartz filler particles are transforming but appear more resistant. This observation suggests that the various solid compounds of the clinker react with the aqueous solution by forming either cement-hydrates, i.e. C-S-H phases, or secondary phases such as Mg-exchanged C-S-H.

Due to mineralogical heterogeneity of the cement, 70% of the map data of Figure 2 was analysed to derive the elemental depth profile depicted in Figure 3. At the cement surface, a max. Mg/Ca ratio of 3 is observed. At a distance of about 140 µm from the surface, the magnesium and calcium concentrations are equal and at 400 µm the magnesium concentration is similar to the bulk concentration of around 0.9 at%. Finally, precipitation of calcite particles is observed on the altered surface of the Cebama cement paste. The high gradient in partial pressure of CO_2 across the interface stimulates the rapid precipitation of solid carbonates, such as calcite. In addition, the elemental depth profile shows a decrease of sulphate in the altered zone. The pH decrease in the cement close to the surface leads to instability of ettringite, and the released sulphate diffuses towards higher pH regions into the cement, where additional ettringite can form.

References

[1] Börsig, N. et al.; *Dalton Trans.* **47**, 11002 (2018).

[2] Moulder, J.F. et al., *Handbook of X-ray Photoelectron spectroscopy*, ULVAC-PHI, Inc., Japan, (1995).

[3] Mullet, M. et al.; *Solid State Chem.* **181**, 81 (2008).

[4] Huber, F. et al.; *Geochim. Cosmochim. Acta* **96**, 154 (2012).

[5] Jordan, N.; Ph. D. dissertation, University of Nice (2008).

[6] Scheinost, A.C. et al.; J. Contam. Hydrol. **102**, 228 (2008).

[7] Börsig, N. et al.; *Geochim. Cosmochim. Acta* **206**, 236 (2017).

[8] Ait Mouheb, N. et al.; Cem. Concr. Res. in preparation (2019).

[9] Bernard, E. et al.; *Appl. Geochem.* **89**, 229 (2018).

7.4 Investigations of radioactive materials by NMR spectroscopy

Th. Sittel, Ch. Adam, N. Finck, M. Trumm, A. Bauer, M. Trumm, A. Geist, U. Müllich, P. J. Panak

In co-operation with:

F. Galluccio[a], E. Macerata[a], M. Mariani[a], E. Mossini[a], M. C. Gullo[b], A. Casnati[b]

[a] Politecnico di Milano, Italy, [b] University of Parma, Italy

Introduction

NMR spectroscopy is a widely used spectroscopic method in organic and inorganic chemistry. A wide variety of experiments can be performed with a single machine, yielding a wealth of chemical information (Figure 1). Experiments are feasible for substances in liquid or solid state and on a broad range of nuclei. This has led to applications of NMR in fields ranging from small molecule spectroscopy to geochemistry and even biomolecular NMR with its focus on protein molecules of several kilodaltons molecular weight.

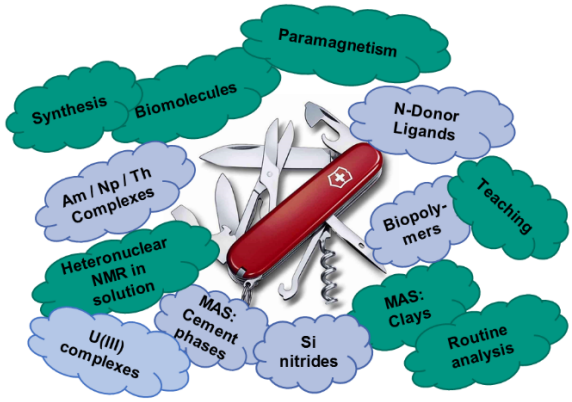

Fig. 1: NMR spectroscopy as the chemists' Swiss army knife.

Our main research activities are in the field of f-element coordination chemistry, thus we are also engaged in the synthesis of new ligands, but also in solid-state spectroscopy and actinide coordination chemistry.

Impact of the solvent polarity on the ligand configuration in Th(IV)-BTP complexes

For the separation of trivalent actinides and lanthanides highly selective ligands are required. Soft N-donor ligands such as bis(triazinyl)pyridines (BTPs) are known for their high selectivity.[1,2] The molecular origin of this selectivity is a topic of fundamental scientific interest. NMR spectroscopy is a valuable tool to determine interactions between metal ions and donor ligands. For actinides and lanthanides, the interactions are dominated by electrostatic interaction. However, due to the overlap of frontier orbitals, the interaction is also partially covalent, resulting in a change of electron density distribution in the ligand. This corresponds directly to the change of the local magnetic field and is therefore precisely observable by the chemical shift.

Figure 2 shows the results of the ^{15}N NMR data analysis of [Th(nPr-BTP)$_3$](OTF$_4$) in THF-d$_8$ (lower spectrum) and methanol-d$_4$ (upper spectrum). For the first time we observed different ligand configurations depending on the solvent used. The ^{15}N NMR spectrum (40.58 MHz, 300 K) recorded in methanol-d$_4$ shows four ^{15}N signals suggesting that the ligand binds asymmetrically to the metal ion. In contrast, only two ^{15}N signals were found in the ^{15}N NMR spectrum recorded in THF-d$_8$ leading to the assumption that the symmetry of the ligand in the complex is preserved.

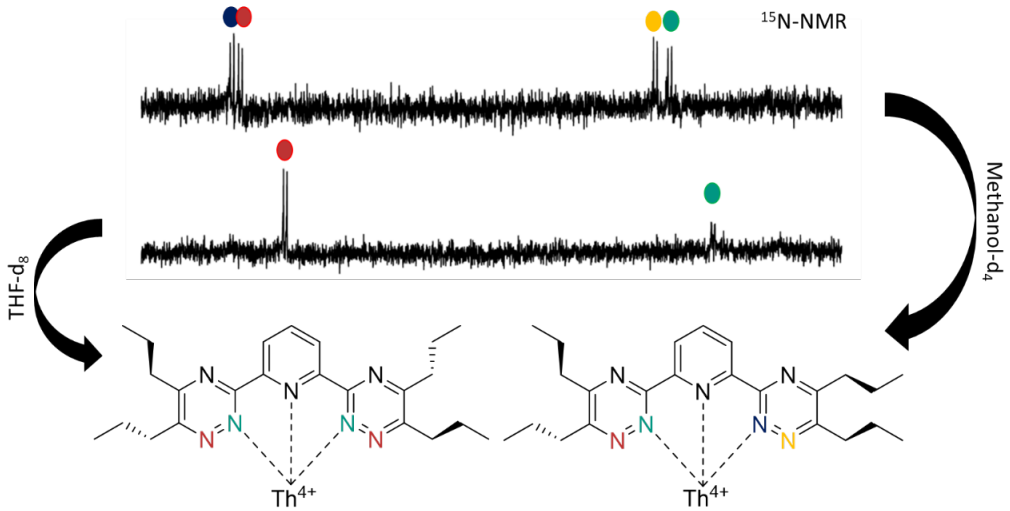

Fig. 2: ^{15}N NMR spectra of [Th(nPr-BTP)$_3$](OTf)$_4$ recorded in THF-d$_8$ and methanol-d$_4$. Depending on the solvent polarity, the stronger solvent-complex interaction in methanol-d$_4$ results in a slightly different ligand leading to twice as many ^{15}N signals as expected.

The suggested ligand structures in the different Th(IV) complexes are shown in Figure 2. Although the Th(IV) ion is complexed by the same nitrogen atoms in both cases, the difference lies within the organization of the nPr side chains. In THF-d_8, the symmetrical organization of the side chains guarantees a minimal repulsion between the three BTP ligands (sym-[Th(nPr-BTP)$_3$]$^{4+}$). This complex structure was also described for the trivalent lanthanide and actinide BTP complexes.[3] In methanol-d_4, this symmetry is broken due to a strong complex-solvent interaction. The side chains of one 1,2,4-triazinyl ring are organized in a way that prevents a fast solvent exchange resulting in twice as many signals in ^{1}H, ^{13}C and ^{15}N spectra (asym-[Th(nPr-BTP)$_3$]$^{4+}$).

To determine whether there is correlation between the ligand configuration in the complex and the solvent polarity, we synthesized [Th(nPr-BTP)$_3$](OTf)$_4$ in a range of deuterated organic solvents. The results show that in polar protic solvents such as methanol or isopropanol asym-[Th(nPr-BTP)$_3$]$^{4+}$ is formed. In contrast, in polar aprotic solvents such as THF or pyridine sym-[Th(nPr-BTP)$_3$]$^{4+}$ is preferably formed. Both complexes are formed simultaneously in cyclohexanol-d_{12} which marks the boundary between polar protic and polar aprotic.

Investigation of clay structures by MAS-NMR spectroscopy

NMR as a versatile spectroscopic method can be used as well for the characterisation of solid substances. However, this requires a special NMR setup that is very different from the normal liquids setup. Signals in the spectra of solids are usually greatly broadened in comparison to those of liquids, as anisotropic inter-actions that cause line broadening (mainly dipolar, quadrupolar and chemical shift anisotropy interactions) cannot be averaged by molecular movement. Dipolar coupling and chemical shift anisotropy can be removed by mimicking molecular motion through fast spinning of the sample in a 4 mm ZrO_2 rotor (up to 15 kHz in the INE NMR setup) around the "magic angle" of 54.74° towards the magnetic field.[4]

In the context of the geochemical research at INE, the interaction of metal ions, especially actinides, with different clay minerals is very important. There are various clay minerals which as a common feature are all made up from octahedral and tetrahedral sheets, but with variations in the filling of the octahedral and tetrahedral sites of the individual minerals. A very important class of clay minerals with a versatile structure are smectites, a subgroup of the phyllosilicates. For example, Al^{3+} ions can be localized in the octahedral layer sheets, and Si in the tetrahedral layer sheets, e.g. pyrophyllite. The incorporation of other ions with different ionic charges leads to changes in layer charge and thereby in the physico-chemical properties, e.g. by substitution of Al^{3+} or other trivalent ions in the tetrahedral silicon sheet. The incorporation of Fe(II) or Fe(III), the most abundant transition metal in the earth's crust, is especially relevant for nuclear waste

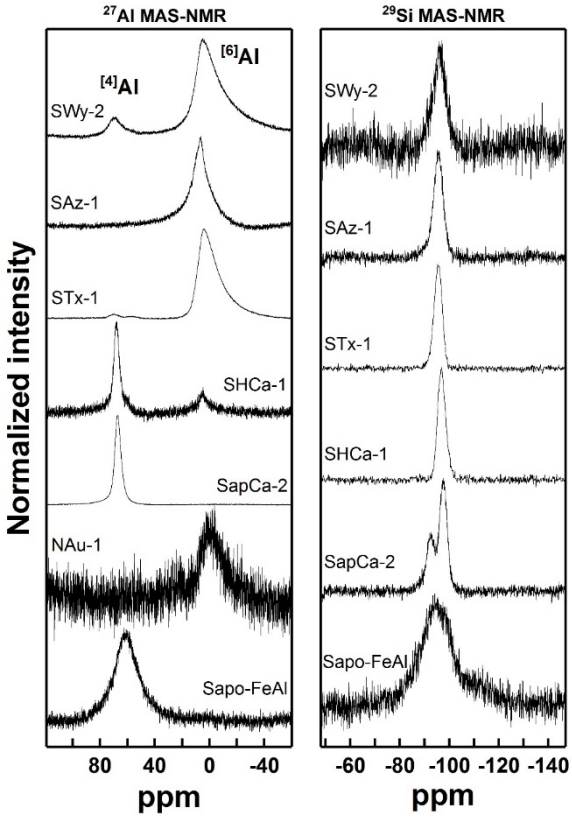

Fig. 3: Experimental ^{27}Al and ^{29}Si MAS-NMR spectra of smectites. The Fe content of the nontronite NAu-1 was too high for ^{29}Si MAS-NMR spectroscopy.

disposal, as the redox couple Fe(II)/Fe(III) influences the clays' specific surface area and reactivity.[5-10]

With ^{27}Al (nuclear spin I = $^5/_2$, natural abundance 100 %) and ^{29}Si (I = $^1/_2$, natural abundance 4.7 %) two NMR active nuclei are available in clay minerals to determine the change in crystal structure at different levels of iron incorporation.[11-13] While iron itself in principle also has an NMR active nucleus (^{57}Fe: I = $^1/_2$, natural abundance 2.1 %) the direct investigation of this metal ion is not possible due to very unfavourable NMR spectroscopic properties as well as the strong paramagnetism of Fe(III). This paramagnetism also leads to a significant line broadening in ^{27}Al and ^{29}Si spectra. In a recent study, we investigated the structure of eight naturally occurring and two synthetic smectites with different charge and charge location, having iron contents between 0.25 % and approx. 35 %. The goal of the study was to determine the distribution of iron within the structural sites and to characterize the local chemical environment. For this, we used ^{27}Al direct excitation MAS NMR spectroscopy as well as ^{29}Si direct excitation and cross-polarization (CP) MAS NMR (Figure 3). In the ^{27}Al spectra, the differences between tetrahedrally coordinated $^{[4]}$Al (signal around 70 ppm) and octahedrally coordinated $^{[6]}$Al (signal around 0 ppm) can be seen very clearly. The relative ratios of the two Al species are determined by their integrals (*cf.* Table 1). ^{29}Si has a much narrower shift range, and signals of different species often overlap and lead to an asymmetrical line broadening. Determination of the

Tab. 1: Distribution of aluminium atoms in different clays as measured by ^{27}Al MAS NMR spectroscopy.

Sample	$^{[4]}Al$		$^{[6]}Al$	
	ppm	%	ppm	%
SWy-2	70	5	5	95
SAz-1	-	-	7	100
STx-1	70	1.5	4	98
SHCa-1	68	77	5	23
SapCa-2	67	100	-	-
NAu-1	-	-	2	100
Sapo-FeAl	61	100	-	-

relative ratios requires fitting of the signal by two or more Gaussian line shapes. However, for example in the saponite SapCa-2 the presence of more than one Si species is obvious. The effects of a high iron content can easily be seen on the broad spectra of the saponite Sapo-FeAl. While this complicates the interpretation of the results, we could clearly show that NMR spectroscopy on minerals containing relatively high concentrations of paramagnetic ions is feasible. Experimental results from NMR spectroscopy are in good agreement with findings by other methods.[14]

NMR spectroscopy on the Am(III)-PTEH complex

We prepared the Lu(III) and Am(III) complexes of 2,6-bis(1-(2-ethylhexyl)-1H-1,2,3-triazol-4-yl)pyridine (PTEH, Figure 4). PTEH is a promising extracting agent to separate An(III) from Ln(III).[15]

$[M(PTEH)_3](CF_3SO_3^-)$ complexes were prepared and characterized extensively by NMR spectroscopy, including direct excitation spectra for ^{1}H and ^{13}C, ^{1}H-^{13}C and ^{1}H-^{15}N correlation spectra, COSY, diffusion-ordered spectroscopy[16, 17] and T_1 relaxation time measurements for the protons.

The most important findings are shown in Figure 4, which shows an overlay of the $^{1}H,^{15}N$-gHMQC correlation spectra for the Lu(III) and Am(III) complexes. Largely differing ^{15}N chemical shifts were observed for the coordinating nitrogen atoms N_1 ($\Delta\delta_{Lu/Am}$ = 259 ppm) and N_8 ($\Delta\delta_{Lu/Am}$ = 330 ppm). The non-coordinating nitrogen atoms N_9 and N_{10} showed only small differences of 14 ppm and 3 ppm, respectively.

This effect is interpreted as a sign for a change in the bonding mode between the ligand and the individual metal ions. The fact that the effect is not propagated into the aromatic ring system beyond the coordinating atoms is a clear indication of a strong Fermi contact interaction, as dipolar effects would be noticeable on all nitrogen atoms. This increased Fermi contact interaction, in turn, is based on an increased share of covalence in the bond. The results are in line with findings for other N-donor ligands studied by NMR spectroscopy.[3, 18]

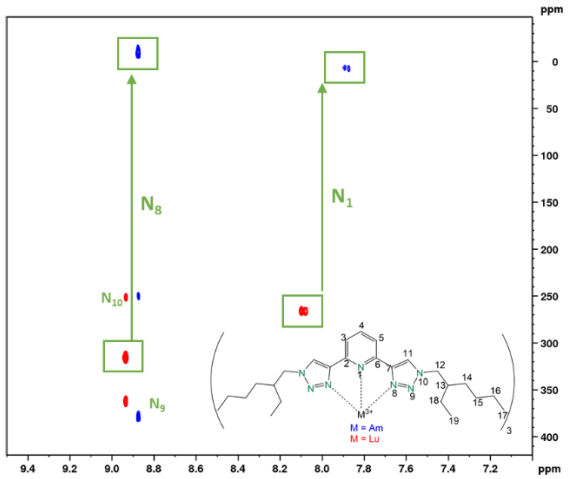

Fig. 4: Overlay of the $^{1}H,^{15}N$-gHMQC spectra for the Lu(III) (red) and Am(III) (blue) complexes of the PTEH ligand.

References

1. Kolarik, Z.; Müllich, U.; Gassner, F., EXTRACTION OF Am(lll) AND Eu(lll) NITRATES BY 2-6-DI-(5,6-DIPROPYL-1,2,4-TRIAZIN-3-YL)PYRIDINES 1. *Solvent Extr. Ion Exch.* **1999,** *17* (5), 1155-1170.
2. Banik, N. L.; Denecke, M. A.; Geist, A.; Modolo, G.; Panak, P. J.; Rothe, J., 2,6-Bis(5,6-dipropyl-1,2,4-triazin-3-yl)-pyridine: Structures of An(III) and Ln(III) 1:3 complexes and selectivity. *Inorganic Chemistry Communications* **2013,** *29*, 172-174.
3. Adam, C.; Kaden, P.; Beele, B. B.; Müllich, U.; Trumm, S.; Geist, A.; Panak, P. J.; Denecke, M. A., Evidence for covalence in a N-donor complex of americium(III). *Dalton Transactions* **2013,** *42* (39), 14068-14074.
4. Duer, M. J., *Introduction to solid state NMR spectroscopy*. 1. publ. ed.; Blackwell: Oxford [u.a.], 2004.
5. Stone, W. E. E.; Sanz, J., Distribution of Ions in the Octahedral Sheet of Micas. In Advanced Chemical Methods for Soil and Clay Mineral Research, Proceedings of the NATO Advanced Study Institute held at the University of Illinois, July 23 - August 4, 1979, Stucki, J. W.; Banwart, W. L., Eds. D. Reidel Publishing Company: Dordrecht, Boston, London, 1980; pp 317 - 329.
6. Stucki, J. W.; Kostka, J. E., Microbial reduction of iron in smectite. *Comptes Rendus Geoscience* **2006,** *338* (6-7), 468-475.
7. Bishop, M. E.; Dong, H. L.; Kukkadapu, R. K.; Liu, C. X.; Edelmann, R. E., Bioreduction of Fe-bearing clay minerals and their reactivity toward pertechnetate (Tc-99). *Geochim. Cosmochim. Acta* **2011,** *75* (18), 5229-5246.
8. Hofstetter, T. B.; Neumann, A.; Schwarzenbach, R. P., Reduction of nitroaromatic compounds by Fe(II) species associated with iron-rich smectites. *Environmental Science & Technology* **2006,** *40* (1), 235-242.
9. Dong, H. L.; Jaisi, D. P.; Kim, J.; Zhang, G. X., Microbe-clay mineral interactions. *Am. Mineral.* **2009,** *94* (11-12), 1505-1519.
10. Jaisi, D. P.; Dong, H. L.; Plymale, A. E.; Fredrickson, J. K.; Zachara, J. M.; Heald, S.; Liu,

C. X., Reduction and long-term immobilization of technetium by Fe(II) associated with clay mineral nontronite. *Chem. Geol.* **2009,** *264* (1-4), 127-138.
11. Mason, J., *Multinuclear NMR*. Plenum Pr.: New York, NY [u.a.], 1987; p XX, 639 S.
12. Kenneth, J. D. M.; Smith, M. E., *Multinuclear solid-state NMR of inorganic materials*. Pergamon: 2002.
13. Thompson, J. G., 29Si AND 27A1 NUCLEAR MAGNETIC RESONANCE SPECTROSCOPY OF 2:1 CLAY MINERALS. *Clay Minerals* **1984,** *19*, 229-236.
14. N. Finck, M.L. Schlegel, K. Dardenne, C. Adam, S. Kraft, A. Bauer, J.-L. Robert, submitted to Physics and Chemistry of Minerals.
15. Ossola, A.; Macerata, E.; Mossini, E.; Giola, M.; Gullo, M. C.; Arduini, A.; Casnati, A.; Mariani, M., 2,6-Bis(1-alkyl-1H-1,2,3-triazol-4-yl)-pyridines: selective lipophilic chelating ligands for minor actinides. *J. Radioanal. Nucl. Chem.* **2018,** *318* (3), 2013-2022.
16. Morris, G. A., Diffusion-Ordered Spectroscopy. In *eMagRes*, John Wiley & Sons, Ltd: 2009.
17. Pelta, M. D.; Morris, G. A.; Stchedroff, M. J.; Hammond, S. J., A one-shot sequence for high-resolution diffusion-ordered spectroscopy. *Magn. Reson. Chem.* **2002,** *40* (13), S147-S152.
18. Adam, C.; Beele, B. B.; Geist, A.; Müllich, U.; Kaden, P.; Panak, P. J., NMR and TRLFS studies of Ln(iii) and An(iii) C5-BPP complexes. *Chem. Sci.* **2015,** *6* (2), 1548-1561.

7.5 Accelerator mass spectrometry (AMS)

F. Quinto, H. Geckeis, D. Glückman, S. Kraft, M. Plaschke, T. Schäfer

In co-operation with:

K. Hain[a], P. Steier[a], Th. Faestermann[b], G. Korschinek[b], U. Mäder[c]

[a]VERA Laboratory, Faculty of Physics, University of Vienna, Währinger Straße 17, A-1090 Vienna, Austria; [b]Physics Department, Technical University of Munich, James-Franck-Straße 1, D-85748 Garching, Germany; [c]Institute of Geological Sciences, University of Bern, Baltzerstrasse 3, CH-3012 Bern, Switzerland.

Introduction

The migration of radionuclides (Rn) away from a deep geological repository for nuclear waste is expected to occur principally by action of groundwater (GW). In crystalline host rock the main migration mechanism is the advection through water conductive fractures. The Rn would be transported after their dissolution in GW or their sorption onto colloidal particles, in particular bentonite colloids generated upon degradation of the geotechnical compacted bentonite barrier (GCBB) surrounding the nuclear waste canisters. Transport in clay host rock as well as through the GCBB would occur via diffusion.

We study the long-term behavior of actinides (An) and ^{99}Tc in natural systems relevant to nuclear waste disposal with both *in situ* Rn tracer tests and the analysis of global fallout in environmental specimens. Samples arising from these experiments present concentrations of the An and ^{99}Tc at levels ≤ fg/g. We carry out such ultra-trace analysis with Accelerator Mass Spectrometry (AMS), currently the most sensitive analytical technique for the determination of An and ^{99}Tc in environmental samples [1].

The AMS measurements of An nuclides were performed at the VERA laboratory (University of Vienna, Austria) employing helium stripping to the 3+ charge state of the An at 1.65 MV terminal voltage [2]. Samples were prepared and measured according to the multi-actinide analysis procedure in which An are concentrated from the sample matrix via iron hydroxide co-precipitation and measured sequentially without previous chemical separation from each other [3].

The AMS measurements of ^{99}Tc were performed at the 14 MV Tandem AMS facility of the Maier-Leibnitz-Laboratorium (MLL) of the Technical University of Munich (TUM, Garching, Germany). At this facility, a Gas-Filled Analyzing Magnet in addition to a 5-fold segmented ionization chamber (GAMS) was available. Such unique GAMS setup offered the capability to effectively suppress the major background source to the mass spectrometric measurement of ^{99}Tc, namely its daughter and stable isobar ^{99}Ru [4].

Migration of An in crystalline host rock

At the Grimsel Test Site (GTS) [5], we have investigated the behavior of An tracers in GW samples through a water conductive feature of the granodiorite rock. In the frame of the CFM run 13-05 [6] we have determined the migration of the ^{233}U, ^{237}Np, ^{242}Pu and ^{243}Am up to 22 months from the starting of the experiment [7]. Furthermore, we have identified in the same GW samples a release from the fracture of ^{241}Am and ^{244}Pu employed 12 years before [7] within the previous *in situ* test CRR run 2 [8]. Following these results and with the aim to study the behavior of the An at the GTS over an even longer time period, we have started investigating the possible migration of global fallout ^{239}Pu, ^{237}Np and ^{236}U through the massive thrust sheet of crystalline rock at the GTS. The global fallout is a known and chronologically defined nuclear contamination source, whose investigation in environmental samples can provide information on the behavior of the An over a time span of 67 years to the present [9].

First information on the behavior of global fallout An at the GTS can be obtained by comparing the concentration of ^{239}Pu, ^{237}Np and ^{236}U in Grimsel GW samples with those in surface water samples collected from the overhead Lake Grimsel. In Fig. 1, the concentration (number of atoms in a sample of 250 ml) of ^{239}Pu, ^{237}Np and ^{236}U measured in Lake Grimsel and in six GW samples are depicted together with those determined in two procedure blanks (Blank_a and Blank_b). The GW samples were collected at different locations that are named: G2, C1, B2, Adus, B5 and F3.

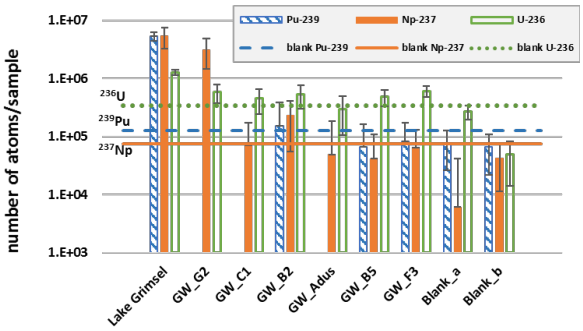

Fig. 1. Concentration of global fallout ^{239}Pu (blue dashed column), ^{237}Np (orange full column) and ^{236}U (green empty column) in Lake Grimsel, Grimsel GW samples and in two procedure blanks (Blank_a and Blank_b). The horizontal lines depict the blank levels of ^{239}Pu (blue dashed line), ^{237}Np (orange continuous line) and ^{236}U (green points line).

A clear global fallout signal is determined in the surface water sample from Lake Grimsel with concentrations of $(5.3 \pm 0.9) \times 10^6$, $(5.4 \pm 2.1) \times 10^6$ and $(1.3 \pm 0.1) \times 10^6$ atoms/250 ml for ^{239}Pu, ^{237}Np and ^{236}U, respectively. As shown in Fig. 1, the An levels

determined in the GW samples are mostly consistent with those found in the procedure blanks, Blank_a and Blank_b, excepting for sample GW_G2 that presents a level of ^{237}Np, equal to (5.3 ± 0.9) × 10^6 atoms/250 ml, significantly higher than the blanks. We also find a concentration of ^{236}U in GW_G2 and GW_F3 that is not consistent with the blank background within one sigma uncertainty, but still very close to it.

Such preliminary results could indicate both the migration of global fallout ^{237}Np in the GW collected at the location G2 and a signature of ^{237}Np from previous *in situ* tracer tests, as demonstrated in [7]. It is interesting to note that the ^{237}Np/^{236}U atom ratio in the GW sample GW_G2 equal to ~5.4, is similar to that found in the surface water sample of Lake Grimsel equal to ~4.3. However, the origin of the ^{237}Np signal in sample GW_G2 and the possible determination of ^{236}U from global fallout in samples GW_G2 and GW_F3 has to be proven with further investigations.

As shown in Fig. 1, the measured levels of ^{239}Pu in GW_B2, GW_B5 and GW_F3 are consistent with the blank background and in GW_G2, GW_C1 and GW_Adus are equal to zero. This result could indicate the retention of Pu in the soil, lake sediments as well as in the fault gauge minerals of the GTS due to sorption and/or filtration processes of Pu(IV) (that is in large part associated to colloids). On the other hand, the determination of ^{237}Np in GW_G2 and possibly of ^{236}U in GW_G2 and GW_F3 could be explained with the preferential migration of U(VI) and Np(V) as dissolved species.

Indeed, in the complex environment of the GTS, the single processes involved in the migration and retention of An cannot be directly identified nor quantified. However, the actual experiment will allow observing the behavior of global fallout An in the long term and on a large scale in a real environment representative of the conditions of a deep geological repository in crystalline host rock.

Development of an analytical method for the determination of An in clay systems at ultra-trace levels

Opalinus clay is under consideration as possible host rock for the geological disposal of HLNW. A particular interest is directed towards the behavior of the An in reducing conditions as those expected in a geological repository in Opalinus clay formations. In reducing conditions, low An solubility and slow An diffusion is expected, correlating with ultra-trace levels of the An diffusing through the clay. In order to verify this assumption, laboratory experiments are planned to study the diffusion of An at low concentration levels under as close as possible natural conditions.

In preparation for these experiments, we have tested an analytical procedure capable of determining several An nuclides in clay materials at ultra-trace concentrations [10]. In the following text, we describe one of the main results of this study.

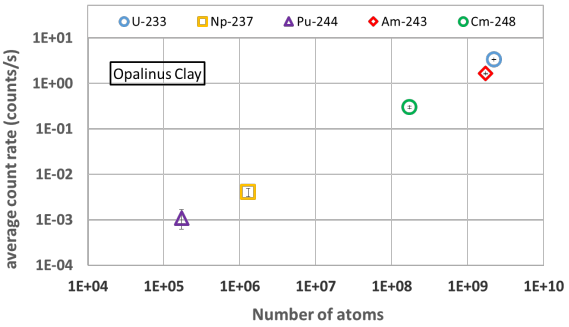

Fig. 2. Average count rate (counts/s) of ^{233}U, ^{237}Np, ^{244}Pu, ^{243}Am and ^{248}Cm as function of their nominal number of atoms in the sample of Opalinus clay spiked with the five An at different concentrations.

Samples simulating specimens obtained after a diffusion experiment were prepared by mixing ca. 100 mg of Opalinus clay, 7 µl of the corresponding synthetic pore water, an An tracer solution and 5 ml 1M HNO_3. The An tracer solution contained ^{233}U, ^{237}Np, ^{244}Pu, ^{243}Am and ^{248}Cm in the relative concentrations resembling the solubility of these An elements in the expected reducing conditions. After a contact time of one week, the samples were submitted to the multi-actinide analysis procedure [3] adapted to the actual sample matrix [10].

As shown in Fig. 2, the simultaneous determination of five An nuclides, whose concentration ranges over four orders of magnitude, is possible down to 10^5 atoms/g in a sample matrix resembling that of a clay sample after a diffusion experiment. These results prove that the diffusion of An through clay in reducing condition can be investigated experimentally at the ultra-trace levels. With the establishment of the actual method, diffusion experiments in reducing condition (and without the addition of any reducing agent) are possible and envisaged for the first time in both laboratory and *in situ* scale.

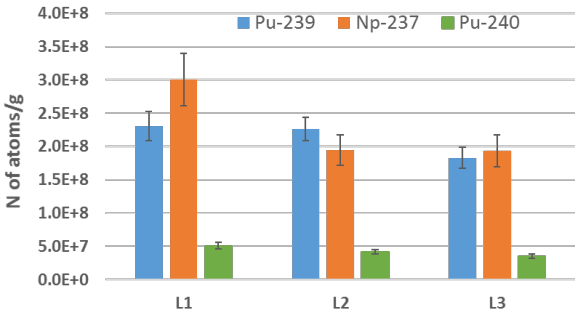

Fig. 3. Numbers of ^{239}Pu, ^{240}Pu ^{237}Np atoms/g in each of the three upper layers of the roof tile L1, L2 and L3.

In another experiment the behavior of global fallout An in a natural clay sample is studied. We have chosen a roof tile being exposed to atmospheric precipitations in the last 100 years covering the period from the pre-nuclear age until now [10]. From the upper surface of the roof tile, three successive layers were collected (L1, L2 and L3), each with a thickness between 110 and 130 µm. From these samples, a concurrent chemical

separation and measurement of the Np and Pu fractions with AMS were performed.

Fig. 3 represents the concentration (number of atoms/g) of ^{239}Pu, ^{240}Pu and ^{237}Np in samples L1, L2 and L3. Clear signals of ^{239}Pu, ^{240}Pu and ^{237}Np were determined in the three investigated layers, indicating the downward migration of the An down to ~360 µm depth. The concentration of ^{239}Pu and ^{237}Np were in the order of magnitude of 10^8 atoms/g. The ^{240}Pu/^{239}Pu isotopic ratio was equal to 0.22 ± 0.03, 0.18 ± 0.02 and 0.19 ± 0.03 in L1, L2 and L3, respectively, and consistent with a global fallout origin, namely 0.18 [9].

We have shown for the first time that the determination of ultra-trace levels of Np and Pu from global fallout is possible in a roof tile [10], providing valuable new information about the behavior of these An in such clay samples exposed to the environment. The analysis of the layers beneath, as well as the mineralogical analysis of the roof tile will provide a better understanding about the relative behavior of the An. The determination of ^{236}U in several layers of the roof tile is as well planned and will allow for the comparison of the behavior of global fallout U with that of Np and Pu.

Diffusion of ^{99}Tc through bentonite

At the GTS, the diffusion of several Rn tracers and, among them ^{99}Tc through bentonite was investigated in the frame of the Long Term In situ Test (LIT). Compacted bentonite rings doped with Rn and ^{99}Tc were positioned in a water conducting shear zone of the GTS in order to simulate the bentonite buffer of an engineered barrier system [11]. In such geometry, the release of Rn into the GW might occur mainly after they have diffused through the bentonite. We have determined the concentration of ^{99}Tc in seven GW samples (each with a volume between 1.7 and 8 ml) collected within a time interval of 129 to 877 d from the starting of the experiment.

As shown in Fig. 4 the concentration of ^{99}Tc in the seven LIT GW samples ranges between ~8×10^6 atoms/ml (~0.8 fg/g) and ~1.2×10^9 atoms/ml (~96 fg/g) in LIT 14-102 and LIT 14-44, respectively. With the GAMS setup and an adapted sample preparation [12], an excellent sensitivity down to 0.5 fg was reached, providing for the first time experimental data on the long-term diffusion (up to ca. 29 months) of ^{99}Tc through bentonite at ultra-trace levels [12]. The access to these low concentration levels will significantly improve the safety assessment of the GCBB.

In addition, a lake water sample (100 ml) from the Wildseemoor (WSM) in Southern Germany was analyzed [12]. The WSM sample presents a concentration of ^{99}Tc equal to ~1×10^6 atoms/ml (~0.5 fg/g), representing a first determination of the level of global fallout ^{99}Tc in a lake sample of Southern Germany [12]. This result paves the way to further investigations of global fallout derived ^{99}Tc in a variety of natural samples, like soil, sediments, peat bog and clay profiles. Such an extensive study would provide a direct observation of the behavior of this long-lived fission product in the environment.

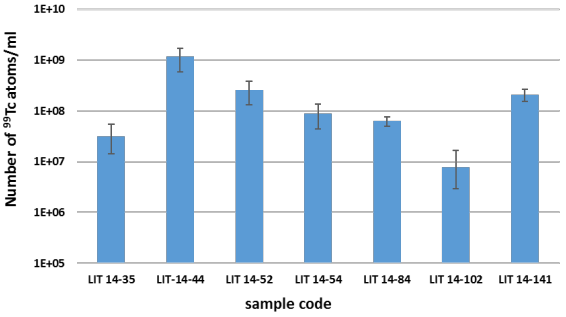

Fig. 4. Concentration of ^{99}Tc (number of atoms/ml) in the seven GW samples from the in situ diffusion test (LIT) at the GTS.

References

[1] P. Steier et al., *Nucl. Instrum. Methods Phys. Res., Sect. B*, **268**, 1045 (2010).

[2] S. R. Winkler et al., *Nucl. Instrum. Methods Phys. Res., Sect. B*, **361**, 458 (2015).

[3] F. Quinto et al., *Anal. Chem.*, **87**, 5766 (2015).

[4] D. Koll et al., F. *Nucl. Instrum. Methods Phys. Res., Sect. B* **438**, 180 (2019).

[5] http://www.grimsel.com/

[6] http://grimsel.com/gts-phase-vi/cfm-section/cfm-introduction/ /

[7] F. Quinto et al., *Anal. Chem.*, **89**, 7182 (2017).

[8] H. Geckeis et al., *Radiochim. Acta*, **92**, 765 (2004).

[9] M. A. Denecke et al., Sources and Behaviour of Actinide Elements in the Environment. In Experimental and Theoretical Approaches to Actinide Chemistry: From Fundamental Systems to Practical Applications, 2016; pp 378-444.

[10] Master Thesis D. Glückman. Development of an analytical method for the determination of actinides in clay systems at ultra-trace levels with Accelerator Mass Spectrometry (AMS) (2018).

[11] L. Schlieckenrieder et al., Colloid Formation and Migration Project: Site instrumentation and initiation of the long-term in-situ test; National Cooperative for the Disposal of Radioactive Waste: Wettingen, Switzerland, (2017).

[12] F. Quinto et al., *Anal. Chem.*, **91**, 4585 (2019).

7.6 Computational chemistry

R. Polly, B. Schimmelpfennig, M. Trumm

Introduction

Computational Chemistry using ab initio, first principle and classical mechanics methods at KIT-INE provides valuable fundamental insights on a molecular scale, greatly assisting, supporting and complementing experimental investigations in the field of nuclear waste disposal. There is a wide range of applications for Computational Chemistry at INE: from providing detailed structures of complex chemical systems including actinides in solution, at surfaces or solid phases, thermodynamic data, spectroscopic information for TRLFS or reproducing experimental XAS and XES measurements, to perform simulations and visualization of complex chemical reactions. Hence, the considered systems vary from molecular species in the gas phase over small complexes in solution to bulk phases or mineral/liquid interfaces at ambient conditions. The synergistic effects at INE resulting from performing theoretical and experimental research together in one house are enormous.

New theoretical methods and the constantly improving hardware allow a steady refinement of the description of actinide systems at the electronic structure level. These improvements also increase the accuracy and reliability of quantum chemistry as a predictive tool.

Incorporation of radionuclides in hydroxycarbonate and hydroxychloride green rust GR(CO_3^{-2}) and GR(Cl^-)

Deep geological disposal is presently considered as the preferred option for the safe management of high-level nuclear waste (HLW) forms, i.e. spent nuclear fuel and vitrified fuel reprocessing residues. In such underground facilities, the HLW will be confined in steel canisters which are foreseen to be surrounded by consecutive manmade (engineered) and natural (host rock) barriers.

Iron (Fe) is the fourth most abundant element in the earth crust and - in the presence of water - commonly found in the form of oxides, hydroxides, or oxide-hydroxides. In a deep geological repository, neutral to alkaline pH values and anoxic conditions are expected to prevail. Iron containing corrosion products resulting from anoxic HLW canister degradation may serve as a major sink for radionuclides released from a breached canister. Under the expected redox conditions Fe(II) oxides are electron acceptors and form mixed-valent Fe minerals [Fe(II)-Fe(III)] such as magnetite and green rust (GR [1], cf. section 8.3). These mixed-valent iron minerals have received a significant amount of attention over the recent decades, especially in the environmental sciences community. They are intrinsic and essential parts of biogeochemical cycling of metals and organic carbon and play an important role regarding the mobility, toxicity, and redox transformation of organic and inorganic pollutants, such as radionuclides. GR compounds are made of brucite-like layers of Fe(II)/Fe(III)-hydroxide with anions and water in the interlayer.

In the present study we focused on the structures of hydroxycarbonate GR(CO_3^{-2}) $[Fe_4^{II}Fe_2^{III}(OH)_{12}]^{2+}\cdot[CO_3^{-2}\cdot 3H_2O]^{2-}$ and hydroxychloride GR(Cl^-) $[Fe_{2,3}^{II}Fe^{III}(OH)_{6,8}]^{+}\cdot[Cl^-\cdot 3H_2O]^-$. For the calculations on GR(CO_3^{-2}) the experimental results of Aissa *et al.* [2] concerning the structural information and the results of Rusch *et al.* [3] reporting the ferrimagnetic properties of GR(CO_3^{-2}) were very helpful to set up our first principle calculations. Refait *et al.* [4] pointed out that there are two possibilities of GR(Cl^-) with an Fe(II):Fe(III) ratio of 2:1 ($[Fe_2^{II}Fe^{III}(OH)_6]^+\cdot[Cl^-\cdot 3H_2O]^-$) and 3:1 ($[Fe_3^{II}Fe^{III}(OH)_8]^+\cdot[Cl^-\cdot 3H_2O]^-$), respectively, and we will consider both of these possible structures here. In a second step we studied the incorporation of Ln^{3+}, An^{3+} into GR(CO_3^{-2}) and Iodide (I^-) into GR(Cl^-) . The results are compared with available experimental data [5,6].

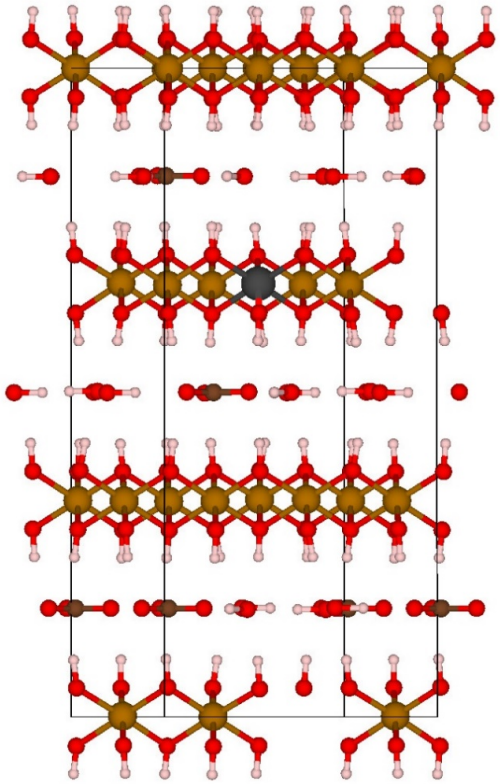

Fig. 1: Structure of $Fe^{II\text{-}III}$ hydroxycarbonate GR(CO_3^{-2}) $[Fe_4^{II}Fe_2^{III}(OH)_{12}]^{2+}\cdot[CO_3^{-2}\cdot 3H_2O]^{2-}$.

From a theoretical perspective, open shell cases such as Fe(II)/Fe(III) are very difficult to tackle. Here we present density functional (DFT+U) calculations on

pure Fe^{II-III} hydroxycarbonate GR(CO_3^{-2}) and hydroxychloride GR(Cl^-). We find that the DFT+U method (U=4.6 eV, J=0.544 eV) [7]) is actually capable to determine the structural parameters (s. Table 1,2,4 and 5), the charges of the [Fe(II)-Fe(III)] ions as well as the magnetic properties of GR(CO_3^{-2}) and GR(Cl^-).

Table 1: Crystallographic data of the pure bulk phase of GR(CO_3^{-2}) (all distances in pm, all angles in °).

	Experimental data [1,2]	DFT+U
V	1190.34	1226.29
a	317.6	320.5
b	317.6	323.5
c	2271.2	2288.1
Interlayer distance	757	763
α	90	89.98
β	90	90.03
γ	120	120.45

Table 2: Interatomic distances for the pure bulk phase of GR(CO_3^{-2}) (all distances in pm).

	Experimental data [1,2]	DFT+U
Fe-OH	209.6	212.0
OH-OH	273.6	276.9
OH-C	333.1	331.6
O-O	262.9	260.4
	278.7	278.9
C-O	117.9	129.7

With these very encouraging results, we proceeded in a second step to study the incorporation of Ln^{3+} and An^{3+} into GR(CO_3^{-2}) and compared calculated results to available experimental data [5].

Table 3: Ln/Am-O distances for the incorporation of Ln^{3+}/An^{3+} into GR(CO_3^{-2}) (all distances in pm).

GR(SO_4^{2-}) [5]	
Am^{3+}-O	242
GR(CO□3□ − 2□)	
La^{3+}-O	240
Eu^{3+}-O	230
Am^{3+}-O	233
Cm^{3+}-O	233

As evident from Table 3, the results we determined for GR(CO_3^{-2}) are in fair agreement with the data for GR(SO_4^{2-}) [5]. The cell parameters of GR(SO_4^{2-}) (see [1,2]) are slightly larger than those of GR(CO_3^{-2}) and hence our result is fully consistent with this data.

For GR(Cl^-) we used the same theoretical approach as outlined above. As pointed out earlier, Refait *et al.* [4] found GR(Cl^-) with different Fe(II):Fe(III) ratios, 2:1 and 3:1. We determined the structures of both species and compared those with the experimental data of Refait *et al.* [4]. Interestingly, although they found two species, Refait *et al.* [4] report only one structure not specifying the corresponding Fe(II):Fe(III) ratio.

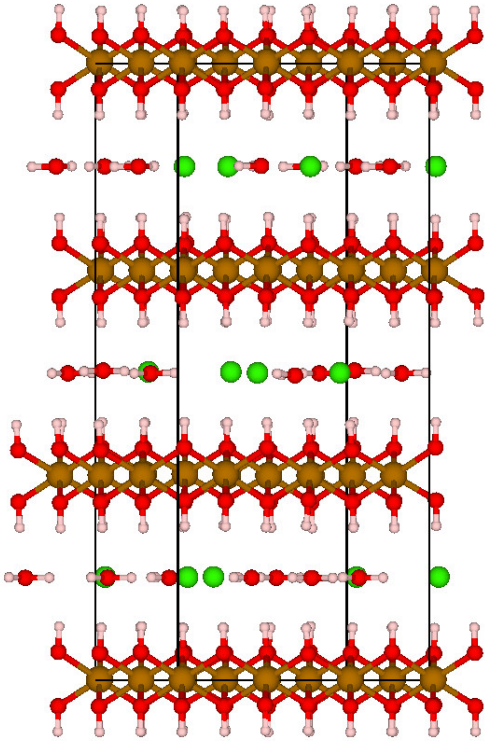

Fig. 2: Structure of Fe^{II-III} hydroxychloride GR(Cl^-) $[Fe_2^{II}Fe^{III}(OH)_6]^+ \cdot [Cl^- \cdot 3H_2O]^-$.

Table 4: Crystallographic data of the pure bulk phase of GR(Cl^-) (all distances in pm).

	Experimental data [1,4]	DFT+U	
Fe(II):Fe(III)		2:1	3:1
a	319.0	322.8	321.9
b	319.0	322.0	322.7
c	2385.6	2377.3	2360.5
Interlayer distance	795	789	787

Table 5: Interatomic distances for the pure bulk phase of GR(Cl^-) (all distances in pm).

	Experimental data [1,4]	DFT+U	
Fe(II):Fe(III)		2:1	3:1
Fe-OH	209	212.5	212.5
OH-OH	277	274.9	277.5
OH-H_2O	300	297.1	294.8
OH-OH	319	323.5	321.4
Cl-H_2O	309	309.7	313.0
Cl-OH	320	314.4	321.6

For both GR(Cl^-) species we see an excellent agreement of the theoretically determined crystallographic data and interatomic distances. This result is the foundation for a further study of GR(Br^-) and GR(I^-) and the

incorporation of I^- into GR(Cl^-) as well as the determination of the corresponding thermodynamic data.

Quantum-chemical calculation of An UV/Vis/NIR and HR-XANES-spectra of actinide compounds

It is one of the main aims of the quantum chemical group to provide – in addition to thermodynamic and structural data – as well spectroscopic data in order to support the interpretation of experimental observations. 2018 was spent on systematic studies of the bare actinide ions in order to assess the requirements on basis sets and correlation treatment to describe electron excitation spectra of actinide systems with sufficient accuracy. We found on the one hand large basis sets of quintuple-zeta quality - especially in the case of Cm(III), where spin-orbit effects are of second-order only - and about 1200 electronic states of spin multiplicities ranging from eight to two to be required. On the other hand, preliminary calculations showed that basis sets of triple-zeta quality are sufficient for the ligands, keeping the computational demands reasonable.

Additional difficulties we had to overcome were symmetry broken solutions in the extended Multistate XMS-CASPT2 of electron correlations as implemented in the MOLCAS package, which required a grouping of quasi-degenerate states. We used approximate values of the total atomic angular momentum at the actinide center for this challenge. Still, the assignment of electronic states was hampered by molecular orbitals mixing the irreducible representations of the molecular point group. We implemented a small program which uses Hartree-Fock orbitals with correct point-group symmetry behavior and imposing higher supersymmetry by restricting rotations to irreducible representations in the CASSCF calculations. Such an accurate description is also a prerequisite for calculating magnetic properties needed in the interpretation of paramagnetic NMR.

The current bottleneck is the huge number of electronic states to be included and the CPU-time demanding MS-CASPT2 calculations with approximately one hour per electronic state and no efficient way to split the huge calculations into many smaller tasks or the use of efficient parallelization. Calculations of spectra for Cm(III) and Am(III) aquo complexes with different coordination numbers in the first shell are in progress. A special focus is on the shift in the fluorescence between eight- and nine-fold coordination of Cm(III).

Initial studies were started on actinyl XANES-spectra with excitations from either the actinide 3d-shell or core orbitals located at the ligands. Such calculations are as well carried out with the MOLCAS package. Unfortunately, no symmetry can be used for such calculations and the active spaces in the RASSCF lead to huge demands in CPU-time for a complete description of the $3d^9 5f^n$ manifold including spin-orbit coupling. Qualitatively correct spectra can be obtained with moderate effort, but a more balanced description including excitations from yl-bonds to antibonding orbitals is a challenge for finding suitable approximations. Preliminary calculations on the bare yl-ions (Fig. 3) indicate that excitations of 3d inner shell electrons to antibonding 5f orbitals can be only explained on the basis of a simple one-electron excitation model in case of a very restricted description of the active space. These calculations are in agreement with the work of Sergentu et al [8]. Including bonding-antibonding excitations gives instead a picture of a metastable state in a plethora of multiply excited configurations embedded in the continuum of the system with an effectively increased oxidation state of the actinide. The studies of such spectra in combination with an analysis of the covalency in the ground state are in progress.

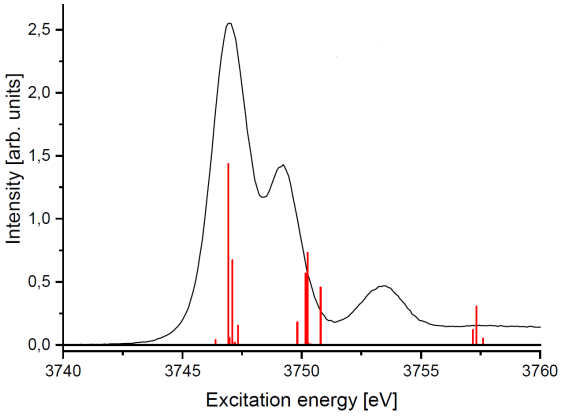

Fig. 3: Calculation of transitions leading to the Np M_5 ($3d_{5/2}$) XANES of neptunyl NpO_2^{2+} (red sticks) applying the RASPT2/ANO-VTZ multireference method with minimal active space (3d/5f). Already this - quite small - calculation reproduces the 3 peaks observed in the Np M_5 HR-XANES experiment (assigned to 5fδφ, 5fπ and 5fσ* transitions, black line) quite well and allows a better understanding of the experimental data.*

Additionally, we have performed extensive studies on aqueous Pu(III) and Pu(IV) ions. Reported coordination numbers in the literature for both aqueous ions range from 8 to 10. To shed further light on the coordination we performed a combined Vis/NIR and theoretical study.

From optimized $Pu(H_2O)_n$ (n=8, 9, 10) structures, absorption spectra were computed on the SO-CASPT2 level. The usage of symmetry blocking of orbitals as described earlier allows a correct description of the multi-reference orbitals in each ligand field. Through a large active space we described all quasi-forbidden 5f-5f transitions as well as several 5f-6d excitations. The excellent agreement between experimental and theoretical spectra allows an assignment of the majority of features in the measured data (Fig. 4).

For Pu(III) we find the nona-coordinated ion to be sufficient to reproduce the measurement accurately. For Pu(IV) a mixture of 8- and 9-fold coordinated aquo ions results in the best fit. The first 5f-6d excitations contribute in wave lengths <370nm for Pu(III) and <190nm for Pu(IV). Another noticeable difference for both ions is the zero-field splitting of the ground state. Whereas the Pu(III) ground-state splitting is less than 150 cm^{-1}, a splitting of up to 1200 cm^{-1} was computed for Pu(IV), depending on the ligand field.

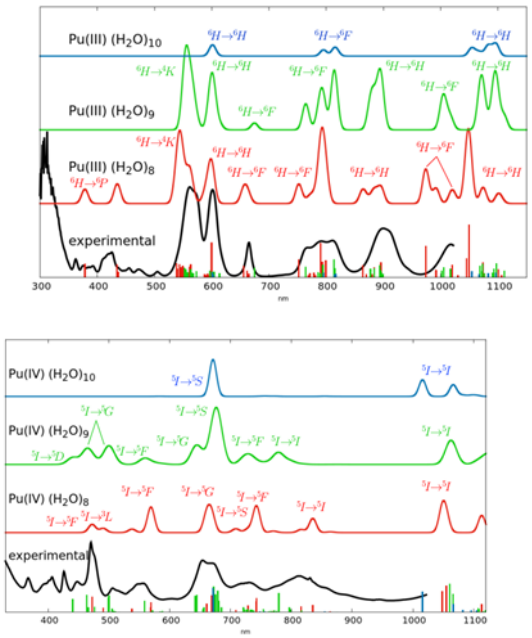

Fig. 4: Measured versus computed Vis/NIR absorption spectra for aqueous Pu(III) (top) and Pu(IV) ions (bottom).

References

[1] M. Usman *et al.*, Chem. Rev. **118**, 3251 (2018).

[2] R. Aissa *et al.*, J. Phys. Chem. Solids **67**, 1016 (2006).

[3] B. Rusch *et al.,* Solid State Sciences 10, 40 (2008)

[4] P. Refait *et al.,* Corros. Sci. 40, 1547 (1998)

[5] N. Finck *et al.*, Environ. Sci. Technol. **50**, 10428 (2016)

[6] PhD thesis of T. Platte, KIT-INE (in prep.)

[7] M. J. Wenzel, G. Steinle-Neumann, Phys. Rev. B **75**, 214430 (2007)

[8] D.-C. Sergentu *et al.,* J. Phys. Chem. Lett. **9**, 5583 (2018)

8 (Radio-)chemical analysis

At INE, a plain cornucopia of instrumentation for the analysis of radioactive samples is available. Our special skills are in handling of radioactive material, separation procedures for element and isotope analysis, as well as operation and maintenance of glove box adapted instrumentation. For external clients we provide analytical service in the fields of decommissioning of nuclear installations, nuclear waste declaration, nuclear pharmacy and others. We have a special focus on mass spectrometry for trace element analysis and speciation studies of actinides and fission products. In favour of that, hyphenated techniques, like Sector Field (SF)-ICP-MS or Collision Cell Quadrupole (CC-Q)-ICP-MS coupled to species sensitive methods, e.g., to capillary electrophoresis (CE) or ion chromatography (IC), are adapted and further developed. Another focus is Accelerator Mass Spectrometry (AMS) for the supersensitive determination of actinides below ppq levels and ^{99}Tc at the ppq levels, achieved in close cooperation with international AMS facilities (see chapter 8.5 for further details). Method development is also integrated in research projects, e.g. in the context of decommissioning or large-scale field experiments. In addition, the analytical unit supports the INE infrastructure, is involved in various teaching activities and is responsible for education of chemical laboratory assistants.

M. Plaschke, A. Bauer, N. Adam, N. Ait Mouheb, M. Altmaier, M. Böttle, M. Bouby, M. Brandauer, N. Cevirim-Papaioannou, D. Fellhauer, M. Fuss, J. Gaona Martinez, A. Geist, F.W. Geyer, F. Heberling, A. Fried, T. Kisely, S. Kraft, S. Kuschel, S. Moisei-Rabung, U. Müllich, F. Quinto, F. Rinderknecht, E. Rolgejzer, B. Schacherl, T. Schäfer, D. Schild, A. Seither, W. Tobie, C. Walschburger, and H. Geckeis.

In co-operation with:
T. Gil-Díaz[a], C.-O. Krauß[b], A. Heneka[b], and S. Gentes[b]

[a] Doctorante en Géochimie et Ecotoxicologie, Université de Bordeaux, F-33615 Pessac, France
[b] Department of Deconstruction and Decommissioning of Conventional and Nuclear Buildings, Institute for Technology and Management in Construction (TMB), KIT Campus South

Instrumentation

Our routine instrumentation is kept up-to-date, e.g., in 2018 a state-of-the-art Q-ICP-MS (Perkin Elmer NEXION 2000) is installed. The instrument offers new analytical capabilities like the effective suppression of poly-nuclear interferences by the universal cell technology or the single nanoparticles analysis. A new glove box adaptation is designed and engineered by INE technicians. The nuclear operation of the instrument will start beginning of 2019. Table 1 presents the spectrum of analytical techniques available at INE.

Inter-Laboratory Comparison

^{241}Am and ^{243}Am and their Np daughters strongly contribute to the long-term radiotoxicity of radioactive waste and, therefore, a Certified Reference Material (CRM) is needed for their accurate determination. The INE lab participated together with eight other international laboratories, noted for radio-analytic chemistry, in an Inter-Laboratory Comparison (ILC) for the certification process of the first ^{243}Am CRM. CEA Marcoule and JRC-Geel organized the ILC. The objectives of the ILC were (a) a performance test of the participating laboratories, (b) an external control of the values determined by the certification process of JRC-Geel and (c) finally to provide the first CRM of ^{243}Am. In the frame of this ILC, the determination of the following measurands was required: the contents in (mol/kg) of ^{243}Am, ^{241}Am and total Am (indicated as [^{243}Am], [^{241}Am] and total [Am], respectively), and the two isotope ratios n(^{241}Am)/n(^{243}Am) and n(^{242m}Am)/n(^{243}Am) in (mol/mol). INE used two analytical methods for the determination of the Am content with SF-ICP-MS. With method 1, the [^{241}Am] and [^{243}Am] were obtained with a standard addition method, by adding a ^{243}Am reference material (Eckert und Ziegler, Germany) to the ^{243}Am CRM. With method 2, [^{241}Am] and [^{243}Am] were quantified by an external calibration using a ^{238}U CRM (SLRS-6, National Research Council Canada). The results obtained with these two methods are consistent within the uncertainty of the measurements. In both methods, the total [Am] was obtained summing up the [^{241}Am] and [^{243}Am]. It is important to note that in method 2 the estimate of the total [Am] is independent from the ^{241}Am/^{243}Am ratio of the pure ^{243}Am CRM.

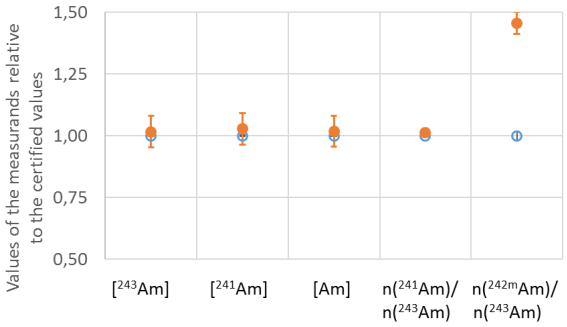

Fig. 1: ILC of a ^{243}Am CRM: determination of [^{243}Am], [^{241}Am], [Am], n(^{241}Am)/n(^{243}Am), n(^{242m}Am)/n(^{243}Am) by INE (orange circles) relative to the certified values (blue circles), see text.

In Fig. 1 the ratios of the results of the INE lab for the five different measurands to the corresponding certified values are depicted. For the four measurands [^{243}Am], [^{241}Am], [Am] and n(^{241}Am)/n(^{243}Am), the

values determined by the certification authority are confirmed by the ILC (including INE) and, therefore, accepted as certified values [1]. For the isotope ratio n(^{242m}Am)/n(^{243}Am) a bias, most probably due to the different methods of determination, between the ILC (including INE, see Fig. 1) and the certification authority is obvious. Therefore, this value is not given as certified but only as indicative value [1]. Even though the INE results comprised a slight overestimation of the measurands [^{243}Am], [^{241}Am] and [Am], they agree with the certified values confirmed by the ILC.

Table 1: Analytical techniques available at INE

Element and Isotope Analysis
Quadrupole Inductively Coupled Plasma Mass Spectrometry (Q-ICP-MS)
Collision Cell Q-ICP-MS (CC-Q-ICP-MS)
Sector Field ICP-MS (SF-ICP-MS)
ICP Optical Emission Spectrometry (ICP-OES)
Nuclear Spectroscopic Methods
Alphaspectrometry
Liquid Scintillation Counting (LSC, conventional/high sensitivity)
Gammaspectrometry (with auto-sampler)
Other Methods
Ion Chromatography (IC)
Gas Chromatography (GC)
Carbon Analysis (TOC, DOC, TIC, NPOC)
Specific Surface Area Analysis (BET)
Differential Thermal Analysis (DTA)
Dilatometry
Fusion and Microwave Digestions

External clients

Analytical service is offered to external clients, e.g. in the fields of nuclear waste declaration or nuclear pharmacy.

Nuclear pharmacy

In 2018 a new co-operation in the field of nuclear pharmacy with the Norwegian company *Oncoinvent AS* (www.oncoinvent.com) started. The radiopharmaceutical Radspherin® is a novel alpha-emitting microsphere, containing ^{224}Ra and designed for treatment of metastatic cancers in body cavities. The active component is incorporated in inorganic microparticles of Ca_2CO_3 acting as carriers in the human body. This allows for a relative slow degradation in the body and a regional retention of effective radiation dose. First samples of this drug were analyzed in 2018 with regard to toxic heavy metal trace impurities. First clinical indication will be treatment of peritoneal carcinomatosis originating from ovarian cancer [2]. In addition, INE continued the longtime cooperation with the *Bayer* company (www.pharma.bayer.com) for the quality control analysis of Xofigo®, containing the short half-live and short range ^{223}Ra alpha emitter as active component.

Nuclear waste treatment and decommissioning of nuclear facilities (KTE-TEAL)

Since several decades, INE provides analytical service for KTE-TEAL (Kerntechnische Entsorgung Karlsruhe GmbH, Technische Einrichtung Analytische Labore). The origin of the samples are the different waste treatment facilities of KTE, mainly the incineration facility (producing ashes) and the evaporation plant (producing LAW liquid concentrates). Annually averaged samples from the different waste treatment facilities as well as samples from decommissioning of nuclear facilities (e.g., demolition waste) and others (e.g., wipe tests) are analysed. At INE, isotope concentrations and nuclide vectors are determined by the combination of nuclear and mass spectroscopy techniques. The main purpose of these determinations is the waste declaration according to the conditions of acceptance for the Konrad nuclear waste repository for low- and intermediate-level nuclear waste. The analysed nuclides include neutron activation and fission products (^{55}Fe, ^{63}Ni, ^{90}Sr), as well as actinides (^{233,234,235,236,238}U, ^{238,239,240,241,242}Pu and $^{242,243+244}$Cm). In 2018, radionuclides (RN) including the fission product ^{99}Tc were analysed in the first samples from the decommissioning of the former Vitrification Plant Karlsruhe (VEK).

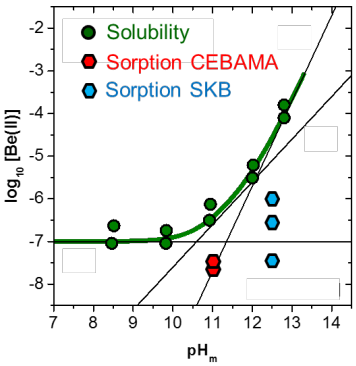

Fig. 2: Solubility of Be(II) in 0.1 M KCl as quantified by Q-ICP–MS. The green curve is calculated with thermodynamic data derived in this work; first results from Be(II) sorption experiments conducted with two cement formulations (CEBAMA and SKB) are included (see text).

Other fields of analytical services

Our analytical capabilities are also requested in other fields of application, e.g., the behavior of engineered nanoparticles (i.e., CeO_2) in a combustion chamber for consumer waste or the analysis of a bio tenside with applications in agriculture, environmental protection, remediation or pharmacy.

Analysis for INE R&D

In the following, selected INE R&D topics are addressed from the analytical perspective.

Cementitious systems

Beryllium solubility and sorption

In the context of the EU collaborative project on Cement-Based Materials, Properties, Evolution, Barrier Functions (CEBAMA), one of the ongoing research activities at INE focuses on the solubility and sorption of beryllium in cementitious systems. The main objectives are the development of comprehensive thermodynamic and activity models for the system Be^{2+}–Na^{+}–

K^+–Ca^{2+}–H^+–Cl^-–HCO_3^-–CO_3^{2-}–OH^-–H_2O(l), the determination of robust solubility upper limit concentrations for source term estimations, and the quantitative assessment of the uptake of Be(II) by cementitious materials. For this purpose, comprehensive Be(II) solubility studies in alkaline NaCl, KCl and $CaCl_2$ solutions, and Be(II) sorption studies on different cementitious materials are performed at INE. In Fig. 2 solubility data determined for β-$Be(OH)_2$(cr) are compared with the first experimental results on Be(II) uptake by two different cement formulations. Be is analyzed by Q-ICP-MS with LOD in the range of 1 ng/L.

Influence of additives on Thorium solubility

The influence of selected cement additives and model organic compounds on the solubility and sorption of RN in cementitious environments is investigated in the framework of the BMWi GRaZ project (Geochemische Radionuklidrückhaltung an Zementalterationsphasen). In a series of screening experiments, gluconate and citrate were identified as relevant organic additives enhancing the solubility of Nd(III), Th(IV) and U(VI) in alkaline solutions of intermediate ionic strength systems such as those potentially forming in specific clay formations (e.g. cretaceous argillites in northern Germany). Based on these results, comprehensive Th(IV) solubility studies in alkaline NaCl, $MgCl_2$ and $CaCl_2$ solutions are performed at INE. Fig 3 shows solubility data of $Th(OH)_4$(ncr, hyd) as a function of pH at fixed gluconate concentration of [GLU]tot = 10^{-2} M in 2.5 M NaCl solution. The results obtained in this study will lead to the development of comprehensive chemical, thermodynamic and activity models for the system Th^{4+}–Na^+–Mg^{2+}–Ca^{2+}–H^+–GLU—Cit^{3-}–Cl^-–OH^-–H_2O(l).

Natural environments

Tin and Selenium sorption in river sediments

In a study together with the University of Bordeaux the development of RN distribution scenarios after a potential nuclear reactor accident is addressed. After wet deposition, RN may be immobilized in river sediments, transported as aqueous species or adsorbed at suspended particular matter. After migration to the sea they can either desorb into seawater or adsorb on suspended particular matter and, finally, sediment at the seafloor. In the present study, adsorption and desorption of ^{113}Sn and ^{75}Se, as representatives of nuclear fission products, on natural sediments from the Garonne and Rhone Rivers (France) in sea- and freshwater solutions, respectively, was investigated.

^{113}Sn (present as Sn^{2+}) shows very strong quasi-instantaneous (<0.5 h) adsorption to the river sediments. As ^{113}Sn also adsorbed at the container walls in the batch-type adsorption experiments only rough estimates for K_D-values could be derived. K_D values for Garonne Sediment in freshwater are about 8000 L/g for low solid-liquid ratios (S/L) equal to 10 mg/L and decrease to about 300 L/g at S/L of 1000 mg/L. In seawater lower K_D values are observed: about 1000 L/g at 10 mg/L decreasing to about 200 L/g at 1000 mg/L S/L. ^{75}Se (present in solution as SeO_4^{2-}) showed very weak adsorption, which could only be determined at the highest S/L ratio (1000 mg/L). K_D at these conditions was 0.04 L/g for Garonne sediments in sea- and freshwater. Although adsorption is weak, the kinetic is so fast that it could not be time-resolved by gamma spectrometry. For desorption of ^{75}Se from the Rhone sediments the following trends could be observed: (a) desorption in seawater is generally very low, (b) desorption in freshwater strongly depends on the preceding sorption medium, i.e. after adsorption in seawater (cw. freshwater) desorption is increased by a factor of two. As expected, desorption kinetics is much slower compared to the adsorption (time span for desorption ~22 h). The analytical group supported the study in particular with the analysis of ca. 500 samples by gamma spectroscopy.

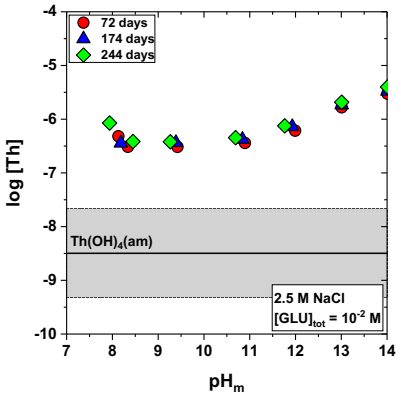

Fig. 3: Solubility of Th(IV) as a function of pH at $[GLU]_{tot}$ = 10^{-2} M in 2.5 M NaCl solution., see text.

Migration of RN from a bentonite source in a granitic shear-zone

In the course of the Colloid formation and Migration experiment (CFM) at the Grimsel Test Site (GTS) analysis of the samples originating from the Long-term In-situ Test (LIT) were in focus. LIT analysis consists in the monitoring of a bentonite source including the isotopes ^{45}Ca, ^{75}Se, ^{99}Tc, ^{137}Cs, ^{233}U, ^{237}Np, ^{241}Am and ^{242}Pu and the conservative tracer Amino-G. The source was emplaced in the shear zone in May 2014 for the better understanding of real *in-situ* conditions in a bentonite-based geotechnical barrier. The experiment was stopped after 4.5 years in October 2018 by injecting epoxy resin in the near-field of the bentonite source followed by overcoring and disassembling of the core. The experiment was monitored *in-situ* and regularly collected samples have been submitted to off-site analysis. The analytic plan included various techniques to investigate elemental and RN composition (i.e., by SF-ICP-MS), colloid size and concentration, pH, Eh_{SHE}, fluorescence and conductivity. A closer look at the analytical data and their interpretation can be found in Chapter 5.3. For the ultra-trace analysis of the actinides and ^{99}Tc please go to chapter 8.5.

Extraction chemistry

The coordination chemistry group performs solvent extraction studies, mainly in support of the EURATOM GENIORS programme. Current work deals with optimising some of the processes developed in preceding projects. This requires determining concentrations of both RN and inactive metallic species in organic and aqueous phase samples from solvent extraction experiments. Analysis of numerous samples is typically performed by gamma and alpha spectrometry and by ICP-MS.

Decommissioning

For the deconstruction of selected parts of a nuclear reactor, the waterjet abrasive suspension cutting technique (WASS) provides several advantages towards conventional cutting techniques: (1) it can be used in a remote controlled mode for components at places difficult to be reached, with challenging geometries or with inherent mechanical stress; (2) it is a cold cutting technique with which the formation of aerosols is avoided, and (3) it can be used submerging with water the items to be deconstructed, taking in this way advantage of the shielding effect of water. However, during the cutting of steel components, a mixture of abrasive and radioactive steel particles from the cut components is generated, the so-called secondary waste. Depending on the operational conditions, the amount of this secondary waste is substantial. This is the reason why the use of WASS in the deconstruction of nuclear facilities is up-to-now limited to some selected applications.

An approach with good prospects to reduce the amount of secondary waste is represented by the joint KIT (INE and TMB) project "Magnet-Separation von Korngemischen zur Minimierung von Sekundärabfällen im Rückbau kerntechnischer Anlagen" (MaSK). Within this project, a multi-step mechanic and magnetic separation device (called MaSK-Rig) was constructed and successfully tested. It could be demonstrated that the separation of magnetic steel particles from the grain suspension can be markedly improved using the MaSK-Rig compared to a previous prototype separation device. The separation efficiency is quantified at INE by the analysis of the steel fraction in the secondary waste by, i.e., ICP-OES [3].

References

[1] M. Crozet and D. Roudil, NoteTechnique DEN/DMRC/CETAMA (2017).

[2] Westrøm, S. et al., *Nucl. Med. Biol.*, **51**, 1 (2017).

[3] Brandauer, M., Geckeis, H., Gentes, S., Heneka, A., Krauß, C.-O., Plaschke, M., Schild, D., Tobie, W., ***DEM 2018*** *- Dismantling Challenges: Industrial Reality, Prospects and Feedback Experience,* Avignon – 2018, October 22-24*, Avignon,* France.

9 Radiation protection research

Radiation Protection Research at KIT-INE deals with assessing radiation exposures by estimation of doses from external radiation fields and with effects of ionizing radiation on materials. The basis for research is the recording and evaluation of radiation exposures by sources of natural and artificial origin. In particular, mixed photon, beta and / or neutron radiation fields are investigated, with simulations contributing to a deeper understanding of the radiation fields. Our studies related to radiation protection summarized in this section are related to numerical evaluation of radiation field around casks loaded with spent nuclear fuel and the respective exposure to workers in generic deep geological repositories and are related to uncertainty assessment in nanodosimetry using Monte-Carlo calculations. Close collaborations are established with national and internationals partners in networks such as "Strahlung und Umwelt" in Competence Alliance Radiation Research (KVSF), the expert group "Dosimetry" (AKD) from the German-Swiss Fachverband für Strahlenschutz e.V. and the European Radiation Dosimetry Group (EURADOS).

9.1 Emplacement of an equal amount of high-level nuclear waste in rock salt and claystone: exposure scenarios of workers

F. Becker, R. Dagan, B. Pang[1], H. Saurí Suárez[2], H. Wu

[1]present address: College of Physics and Energy, Shenzhen University, China; [2]present address: Balcke-Dürr Nuklear Service, Karlsruhe

Introduction

In various concepts for a deep-geological disposal facility of high-level nuclear waste, spent nuclear fuel (SNF) assemblies are planned to be contained inside shielding casks. Besides long-term safety aspects of radionuclide containment, shielding casks are projected to reduce the emitted radiation an in turn the amount of radiation received by workers. An evaluation of the emitted radiation is necessary to assess the dose workers may receive when they are handling such casks. This evaluation can be performed with Monte-Carlo codes like MCNP6 [1]. For a POLLUX® type shielding cask containing uranium dioxide (UOX) and mixed oxide (MOX) fuel assemblies, the radiation field and dosimetry is ruled mainly by neutrons, backscattered neutrons also play an important role [2]. Within the ENTRIA project [3] the radiation fields and exposure in a final disposal in a rock salt and a claystone repository were simulated with MCNP6.

Emplacement of an equal amount of high-level nuclear waste in rock salt and claystone

Some results of exposure scenarios of workers for the emplacement of an equal amount of waste in rock salt and claystone are summarized here. For more details of the investigations, we refer to publication [4].

According to average composition of SNF from German reactors to be disposed of [5], a representative waste inventory consisting of ~90% UOX and ~10% MOX SNF assemblies was used. For a rock salt depository POLLUX®-10 casks containing nine UOX and one MOX fuel rods with an average burnup of 55 GWd/tHM and a cooling time of 50 years after unloading from reactor were considered. The same waste inventory and cask were taken for the claystone case, but a lower waste load per cask was selected to account for the constraint in argillaceous host rock. In order to keep the thermal impact below the level of heat-induced irreversible alteration of clay minerals, eight UOX and one MOX fuel rods were split into three "triple" casks, one "U2M" cask and two "U3" casks. The least common multiple of casks with the same amount of waste would be three POLLUX®-10 and ten triple casks.

The simulated emplacement scenario in an emplacement drift consists of four steps [4]. In a first step, a cask is transported with a train, consisting of a carriage loaded with a cask, an electric locomotive, and a drivers cab of locomotive. A phantom sitting in the drivers cab is employed to determine the personal dose equivalent $H_P(10)$. For the hypothetical example to dispose of a cask, one km of transport with a speed of 5 km/h is assumed. In a second step of 10 min duration, the cask is positioned under a storage equipment at the emplacement position, in order to elevate the cask from the carriage to allow the entity locomotive and carriage to drive back. At the third step lasting ten minutes, the entity locomotive and carriage is driven back and the cask is placed on the ground with the help of a storage equipment. In the 10-minute fourth step, the entity locomotive and carriage connects to the rail mounted storage equipment and moves it to the next emplacement position. Figure 1 summarizes the respective amount of dose ($H_P(10)$) as function of distance covered.

As a result, the dose for the emplacement of the same amount of SNF yields a 60% higher dose for the investigated scenario with U2M and U3 casks compared to the one with POLLUX®-10 casks. Neglecting the distance of 1000 m to access the emplacement position, for the claystone scenario about 60 % more emplacement drift space is required than for the rock salt case.

Outlook

Our studies [2] on POLLUX casks containing UOX and MOX fuel assemblies showed that the radiation field and in turn the individual personal dose of workers is dominated by neutrons. The employed Monte Carlo codes used existing physics models and nuclear data to model neutron transport in various materials

and geometries, but so far, only the "standard" models and databases were employed.

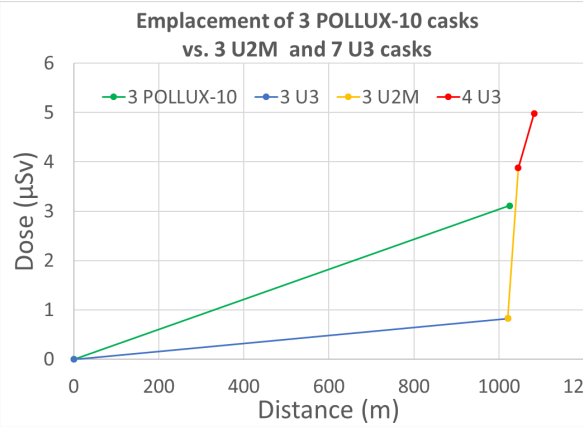

Fig. 1: Comparison of the emplacement of three POLLUX®-10 casks compared to the emplacement of three U3 plus three U2M plus four U3 casks.

However, in the last decade it was shown theoretically [6,7,8] and experimentally [9] that the neutron scattering formalism in default Monte Carlo simulations is not accurate, in particular in the vicinity of resonances. Hence, the investigation of the impact of improved energy dependent scattering kernel formalism in Monte Carlo simulations relating to radiation dose assessments is one of the main topics of future investigations. This includes among others additional predicted absorption due to the up-scattered neutrons into the resonances and consequently a shifted nuclide inventory vector, which eventually alters the radiation field within the repository. Further on, for many cases, the physical model for neutron scattering must take into account the motion of the target nuclei: in the thermal energy region the motion of the target nuclei can cause significant changes, resulting in a different neutron interaction probability.

At thermal energies, the scattering phenomena is governed by the well-known S(α,β) scattering kernel. In this case, the molecular binding of the nuclide grid affects directly the scattering physics of the interacting neutron. If the S(α,β) scattering kernel is not available, the free gas model (FGM) is usually employed in order to determine the kinematics of the scattered neutron.

A second future task is the investigation of effects of the interactions of neutrons with the grid elements of casks in a repository. This concerns their absorption and in particular their back scattering (reflection). A special attention should be focused on the walls of a repository, which have shown [2] to be a major contributor to the overall dose.

Acknowledgements

In the context of the ENTRIA project, the German Federal Ministry of Education and Research (BMBF) financially supported the work (grant number 15S9082E).

References

[1] D. B. Pelowitz et al., *MCNP6™ User's Manual Version 1.0.* Los Alamos National Laboratory, LA-CP-13-00634 (2013).

[2] B. Pang B. et al., *Radiation Protection Dosimetry* **170,** 387–92 (2016)

[3] ENTRIA - Disposal Options for Radioactive Residues: Interdisciplinary Analyses and Development of Evaluation Principles. Available on http://www.entria.de (4 May 2018, date last accessed).

[4] H. Saurí Suárez, *Individual dosimetry in disposal facilities for high-level nuclear waste*, Ph.D. thesis, urn:nbn:de:swb:90-840326, KITopen ID: 1000084032 (2018).

[5] F. Peiffer and A. McStocker, *Bericht zum Arbeitspaket 3 Vorläufige Sicherheitsanalyse für den Standort Gorleben,* GRS-278 (2011).

[6] R. Dagan et al., *Nuclear Data Sheets***, 118,** 179–182 (2014).

[7] B. Becker et al., *Annals of Nuclear Energy,* **36,** 470-474 (2009).

[8] R. Dagan et al., *Annals of Nuclear Energy* **32,** 367-377 (2005).

[9] T. Ro et al., *Journal of the Korean Physical Society*, **55,** 1389-1393 (2009).

9.2 Participation in EURADOS exercise on uncertainty assessment in micro- and nanodosimetry using Monte-Carlo calculations

B. Heide

A benchmark exercise of the European Radiation Dosimetry Group (EURADOS) was designed to evaluate microdosimetric as well as nanodosimetric results obtained with respect to a liquid water target. Such a target is often used as representative of biological material in dosimetry calculations.

The results of the benchmark exercise were published elsewhere [1]. In the following, we will focus on a by-product which was discovered in the framework of the exercise. In order to calculate the total specific energy spectrum, the total yield of Auger plus Coster – Kronig electrons and the total yield of internal conversion (IC) electrons were given in the exercise: 24.9% and 0.94%. It was observed that there is a difference visible in the spectrum depending on whether the yields were taken explicitly into account or, as usually done, a constant number of electrons per decay, namely 26 (=25 + 1), were applied. The difference can be inferred from Fig. 1.

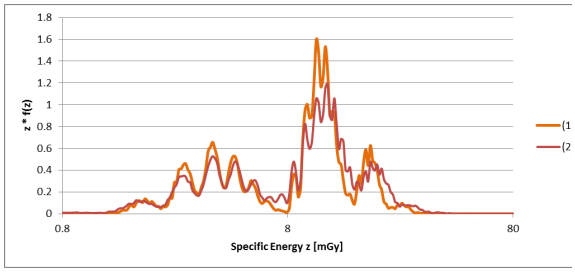

Fig. 1: Total specific energy spectrum. Curve (1) refers to the yield of Auger and Coster-Kronig electrons (24.90%) as well as to the yield of IC electrons (0.94%). Curve (2) was generated using a constant number of electrons per decay: 26 (= 25 + 1).

Reference

[1] C. Villagrasa et al., *Radiation Protection Dosimetry*, **ncy240**, https://doi.org/10.1093/rpd/ncy240 (2018)

10 Geoenergy

The Karlsruhe Institute of Technology has defined a broad research program on Enhanced Geothermal Systems (EGS) technology development. Research activities cover the whole process chain of geothermal exploration, engineering and production including system integration and social acceptance and span from fundamental to applied research across scales [1]. Compared to a nuclear waste disposal research, the conditions at a geothermal site are characterized by elevated temperature, flow rate and pressure conditions. Therefore, the influence of hydraulic processes extends even further: not only the direct hydraulic observables like flow / pressure fields or tracer propagation is affected by the petrophysical setting, but the changes in the system setting due to mechanical and chemical interaction become important. In this context, the geoenergy research at INE concerns mainly physical and chemical processes in the thermal water circuit and in fractured reservoir systems. The technical feasibility of EGS in fractured crystalline basement was demonstrated first at the Soultz-sous Forêts project, France [2]. Major conclusion from this project are that effective enhancement of hydraulic yield under environmentally friendly condition, e.g., reducing induced seismicity, are technically feasible during reservoir engineering and operation. However, both was achieved by reducing the injection wellhead pressure at the expense of economic viability. For the further development of EGS, this learning curve needs to be continued in the field of controlled high-flowrate injection on existing fractures. In the surface facilities, scaling and corrosion remains an issue. This opens three major fields of investigation of the geothermal research at INE in 2018: (1) exploration for naturally permeable fracture zones, (2) monitoring of high flowrate injection, and (3) characterization of scalings in geothermal power plants.

N. Cornejo, N. Haaf, F. Heberling, M. Pavez, K. Schätzler, E. Schill

In co-operation with:

S. Held[a], T. Kohl[a]

[a] AGW, Karlsruhe Institute of Technology, Germany

Introduction

The environmentally friendly development of deep geothermal energy addresses key issues such as perceptible seismicity during enhancement of the reservoir performance and operation, as well as radioactive scaling. Recent development in enhancing and operating geothermal systems have revealed the importance of the utilization of natural flow paths [2]. In this context, the research at INE focuses on the advancement of electromagnetic methods to detect, characterize and monitor preferential flow.

The research in the Helmholtz program *Renewable Energies* at INE is completed among others in two EC H2020 projects:

1) Deployment of deep enhanced geothermal systems for sustainable energy business (DEEPEGS, www.deepegs.eu/)
2) Cooperation in Geothermal energy research Europe-Mexico for development of Enhanced Geothermal Systems and Superhot Geothermal Systems (GEMex, www.gemex-h2020.eu/)

In 2018, research at INE has contributed to the detection of natural fluid pathways in fault zones. Pathways in naturally fractured reservoirs are often linked to the damage zone of faults. Natural faults are typically segmented and reveal a considerable tortuosity. Depending on the orientation of the single segments of the fault in the ambient stress field, permeability ranges from impermeable to highly permeable. Therefore, new methods such as 3D inversion of magnetotelluric data have been applied to visualize segments with preferential fluid pathways [3].

Monitoring of fluid injection bases on such 3D visualization of the initial condition. Passive electromagnetic techniques (e.g. magnetotellurics) are traditionally used for geothermal exploration and a few recent studies have demonstrated its potential for monitoring reservoir development. One of the main challenges is though the presence of cultural noise and/or variability of the Earth magnetic field that can obfuscate the electromagnetic signals of interest. INE has contributed to the investigation of the benefits and drawbacks of active electromagnetic surveying using controlled-sources to tackle this challenge [4].

Significant steps forward in magnetotelluric monitoring have been achieved in 2018 with regards to the identification of signals related to fluid injection and induced seismicity [6]. A processing procedure has been established to address the separation of uncorrelated noise from the likewise uncorrelated relatively high-frequency perturbation that originate from reservoir engineering and represent the sought-for signal.

High-resolution visualization of preferential magmatic and geothermal fluid pathways using electric conductivity at Villarrica volcano, S-Chile

Preferential fluid pathways along regional fault systems are crucial for the spatial localization of volcanic and geothermal manifestations. Differences in electric properties of fluids and hydrothermal alteration products against the unaltered matrix allow for visualization of such pathways. Unfavourable geometry resulting from the fluid pathways in regional faults often being

aligned along the geo-electric strike can be overcome by using 3D inversion of magnetotelluric data. For a section in the 1400 km long Liquiñe-Ofqui Fault System (LOFS), we demonstrate the potential of 3-D inversion of magnetotelluric data from a dense station network [3].

Five out of six electric resistivity anomalies at intermediate depth are connected to volcanic or geothermal surface manifestations (Fig. 1). Deep and highly conductive anomalies are detected in the vicinity of the volcanic chain and where the LOFS is cross-cut by a fault that belongs to the Andean transversal fault system. The anomaly underneath the volcanic chain coincides with a volcanically and seismically active zone at depth that is linked to the recent lateral eruption in 2015; the anomaly related to the fault crossing reveals a vertical pathway extending to the surface. Phase tensor analyses indicate a structural origin of the latter anomaly that may be connected to a line of volcanic cones that occurs in the NE of the Villarrica volcano.

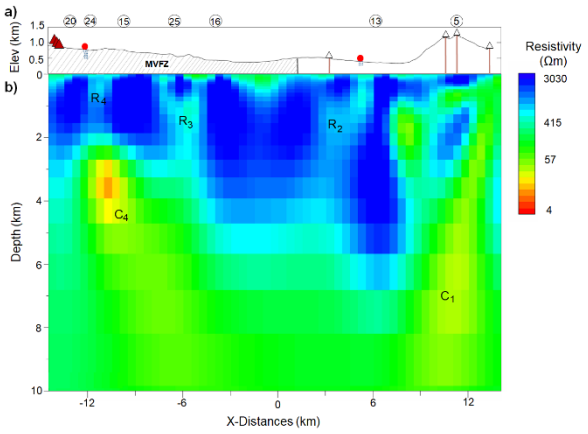

Fig. 1: a) Elevation and major geological features including Moccha-Villarrica fault zone, the monogenetic cones and thermal springs along a representative section of the 1400 km long Liquiñe-Ofqui Fault System (LOFS). b) 3-D inverted electrical resistivity distribution subparallel to the LOFS. High and intermediated conductivity anomalies are labelled with C1 / C4 and R2 / R3, respectively.

Monitoring geothermal reservoir developments with the controlled-source electro-magnetics method: a calibration study on the Reykjanes geothermal field

In order to investigated the benefits and drawbacks of active electromagnetic surveying by controlled source electromagnetic (CSEM), time-lapse surveys were carried out over the Reykjanes geothermal field in Iceland before (baseline) and after (monitor) the thermal stimulation of the supercritical RN-15/IDDP-2 geothermal well. It results that when similar CSEM equipment is used during the baseline and monitor surveys and systematically d-GPS positioned, the remaining key parameter controlling the survey repeatability is in the level of external noise. Since the influence of external noise on CSEM data can be artificially reduced (e.g. by increasing the transmitter dipolar moment), it offers the

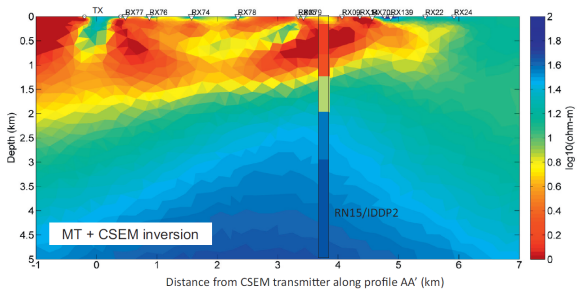

Fig. 2: Resistivity model (log scale) obtained from 2.5D inversion of the CSEM and MT data.

possibility to adapt the survey design to increase the chance of detecting the time-lapse signals of interest. On the contrary, little control is possible on the passive magnetotelluric signal to noise ratio and hence repeatability.

The time-lapse EM survey acquired over the Reykjanes geothermal reservoir showed that a high CSEM survey repeatability can be achieved with electric field measurements (within a few percent). To assess the quality of our CSEM dataset, we inverted the data and confronted the resulting resistivity model with the resistivity logged in the RN-15/IDDP-2 well. We obtained a good match down to 2-3km depth, i.e. enough to image the cap rock and the liquid-dominated reservoir but not deep enough to image the reservoir in supercritical conditions. To obtain such an image, we had to jointly invert legacy magnetotelluric data with our CSEM data (Fig. 2).

Comparing results from baseline and monitoring CSEM did not reveal any permanent changes in electric resistivity related to the stimulation of the RN-15/IDDP-2 well.

Processing of magnetotelluric data for monitoring changes during drilling operation

Long-term magnetotelluric monitoring of different injection and production experiments at the Rittershoffen geothermal site in Alsace (France) provided a first continuous data set over several month, covering the end of drilling phase of GRT2 [5], mostly, production from, but also injection into this well, injection into GRT1 and a circulation experiment. Transfer functions showed particular variation pattern for different operations, i.e. an increase in uncertainty, conductivity and phase during test operation with a preferential direction sub-parallel to minimum principal stress, i.e. perpendicular to the expected extension of the fractures controlling the reservoir. In particular fluid injection, either into GRT2 or GRT1 causes a strong decrease in resistivity by up to one order of magnitude in the YX component between about 8–25 s of period.

A similar experiment was carried out during drilling and reservoir engineering of the RN-15/IDDP-2 well on the Reykjanes peninsular in Iceland [6]. During and after deepening of the RN-15 to 4665m (IDDP-2 well) a magnetotelluric dataset was acquired between November 2016 and January 2017. The drilling progress during this period was accompanied by partial and up

to total circulation loss and induced seismicity. Two continuous running MT stations, GUN and RAH, were installed on the Reykjanes peninsula. RAH and GUN are located about 6 and 1 km away from IDDP-2. Both MT stations are equipped with two electric dipoles in N-S and E-W direction, as well as three magnetic sensors oriented in N, E and vertical direction. MT monitoring was carried out with a sampling frequency of 512 Hz. Processing revealed the bad data quality of RAH. Consequently, MT data were processed using single site method with the bounded influence remote reference processing (birrp).

Due to the high frequency of the perturbations applied during drilling and reservoir engineering and the therefore presumed high frequency of changes in the electromagnetic field, in MT monitoring, conventional processing of MT data as applied in exploration with

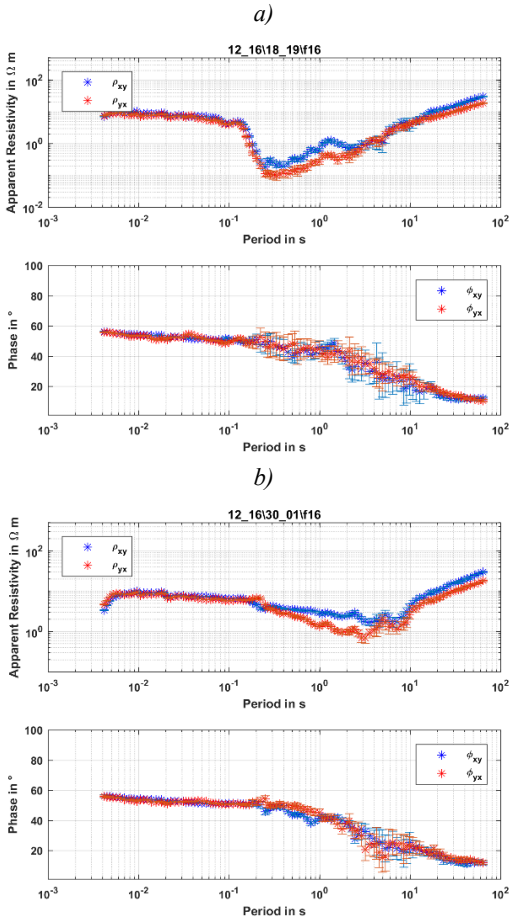

Fig. 3: Representative end-member types of transfer functions (top: apparent resistivity, bottom phase) with a) a resistivity low (>10^{-1} Ωm) at periods of a few tens of seconds from December 18th to 19th, 2016 and b) a resistivity low (>1 Ωm) at periods of up to 10 s from November 30th to December 1st, 2016.

the aim to obtain smoothest distribution must be questioned.

Here we demonstrated that low perturbations represented by low error bars in the transfer functions are not improved by remote referencing. In contrast, the changes in electric resistivity, which have been related to fluid injection in comparable studies, e.g. [5], appear as uncorrelated noise in the remote referenced processing. To eliminate only the uncorrelated noise that originates from operations at the surface, we propose to apply notch filters of the respective frequencies. In the case of high frequency signal an improvement of filtering is achieved by decimation of the sampling frequency prior to the filtering.

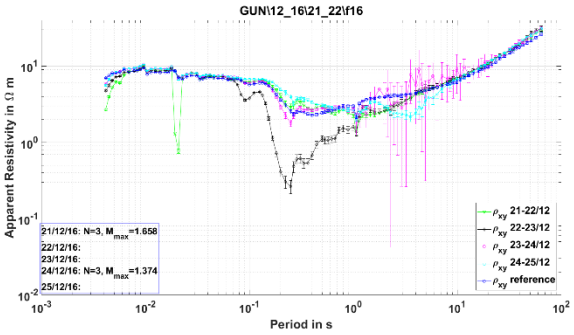

Fig. 4: Comparison of apparent resistivities versus period monitored between December 21st and 25th, 2016 with the occurrence of seismic events during deepening of the RN-15/IDDP-2 well.

Resulting apparent resistivities reveal significant variability in the single-site processed transfer functions (calculated for 48 h) over the time period of November 30th, 2016 to December 1st, 2016 at the GUN station (Fig. 3). Typically, temporal variations in electric resistivity occurs between 10^{-1} and 10 s. Changes in the phase are not observed. One end-member type shows apparent resistivities down to about 10^{-1} Ωm at periods of a few tens of seconds (Fig. 3a). The opposite end-member type reveals apparent resistivities down to 1 Ωm at periods up to 10 s (Fig. 3b). Note that such decrease in resistivity has been attribute in other geothermal projects such as Rittershoffen (France) to fluid injection [5].

These first results indicate a correlation between fluid loss, induced seismicity and low resistivity in the magnetotelluric data. In Fig. 4, a representative example shows the decrease in resistivity 48-24h prior to a cluster of three seismic event with magnitudes M>0.8 including a major event of M=1.4 on December 24th, 2016. The resistivity decrease that is observed between December 22nd and 23th, 2016 is fully reversed after the occurrence of the event. Note that full reversion is also indicated f December 21st, 2016.

References

[1] Meller, C., et al., *Energy Technology* (2016)

[2] Schill, E., et al., *Geothermics* (2017).

[3] Pavez, M., et al., *Journal of volcanology and geothermal research* (subm.)

[4] Darnet, M., et al., *Journal of volcanology and geothermal research* (2018).

[5] Abdelfettah, Y., et al., *Geothermics* (2018)

[6] Haaf, N. et al., *Proceedings of the 44th Stanford Geothermal Workshop, 2018* (subm.).

11 Publications

2018

ISI/SCOPUS

1. Abdelfettah, Y.; Sailhac, P.; Larnier, H.; Matthey, P. D.; Schill, E., Continuous and time-lapse magnetotelluric monitoring of low volume injection at Rittershoffen geothermal project, northern Alsace - France. *Geothermics* **2018,** *71*, 1-11.
2. Adam, N.; Trumm, M.; Smith, V. C.; Macgillivray, R. T. A.; Panak, P. J., Incorporation of transuranium elements: Coordination of Cm(iii) to human serum transferrin. *Dalton transactions* **2018,** *47* (41), 14612-14620.
3. Bae, S.; Sihn, Y.; Kyung, D.; Yoon, S.; Eom, T.; Kaplan, U.; Kim, H.; Schäfer, T.; Han, S.; Lee, W., Molecular Identification of Cr(VI) Removal Mechanism on Vivianite Surface. *Environmental science & technology* **2018,** *52* (18), 10647-10656.
4. Baumann, A.; Gaona, X.; Yalçıntaş, E.; Dardenne, K.; Prüßmann, T.; Rothe, J.; Duckworth, S.; Altmaier, M.; Geckeis, H., Impact of nitrate on the redox chemistry and solubility of Tc(IV) in alkaline, dilute to concentrated aqueous NaCl solutions. *Applied geochemistry* **2018,** *98*, 321-330.
5. Baumann, A.; Yalçıntaş, E.; Gaona, X.; Polly, R.; Dardenne, K.; Prüßmann, T.; Rothe, J.; Altmaier, M.; Geckeis, H., Thermodynamic description of Tc(IV) solubility and carbonate complexation in alkaline $NaHCO_3$-Na_2CO_3-NaCl systems. *Dalton transactions* **2018,** *47* (12), 4377-4392.
6. Becker, F.; Behrens, R.; Busch, F.; Figel, M.; Lorenz, B.; Otto, T., Dosimetrie - Neue Messgrößen der ICRU. *Strahlenschutz-Praxis* **2018,** *24* (1), 8-25.
7. Beuth, T.; Bracke, G.; Chaudry, S.; Lommerzheim, A.; Mayer, K. M.; Metz, V.; Mönig, J.; Mrugalla, S.; Orzechowski, J.; Plischke, E.; Röhlig, K. J.; Rübel, A.; Stolzenberg, G.; Wolf, J.; Wollrath, J., Wahrscheinlichkeitsklassen und Umgang mit unwahrscheinlichen Entwicklungen. *Atw* **2018,** *63* (11/12), 593-600.
8. Börsig, N.; Scheinost, A. C.; Shaw, S.; Schild, D.; Neumann, T., Retention and multiphase transformation of selenium oxyanions during the formation of magnetite via iron(II) hydroxide and green rust. *Dalton transactions* **2018,** *47* (32), 11002-11015.
9. Brkljača, Z.; Namjesnik, D.; Lützenkirchen, J.; Předota, M.; Preočanin, T., Quartz/Aqueous Electrolyte Solution Interface: Molecular Dynamic Simulation and Interfacial Potential Measurements. *The journal of physical chemistry <Washington, DC> / C* **2018,** *122* (42), 24025-24036.
10. Çevirim-Papaioannou, N.; Yalçıntaş, E.; Gaona, X.; Altmaier, M.; Geckeis, M., Solubility of U(VI) in chloride solutions. II. The stable oxides/hydroxides in alkaline KCl solutions: Thermodynamic description and relevance in cementitious systems. *Applied geochemistry* **2018,** *98*, 237-246.
11. Çevirim-Papaioannou, N.; Yalçıntaş, E.; Gaona, X.; Dardenne, K.; Altmaier, M.; Geckeis, H., Redox chemistry of uranium in reducing, dilute to concentrated NaCl solutions. *Applied geochemistry* **2018,** *98*, 286-300.
12. Dagan, R.; Herm, H.; Metz, V.; Becker, B., Determination of minor actinides in irradiated fuel rod components. *Atw* **2018,** *63* (10), 526-528.
13. Darnet, M.; Wawrzyniak, P.; Coppo, N.; Nielsson, S.; Schill, E.; Fridleifsson, G. Ó., Monitoring geothermal reservoir developments with the Controlled-Source Electro-Magnetic method - A calibration study on the Reykjanes geothermal field [in press]. *Journal of volcanology and geothermal research* **2018**.
14. Di Bernardo, P.; Endrizzi, F.; Melchior, A.; Zhang, Z. C.; Zanonato, P. L.; Rao, L. F., Complexation of Th(IV) with sulfate in aqueous solution at 10-70 degrees C. *J Chem Thermodyn* **2018,** *116*, 273-278.
15. Drake, H.; Mathurin, F. A.; Zack, T.; Schafer, T.; Roberts, N. M. W.; Whitehouse, M.; Karlsson, A.; Broman, C.; Astrom, M. E., Incorporation of Metals into Calcite in a Deep Anoxic Granite Aquifer. *Environmental Science & Technology* **2018,** *52* (2), 493-502.
16. Endrizzi, F.; Gaona, X.; Marques Fernandes, M.; Baeyens, B.; Altmaier, M., Solubility and hydrolysis of U(VI) in 0.5 mol/kg NaCl solutions at T = 22 and 80°C. *The journal of chemical thermodynamics* **2018,** *120*, 45-53.

17. Ferrari, P.; Bakhanova, E.; Becker, F.; Campani, L.; Chumak, V.; Jansen, J.; Jovanovic, Z.; Khan, S.; Kristic, D.; Mariotti, F.; Connor, U.; Pierotti, L.; Principi, S.; Clairand, I.; Knezevic, Z., EURADOS Working Group-12 Studies in Interventional Radiology for Medical Staff Dosimetry. *Il nuovo cimento / C* **2018,** *41*, Article:-217.

18. Fröhlich, D. R.; Panak, P. J., A thermodynamical study on the complex formation of Cm(III) with methacrylate. *Applied geochemistry* **2018,** *92*, 104-109.

19. Gaona, X.; Kulik, D. A.; Macé, N.; Wieland, E., Corrigendum to "Aqueous-solid solution thermodynamic model of U(VI) uptake in C-S-H phases" [Appl. Geochem. 27 (2012), 81–95] (Erratum). *Applied geochemistry* **2018,** *90*, 150.

20. Gonzalez-Siso, M. R.; Gaona, X.; Duro, L.; Altmaier, M.; Bruno, J., Thermodynamic model of Ni(II) solubility, hydrolysis and complex formation with ISA. *Radiochimica Acta* **2018,** *106* (1), 31-45.

21. Grunwaldt, J.-D.; Lichtenberg, H.; Rothe, J., Inauguration Workshop of the CAT-ACT Beamline for Catalysis and Radionuclide Research at ANKA. *Synchrotron radiation news* **2018,** *31* (1), 16-19.

22. Haas-Nuesch, R.; Heberling, F.; Schild, D.; Rothe, J.; Dardenne, K.; Jahniche, S.; Eiche, E.; Marquardt, C.; Metz, V.; Schafer, T., Mineralogical characterization of scalings formed in geothermal sites in the Upper Rhine Graben before and after the application of sulfate inhibitors. *Geothermics* **2018,** *71*, 264-273.

23. Halleröd, J.; Ekberg, C.; Authen, T.; Bertolo, L.; Lin, M.; Grüner, B.; Švehla, J.; Wagner, C.; Geist, A.; Panak, P.; Aneheim, E., On the Basic Extraction Properties of a Phenyl Trifluoromethyl Sulfone-Based GANEX System Containing $CyMe_4$-BTBP and TBP. *Solvent extraction and ion exchange* **2018,** *36* (4), 360-372.

24. Häußler, V.; Amayri, S.; Beck, A.; Platte, T.; Stern, T. A.; Vitova, T.; Reich, T., Uptake of actinides by calcium silicate hydrate (C-S-H) phases. *Applied geochemistry* **2018,** *98*, 426-434.

25. Heberling, F.; Metz, V.; Böttle, M.; Curti, E.; Geckeis, H., Barite recrystallization in the presence of ^{226}Ra and ^{133}Ba. *Geochimica et cosmochimica acta* **2018,** *232*, 124-139.

26. Held, S.; Schill, E.; Schneider, J.; Nitschke, F.; Morata, D.; Neumann, T.; Kohl, T., Geochemical characterization of the geothermal system at Villarrica volcano, Southern Chile; Part 1: Impacts of lithology on the geothermal reservoir. *Geothermics* **2018,** *74*, 226-239.

27. Herm, M.; Dagan, R.; González-Robles, E.; Müller, N.; Metz, V., Comparison of calculated and measured radionuclide inventory of a Zircaloy-4 cladding tube plenum section. *MRS advances* **2018,** *3* (19), 1031-1037.

28. Janicki, R.; Lindqvist-Reis, P., Eu(III) and Cm(III) tetracarbonates: in the quest for the limiting species in solution. *Dalton transactions* **2018,** *47* (7), 2393-2405.

29. Jo, Y.; Lee, J. Y.; Yun, J.-I., Adsorption of uranyl tricarbonate and calcium uranyl carbonate onto γ-alumina. *Applied geochemistry* **2018,** *94*, 28-34.

30. Jordan, N.; Franzen, C.; Lützenkirchen, J.; Foerstendorf, H.; Hering, D.; Weiss, S.; Heim, K.; Brendler, V., Adsorption of selenium(VI) onto nano transition alumina. *Environmental science / Nano* **2018,** *5* (7), 1661-1669.

31. Kienzler, B., Corrosion processes of alloyed steels in salt solutions. *Atw* **2018,** *63* (2), 104-110.

32. Kienzler, B.; Geckeis, H., Radioactive wastes and disposal options. *The European physical journal / Web of Conferences* **2018,** *189*, 00014.

33. Kotz, F.; Schneider, N.; Striegel, A.; Wolfschläger, A.; Keller, N.; Worgull, M.; Bauer, W.; Schild, D.; Milich, M.; Greiner, C.; Helmer, D.; Rapp, B. E., Glassomer-Processing Fused Silica Glass Like a Polymer. *Advanced materials* **2018,** *30* (22), 1707100.

34. Kotz, F.; Schneider, N.; Striegel, A.; Wolfschläger, A.; Keller, N.; Worgull, M.; Bauer, W.; Schild, D.; Milich, M.; Greiner, C.; Helmer, D.; Rapp, B. E., Nanocomposites: Glassomer-Processing Fused Silica Glass Like a Polymer (Adv. Mater. 22/2018). *Advanced materials* **2018,** *30* (22), 1870151.

35. Kulenkampff, J.; Stoll, M.; Gründig, M.; Mansel, A.; Lippmann-Pipke, J.; Kersten, M., Time-lapse 3D imaging by positron emission tomography of Cu mobilized in a soil column by the herbicide MCPA. *Scientific reports* **2018,** *8* (1)

36. Lindqvist-Reis, P.; Réal, F.; Janicki, R.; Vallet, V., Unraveling the Ground State and Excited State Structures and Dynamics of Hydrated Ce^{3+} Ions by Experiment and Theory. *Inorganic chemistry* **2018,** *57* (16), 10111-10121.

37. Lippold, H.; Karimzadeh, L.; Kulenkampff, J.; Wissmeier, L.; Stuhlfauth, C.; Stoll, M.; Lippmann-Pipke, J., Effect of pH on the mobility of the herbicide MCPA in a sand-goethite column: 1D and 2D reactive transport modeling. *Applied geochemistry* **2018,** *98*, 345-350.

38. Lützenkirchen, J.; Finck, N., Treatment of temperature dependence of interfacial speciation by speciation codes and temperature congruence of oxide surface charge. *Applied Geochemistry* **2019,** *102*, 26-33.

39. Lützenkirchen, J.; Franks, G. V.; Plaschke, M.; Zimmermann, R.; Heberling, F.; Abdelmonem, A.; Darbha, G. K.; Schild, D.; Filby, A.; Eng, P.; Catalano, J. G.; Rosenqvist, J.; Preocanin, T.; Aytug, T.; Zhang, D.; Gan, Y.; Braunschweig, B., The surface chemistry of sapphire-c: A literature review and a study on various factors influencing its IEP. *Advances in colloid and interface science* **2018,** *251*, 1-25.

40. Lützenkirchen, J.; Scharnweber, T.; Ho, T.; Striolo, A.; Sulpizi, M.; Abdelmonem, A., A set-up for simultaneous measurement of second harmonic generation and streaming potential and some test applications. *Journal of colloid and interface science* **2018,** *529*, 294-305.

41. Lützenkirchen, J.; Sjoberg, S., Speciation and equilibria in the H^+-Al^{3+} - polyacrylic acid system. *Monatsh Chem* **2018,** *149* (2), 423-429.

42. Mayordomo, N.; Foerstendorf, H.; Liitzenlcirchen, J.; Heim, K.; Weiss, S.; Alonso, U.; Missana, T.; Schmeide, K.; Jordan, N., Selenium(IV) Sorption Onto gamma-Al_2O_3: A Consistent Description of the Surface Speciation by Spectroscopy and Thermodynamic Modeling. *Environmental Science & Technology* **2018,** *52* (2), 581-588.

43. McNeece, C. J.; Lützenkirchen, J.; Hesse, M. A., Chromatographic analysis of the acidity-salinity transport system. *Journal of contaminant hydrology* **2018,** *216*, 27-37.

44. Meixner, J.; Grimmer, J. C.; Becker, A.; Schill, E.; Kohl, T., Comparison of different digital elevation models and satellite imagery for lineament analysis: Implications for identification and spatial arrangement of fault zones in crystalline basement rocks of the southern Black Forest (Germany). *J Struct Geol* **2018,** *108*, 256-268.

45. Meller, C.; Schill, E.; Bremer, J.; Kolditz, O.; Bleicher, A.; Benighaus, C.; Chavot, P.; Gross, M.; Pellizzone, A.; Renn, O.; Schilling, F.; Kohl, T., Acceptability of geothermal installations: A geoethical concept for GeoLaB. *Geothermics* **2018,** *73*, 133-145.

46. Montoya, V.; Baeyens, B.; Glaus, M. A.; Kupcik, T.; Fernandes, M. M.; Van Laer, L.; Bruggeman, C.; Maes, N.; Schafer, T., Sorption of Sr, Co and Zn on illite: Batch experiments and modelling including Co in-diffusion measurements on compacted samples. *Geochimica Et Cosmochimica Acta* **2018,** *223*, 1-20.

47. Mossini, E.; Macerata, E.; Wilden, A.; Kaufholz, P.; Modolo, G.; Iotti, N.; Casnati, A.; Geist, A.; Mariani, M., Optimization and Single-Stage Centrifugal Contactor Experiments with the Novel Hydrophilic Complexant PyTri-Diol for the i-SANEX Process. *Solvent extraction and ion exchange* **2018,** *36* (4), 373-386.

48. Necib, S.; Bucur, C.; Caes, S.; Cochin, F.; Cvetković, B. Z.; Fulger, M.; Gras, J. M.; Herm, M.; Kasprzak, L.; Legand, S.; Metz, V.; Perrin, S.; Sakuragi, T.; Suzuki-Muresan, T., Overview of ^{14}C release from irradiated zircaloys in geological disposal conditions. *Radiocarbon* **2018,** *60* (6), 1757-1771.

49. Prieur, D.; Epifano, E.; Dardenne, K.; Rothe, J.; Hennig, C.; Scheinost, A. C.; Neuville, D. R.; Martin, P. M., Peculiar Thermal Behavior of UO_2 Local Stucture. *Inorganic chemistry* **2018,** *57* (23), 14890-14894.

50. Pupier, M.; Nuzillard, J.-M.; Wist, J.; Schlörer, N. E.; Kuhn, S.; Erdelyi, M.; Steinbeck, C.; Williams, A. J.; Butts, C.; Claridge, T. D. W.; Mikhova, B.; Robien, W.; Dashti, H.; Eghbalnia, H. R.; Farès, C.; Adam, C.; Kessler, P.; Moriaud, F.; Elyashberg, M.; Argyropoulos, D.; Pérez, M.; Giraudeau, P.; Gil, R. R.; Trevorrow, P.; Jeannerat, D., NMReDATA, a standard to report the NMR assignment and parameters of organic compounds. *Magnetic resonance in chemistry* **2018,** *56* (8), 703-715.

51. Rai, D.; Kitamura, A.; Altmaier, M.; Rosso, K. M.; Sasaki, T.; Kobayashi, T., A Thermodynamic Model for ZrO_2(am) Solubility at 25 °C in the Ca^{2+}–Na^+–H^+–Cl^-–OH^-–H_2O System: A Critical Review. *Journal of solution chemistry* **2018,** *47* (5), 855-891.

52. Rai, D.; Kitamura, A.; Altmaier, M.; Rosso, K. M.; Sasaki, T.; Kobayashi, T., Correction to: A Thermodynamic Model for ZrO_2(am) Solubility at 25 °C in the Ca^{2+}–Na^+–H^+–Cl^-–OH^-–H_2O System: A Critical Review. *Journal of solution chemistry* **2018,** *47* (6), 1138.

53. Rojo, H.; Scheinost, A. C.; Lothenbach, B.; Laube, A.; Wieland, E.; Tits, J., Retention of selenium by calcium aluminate hydrate (AFm) phases under strongly-reducing radioactive waste repository conditions. *Dalton transactions* **2018,** *47* (12), 4209-4218.

54. Saleh, A. S.; Lee, J. Y.; Jo, Y.; Yun, J. I., Uranium(VI) sorption complexes on silica in the presence of calcium and carbonate. *J Environ Radioactiv* **2018,** *182*, 63-69.

55. Sauri Suarez, H.; Becker, F.; Klix, A.; Pang, B.; Döring, T., Neutron flux measurements on a mock-up of a storage cask for high-level nuclear waste using 2.5 MeV neutrons. *Journal of radiological protection* **2018,** *38* (3), 881-891.

56. Sulpizi, M.; Lützenkirchen, J., Atypical titration curves for $GaAl_{12}$ Keggin-ions explained by a joint experimental and simulation approach. *The journal of chemical physics* **2018,** *148* (22), Article:-222836.

57. Tasi, A.; Gaona, X.; Fellhauer, D.; Böttle, M.; Rothe, J.; Dardenne, K.; Polly, R.; Grivé, M.; Colàs, E.; Bruno, J.; Källstrom, K.; Altmaier, M.; Geckeis, H., Thermodynamic description of the plutonium – α–d–isosaccharinic acid system ii: Formation of quaternary Ca(II)–Pu(IV)–OH–ISA complexes. *Applied geochemistry* **2018,** *98*, 351-366.

58. Tasi, A.; Gaona, X.; Fellhauer, D.; Böttle, M.; Rothe, J.; Dardenne, K.; Schild, D.; Grivé, M.; Colàs, E.; Bruno, J.; Källström, K.; Altmaier, M.; Geckeis, H., Redox behavior and solubility of plutonium under alkaline, reducing conditions. *Radiochimica acta* **2018,** *106* (4), 259-279.

59. Tasi, Á. G.; Gaona, X.; Fellhauer, D.; Böttle, M.; Rothe, J.; Dardenne, K.; Polly, K.; Grivé, M.; Colàs, E.; Bruno, J.; Källström, K.; Altmaier, M.; Geckeis, H., Thermodynamic description of the plutonium – α-D-isosaccharinic acid system I: Solubility, complexation and redox behavior. *Applied geochemistry* **2018,** *98*, 247-264.

60. Trumm, M., On the Isotropy of Induced Multipole Moments in Heavy Ion Complexes. *J Comput Chem* **2018,** *39* (7), 373-379.

61. Vespa, M.; Lothenbach, B.; Dähn, R.; Huthwelker, T.; Wieland, E., Characterisation of magnesium silicate hydrate phases (M-S-H): A combined approach using synchrotron-based absorption-spectroscopy and ab initio calculations. *Cement and concrete research* **2018,** *109*, 175-183.

62. Virtanen, S.; Meriläinen, S.; Eibl, M.; Rabung, T.; Lehto, J.; Huittinen, N., Sorption competition and kinetics of trivalent cations (Eu, Y and Cm) on corundum (α-Al_2O_3): A batch sorption and TRLFS study. *Applied geochemistry* **2018,** *92*, 71-81.

63. Vitova, T.; Pidchenko, I.; Biswas, S.; Beridze, G.; Dunne, P. W.; Schild, D.; Wang, Z.; Kowalski, P. M.; Baker, R. J., Dehydration of the Uranyl Peroxide Studtite, $[UO_2(\eta^2\text{-}O_2)(H_2O)_2]\cdot 2H_2O$, Affords a Drastic Change in the Electronic Structure: A Combined X-ray Spectroscopic and Theoretical Analysis. *Inorganic chemistry* **2018,** *57* (4), 1735-1743.

64. Vitova, T.; Pidchenko, I.; Fellhauer, D.; Pruessmann, T.; Bahl, S.; Dardenne, K.; Yokosawa, T.; Schimmelpfennig, B.; Altmaier, M.; Denecke, M.; Rothe, J.; Geckeis, H., Exploring the electronic structure and speciation of aqueous and colloidal Pu with high energy resolution XANES and computations. *Chemical communications* **2018,** *54* (91), 12824-12827.

65. Weßling, P.; Trumm, M.; Geist, A.; Panak, P. J., Stoichiometry of An(III)–DMDOHEMA complexes formed during solvent extraction. *Dalton transactions* **2018,** *47* (32), 10906-10914.

66. Whittaker, D.; Geist, A.; Modolo, G.; Taylor, R.; Sarsfield, M.; Wilden, A., Applications of Diglycolamide Based Solvent Extraction Processes in Spent Nuclear Fuel Reprocessing, Part 1: TODGA. *Solvent extraction and ion exchange* **2018,** *36* (3), 223-256.

Invited talks

67. Adam, N.; Adam, C.; Keskitalo, M.; Pfeuffer-Rooschuez, J.; Ditter, A.-L.; Smith, V. C.; MacGillivray, R. T. A.; Panak, P. J., *Interaction of human serum albumin with Cm(III) using time-resolved laser fluorescence spectroscopy (TRLFS) and NMR*, 18th Radiochemical Conference (RadChem 2018), Marienbad, Czech Republic, **2018**.

68. Altmaier, M.; Geckeis, H., *Research on radiochemistry and geochemistry at KIT-INE, Germany, in support of the Nuclear Waste Disposal Safety Case,* Korean Radioactive Waste Society Annual Meeting, Jeju, Republic of Korea, **2018**.

69. Altmaier, M., *Radiochemical and geochemical Research at the Institute for Nuclear Waste Disposal at the Karlsruhe Institute of Technology,* f-ELEMENT Seminar Series Cologne, Köln, **2018**.

70. Altmaier, M., *CORI - cement-organic-radionuclide-interactions,* IGD-TP 8th Exchange Forum, Berlin, **2018**.

71. Becker, F., *Neue Regelungen zu Dosisgrenzwerten*, Symposium: Was bringt uns die neue Strahlenschutzverordnung?, Aschaffenburg, Germany, **2018**.

72. Fellhauer, D.; Schepperle, J.; Schramm, T.; Gaona, X.; Schild, D.; Walter, O.; Rothe, J.; Altmaier, M.; Geckeis, H., *Solubility, hydrolysis and solid phase formation of hexavalent Pu in alkaline NaCl solutions*, Plutonium Futures - The Science: A Topical Conference on Plutonium and Actinides, San Diego, USA, **2018**.

73. Geckeis, H., *Retrieving waste from the Asse salt mine – facts and challenges*, United States Nuclear Waste Technical Review Board, Spring Board Meeting, Washington DC, USA, **2018**.

74. Geckeis, H., *Zur Chemie des "elementaren Bösen" - Chemische Aspekte der nuklearen Entsorgung*, Seminarvortrag auf Einladung des GDCH-Jungchemikerforums der Universität Chemnitz, Chemnitz, Germany, **2018**.

75. Geckeis, H., *Aspects of environmental actinide behavior*, Xingda lecture, College of chemistry and molecular engineering, Peking University, Peking, China, **2018**.

76. Geckeis, H., *Aspects of environmental actinide behavior*, Journées d'Etude de la Chimie sous Rayonnement et de la Radiochimie, Strasbourg, France, **2018**.

77. Geckeis, H., *Safety for 1 Million Years! The Scientific Challenge of Radioactive Waste Disposal*, Forster Summer School 2018, Global Change – Technological, Societal and Ecological Transitions on the Move, Mainz, Germany, **2018**.

78. Geckeis, H.; Zavarin, M.; Salbu, B.; Lind, O. C.; L., S., *Environmental chemistry of Plutonium*, American Nuclear Society meeting, Plutonium Futures – The Science 2018, San Diego, USA, **2018**.

79. Heberling, F., *3D Molecular Structure of Mineral-Water-Interfaces, Studied by X-ray Surface Diffraction*, MAINZ Summer School "Investigating Solid-Liquid Interfaces – Complementary Theoretical and Experimental Approaches", Mainz, Germany, **2018**.

80. Heberling, F., *Mineralogical characterization of scalings formed in the presence of a sulfate inhibitor – links between scale formation and corrosion*, German Geothermal Congress, Essen, Germany, **2018**.

81. Heberling, F.; Polly, R., *Molecular scale structure of the calcite(104)-water-interface and interfacial reactions of Selenite ($Se(IV)O_3^{2-}$), insights from experiment and theory*, 255th ACS National Meeting & Expo, New Orleans, USA, **2018**.

82. Herm, M., *^{14}C inventory in irradiated Zircaloys*, EC CAST (CArbon-14 Source Term) Final Symposium, Lyon, France, **2018**.

83. Joseph, C.; Balboni, E.; Baumer, T.; Treinen, K.; Kersting, A. B.; Zavarin, M., *Desorption kinetics of plutonium from altered nuclear melt glass colloids*, 256th ACS conference, Boston, USA, 2018.

84. Metz, V., *Research on high-level waste at KIT-INE in the context of prolonged interim storage and the new site-selection process for a deep geological repository in Germany*, Korean Radioactive Waste Society (KRS) Fall Meeting, Jeju, Republic of Korea, **2018**.

85. Metz, V., *Auswirkungen der (verlängerten) Oberflächenlagerung hochradioaktiver Abfälle auf die anschließende Tiefenlagerung*, Eingeladener Vortrag im Bundesamt für kerntechnische Entsorgungssicherheit (BfE), Berlin, Germany, **2018**.

86. Quinto, F.; Geckeis, H.; Hain, K.; Mäder, U.; Plaschke, M.; Schäfer, T.; Steier, P., *Ultra-trace analysis with AMS of actinides from global fallout and in-situ tracer tests*, Plutonium Futures - The Science: A Topical Conference on Plutonium and Actinides, San Diego, USA, **2018**.

87. Rothe, J., *XAFS spectroscopy - an ideal tool to unravel molecular scale structures and processes in the context of the nuclear waste disposal safety case*, 17th Symposium on Remediation, Jena, Germany, **2018**.

88. Schacherl, B., *Strukturelle Untersuchungen von Neptunium auf Illit mit hochauflösender Röntgenabsorptionsspektroscopie*, Finalrunde des WiN Germany Preises 2018, Mitgliederversammlung Women in Nuclear, Garching, Germany, **2018**.

89. Skerencak-Frech, A., *Radionuclide chemistry in Nuclear Waste Disposal – application of modern spectroscopy for molecular process understanding and actinide thermodynamics*, 35th International Conference on Solution Chemistry, Szeged, Hungary, **2018**.

Oral and poster presentations

90. Ait Mouheb, N.; Montoya, V.; Schäfer, T.; Metz, V.; Geckeis, H., *Radionuclide/toxic elements migration in the low pH cement / clay interface*, 8th Reactive Transport PhD Workshop, Villingen-Schwenningen, Germany, **2018**.

91. Ait Mouheb, N.; Montoya, V.; Schild, D.; Soballa, E.; Adam, C.; Schäfer, T., *Experimental findings and modelling of the hydration of low pH cements – relevance of C-A-S-H phases*, 3rd International Symposium on Cement-based Materials for Nuclear Wastes (NUWCEM 2018), Avignon, France, **2018**.

92. Altmaier, M.; Montoya, V.; Duro, L.; Valls, A.; Holt, E.; Claret, F.; Mäder, U.; Grambow, B.; Idiart, A., *CEBAMA – a project on cement-based-materials within the EC Horizon 2020 frame*, 3rd International Symposium on Cement-based Materials for Nuclear Wastes (NUWCEM 2018), Avignon, France, **2018**.

93. Altmaier, M.; Brandt, F.; Brendler, V.; N.; Chiorescu, I.; Colas, E.; Endrizzi, F.; Gaona, X.; Gray, A.; Grive, M.; Hagemann S.; Huittinen, N.; Koke, C.; Kulik, D.A.; Krüger, S.; Lee, J.-Y.; Maiwald, M.; Miron, D.; Panak, P.J.; Poonoosamy, J.; Skerencak-Frech, A.; Steudtner, R.; Thoenen, T., *Studies on radionuclide chemistry at elevated temperature conditions within the collaborative THERMAC project,* International Symposium on Solubility Phenomena and Related Equilibrium Processes (ISSP 2018), Tours, France, **2018**.

94. Altmaier, M.; Schepperle, J.; Yalcintas, E.; Cevirim-Papaioannou, N.; Fellhauer, D.; Gaona, X.; Geckeis, H., *Studies on An(IV)-hydroxo-carbonate complex formation along the An(IV) = Th, U, Np, Pu series,* American Chemical Society meeting, Boston, USA, **2018**.

95. Altmaier, M.; Endrizzi, F.; Lee, J.-Y.; Fellhauer, D.; Gaona, X., *Studies on actinide chemistry at elevated temperatures at KIT-INE within the German collaborative ThermAc project,* American Chemical Society meeting, Boston, USA, **2018**.

96. Altmaier, M.; Fellhauer, D.; Metz, V., *Geochemistry in support of potential emergency measures for Schachtanlage Asse II – (4). Radionuclide source terms, solubility and retention processes,* 9th US/German Workshop Salt Repository Research, Design and Operation, Hanover, Germany, September **2018**.

97. Altmaier, M.; Cevirim-Papaioannou, N.; Yalcintas, E.; Gaona, X.; Geckeis, H., *Solution chemistry of uranium in cementitious systems - Redox chemistry, solubility and hydrolysis of uranium in dilute to concentrated saline systems and high pH conditions,* 3rd International Symposium on Cement-based Materials for Nuclear Wastes (NUWCEM 2018), Avignon, France, **2018**.

98. Altmaier, M., *Studies on Radionuclide-Organic Interactions at KIT,* K3Trilateral Workshop KIT-INE, KAERI and KAIST, Jeju, Republic of Korea, **2018**.

99. Altmaier, M., *CEBAMA – EC HORIZON2020 Project on Cement-Based-Materials,* IGD-TP 8th Exchange Forum, Berlin, **2018**.

100. Beck, A.; Pidchenko, I.; Fellhauer, D.; González-Robles, E.; Dardenne, K.; Rothe, J.; Altmaier, M.; Herm, M.; Geckeis, H.; Vitova, T., *U/Pu M4,5 edge HR-XANES investigations (i) of aqueous/colloidal Pu and (ii) at the Zircaloy cladding/spent nuclear fuel interface*, 17th International Conference on X-Ray Absorption Fine Structure (XAFS 2018), Krakau, Poland, **2018**.

101. Becker, F., *Welches sind die gebräuchlichsten Monte-Carlo-Codes zur Anwendung im Strahlenschutz und in der Dosimetrie?*, 88. Arbeitskreis "Dosimetrie" (AKD) im Deutsch-Schweizerischen Fachverband für Strahlenschutz, Dresden, Germany, **2018**.

102. Becker, F.; Suarez, H. S.; Pang, B.; Metz, V.; Geckeis, H., *Monte-Carlo simulations for individual dosimetry in disposal facilities for spent nuclear fuel*, 5th European IRPA Congress, Den Haag, The Netherlands, **2018**.

103. Bourg, S.; Geist, A.; Adnet, J.-M.; Rhodes, C.; Hanson, B., *GENIORS, a European Project on Advanced Fuel Recycling Strategies - Consolidating the Outcome of Preceding Projects*, 18th Radiochemical Conference, Mariánské Lázně, Czech Republic, **2018**.

104. Bourg, S.; Geist, A.; Adnet, J.-M.; Rhodes, C.; Hanson, B., *GENIORS, the Current European Actinide Separations Programme - Consolidating the Outcome of Preceding Projects*, 42nd Annual Actinide Separations Conference, Charleston, USA, **2018**.

105. Bourg, S.; Geist, A.; Adnet, J.-M.; Rohdes, C.; Hanson, B., *GENIORS, a EU project on MOX fuel reprocessing in GEN IV systems*, Actinide and Fission Product Partitioning and Transmutation: 15th Information Exchange Meeting, Manchester, Great Britain, **2018**.

106. Brandauer, M., *Abrasive waste treatment technologies for the reduction of secondary radioactive waste*, Japanese-German Student Nuclear Decommissioning Symposium, Tsuruga, Japan, **2018**.

107. Brandauer, M., *Experimentelle Untersuchungen zur Separation von Korngemischen in einem Stabmagnetfilter*, KTG-Sitzung, Berlin, Germany, **2018**.

108. Brandauer, M., *Introduction to the KIT decommissioning R&D*, IAEA Regional Workshop on Application of State-of-the-Art Methodologies and Technologies for Decommissioning, Karlsruhe, Germany, **2018**.

109. Brandauer, M., *Karlsruhe Institute of Technology. A center of decommissioning education and research*, Dialogue with Taiwan on Nuclear Decommissioning in Baden-Württemberg, Germany – 35 Years of Experience and Competence, Taipeh, Taiwan, **2018**.

110. Brandauer, M., *New developments in decontamination and dismantling techniques*, 10th Summer School on Nuclear Decommissioning and Waste Management, Ispra, Italy, **2018**.

111. Brandauer, M., *New technologies for concrete surface decontamination*, Stillegung - Abbau kerntechnischer Anlagen, Karlsruhe, Germany, **2018**.

112. Brandauer, M., *Situation of decommissioning of commercial nuclear power plants in Europe*, International Symposium, Wakasa Wan Energy Research Center, Tsuruga, Japan, **2018**.

113. Brandauer, M.; Geckeis, H.; Gentes, S.; Heneka, A.; Krauß, C. O.; Plaschke, M.; Schild, D.; Tobie, W., *Presentation of a separation method for the reduction of secondary waste from the waterjet abrasive suspension cutting technique*, International Conference on Dismantling Challenges: Industrial Reality, Prospects and Feedback Experience (DEM 2018), Avignon, France, **2018**.

114. Busser, C.; Faestermann, T.; Gomez-Guzman, J. M.; Hain, K.; Kinast, A.; Koll, D.; Korschinek, G.; Kortmann, F.; Krieg, D.; Lebert, M.; Lierse von Gostomski, C.; Ludwig, P.; Quinto, F., *Improving the accuracy in the analysis of ^{99}Tc using AMS*, 82. Jahrestagung der DPG und DPG-Frühjahrstagung der Sektion Atome, Moleküle, Quantenoptik und Plasmen (SAMOP), Fachverband Massenspektrometrie, Erlangen, Germany, **2018**.

115. Delavernhe, L.; Joseph, C.; Montoya, V.; Moisei-Rabung, S.; Glaus, M. A.; Trumm, M.; Kupcik, T.; Lützenkirchen, J.; Schuhmann, R.; Emmerich, K.; Schäfer, T., *Influence of interlayers on the diffusion of HTO, $^{36}Cl^-$, and $^{85}Sr^{2+}$ through smectites*, 25. Koordinierungsgespräch KIT/INE – PSI/LES, PSI Villigen, Schweiz, **2018**.

116. Duckworth, S.; Baumann, A.; Gaona, X.; Altmaier, M.; Geckeis, H., *Impact of sulfate on the on the solubility of Tc(IV) under reducing conditions*, 10th International Symposium on Technetium and Rhenium – Science and Utilization, Moscow, Russia, **2018**.

117. Fellhauer, D.; Schepperle, J.; Schramm, T.; Gaona, X.; Schild, D.; Walter, O.; Rothe, J.; Altmaier, M.; Geckeis, H., *Solubility and solid phase formation of plutonium(VI) in alkaline NaCl solutions*, International Symposium on Solubility Phenomena and Related Equilibrium Processes (ISSP 2018), Tours, France, **2018**.

118. Ferrari, P.; Bakhanova, E.; Becker, F.; Campani, L.; Chumak, V.; Jansen, J.; Jovanovic, Z.; Khan, S.; Kristic, D.; Mariotti, F.; Connor, U.; Pierotti, L.; Principi, S.; Clairand, I.; Knezevic, Z., *EURADOS Working Group-12 Studies in Interventional Radiology for Medical Staff Dosimetry*, XVIII Convegno Nazionale - SIRR2018, Rom, Italy, **2018**.

119. Finck, N.; Schlegel, M. L.; Adam, D.; Dardenne, K.; Bauer, A.; Robert, J. L., *Iron speciation in smectites of different charge and charge location*, 17th International Conference on X-Ray Absorption Fine Structure (XAFS 2018), Krakau, Polen, : **2018**.

120. Friedrich, S., *Defined removal of highly reinforced concrete structures (DefAhS)*, International Workshop on Application of Advanced Plant Information Systems for Nuclear Decommissioning and Life-Cycle Management, Lillehammer, Norway, **2018**.

121. Gaona, X.; Baumann, A.; Duckworth, S.; Yalcintas, E.; Polly, R.; Altmaier, M.; Geckeis, H., *Solubility, complexation and redox behaviour of Tc(IV): effect of carbonate, sulfate and nitrate*, American Chemical Society meeting, Boston, USA, **2018**.

122. Gaona, X., Cevirim-Papaioannou, N.; Ait-Mouheb, N.; Böttle, M.; Altmaier, M., *Solubility, hydrolysis and sorption of Be(II) in the context of cementitious systems,* International Symposium on Solubility Phenomena and Related Equilibrium Processes (ISSP 2018), Tours, France, **2018**.

123. Gaona, X.; Grambow, B.; Altmaier, M.; Geckeis, H., *Development and improvement of thermodynamic understanding for the nuclear waste disposal Safety Case*, IGD-TP Exchange Forum, Berlin, Germany, **2018**.

124. Gaona, X.; Tasi, A.; Fellhauer, D.; Rabung, T.; Rothe, J.; Polly, R.; Grivé, M.; Colàs, E.; Bruno, J.; Källström, K.; Altmaier, M.; Geckeis, H., *Solution chemistry of Pu in alkaline reducing systems: redox, solubility and complexation with organic ligands*, American Chemical Society meeting, Boston, USA, **2018**.

125. Gentes, S.; Brandauer, M., *Rückbau kerntechnischer Anlagen: Kein Thema für sich! Der wichtige Beitrag von Forschung und Lehre*, Ausstellung des KIT-Zentrums Energie im Karlsruher Rathaus, Karlsruhe, Germany, **2018**.

126. Heide, B., *Different Actions Taken to Generate the Specific Energy Distribution*, EURADOS Annual Meeting, Working Group 6 meeting, Lisbon, Portugal, **2018**.

127. Heneka, A.; Brandauer, M.; Geckeis, H.; Gentes, S.; Krauß, C. O.; Plaschke, M.; Schild, D.; Tobie, W., *Magnetic filter system for the treatment of secondary waste from the water jet abrasive suspension cutting technique*, 49th Annual Meeting on Nuclear Technology (AMNT 2018), Berlin, Germany, **2018**.

128. Heneka, A.; Brandauer, M.; Geckeis, H.; Gentes, S.; Krauß, C. O.; Plaschke, M.; Schild, D.; Tobie, W., *Verbesserung eines Magentseparationsverfahrens zur Behandlung des Sekundärabfalls der Wasser-Abrasiv-Suspensions-Schneidtechnik*, IFAT 2018 : Weltleitmesse für Wasser-, Abwasser-, Abfall- und Rohstoffwirtschaft, Munich, Germany, **2018**.

129. Herm, M., *Formation and status of ^{14}C in activated steel*, EC CAST (CArbon-14 Source Term) Final Symposium, Lyon, France, **2018**.

130. Herm, M.; González-Robles, E.; Müller, N.; Dardenne, K.; Rothe, J.; Schild, D.; García, C.; Dagan, R.; Metz, V., *Research activities on safety of extended dry storage of spent nuclear fuel at KIT-INE*, 2nd Workshop on Safety of Extended Dry Storage of Spent Nuclear Fuel, Garching, Germany, **2018**.

131. Herm, M.; González-Robles, E.; Müller, N.; König, T.; Dardenne, K.; Rothe, J.; Schild, D.; Dagan, R.; Metz, V., *Radionuclides present at inner cladding surfaces of irradiated PWR fuel rod segments in the context of safety of extended dry storage of spent nuclear fuel*, KEK, Seminar, Boston, MA, USA, **2018**.

132. Herm, M.; González-Robles, E.; Müller, N.; König, T.; Dardenne, K.; Rothe, J.; Schild, D.; Dagan, R.; Metz, V., *Radionuclides present at inner cladding surfaces of irradiated PWR fuel rod segments in thecontext of safety of extended dry storage of spent nuclear fuel*, Materials Research Society (MRS), scientific basis for nuclear waste management (SBNWM), Boston, MA, USA, **2018**.

133. Herm, M.; González-Robles, E.; Müller, N.; Schild, D.; Dardenne, K.; Rothe, J.; García, C.; Dagan, R.; Metz; V., *Radionuclide containing solid phases on inner surfaces of Zircaloy-4 from plenum and fuel section of a PWR fuel rod*, 29th International Spent Nuclear Fuel Workshop, Sheffield, UK, **2018**.

134. Idiart, A.; Laviña, M.; Coene, E.; Montoya, V.; Kosakowski, G.; Cochepin, B.; Munier, I.; Samper, J.; Meeussen, J.; Deissmann, G.; Rohmen, S.; Vopalka, D., *Reactive transport processes at a low-pH concrete / clay interface: a benchmark modelling study*, 3rd International Symposium on Cement-based Materials for Nuclear Wastes (NUWCEM 2018), Avignon, France, **2018**.

135. Lee, J.-Y.; Fellhauer, D.; Gaona, X.; Vespa, M.; Schild, D.; Walter, O.; Altmaier, M., *Temperature effect on solid transformation and redox behavior of Np(V)*, International Symposium on Solubility Phenomena and Related Equilibrium Processes (ISSP 2018), Tours, France, **2018**.

136. Lewis, F. W.; Zaytsev, A.; Bulmer, R.; Wilden, A.; Modolo, G.; Wessling, P.; Geist, A.; Panak, P. J., *Studies on new bis-triazine ligands in spent nuclear fuel reprocessing: tuning the aliphatic part and its effects on extraction properties*, International Nuclear Engineering Conference (INEC 2018), Manchester, UK, **2018**.

137. Li, W. B.; Belchior, A.; Beuve, M.; Bug, M. U.; di Maria, S.; Dressel, T.; Friedland, W.; Heide, B.; Hocine, N.; Klapproth, A.; Li, C. Y.; Li, J. L.; Multhoff, G.; Poignant, F.; Xie, X. Z.; Villagrasa, C., *Comparison of Monte Carlo simulated physical radiation quantities for gold nanoparticles irradiated by xrays and assessment of potential indication for targeted breast cancer treatment Assessing the contribution of cross-sections to the uncertainty of Monte Carlo calculations in micro- and nano-dosimetry*, Geant4 International User Conference, Bordeaux, France, **2018**.

138. Modolo, G.; Wilden, A.; Geist, A., *Actinide-lanthanide separation - the crucial point during the recycling of minor actinides from used nuclear fuel*, 10th International Conference on f-Elements (ICFE 2018), Lausanne, Switzerland, **2018**.

139. Montoya, V.; Ait Mouheb, N.; Schäfer, T., *Reactive transport modelling of radionuclides migration in the low pH cement/clay interface*, 3rd International Symposium on Cement-based Materials for Nuclear Wastes (NUWCEM 2018), Avignon, France, **2018**.

140. Munoz, A. G.; Schild, D., *Corrosion of austenitic steel in geochemical near-field conditions of high-level radioactive waste rock repositories*, The Annual Congress of the European Federation of Corrosion (2018), Krakau, Poland, **2018**.

141. Munoz, A. G.; Schild, D., *Corrosion of steel in high-level radioactive waste rock repositories: kinetics and thermodynamics*, Corrosion Conference and Expo 2018, Phoenix, USA, **2018**.

142. Plaschke, M.; Quinto, F.; Geyer, F.; Geckeis, H., *Analysis of isobaric interferences in the analysis of Tc-99 with SF-ICPMS*, 82. Jahrestagung der DPG und DPG-Frühjahrstagung der Sektion Atome, Moleküle, Quantenoptik und Plasmen (SAMOP), Fachverband Massenspektrometrie, Erlangen, Germany, **2018**.

143. Plaschke, M.; Quinto, F.; Geyer, F.; Walschburger, C.; Hahn, E.; Lemmer, D.; Eissler, A.; Busser, C.; Faestermann, T.; Gomez-Guzman, J. M.; Hain, K.; Kroll, D.; Korschinek, G.; Ludwig, P.; Geckeis, H., *Massenspektrometrische Analytik von ^{99}Tc - von der Quelle bis zum Aquifer*, 8. RCA Workshop, Dresden, Germany, **2018**.

144. Polly, R.; Schimmelpfennig, B.; Vozarova, N.; Platte, T.; Finck, N.; Geckeis, H., *Incorporation of radionuclides in green rust*, ATAS 2018, Nice, France, **2018**.

145. Polly, R.; Schimmelpfennig, B.; Vozarova, N.; Platte, T.; Finck, N.; Geckeis, H., *Incorporation of radionuclides in green rust*, STC 2018, Halle (Saale), Germany, **2018**.

146. Quinto, F., *Ultra-trace analysis with AMS of actinides from in-situ radionuclide tracer tests at the Grimsel test site (Switzerland)*, Seminar, Abteilung Nuklearchemie der Universität zu Köln, Köln, Germany, **2018**.

147. Quinto, F.; Blechschmidt, I.; Plaschke, M.; Schäfer, T.; Steier, P.; Geckeis, H., *Investigating the long-term behaviour of actinides in repository relevant conditions with the multi-actinides analysis and AMS*, Seminar, Johannes Gutenberg-Universität, Mainz, Germany, **2018**.

148. Quinto, F.; Busser, C.; Faestermann, T.; Geckeis, H.; Gomez-Guzman, J.-M.; Hain, K.; Koll, D.; Korschinek, G.; Ludwig, P.; Plaschke, M.; Schäfer, T., *Ultra-trace analysis of Tc-99 with AMS in environmental samples*, 82. Jahrestagung der DPG und DPG-Frühjahrstagung der Sektion Atome, Moleküle, Quantenoptik und Plasmen (SAMOP), Fachverband Massenspektrometrie, Erlangen, Germany, **2018**.

149. Rothe, J.; Bahl, S.; Bohnert, E.; Dardenne, K.; González-Robles, E.; Herm, M.; Kienzler, B.; Metz, V.; Müller, N.; Schild, D.; Vitova, T.; Geckeis, H., *XAFS and μ-XANES/XRF investigation of highly radioactive spent nuclear fuel fragments at the KIT synchrotron source*, 17th International Conference on X-Ray Absorption Fine Structure (XAFS 2018), Krakau, Poland, **2018**.

150. Rothe, J.; Dardenne, K.; Vitova, T.; Gaona, X.; Altmaier, M.; Geckeis, H., *Use of advanced spectroscopic techniques for the characterization of Tc aqueous species and solid compounds: ACT beamline at KIT synchrotron source*, International Symposium on Technetium and Rhenium – Science and Utilization, Moscow, Russia, **2018**.

151. Salee, P.; Bouby, M., *Leaching studies of valuable/toxic metal ions from secondary Mining Waste Residues (MWR) by using bio- or organic ligands*, ICIA-International Conference on Ion Analysis, Berlin, Germany, **2018**.

152. Schacherl, B.; Joseph, S.; Beck, A.; Rieder, F.; Dardenne, K.; Fellhauer, D.; Bohnert, E.; Kupcik, T.; Rothe, J.; Geckeis, H.; Vitova, T., *Structural investigations of Np sorbed on illite by M_5-edge HR-XANES and L_3-edge EXAFS spectroscopy*, 4th International Workshop on Advanced Techniques for Actinide Spectroscopy (ATAS 2018), Nice, France, **2018**.

153. Stoll, M.; Huber, F. M.; Meinel, D.; Enzmann, F.; Trumm, M.; Schill, E.; Schäfer, T., *Experimental and numerical investigations on the effect of fracture geometry and aperture distribution on flow and solute transport in natural fractures*, 26. Tagung der Fachsektion Hydrogeologie e.V. (26. FH-DGGV-Tagung), Bochum, Germany **2018**.

154. Tasi, A. G.; Gaona, X.; Fellhauer, D.; Rabung, T.; Rothe, J.; Grivé, M.; Colàs, E.; Bruno, J.; Källström, K.; Altmaier, M.; Geckeis, H., *Redox, solubility and sorption behavior of plutonium in the presence of α-D-isosaccharinic acid and cement*, 35th International Conference on Solution Chemistry (ICSC 2018), Szeged, Hungary, **2018**.

155. Villagrasa, C.; Bordage, M.-C.; Bug, M.; Chiriotti, S.; Friedland, W.; Gargioni, E.; Heide, B.; Nettelbeck, H.; Parisi, A.; Rabus, H., *Assessing the contribution of cross-sections to the uncertainty of Monte Carlo calculations in micro- and nano-dosimetry*, Geant4 International User Conference, Bordeaux, France, **2018**.

156. Vozarova, N.; Finck, N.; Schild, D.; Dardenne, K.; Montoya, V.; Geckeis, H., *Sorption of Eu(III) and Am(III) on Magnetite in NaCl Brine*, Goldschmidt Conference (2018), Boston, USA, **2018**.

157. Weßling, P.; Trumm, M.; Geist, A.; Panak, P. J., *Determining the stoichiometry of An(III)-DMDOHEMA complexes formed during extraction*, 18th Radiochemical Conference (RadChem 2018), Mariánské Lázně, Czech Republic, **2018**.

158. Yalcintas, E.; Reed, D. T.; Gaona, X.; Dardenne, K.; Altmaier, M., *Complexation behavior of U(IV) in the presence of EDTA and its long-term effect on UO_2(am,hyd) solubility*, International Symposium on Solubility Phenomena and Related Processes (ISSP 18), Tours, France, **2018**.

159. Zellmann, E., *Erstellung einer Datenbank des Rückbaus kerntechnischer Anlagen : Analysetool, Wissensspeicher und Instrument zur Erkundung offener Fragestellungen*, 49th Annual Meeting on Nuclear Technology (AMNT 2018), Berlin, Germany, **2018**.

Proceedings

160. Ait Mouheb, N.; Montoya, V.; Schild, D.; Soballa, E.; Adam, C.; Geyer, F.; Schäfer, T., *Characterization and sorption properties of low pH cements*, In Altmaier et al. (2018) Proceedings of the Second Annual Workshop of the HORIZON 2020 CEBAMA Project. , KIT Scientific report KIT-SR 7752: **2018**.

161. Altmaier, M.; Montoya, V.; Duro, L.; Valls, A., *Proceedings of the Second Annual Workshop of the HORIZON 2020 CEBAMA Project*, KIT Scientific report KIT-SR 7752: **2018**.

162. Altmaier, M.; Buhmann, D.; Fellhauer, D.; Förster, B.; Metz, V.; Mönig, J.; Poppei, J.; Wissmeier, L., *Geochemistry in support of potential emergency measures for Schachtanlage Asse II,* Proceedings of the 9th US/German Workshop Salt Repository Research, Design and Operation, (Eds.: Hammer, J.; Hansen, F.D.; Maniats, G.; Fahland , S.; Bollingerfehr, W.; Enste, G.; Bühler, M.), BGR Hanover, Germany, **2018**.

163. Brandauer, M.; Geckeis, H.; Gentes, S.; Heneka, A.; Krauß, C.-O.; Plaschke, M.; Schild, D.; Tobie, W., *Vorstellung eines Magnetfiltersystems zur Behandlung von Sekundärabfällen der Wasser-Abrasiv-Suspensions-Schneidtechnik*, 49. Jahrestagung Kerntechnik / 49th Annual Meeting on Nuclear Technology (AMNT 2018), Berlin, Germany, INFORUM GmbH, Berlin: **2018**.

164. Fellhauer, D.; Schepperle, J.; Schramm, T.; Gaona, X.; Schild, D.; Walter, O.; Rothe, J.; Altmaier, M.; Geckeis, H., *Solubility, hydrolysis and solid phase formation of hexavalent Pu in alkaline NaCl solutions*, Plutonium Futures: The Science, San Diego, USA, ANS, New York (NY): **2018**; pp 15-16.

165. Ginjaume, M.; Clairand, I.; Carinou, E.; Ciraj Bjelac, O.; Ferari, P.; Sansmerce, M.; Farah, J.; Becker, F.; Chumak, V.; Daures, J.; Domienik, J.; Jovanovic, Z.; Kopec, R.; Krstic, D.; Szumaska, A.; Nikodemova, D.; Teles, P.; Principi, S.; Vanhavere, F.; Knezevic, Z., *Overview of the Activities on Eye Lens Dosimetry within EURADOS WG 12 (Dosimetry in medical imaging)*, 14th International Congress of the International Radiation Protection Association, Cape Town, South Africa, **2018**; p 773.

166. Gyekye, P. K.; Becker, F.; Emi-Reynolds, G., *Investigations into Radiation Dose Distribution in a Computed Tomography Fluoroscopy Room: Monte Carlo Studies*, 14th International Congress of the International Radiation Protection Association, Cape Town, South Africa, **2018**; pp 1245-1250.

167. Herm, M.; Gonzalez-Robles, E.; Böttle, M.; Müller, N.; Bohnert, E.; Dagan, R.; Caruso, S.; Kienzler, B.; Metz, V.; Geckeis, H., *^{14}C inventory in irradiated zircaloys. Summary of work performed by KIT-INE within WP2 and WP3 of the CAST project*, Abstracts of the EC CAST Final Symposium, Lyon, France, **2018**; pp 30-31.

168. Herm, M.; Gonzalez-Robles, E.; Böttle, M.; Müller, N.; Bohnert, E.; Dagan, R.; Caruso, S.; Kienzler, B.; Metz, V.; Geckeis, H., *Summary of work performed by KIT-INE within WP2 and QP3 of the CAST project. Formation and Status of ^{14}C in activated steel*, Abstracts of EC CAST Final Symposium, Lyon, France, **2018**; pp 17-18.

169. Herm, M.; González-Robles, E.; Müller, N.; Dardenne, K.; Rothe, J.; Schild, D.; García, C.; Dagan, R.; Metz, V., *Research activities on safety of extended dry storage of spent nuclear fuel at KIT-INE*, Abstracts of 2nd workshop on safety of extended dry storage of spent nuclear fuel, **2018**.

170. Herm, M.; González-Robles, E.; Müller, N.; König, T.; Dardenne, K.; Rothe, J.; Schild, D.; Dagan, R.; Metz, V., *Radionuclides present at inner cladding surfaces of irradiated PWR fuel rod segments in the context of safety of extended dry storage of spent nuclear fuel*, Abstracts of Materials Research Society (MRS), scientific basis for nuclear waste management (SBNWM), Boston, MA, USA, **2018**.

171. Herm, M.; González-Robles, E.; Müller, N.; Schild, D.; Dardenne, K.; Rothe, J.; García, C.; Dagan, R.; Metz, V., *Radionuclide containing solid phases on inner surfaces of Zircaloy-4 from plenum and fuel section of a PWR fuel rod*, Abstracts of Spent Fuel Workshop 2018, Sheffield, UK, **2018**.

172. K. German; X. Gaona; Ozawa, M.; Obruchnikova, Y.; Johnstone, E.; Maruk, A.; Chotkowski, M.; Troshkina, I.; Safonov, A., *Proceedings and selected lectures of the 10th International Symposium on Technetium and Rhenium – Science and Utilization*, Moscow, Russia, Publishing House Granica: **2018**.

173. Köpke, R.; Haaf, N.; Limberger, F.; Wang, J.; Peters, M.; Gaucher, E.; Schill, E.; Kohl, T., *First results from stimulation assessment and monitoring of the 426°C geothermal well RN-15/IDDP-2 (H2020-DEEPEGS project)*, Ideen und Innovationen für die Energie von morgen : Wissenschaftliche Beiträge des KIT zu den Jahrestagungen 2014, 2016 und 2017 des KIT-Zentrums Energie. Ed.: W. Breh, KIT Scientific Publishing, Karlsruhe: **2018**; pp 91-96.

174. Munoz, A. G.; Schild, D., *Corrosion of steel in high-level radioactive waste rock repositories: kinetics and thermodynamics*, Proceedings of NACE Corrosion Conference and Expo, Phoenix, USA, NACE International, Houston (TX): **2018**; pp Paper-11707.

175. Quinto, F.; Geckeis, H.; Hain, K.; Mäder, U.; Plaschke, M.; Schäfer, T.; Steier, P., *Ultra-trace analysis with AMS of actinides from global fallout and in-situ tracer tests*, Plutonium Futures - The Science : A Topical Conference on Plutonium and Actinides, San Diego, USA, ANS, LaGrange Park (IL): **2018**; pp 300-303.

176. Schnurr, A.; Powell, B., *Examination of the effect of alpha radiolysis on Pu(IV/V) sorption to minerals using multiple Pu isotopes*, Plutonium Futures: The Science 2018, San Diego, USA ANS, La Grange Park (IL): **2018**; pp 18-19.

177. Tasi, A. G.; Gaona, X.; Fellhauer, D.; Rabung, T.; Rothe, J.; Grivé, M.; Colàs, E.; Bruno, J.; Källström, K.; Altmaier, M.; Geckeis, H., *Redox, solubility and sorption behavior of plutonium in the presence of α-D-isosaccharinic acid and cement*, Programm & Abstract Book, 35th International Conference on Solution Chemistry, Szeged, Hungary, Hungarian Chemical Society: **2018**; p 69.

178. Vehmas, T.; Leivo, M.; Holt, E.; Alonso, M. C.; García, J. L.; Fernández, A.; Isaacs, M.; Rastrick, E.; Read, D.; Vašíček, R.; Hloušek, J.; Hausmannová, L.; Večerník, P.; Červinka, R.; Havlová, V.; Lange, S.; Klinkenberg, M.; Bosbach, D.; Deissmann, G.; Montoya, V.; Ait Mouheb, N.; Adam, C.; Schild, D.; Schäfer, T., *Cebama reference mix design for low-pH concrete and paste, preliminary characterisation*, In Altmaier et al. (2018) Proceedings of the Second Annual Workshop of the HORIZON 2020 CEBAMA Project. , KIT Scientific report KIT-SR 7752: **2018**.

179. Vitova, T., *Pu electronic structure and speciation applying Pu M5 edge HR-XANES and RIXS*, Plutonium Futures: The Science 2018, San Diego, USA, ANS, La Grange Park (IL): **2018**; p 377.

180. Zellmann, E.; Brandauer, M.; Gentes, S., *Implementation of a Nuclear Decommissioning Database - A Basis for Knowledge Management and Future Research*, 49. Jahrestagung Kerntechnik / 49th Annual Meeting on Nuclear Technology (AMNT 2018), Berlin, Germany, INFORUM GmbH, Berlin: **2018**; pp CD-ROM.

Reports

181. Bruno, J.; Gonzalez-Siso, M. R.; Duro, L.; Gaona, X.; Altmaier, M. *Key master variables affecting the mobility of Ni, Pu, Tc and U in the near field of the SFR repository. Main experimental findings and PA implications of the PhD thesis*; SKB Technical Report TR-18-01, **2018**.

182. Finck, N.; Ait Mouheb, N.; Montoya, V.; Rothe, J. *Determination of Fe speciation in low pH cementitious materials*; **2018**.

183. Finck, N.; Montoya, V.; Ait Mouheb, N.; Schäfer, T. *Determination of Fe speciation in low pH cementitious materials*; **2018**.

184. Herm, M.; Visser-Týnová, E.; Heikola, T.; Ollila, K.; González-Robles, E.; Böttle, M.; Müller, N.; Bohnert, E.; Dagan, R.; Caruso, S.; Kienzler, B.; Metz, V. *Final report on C-14 release from steels under low pH and acidic conditions (D2.16)*; **2018**.

185. Kaplan, U.; Bouby, M.; Rabung, T.; Schild, D.; Kaden, P.; Schäfer, T. *Characteriztion of natural organic matter (NOM) derived from different layers within Boom Clay (BC) – Formation and their radionuclide interaction*; **2018**.

Dissertations

186. Baumann, A., *Untersuchungen zur aquatischen Chemie von Technetium im Kontext nuklearer Entsorgung: Redoxverhalten, Löslichkeit und Komplexchemie von Tc(IV) in Elektrolytlösungen*. Ph.D. thesis, Karlsruher Institut für Technologie (KIT), **2018**.

187. Cevirim-Papaioannou, N., *Redox chemistry, solubility and hydrolysis of uranium in dilute to concentrated salt systems.* Ph.D. thesis, Karlsruher Institut für Technologie (KIT), **2018**.

188. Saurí Suárez, H., *Individual dosimetry in disposal facilities for high-level nuclear waste*. Ph.D. thesis, Karlsruher Institut für Technologie (KIT), **2018**.

189. Stoll, M., *Colloid mobility controlling processes in single fractures – a bottom-up approach*. Ph.D. thesis, Digitale Bibliothek Thüringen, **2018**.

190. Tasi, A. G., *Solubility, redox and sorption behavior of plutonium in the presence of α-D-isosaccharinic acid and cement under reducing conditions*. Ph.D. thesis, Karlsruher Institut für Technologie (KIT), **2018**.

2019

ISI/SCOPUS

1. Adam, N.; Adam, C.; Keskitalo, M.; Pfeuffer-Rooschuz, J.; Panak, P. J., Interaction of Cm(III) with human serum albumin studied by time-resolved laser fluorescence spectroscopy and NMR. *J Inorg Biochem* **2019,** *192*, 45-51.

2. Ayabe, T.; Costes, J. P.; Vendier, L.; Geist, A.; Takeda, M.; Takahashi, M., Contribution of Gd-155 Mossbauer data to the study of the magnetic interaction in heterodinuclear 3d-Gd (3d=Cu, Ni) coordination complexes. *Dalton T* **2019,** *48* (20), 6872-6878.

3. Barisic, A.; Lützenkirchen, J.; Lefevre, G.; Begovic, T., The influence of temperature on the charging of polytetrafluoroethylene surfaces in electrolyte solutions. *Colloid Surface A* **2019,** *579*.

4. Döpke, M. F.; Lützenkirchen, J.; Moultos, O. A.; Siboulet, B.; Dufreche, J. F.; Padding, J. T.; Hartkamp, R., Preferential Adsorption in Mixed Electrolytes Confined by Charged Amorphous Silica. *J Phys Chem C* **2019,** *123* (27), 16711-16720.

5. Dumas, T.; Fellhauer, D.; Schild, D.; Gaona, X.; Altmaier, M.; Scheinost, A. C., Plutonium Retention Mechanisms by Magnetite under Anoxic Conditions: Entrapment versus Sorption. *Acs Earth Space Chem* **2019,** *3* (10), 2197-2206.

6. Endrizzi, F.; Gaona, X.; Zhang, Z. C.; Xu, C.; Rao, L. F.; Garcia-Perez, C.; Altmaier, M., Thermodynamic description of U(VI) solubility and hydrolysis in dilute to concentrated NaCl solutions at T=25, 55 and 80 degrees C. *Radiochim Acta* **2019,** *107* (8), 663-678.

7. Epifano, E.; Naji, M.; Manara, D.; Scheinost, A. C.; Hennig, C.; Lechelle, J.; Konings, R. J. M.; Gueneau, C.; Prieur, D.; Vitova, T.; Dardenne, K.; Rothe, J.; Martin, P. M., Extreme multi-valence states in mixed actinide oxides. *Commun Chem* **2019,** *2*.

8. Ferrari, P.; Becker, F.; Jovanovic, Z.; Khan, S.; Bakhanova, E.; Principi, S.; Kristic, D.; Pierotti, L.; Mariotti, F.; Faj, D.; Turk, T.; Nikezic, D.; Bertolini, M., Simulation of H-p(10) and effective dose received by the medical staff in interventional radiology procedures. *J Radiol Prot* **2019,** *39* (3), 809-824.

9. Finck, N.; Bouby, M.; Dardenne, K., Fate of Lu(III) sorbed on 2-line ferrihydrite at pH 5.7 and aged for 12 years at room temperature. I: insights from ICP-OES, XRD, ESEM, AsFlFFF/ICP-MS, and EXAFS spectroscopy. *Environ Sci Pollut R* **2019,** *26* (6), 5238-5250.

10. Finck, N.; Schlegel, M. L.; Dardenne, K.; Adam, C.; Kraft, S.; Bauer, A.; Robert, J. L., Structural iron in smectites with different charge locations. *Phys Chem Miner* **2019,** *46* (7), 639-661.

11. Fröhlich, D. R.; Koke, C.; Maiwald, M. M.; Chomyn, C.; Plank, J.; Panak, P. J., A spectroscopic study of the complexation reaction of trivalent lanthanides with a synthetic acrylate based PCE-superplasticizer. *Spectrochim Acta A* **2019,** *207*, 270-275.

12. Fröhlich, D. R.; Panak, P. J., The complexation of Eu(III) and Cm(III) with polyacrylate as a model compound for complex polycarboxylates studied by laser fluorescence spectroscopy. *J Lumin* **2019,** *212*, 166-170.

13. Garcia, D.; Lützenkirchen, J.; Petrov, V.; Siebentritt, M.; Schild, D.; Lefevre, G.; Rabung, T.; Altmaier, M.; Kalmykov, S.; Duro, L.; Geckeis, H., Sorption of Eu(III) on quartz at high salt concentrations. *Colloid Surface A* **2019,** *578*.

14. Ginjaume, M.; Carinou, E.; Brodecki, M.; Clairand, I.; Domienik-Andrzejewska, J.; Exner, L.; Ferrari, P.; Jovanovic, Z.; Krstic, D.; Principi, S.; Van Hoey, O.; Vanhavere, F., Effect of the radiation protective apron on the response of active and passive personal dosemeters used in interventional radiology and cardiology. *J Radiol Prot* **2019,** *39* (1), 97-+.

15. Herdzik-Koniecko, I.; Wagner, C.; Trumm, M.; Müllich, U.; Schimmelpfennig, B.; Narbutt, J.; Geist, A.; Panak, P. J., Do An(III) and Ln(III) ions form heteroleptic complexes with diglycolamide and hydrophilic BT(B)P ligands in solvent extraction systems? A spectroscopic and DFT study. *New J Chem* **2019,** *43* (16), 6314-6322.

16. Horne, G. P.; Mezyk, S. P.; Moulton, N.; Peller, J. R.; Geist, A., Time-resolved and steady-state irradiation of hydrophilic sulfonated bis-triazinyl-(bi)pyridines - modelling radiolytic degradation. *Dalton T* **2019,** *48* (14), 4547-4554.

17. Joseph, C.; Balboni, E.; Baumer, T.; Treinen, K.; Kersting, A. B.; Zavarin, M., Plutonium Desorption from Nuclear Melt Glass-Derived Colloids and Implications for Migration at the Nevada National Security Site, USA. *Environ Sci Technol* **2019,** *53* (21), 12238-12246.

18. Klass, L.; Wilden, A.; Kreft, F.; Wagner, C.; Geist, A.; Panak, P. J.; Herdzik-Koniecko, I.; Narbutt, J.; Modolo, G., Evaluation of the Hydrophilic Complexant N,N,N',N'-tetraethyldiglycolamide (TEDGA) and its Methyl-substituted Analogues in the Selective Am(III) Separation. *Solvent Extr Ion Exc* **2019,** *37* (5), 297-312.

19. Koke, C.; Skerencak-Frech, A.; Panak, P. J., Thermodynamics of the complexation of curium(III) with chloride in alkali and alkali earth metal solutions at elevated temperatures. *J Chem Thermodyn* **2019,** *131*, 219-224.

20. Koll, D.; Busser, C.; Faestermann, T.; Gomez-Guzman, J. M.; Hain, K.; Kinast, A.; Korschinek, G.; Krieg, D.; Lebert, M.; Ludwig, P.; Quinto, F., Recent developments for AMS at the Munich tandem accelerator. *Nucl Instrum Meth B* **2019,** *438*, 180-183.

21. Lee, J. Y.; Amayri, S.; Montoya, V.; Fellhauer, D.; Gaona, X.; Altmaier, M., Solubility and stability of liebigite, $Ca_2UO_2(CO_3)_3 \cdot 10H_2O$(cr), in dilute to concentrated NaCl and $NaClO_4$ solutions at T=22-80°C. *Appl Geochem* **2019,** *111,* 104374.

22. Liu, J. T.; Wu, H.; Zhang, F.; Liu, S. C.; Liu, Z. X.; Yan, H. Z., Improvement in the method for borehole caliper measurement based on azimuthal gamma-gamma density well logging. *Appl Radiat Isotopes* **2019,** *145*, 68-72.

23. Lützenkirchen, J.; Barisic, A.; Lefevre, G.; Begovic, T., Electrokinetic mobility, pH and conductance/conductivity data for aqueous silica and PTFE suspension of controlled composition for selected temperature ranges. *Data Brief* **2019,** *25*, 104354.

24. Lützenkirchen, J.; Finck, N., Treatment of temperature dependence of interfacial speciation by speciation codes and temperature congruence of oxide surface charge. *Appl Geochem* **2019,** *102*, 26-33.

25. Maiwald, M. M.; Fellhauer, D.; Skerencak-Frech, A.; Panak, P. J., The complexation of neptunium(V) with fluoride at elevated temperatures: Speciation and thermodynamics. *Appl Geochem* **2019,** *104*, 10-18.

26. Malmbeck, R.; Magnusson, D.; Bourg, S.; Carrott, M.; Geist, A.; Heres, X.; Miguirditchian, M.; Modolo, G.; Müllich, U.; Sorel, C.; Taylor, R.; Wilden, A., Homogenous recycling of transuranium elements from irradiated fast reactor fuel by the EURO-GANEX solvent extraction process. *Radiochim Acta* **2019,** *107* (9-11), 917-929.

27. Molodtsov, K.; Schymura, S.; Rothe, J.; Dardenne, K.; Schmidt, M., Sorption of Eu(III) on Eibenstock granite studied by microTRLFS: A novel spatially-resolved luminescence-spectroscopic technique. *Sci Rep* **2019,** *9* (1), 6287.

28. Müller, K.; Foerstendorf, H.; Steudtner, R.; Tsushima, S.; Kumke, M. U.; Lefevre, G.; Rothe, J.; Mason, H.; Szabo, Z.; Yang, P.; Adam, C. K. R.; Andre, R.; Brennenstuhl, K.; Chiorescu, I.; Cho, H. M.; Creff, G.; Coppin, F.; Dardenne, K.; Den Auwer, C.; Drobot, B.; Eidner, S.; Hess, N. J.; Kaden, P.; Kremleva, A.; Kretzschmar, J.; Kruger, S.; Platts, J. A.; Panak, P. J.; Polly, R.; Powell, B. A.; Rabung, T.; Redon, R.; Reiller, P. E.; Rosch, N.; Rossberg, A.; Scheinost, A. C.; Schimmelpfennig, B.; Schreckenbach, G.; Skerencak-Frech, A.; Sladkov, V.; Solari, P. L.; Wang, Z. M.; Washton, N. M.; Zhang, X. B., Interdisciplinary Round-Robin Test on Molecular Spectroscopy of the U(VI) Acetate System. *Acs Omega* **2019,** *4* (5), 8167-8177.

29. Neill, T. S.; Morris, K.; Pearce, C. I.; Abrahamsen-Mills, L.; Kovarik, L.; Kellet, S.; Rigby, B.; Vitova, T.; Schacherl, B.; Shaw, S., Silicate stabilisation of colloidal UO_2 produced by uranium metal corrosion. *J Nucl Mater* **2019,** *526*.

30. Quinto, F.; Busser, C.; Faestermann, T.; Hain, K.; Koll, D.; Korschinek, G.; Kraft, S.; Ludwig, P.; Plaschke, M.; Schäfer, T.; Geckeis, H., Ultratrace Determination of Tc-99 in Small Natural Water Samples by Accelerator Mass Spectrometry with the Gas-Filled Analyzing Magnet System. *Anal Chem* **2019,** *91* (7), 4585-4591.

31. Renz, T.; Plaschke, M.; Quinto, F.; Bauer, A.; Lagos, M.; Taubald, H.; Geckeis, H., Adaptation of an Analytical Procedure for Concurrent Determination of Np and Pu in clay samples. *Clay Clay Miner* **2019,** *67* (3), 183-189.

32. Rohde, V.; Böringer, S.; Tübke, B.; Adam, C.; Dahmen, N.; Schmiedl, D., Fractionation of three different lignins by thermal separation techniques—A comparative study. *GCB Bioenergy* **2019,** *11*, 206-217.

33. Rothe, J.; Altmaier, M.; Dagan, R.; Dardenne, K.; Gaona Martinez, J.; González-Robles Corrales, E.; Herm, M.; Metz, V.; Pidchenko, I.; Vitova, T.; Geckeis, H., Fifteen years of radionuclide research at the KIT synchrotron source in context of the nuclear waste disposal safety case. *Geosciences* **2019,** *9*, 91.

34. Selmani, A.; Lützenkirchen, J.; Kucanda, K.; Dabic, D.; Redel, E.; Marion, I. D.; Kralj, D.; Jurasin, D. D.; Sikiric, M. D., Tailoring the stability/aggregation of one-dimensional TiO_2(B)/titanate nanowires using surfactants. *Beilstein J Nanotech* **2019,** *10*, 1024-1037.

35. Skerencak-Frech, A.; Taube, F.; Zanonato, P. L.; Acker, M.; Panak, P. J.; Di Bernardo, P., A potentiometric and microcalorimetric study of the complexation of trivalent europium with lactate: The ionic strength dependency of log β'_n, $\Delta_r H_{m,n}$ and $\Delta_r S_{m,n}$. *Thermochim Acta* **2019,** *679,* 178316.

36. Smith, A. L.; Verleg, M. N.; Vlieland, J.; de Haas, D.; Ocadiz-Flores, J. A.; Martin, P.; Rothe, J.; Dardenne, K.; Salanne, M.; Gheribi, A. E.; Capelli, E.; van Eijck, L.; Konings, R. J. M., In situ high-temperature EXAFS measurements on radioactive and air-sensitive molten salt materials. *J Synchrotron Radiat* **2019,** *26*, 124-136.

37. Stoll, M.; Huber, F. M.; Trumm, M.; Enzmann, F.; Meinel, D.; Wenka, A.; Schill, E.; Schäfer, T., Experimental and numerical investigations on the effect of fracture geometry and fracture aperture distribution on flow and solute transport in natural fractures. *J Contam Hydrol* **2019,** *221*, 82-97.

38. Taube, F.; Drobot, B.; Rossberg, A.; Foerstendorf, H.; Acker, M.; Patzschke, M.; Trumm, M.; Taut, S.; Stumpf, T., Thermodynamic and Structural Studies on the Ln(III)/An(III) Malate Complexation. *Inorganic chemistry* **2019,** *58* (1), 368-381.

39. Vasiliev, A. N.; Banik, N. L.; Marsac, R.; Kalmykov, S. N.; Marquardt, C. M., Determination of complex formation constants of neptunium(V) with propionate and lactate in 0.5-2.6 m NaCl solutions at 22-60°C using a solvent extraction technique. *Radiochim Acta* **2019,** *107* (7), 623-634.

40. Villagrasa, C.; Bordage, M.-C.; Bueno, M.; Bug, M.; Chiriotti, S.; Gargioni, E.; Heide, B.; Nettelbeck, H.; Parisi, A.; Rabus, H., Assessing the contribution of cross-sections to the uncertainty of Monte Carlo calculations in micro- and nanodosimetry. *Radiation protection dosimetry* **2019,** *183* (1-2), 11-16.

41. Vitova, T.; Geckeis, H.; Bagus, P. S., Probing Actinide Covalency: Plutonium Electronic Structure Studies Using High Energy Resolution X-Ray Spectroscopy. *Actinide research quarterly* **2019,** *Second Quarter 2019*.

42. Vogt, M.; Hopp, J.; Gail, H. P.; Ott, U.; Trieloff, M., Acquisition of terrestrial neon during accretion - A mixture of solar wind and planetary components. *Geochim Cosmochim Ac* **2019,** *264*, 141-164.

43. Wessling, P.; Trumm, M.; Macerata, E.; Ossola, A.; Mossini, E.; Gullo, M. C.; Arduini, A.; Casnati, A.; Mariani, M.; Adam, C.; Geist, A.; Panak, P. J., Activation of the Aromatic Core of 3,3 '-(Pyridine-2,6-diylbis(1H-1,2,3-triazole-4,1-diyl))bis(propan-1-ol)-Effects on Extraction Performance, Stability Constants, and Basicity. *Inorg Chem* **2019,** *58* (21), 14642-14651.

44. Wilden, A.; Kowalski, P. M.; Klass, L.; Kraus, B.; Kreft, F.; Modolo, G.; Li, Y.; Rothe, J.; Dardenne, K.; Geist, A.; Leoncini, A.; Huskens, J.; Verboom, W., Unprecedented Inversion of Selectivity and Extraordinary Difference in the Cornplexation of Trivalent f Elements by Diastereomers of a Methylated Diglycolamide. *Chem-Eur J* **2019,** *25* (21), 5507-5513.

45. Woodhead, D.; McLachlan, F.; Taylor, R.; Müllich, U.; Geist, A.; Wilden, A.; Modolo, G., Nitric Acid Extraction into a TODGA Solvent Modified with 1-Octanol. *Solvent Extr Ion Exc* **2019,** *37* (2), 173-190.

46. Yalcintas, E.; Cevirim-Papaioannou, N.; Gaona, X.; Fellhauer, D.; Neck, V.; Altmaier, M., Solubility of U(VI) in chloride solutions. III. The stable oxides/hydroxides in $MgCl_2$ systems: Pitzer activity model for the system UO_2^{2+}–Na^+–K^+–Mg^{2+}–H^+–OH^-–Cl^-–H_2O(l). *J Chem Thermodyn* **2019,** *131*, 375-386.

47. Yin, Z.; Lützenkirchen, J.; Finck, N.; Celaries, N.; Dardenne, K.; Hansen, H. C. B., Adsorption of arsenic(V) onto single sheet iron oxide: X-ray absorption fine structure and surface complexation. *J Colloid Interf Sci* **2019,** *554*, 433-443.

48. Yokosawa, T.; Prestat, E.; Polly, R.; Bouby, M.; Dardenne, K.; Finck, N.; Haigh, S. J.; Denecke, M. A.; Geckeis, H., Fate of Lu(III) sorbed on 2-line ferrihydrite at pH 5.7 and aged for 12 years at room temperature. II: insights from STEM-EDXS and DFT calculations. *Environ Sci Pollut R* **2019,** *26* (6), 5282-5293.

49. Zavarin, M.; Zhao, P.; Joseph, C.; Begg, J. D.; Boggs, M. A.; Dai, Z.; Kersting, A. B., Hydrothermal Alteration of Nuclear Melt Glass, Colloid Formation, and Plutonium Mobilization at the Nevada National Security Site, U.S.A. *Environ Sci Technol* **2019,** *53* (13), 7363-7370.

50. Zegke, M.; Zhang, X. B.; Pidchenko, I.; Hlina, J. A.; Lord, R. M.; Purkis, J.; Nichol, G. S.; Magnani, N.; Schreckenbach, G.; Vitova, T.; Love, J. B.; Arnold, P. L., Differential uranyl(v) oxo-group bonding between the uranium and metal cations from groups 1, 2, 4, and 12; a high energy resolution X-ray absorption, computational, and synthetic study. *Chem Sci* **2019,** *10* (42), 9740-9751.

published online in advance:

51. Dubos, J. L.; Orberger, B.; Milazzo, J. M.; Blancher, S. B.; Wallmach, T.; Lützenkirchen, J.; Banchet, J., Agglomeration potential evaluation of industrial Mn dusts and sludges based on physico-chemical characterization. *Powder technology* **2019,** *360*, 1079-1091.

52. Epifano, E.; Prieur, D.; Martin, P. M.; Gueneau, C.; Dardenne, K.; Rothe, J.; Vitova, T.; Dieste, O.; Wiss, T.; Konings, R. J. M.; Manara, D., Melting behaviour of uranium-americium mixed oxides under different atmospheres. *J Chem Thermodyn* **2020,** *140*.

53. Grambow, B.; Lopez-Garcia, M.; Olmeda, J.; Grive, M.; Marty, N. C. M.; Grangeon, S.; Claret, F.; Lange, S.; Deissmann, G.; Klinkenberg, M.; Bosbach, D.; Bucur, C.; Florea, I.; Dobrin, R.; Isaacs, M.; Read, D.; Kittnerova, J.; Drtinova, B.; Vopalka, D.; Cevirim-Papaioannou, N.; Ait-Mouheb, N.; Gaona, X.; Altmaier, M.; Nedyalkova, L.; Lothenbach, B.; Tits, J.; Landesman, C.; Rasamimanana, S.; Ribet, S., Retention and diffusion of radioactive and toxic species on cementitious systems: Main outcome of the CEBAMA project. *Appl Geochem* **2020,** *112*.

54. Huang, L.-Z.; Wei, X.; Gao, E.; Zhang, C.; Hu, X.-M.; Chen, Y.; Liu, Z.; Finck, N.; Lützenkirchen, J.; Dionysiou, D. D., Single Fe atoms confined in two-dimensional MoS_2 for sulfite activation: A biomimetic approach towards efficient radical generation [in press]. *Applied catalysis / B* **2019**, 118459.

55. Kölbel, L.; Kölbel, T.; Sauter, M.; Schäfer, T.; Siefert, D.; Wiegand, B., Identification of fracture zones in geothermal reservoirs in sedimentary basins: A radionuclide-based approach. *Geothermics* **2019,** *85*.

56. Morelova, N.; Finck, N.; Lutzenkirchen, J.; Schild, D.; Dardenne, K.; Geckeis, H., Sorption of americium / europium onto magnetite under saline conditions: Batch experiments, surface complexation modelling and X-ray absorption spectroscopy study. *J Colloid Interface Sci* **2020,** *561*, 708-718.

57. Vitova, T.; Pidchenko, I.; Schild, D.; Prüssmann, T.; Montoya, V.; Fellhauer, D.; Gaona, X.; Bohnert, E.; Rothe, J.; Baker, R. J.; Geckeis, H., Competitive Reaction of Neptunium(V) and Uranium(VI) in Potassium-Sodium Carbonate-Rich Aqueous Media: Speciation Study with a Focus on High-Resolution X-ray Spectroscopy. *Inorg Chem* **2020,** *59* (1), 8-22.

58. Zaytsev, A. V.; Bulmer, R.; Kozhevnikov, V. N.; Sims, M.; Modolo, G.; Wilden, A.; Waddell, P. G.; Geist, A.; Panak, P. J.; Wessling, P.; Lewis, F. W., Exploring the Subtle Effect of Aliphatic Ring Size on Minor Actinide-Extraction Properties and Metal Ion Speciation in Bis-1,2,4-Triazine Ligands. *Chemistry* **2020,** *26* (2), 428-437.

Invited talks

59. Altmaier, M., *Cement properties and barrier functions in repository environments, CEBAMA project,* EURADWASTE'19, Pitesti, Romania, **2019**.

60. Altmaier, M.; Fellhauer, D.; Kienzler, B., *Research at the Institute for Nuclear Waste Disposal (KIT-INE), Karlsruhe, Germany, in support of the Nuclear Waste Disposal Safety Case,* Pacific Northwest National Laboratories, USA, **2019**.

61. Altmaier, M.; Brandt, F.; Brendler, V.; Campos, I.; Cevirim-Papaioannou, N.; N.; Chiorescu, I.; Colas, E.; Curtius, H.; Endrizzi, F.; Fellhauer, D.; Franzen, C.; Gaona, X.; Gray, A.; Grive, M.; Hagemann S.; Huittinen, N.; Koke, C.; Kulik, D.A.; Krüger, S.; Lee, J.-Y.; Maiwald, M.; Miron, D.; Panak, P.J.; Poonoosamy, J.; Skerencak-Frech, A.; Steudtner, R.; Thoenen, T., *Verbundprojekt ThermAc: Aufklärung von Thermodynamik und Speziation von Actiniden bei höheren Temperaturen in Kombination von Schätzmethoden, spektroskopischen und quantenchemischen Methoden,* 4. Projektstatusgespräch zur BMBF-geförderten Nuklearen Sicherheitsforschung, Karlsruhe, **2019**.

62. Altmaier, M.; Geckeis, H., *Research on radiochemistry and geochemistry at KIT-INE, Germany, in support of the Nuclear Waste Disposal Safety Case,* GDCH Geschäftsstelle Frankfurt, Besuch Delegation der East China University of Technology, Frankfurt, **2019**.

63. Finck, N.; Vozarova, N.; Cakir-Wuttke, P.; Schlegel, M. L.; Montoya, V.; Lützenkirchen, J.; Schild, D.; Dardenne, K.; Geckeis, H., *Steel corrosion and actinide retention by Fe-corrosion phases under anaerobic saline conditions*, 7. Workshop des BMWi-Verbundprojektes GRaZ, Saarbrücken, Germany, **2019**.

64. Geist, A., *Studies on N-donor–actinide coordination chemistry at KIT-INE*, Florida State University, Tallahassee, USA, **2019**.

65. Geist, A., *Current trends in actinide separation by solvent extraction using nitrogen donor ligands*, Autumn School, "The Chemistry of f Elements", Dresden, Germany, **2019**.

66. Glückman, D.; Quinto, F.; Hain, K.; Joseph, C.; Montoya, V.; Steier, P.; Geckeis, H., *Ultra-trace determination of actinides in clay systems with accelerator mass spectrometry & development of a diffusion setup for reducing conditions*, Institut für Kernchemie, Universität Mainz, Mainz, Germany, **2019**.

67. Quinto, F.; Faestermann, T.; Hain, K.; Koll, D.; Korschinek, G.; Kraft, S.; Ludwig, P.; Plaschke, M.; Schäfer, T.; Steier, P.; Geckeis, H., *Accelerator Mass Spectrometry as a powerful tool to study the environmental behavior of actinides and Tc-99 at femtogram and attogram levels*, Institut de Chimie de Nice, Université Nice Sophia Antipolis - Université Côte d'Azur, Nice, France, **2019**.

68. Rothe, J., *Röntgenspektroskopische Untersuchungen an hochradioaktiven nuklearen Abfällen (HLW)*, Seminarvortrag, Institut für Radioökologie und Strahlenschutz, Leibniz Universität Hannover, Hannover, Germany, **2019**.

69. Rothe, J., *XAS based investigations of highly radioactive nuclear waste forms at the KIT synchrotron light source (KARA)*, Invited Seminar Talk, Shanghai Institute of Applied Physics (SINAP), Chinese Academy of Sciences, Shanghai, China, **2019**.

70. Schacherl, B., *How redox reactions at a clay mineral surface influence the sorption of neptunium*, 50th AMNT 2019 Young Scientists Workshop, Berlin, Germany, **2019**.

71. Schätzler, K., *Energiequellen und Infrastrukturoptionen nachhaltiger Quartierswärmesysteme*, FVEE-Veranstaltung auf den Berliner Energietagen, Session 6.06: Neue Wege für die Quartierswärmeversorgung, Berlin, Germany, **2019**.

72. Schill, E., *Enhanced Geothermal Systems: challenges and achievements for an environmentally friendly technology development*, University of Alberta - Centennial Centre of Interdisciplinary Sciences (CCIS), Joint seminar between (1) Institute of Geophysical Research and (2) Future Energy Systems, **2019**.

73. Schill, E., *Hydraulic stimulation: experience with induced seismicity and electromagnetic monitoring*, European PhD Day, GFZ Potsdam, Germany, **2019**.

74. Schill, E., *Towards forecasting seismic activity induced during reservoir engineering by magnetotelluric methods*, TU Berlin, Berlin, Germany, **2019**.

75. Vitova, T., *Electronic structure and speciation of actinides applying high energy resolution X-ray absorption and emission spectroscopy*, Seaborg Institute Seminar Series, Los Alamos, USA, **2019**.

76. Vitova, T., *Advanced Structural Studies of Actinide Materials applying High Resolution X-Ray Absorption and Emission Spectroscopy*, Migration 2019, Kyoto, Japan, **2019**.

77. Vitova, T., *Advances in the X-Ray Spectroscopy of the Actinides*, SSRL Annual Users Meeting, Stanford, USA, **2019**.

Oral and poster presentations

78. Ait Mouheb, N.; Montoya, V.; Joseph, C.; Schäfer, T.; Geckeis, H., *Diffusion of tritiated water through low pH cements*, 5th International Workshop on Mechanisms and Modelling of Waste / Cement Interactions, Karlsruhe, Germany, **2019**.

79. Ait Mouheb, N.; Montoya, V.; Schild, D.; Finck, N.; Lützenkirchen, J.; Adam, C.; Joseph, C.; Schäfer, T., *Radionuclide migration in low-pH / cement clay interfaces: Derivation of reactive transport parameters within the CEBAMA*, 9th European Commission Conference on EURATOM Research and Teaching in Radioactive Waste Management (EURADWASTE'19), Pitesti, Romania, **2019**.

80. Altmaier, M., *CO_2-Production rates in saline systems. Relevance in the context of Schachtanlage Asse II,* 10th US/GERMAN Workshop on Salt Repository Research, Design, and Operation, Rapid City, USA, **2019**.

81. Altmaier, M.; Blin, V.; Garcia, D.; Henocq, P.; Ricard, R.; Missana, T., Vandenborre, J., *CORI – collaborative research on Cement-Organics-Radionuclides-Interactions in EURAD,* EURADWASTE'19, Pitesti, Romania, **2019**.

82. Altmaier, M.; Montoya, V.; Duro, L.; Valls, A.; Holt, E.; Claret, F.; Mäder, U.; Grambow, B.; Idiart, A., *Final results from the EC HORIZON2020 CEBAMA project,* Migration 2019, Kyoto, Japan, **2019**.

83. Altmaier, M.; Brandt, F.; Brendler, V.; Campos, I.; Cevirim-Papaioannou, N.; Chiorescu, I.; Colas, E.; Curtius, H.; Endrizzi, F.; Gaona, X.; Gray, A.; Hagemann S.; Huittinen, N.; Koke, C.; Kulik, D.A.; Krüger, S.; Lee, J.-Y.; Maiwald, M.; Miron, D.; Panak, P.J.; Poonoosamy, J.; Skerencak-Frech, A.; Steudtner, R.; Thoenen, T., *Conclusions from the THERMAC project – a dedicated collaborative project to investigate actinide chemistry at elevated temperature conditions,* Migration 2019, Kyoto, Japan, **2019**.

84. Altmaier, M.; Blin, V.; Garcia, D.; Henocq, P.; Ricard, R.; Missana, T., Vandenborre, J., CORI – collaborative research on cement-organics-radionuclides-interactions in EURAD, ABC-Salt VI Workshop, Karlsruhe, Germany, **2019**.

85. Altmaier, M., *Overview of the BMBF funded ThermAc project,* HiTAC - III Workshop 2019, High Temperature Aqueous Chemistry, Karlsruhe, Germany, **2019**.

86. Bartova, B.; Brown, A.; Molinas, M.; Pan, Z.; Lagrange, T.; Faizova, R.; Mazzanti, M.; Schacherl, B.; Beck, A.; Vitova, T.; Kvashnina, K.; Robbert, Y.; Weyer, S.; Bernier-Latmani, R., *Mechanistic insights into U(VI) reduction and the associated uranium isotopic fractionation*, Goldschmidt 2019, Barcelona, Spain, **2019**.

87. Beam, J.; Yalcintas, E.; Reed, D.T.; Gaona, X.; Altmaier, M., *Complexation behaviour of U(IV) in the presence of EDTA and its long term effect on UO_2(am,hyd) solubility,* ABC-Salt VI Workshop, Karlsruhe, Germany, **2019**.

88. Beck, A.; Dardenne, K.; Galanzev, J.; Hardock, K.; Krepper, V.; Rothe, J.; Schacherl, B.; Vitova, T.; Geckeis, H., *Instrumentation for X-ray emission spectroscopy at the KIT-INE radionuclide beamline stations at KARA*, EBS workshop on X-ray Emission Spectroscopy, ESRF, Grenoble, France, **2019**.

89. Beck, A.; Tasi, A.; Fellhauer, D.; Rothe, J.; Schacherl, B.; Galanzew, J.; Dardenne, K.; Altmaier, M.; Pidchenko, I.; Geckeis, H.; Vitova, T., *Pu M5 edge HR-XANES and Pu L3 edge EXAFS investigation of aqueous/colloidal Pu*, Migration 2019, Kyoto, Japan, **2019**.

90. Bourg, S.; Geist, A., *The GENIORS midterm report*, 43rd Annual Actinide Separations Conference, Kingsport, USA, **2019**.

91. Brandauer, M.; Friedrich, S.; Gentes, S.; Schilp, S.; Hartung, F.; Johannes, P., 14. Internationales Symposium Konditionierung radioaktiver Betriebs- und Stilllegungsabfälle (KONTEC 2019), Dresden, Germany, **2019**.

92. Cevirim-Papaioannou, N.; Gaona, X.; Han, S.; Ait Mouheb, N.; M., B.; Gaboreau, S.; Claret, F.; Um, W.; Altmaier, M., *Solubility and sorption of Be(II) in cementitious systems*, Mechanism and Modeling of Waste/Cement Interactions, Karlsruhe, Germany, **2019**.

93. Cevirim-Papaioannou, N.; Gaona, X.; Han, S.; Ait Mouheb, N.; M., B.; Gaboreau, S.; Claret, F.; Um, W.; Altmaier, M., *Beryllium solubility, hydrolysis and sorption in cementitious systems*, Goldschmidt, Barcelona, Spain, **2019**.

94. Cevirim-Papaioannou, N.; Gaona, X.; Han, S.; Ait Mouheb, N.; M., B.; Gaboreau, S.; Claret, F.; Um, W.; Altmaier, M., *Chemistry of beryllium in cementitious systems studied within CEBAMA: solubility, hydrolysis, carbonate complexation and sorption*, EURADWASTE, Pitesti, Romania, **2019**.

95. Cevirim-Papaioannou, N.; J.-L., L.; Gaona, X.; Yalcintas Bethune, E.; Montoya, V.; Fellhauer, D.; Dardenne, K.; Altmaier, M.; Geckeis, H., *Solution chemistry and thermodynamics of U(IV) and U(VI): solubility, hydrolysis and the ternary system Ca-U(VI)-carbonate*, Migration, Kyoto, Japan, **2019**.

96. Cevirim-Papaioannou, N.; Yalcintas, E.; Gaona, X.; Dardenne, K.; Altmaier, M.; Geckeis, H., *Redox chemistry and solubility of uranium in alkaline systems*, Mechanism and Modeling of Waste/Cement Interactions, Karlsruhe, Germany, **2019**.

97. Cevirim-Papaioannou, N.; Yalcintas, E.; Gaona, X.; Dardenne, K.; Altmaier, M.; Geckeis, H., *Solubility, hydrolysis and redox chemistry of uranium in reducing dilute to concentrated salt systems*, ABC-Salt VI Workshop, Karlsruhe, Germany, **2019**.

98. Chaparro, M. C.; Saaltink, M. W., *Reactive transport and tritium transport models in concrete cells for storing radioactive waste*, 5th International Workshop on Mechanisms and Modelling of Waste/Cement Interactions, Karlsruhe, Germany, **2019**.

99. Chaparro, M. C.; Saaltink, M. W., *Geochemical reactions and tritium transport in concrete cells for storing radioactive waste*, Goldschmidt, Barcelona, Spain, **2019**.

100. Cornejo, N.; Schill, E.; Held, S.; Piccardi, L.; Brogi, A.; Liotta, D.; Perez, M.; Carrillo, J.; Garduño, V. H., *Regional structures in the Los Humeros geothermal system: insights for super-hot geothermal fluids location*, European Geothermal Workshop 2019, Karlsruhe, Germany, **2019**.

101. Cornejo, N.; Schill, E.; Perez, M.; Carrillo, J., *Gravity results*, GEMEX Meeting, Geothermiezentrum Bochum, Germany, **2019**.

102. Dagan, R.; Konobeyev, A., *On the validity and usage of the scattering source term within the Boltzmann transport equation*, ICTT- International conference on Transport Theory, Paris, France, **2019**.

103. Duckworth, S.; Gaona, X.; Altmaier, M.; Geckeis, H., *Solution chemistry of Tc in the presence of inorganic and organic ligands in dilute to concentrated salt systems*, ABC Salt Workshop IV 2019, Karlsruhe, Germany, **2019**.

104. Duckworth, S.; Gaona, X.; Altmaier, M.; Geckeis, H., *Interaction of Technetium with sulfate and gluconate under reducing conditions*, Migration Conference 2019, Kyoto, Japan, **2019**.

105. Duckworth, S.; Gaona, X.; Altmaier, M.; Geckeis, H., *Impact of sulfate and gluconate on the solution chemistry of Tc under reducing conditions: solubility, complexation and redox chemistry*, GDCh 2019, Dresden, Germany, **2019**.

106. Fellhauer, D.; Altmaier, M.; Metz, V.; Geckeis, H., *Aquatic radiochemistry and solubility studies in support of potential emergency measures for the Asse II salt mine, Germany*, Migration 2019, Kyoto, Japan, **2019**.

107. Fellhauer, D.; Gaona, X.; Altmaier, M.; Geckeis, H., *On the very low solubility of Np(V) hydroxide solid phases in alkaline solutions containing (sub)millimolar concentrations of* Ca^{2+}, 5th International Workshop on Mechanism and Modelling of Waste – Cement Interactions, Karlsruhe, Germany, **2019**.

108. Fellhauer, D.; Gaona, X.; Altmaier, M.; Geckeis, H., *The impact of (sub)millimolar concentrations of* Ca^{2+} *on the Np(V) solid phase formation in alkaline solutions*, Migration 2019, Kyoto, Japan, **2019**.

109. Fellhauer, D.; Lee, J.-Y.; Gaona, X.; Schild, D.; Altmaier, M., *Redox chemistry of Np(V)/Np(IV) in reducing aqueous solution at T = 23 and 80 °C*, Migration 2019, Kyoto, Japan, **2019**.

110. Fernandez-Rojo, L.; Chaparro, M. C.; Soler, J. M.; Cama, J., *Fractured core experiments to study water-rock-cement interaction under* CO_2 *storage conditions*, 5th International Workshop on Mechanisms and Modelling of Waste/Cement Interactions, Karlsruhe, Germany, **2019**.

111. Fernandez-Rojo, L.; Soler, J. M.; Chaparro, M. C.; Galí, S.; Queralt, I.; Cama, J., *Rock/cement fracture in geological* CO_2 *storage*, Goldschmidt, Barcelona, Spain, **2019**.

112. Finck, N.; Dardenne, K.; Kraft, S.; Rothe, J.; Bosbach, D.; M.A., D., *Investigations in the* $CaMoO_4$-$Na_{0.5}Ln_{0.5}MoO_4$ *(Ln = La, Eu, Yb) solid solution series*, 14th SOLEIL Users' meeting, Gif-sur-Yvette, France, **2019**.

113. Finck, N.; Vozarova, N.; Schlegel, M. L.; Schild, D.; Geckeis, H., *Stainless steel corrosion under anaerobic, highly saline and elevated temperature conditions*, 7th international workshop on long-term prediction of corrosion damage in nuclear waste repositories, Nancy, France, **2019**.

114. Fuchs, S.; Reinsch, T.; Huenges, E.; Kohl, T.; Schill, E., *Breitbandnetzausbau & Wärmwende: Synergien für die geothermische Exploration urbaner Räume*, FVEE – Jahrestagung 2019: Energy Research for Future – Forschung für die Herausforderungen der Energiewende, Berlin, Germany, **2019**.

115. Galanzew, J.; Beck, A.; Schild, D.; Adam, N.; Gaona, X.; März, J.; Butorin, S. M.; Geckeis, H.; Kvashnina, K.; Vitova, T., *Th L3 edge high energy resolution X-ray absorption and emission structural studies of Th compounds*, GDCH Jahrestagung Fachgruppe Nuklearchemie, Dresden, Germany, **2019**.

116. Galanzew, J.; Beck, A.; Schild, D.; Adam, N.; Gaona, X.; März, J.; Butorin, S. M.; Geckeis, H.; Kvashnina, K.; Vitova, T., *Th L3 edge high energy resolution X-ray absorption and emission structural studies of Th compounds*, Journée des Actinides (JdA) 2019, **2019**.

117. Gaona, X.; Cevirim-Papaioannou, N.; Schepperle, J.; Fellhauer, D.; Tasi, A.; Adam, N.; Yalcintas, E.; Dardenne, K.; Rothe, J.; Altmaier, M.; Geckeis, H., *Actinide chemistry in aqueous systems: solubility, complexation and redox processes*, ABC-Salt VI Workshop, Karlsruhe, Germany, **2019**.

118. Gaona, X.; Endrizzi, F.; Lee, J.-Y.; Fellhauer, D.; Cevirim-Papaioannou, N.; Altmaier, M., *Studies on actinide chemistry at elevated temperatures at KIT-INE within the German collaborative ThermAc project*, HiTAC - III Workshop 2019, High Temperature Aqueous Chemistry, Karlsruhe, Germany, **2019**.

119. Gaona, X.; Grambow, B.; Altmaier, M.; Duro, L.; Geckeis, H., *Development and improvement of quality assured thermodynamic understanding for use in performance assessment of nuclear waste disposal*, EURADWASTE'19, Pitesti, Romania, **2019**.

120. Gaona, X.; Grenthe, I.; Plyasunov, A.; Rao, L.; Runde, W.; Grambow, B.; Konings, R. J. M.; Smith, A. L.; Moore, E.; Spahiu, K.; Martinez, J.; Ragoussi, M.-E., *NEA-TDB Update book on U, Np, Pu, Am and Tc: overview, systematic trends and datagaps of relevance to nuclear waste disposal*, Migration 2019, Kyoto, Japan, **2019**.

121. Gaona, X.; Tasi, A.; Adam, N.; Duckworth, S.; Fellhauer, D.; Altmaier, M.; Geckeis, H., *Radionuclide – organic interaction: impact on the solubility of M(III/IV) under repository-relevant pH / Eh conditions*, Migration 2019, Kyoto, Japan, **2019**.

122. Gaona, X.; Yalcintas, E.; Baumann, A.; Altmaier, M.; Geckeis, H., *Thermodynamics of Tc(IV) in aqueous solutions: application to complex mixtures including cementitious systems*, Mechanism and Modeling of Waste/Cement Interactions, Karlsruhe, Germany, **2019**.

123. Garcia, D.; Lützenkirchen, J.; Petrov, V.; Siebentritt, M.; Huguenel, M.; Camels, L.; Schild, D.; Levèvre, G.; Rabung, T.; Altmaier, M.; Kalmykov, S.; Duro, L.; Geckeis, H., *Sorption behavior of di- and trivalent radionuclides on oxide surfaces at high salt concentrations*, Goldschmidt 2019, Barcelona, Spain, **2019**.

124. Geckeis, H.; Gentes, S.; Heneka, A.; Krauß, C. O.; Plaschke, M.; Schild, D.; Tobie, W., *Vorstellung eines Separationssystems zur Behandlung von Sekundärabfällen der Wasser-Abrasiv-Suspensions-Schneidtechnik*, 50th Annual Meeting on Nuclear Technology (AMNT 2019), Berlin, Germany, **2019**.

125. Glückman, D.; Joseph, C.; Quinto, F.; Vogt, M., *Influence of heterogeneity of Opalinus Clay on radionuclide sorption and diffusion from micro- to macroscale*, Kick-off Meeting zum iCross-Projekt, Berlin, Germany, **2019**.

126. Glückman, D.; Quinto, F.; Hain, K.; Joseph, C.; Montoya, V.; Steier, P.; Geckeis, H., *Development of an analytical method for the determination of actinides in clay systems at ultra-trace levels with accelerator mass spectrometry (AMS)*, Frühjahrstagung der Deutschen Physikalischen Gesellschaft, Rostock, Germany, **2019**.

127. Glückman, D.; Quinto, F.; Hain, K.; Joseph, C.; Montoya, V.; Steier, P.; Geckeis, H., *Ultra-trace determination of actinides in clay samples with accelerator mass spectrometry*, Jahrestagung der Fachgruppe Nuklearchemie (GDCh), Dresden, Germany, **2019**.

128. González-Robles, E.; Herm, M.; Müller, N.; Böttle, M.; Fuss, M.; Bohnert, E.; Gaggiano, R.; Metz, V., *Radionuclide release from spent fuel under anoxic / reducing conditions in cementitious solution*, 5th International workshop on mechanisms and modelling of waste - cement interactions, Karlsruhe, Germany, **2019**.

129. Gülce, F.; Feastermann, T.; Hain, K.; Korschinek, G.; Martschini, M.; Pitters, J.; Quinto, F.; Rugel, G.; Steier, P.; Wallner, G.; Welch, J. M., *Method for ultra-trace Determination of Tc-99 from Large Seawater Samples*, International Conference on Environmental Radioactivity (ENVIRA 2019), Prague, Czech Republic, **2019**.

130. Hain, K.; Faestermann, T.; Golser, R.; Gülce, F.; Kern, M.; Korschinek, G.; Martschini, M.; Pitters, J.; Quinto, F.; Sakaguchi, A.; Steier, P.; Wallner, G.; Welch, J.; Yamada, M., *Application of AMS to ultra-low levels of actinides and Tc-99 in the environment*, Migration conference, Kyoto, Japan, **2019**.

131. Han, S.; Cevirim-Papaioannou, N.; Gaona, X.; Um, W.; Altmaier, M., *Uptake of Be(II) by ordinary portland cement in the degradation phase I*, Mechanism and Modeling of Waste/Cement Interactions, Karlsruhe, Germany, **2019**.

132. Han, S.; Cevirim-Papaioannou, N.; Gaona, X.; Um, W.; Altmaier, M., *Sorption of beryllium in fresh ordinary Portland cement paste*, Migration 2019, Kyoto, Japan, **2019**.

133. Heberling, F.; Klacic, T.; Eng, P.; Preocanin, T.; Lützenkirchen, J., *Structure and surface complexation of the calcite-water-interface*, Goldschmidt Conference 2019, Barcelona, Spain, **2019**.

134. Heberling, F.; Klacic, T.; Eng, P.; Preocanin, T.; Lützenkirchen, J., *Structure and chemistry of the calcite-water-interface*, EGU General Assembly 2019, Vienna, Austria, **2019**.

135. Heide, B., *When Should Trajectory Approach Be Replaced by Multiple Scattering Theory for Low Energy Electrons Impinging on a Nanometric Slab of Water Molecules?*, EURADOS WG6 Meeting, Paris-Fontenay, France, **2019**.

136. Heneka, A.; Geckeis, H.; Gentes, S.; Krauß, C. O.; Plaschke, M.; Schild, D.; Tobie, W., *Weiterentwicklung eines Separationsverfahrens zur Behandlung des Sekundärabfalls aus der Wasser-Abrasiv-Suspensions-Schneidtechnik*, 14. Internationales Symposium Konditionierung radioaktiver Betriebs- und Stilllegungsabfälle (KONTEC 2019), Dresden, Germany, **2019**.

137. Joseph, C., *DR-C: Laboratory diffusion experiments*, DR-C follow-up meeting, FANC, Brussels, Belgium, **2019**.

138. Joseph, C.; Balboni, E.; Baumer, T.; Treinen, K.; Kersting, A. B.; Zavarin, M., *Plutoniumdesorption von Kolloiden aus verwitterter nuklearer Glasschmelze von der Nevada National Security Site, USA*, Gesellschaft Deutscher Chemiker (GDCh), Jahrestagung der Fachgruppe Nuklearchemie, Dresden, Germany, **2019**.

139. Joseph, C.; Delavernhe, L.; Montoya, V.; Moisei-Rabung, S.; Glaus, M. A.; Trumm, M.; Kupcik, T.; Schuhmann, R.; Emmerich, K.; Schäfer, T., *Part 1: Influence of interlayers on the diffusion of HTO, $^{36}Cl^-$, and $^{85}Sr^{2+}$ through smectites*, Seminar at the Institute of Resource Ecology, HZDR, Dresden-Rossendorf, Germany, **2019**.

140. Joseph, C.; Stoll, M.; Heberling, F.; Metz, V.; Geckeis, H., *On-going and planned activities in the context of Mont Terri*, 26. Koordinierungsgespräch KIT/INE – PSI/LES, Eggenstein-Leopoldshafen, Germany, **2019**.

141. Joseph, C.; Stoll, M.; Heberling, F.; Metz, V.; Geckeis, H., *Part 2: KIT-INE's activities in the Mont Terri underground rock laboratory (iCross)*, Seminar at the Institute of Resource Ecology, HZDR, Dresden-Rossendorf, Germany, **2019**.

142. Koke, C.; Skerencak-Frech, A.; Panak, P. J., *The complexation and thermodynamics of Cm(III) with F- at T=25 to 200°C studied by time resolved laser fluorescence spectroscopy*, Migration 2019, Kyoto Japan, **2019**.

143. Kose, T.; Chaparro, M. C.; Schilling, F.; Hirsch, A.; Blum, P., *Coupled thermal-hydraulic-chemical modelling of a cement-rock-brine-CO_2 system*, Goldschmidt, Barcelona, Spain, **2019**.

144. Kuzenkova, A.; Fellhauer, D.; Schild, D.; Gaona, X.; Rothe, J.; Romanchuk, A.; Kalmykov, S.; Altmaier, M., *Solubility, speciation and solid phase formation of Pu(VI) in alkaline $CaCl_2$ and NaCl solutions*, Migration 2019, Kyoto, Japan, **2019**.

145. Mayordomo, N.; Rodriguez, D. M.; Molodtsov, K.; Johnstone, E. V.; Rossberg, A.; Heim, K.; Foerstendorf, H.; Schild, D.; Brendler, V.; Müller, K., *^{99}Tc immobilization by aluminum solids containing Fe(II) moieties*, 43rd Symposium 'Scientific Basis for Nuclear Waste Management' (2019), Vienna, Austria, **2019**.

146. Meier, R.; Kitagaki, T.; Kozai, N.; Fellhauer, D.; Kobayashi, T.; Ohnuki, T., *Complexation of actinides with borate and polyborates*, Migration 2019, Kyoto, Japan, **2019**.

147. Modolo, G.; Wilden, A.; Kaufholz, P.; Marie, C.; Vanel, V.; Miguirditchian, M.; Bourg, S.; Casnati, A.; Geist, A., *Selective separation of Am(III) from PUREX raffinate with a TODGA-based solvent using innovative hydrophilic complexing agents*, Proceedings of the Internat. Conf. GLOBAL 2019, Seattle, USA, ANS, La Grange Park (IL): **2019**.

148. Molinas, M.; Faizova, R.; Mazzanti, M.; Schacherl, B.; Galanzew, J.; Vitova, T.; Bernier-Latmani, R., *U(V) is an intermediate in the reduction of U(VI) by Shewanella oneidensis MR-1*, Goldschmidt 2019, Barcelona, Spain, **2019**.

149. Montoya, V.; Ait Mouheb, N.; Schäfer, T.; Finck, N.; Joseph, C.; Geckeis, H., *Multi-method and multi-scale approach for studying chloride-36 migration through low pH cement pastes*, 5th Internal Workshop on Mechanisms and Modelling of Waste / Cement Interactions, Karlsruhe, Germany, **2019**.

150. Munoz, A. G.; Schild, D., *Corrosion mechanisms of austenitic steel in salt rock repositories of high-level radioactive waste*, 235th ECS Meeting, Dallas, USA, **2019**.

151. Cornejo, N.; Schill, E.; Held, S.; Perez, M.; Carrillo, J., *Towards visualization of possible fluid pathways using gravity in Los Humeros and Acoculco geothermal fields*, Latin American Colloquium, Hamburg, Germany, **2019**.

152. Nagatou, K.; Schulz, M.; Arbeiter, F.; weth, A. V. d.; Dagan, R., *Analytical solution of a gas release problem considering permeation with time dependent boundary conditions*, ICTT - International conference on Transport Theory, Paris, France, **2019**.

153. Pavez, M.; Schill, E.; Haaf, N.; Mora-Stock, C.; Díaz, D., *Indication of Forecasting Seismic Activity by Magnetotelluric Methods from Fluid Injection During Reservoir Engineering*, IUGG Meeting, Montreal, Canada, **2019**.

154. Pavez, M.; Schill, E.; Held, S.; Díaz, D.; Kohl, T., *Geothermal Systems Exploration in the Chilean Southern Volcanic Zone by Magnetotelluric Method: a case study at Villarrica Volcano*, 25th Latin American Colloquium, Hamburg, Germany, **2019**.

155. Pavez, M.; Schill, E.; Held, S.; Díaz, D.; Kohl, T., *Geothermal Systems Exploration in the Chilean Southern Volcanic Zone by Magnetotelluric Method: a case study at Villarrica Volcano*, European Geothermal Workshop, Karlsruhe, Germany, **2019**.

156. Platte, T.; Polly, R.; Finck, N.; Mangold, S.; Geckeis, H., *Retention of Iodine by the Fe secondary phases green rust and magentite*, Migration, Kyoto, Japan, **2019**.

157. Polly, R.; Schimmelpfennig, B.; Vozarova, N.; Platte, T.; Heberling, F.; Finck, N.; Geckeis, H., *Density functional theory study of the incorporation of radionuclides in hydroxycarbonate and hydroxychloride Green Rust*, Migration 2019, Kyoto, Japan, **2019**.

158. Popa, K.; Walter, O.; Blanco, O. D.; Beck, A.; Vitova, T., *Reduction-precipitation of U(VI) by Fe(II)-oxalate*, 5th World Congress on Recent Advances in Nanotechnology (RAN'20), Lisabon, Portugal, **2019**.

159. Quinto, F.; Blechschmidt, I.; Faestermann, T.; Hain, K.; Koll, D.; Korschinek, G.; Kraft, S.; Ludwig, P.; Plaschke, M.; Rinderknecht, F.; Schäfer, T.; Steier, P.; Geckeis, H., *Ultra-trace analysis with AMS in nuclear waste disposal research: results from the CFM project at the Grimsel Test Site*, Migration conference, Kyoto, Japan, **2019**.

160. Quinto, F.; Faestermann, T.; Hain, K.; Koll, D.; Korschinek, G.; Ludwig, P.; Plaschke, M.; Schäfer, T.; Geckeis, H., *Safety of Nuclear Waste Disposal: Ultra-trace Determination of ^{99}Tc in Small Natural Water Samples by AMS with the Gas-Filled Analyzing Magnet System*, Workshop "Scientific perspectives for KIMM - Competence Center for Ion Beams in Materials Research and Medicine", Universität der Bundeswehr München, Munich, Germany, **2019**.

161. Quinto, F.; Geckeis, H.; Hain, K.; Plaschke, M.; Schäfer, T.; Steier, P., *Long-term Behavior of Actinides from Global Fallout and In-situ Tracer Tests*, 83. Jahrestagung der DPG und DPG-Frühjahrstagung, Rostock, Germany, **2019**.

162. Rabung, T.; Kienzler, B.; Skerencak-Frech, A.; Schlieker, M.; Fellhauer, D.; Plaschke, M.; Geyer, F.; Walschburger, C.; Kisely, T.; Böttle, M.; Fuss, M.; Altmaier, M.; Metz, V.; Geckeis, H., *Sorption of ^{243}Am(III), ^{242}Pu(VI), ^{237}Np(V), ^{233}U(VI), ^{230}Th(IV), ^{226}Ra(II), ^{137}Cs(I), ^{99}Tc(VII), ^{75}Se(IV) on rock samples from the overburden of the ASSE II salt mine*, Migration 2019, Kyoto Japan, **2019**.

163. Ratnayake, S. Y.; Lützenkirchen, J.; Schild, D.; Finck, N.; Geckeis, H., *Speciation of Thorium in Soils from Sri Lanka*, Goldschmidt Conference, Barcelona, Spain, **2019**.

164. Richnow, H.; Shao, H.; Saadat, A.; Schmidt, D.; Henninger, S.; Kastner, O.; Kohl, T.; Schill, E.; Bauer, S.; Dahmke, A.; Staudacher, L., *Wärmespeicher im urbanen Untergrund – CO_2-freie Wärmeversorgung der Stadt*, FVEE – Jahrestagung 2019: Energy Research for Future – Forschung für die Herausforderungen der Energiewende, Berlin, Germany, **2019**.

165. Rieder, F.; Trumm, M.; Skerencak-Frech, A.; Rabung, T.; Geckeis, H., *Carbonate mediated sorption of Eu(III)/Cm(III) onto clay minerals: Batch sorption, laser spectroscopy and modelling*, Migration 2019, Kyoto, Japan, **2019**.

166. Rodríguez, D. M.; Mayordomo, N.; Brendler, V.; Müller, K.; Schild, D.; Stumpf, T., *Reductive immobilization of ^{99}Tc(VII) by different crystalline phases of iron sulfide (FeS_2)*, Migration 2019, Kyoto, Japan, **2019**.

167. Schacherl, B.; Joseph, C.; Beck, A.; Schnurr, A.; Rieder, F.; Dardenne, K.; Fellhauer, D.; Bohnert, E.; Kupcik, T.; Rothe, J.; Geckeis, H.; Vitova, T., *Structural investigations of Np sorbed on illite by M5-edge HR-XANES and L3-edge EXAFS spectroscopy*, Migration 2019, Kyoto, Japan, **2019**.

168. Schacherl, B.; Joseph, C.; Lavrova, P.; Beck, A.; Schnurr, A.; Rieder, F.; Dardenne, K.; Fellhauer, D.; Kupcik, T.; Rothe, J.; Geckeis, H.; Vitova, T., *Np M5-edge HR-XANES and L3-edge EXAFS spectroscopy on illite samples with 20–140 ppm Np*, EBS workshop on X-ray Emission Spectroscopy, ESRF, Grenoble, France, **2019**.

169. Schäfer, T.; Quinto, F.; Kraft, S.; Rinderknecht, F.; Lanyon, B.; Blechschmidt, I., *Clay nanoparticle and RN release from the geotechnical barrier: Insights from the CFM Long-term In situ Test (LIT) at GTS*, Goldschmidt conference, Barcelona, Spain, **2019**.

170. Schepperle, J.; Yalcintas, E.; Fellhauer, D.; Cevirim-Papaioannou, N.; Gaona, X.; Altmaier, M.; Geckeis, H., *Hydroxo-carbonate complex formation and solubility of tetravalent actinides at alkaline pH conditions,* ABC-Salt VI Workshop, Karlsruhe, Germany, **2019**.

171. Schill, E.; Haaf, N., *Towards forecasting seismic activity induced during reservoir engineering by magnetotelluric methods*, IUGG Meeting, Montreal, Canada, **2019**.

172. Schill, E.; Kohl, T.; Stricker, K.; Schätzler, K.; Grimmer, J., *Geothermal heat storage in the Upper Rhine Graben – the DeepStor project at KIT Campus North*, European Geothermal Workshop, Karlsruhe, Germany, **2019**.

173. Sittel, T.; Adam, C.; Geist, A.; Panak, P. J., *Synthese von 8,8'-Oxybis-3,4-dipropylcinnolin und TRLFS-Untersuchung der Komplexierung mit Cm(III)*, GDCh- Jahrestagung der Fachgruppe Nuklearchemie, Dresden, Germany, **2019**.

174. Sittel, T.; Adam, C.; Geist, A.; Panak, P. J., *Investigation of the ligand configuration in Th(IV) N-donor complexes*, 21st – 15th ISMAR – EUROMAR Joint Conference, Berlin, Germany, **2019**.

175. Skerencak-Frech, A.; Maiwald, M.; Koke, C.; P., P., *Spectroscopic characterization of the Thermodynamics of Actinides at elevated Temperatures*, 3rd International Workshop on High Temperature Aqueous Chemistry – HiTAC (III), Karlsruhe Germany, **2019**.

176. Skerencak-Frech, A.; Rieder, F.; Trumm, M.; Altmaier, M.; Geckeis, H., *Sorption von dreiwertigen Actiniden und Lanthaniden an Tonmineralien bei niedrigen und mittleren Ionenstärken*, 3. Fachworkshop der Bundesgesellschaft für Endlagerung, Braunschweig, Germany, **2019**.

177. Sowoidnich, T.; Link, J.; Heberling, F.; Lützenkirchen, J.; Gil-Díaz, T.; Ludwig, H.-M.; Schäfer, T.; Haist, M., *Influence of hydration on the rheological behavior of tricalcium silicate paste*, 2nd international RILEM Conference, Rheology and Processing of Construction Materials, Dresden, Germany, **2019**.

178. Stern, T.; Reich, T.; Platte, T.; Vitova, T., *M5-Kante HR-XANES Untersuchung zur Sorption von Plutonium(IV) an Kaolinit*, GDCh Jahrestagung Fachgruppe Nuklearchemie, Dresden, Germany, **2019**.

179. Vitova, T.; Beck, A.; Schacherl, B.; Galanzew, J.; Prüßmann, T.; Bahl, S.; Pidchenko, I.; Bagus, P.; Jolly, Y.; Kowalski, P. M.; Dardenne, K.; Rothe, J.; Geckeis, H., *Structural studies of actinide materials applying high resolution X-ray absorption and emission spectroscopy*, EBS workshop on X-ray Emission Spectroscopy, Grenoble, France, **2019**.

180. Vitova, T.; Beck, A.; Tasi, A.; Fellhauer, D.; Pidchenko, I.; Bagus, P. S.; Joly, Y.; Dardenne, K.; Rothe, J.; Altmaier, M.; Geckeis, H., *Exploring the electronic structure and speciation of aqueous and colloidal Pu with high energy resolution XANES and computations*, Journee des Actinides (JdA), Erice, Italien, **2019**.

181. Vitova, T.; Beck, A.; Tasi, A.; Fellhauer, D.; Pidchenko, I.; Dardenne, K.; Rothe, J.; Altmaier, M.; Geckeis, H., *Exploring the electronic structure and speciation of aqueous and colloidal Pu with high energy resolution XANES and computations*, Jahrestagung Fachgruppe Nuklearchemie, Dresden, Germany, **2019**.

182. Vitova, T.; Pidchenko, I.; Prüßmann, T.; Bahl, S.; Beck, A.; Schacherl, B.; Galanzew, J.; Dardenne, K.; Rothe, J.; Geckeis, H., *Structural properties of actinides applying M4,5 edge high resolution XANES and 3d4f RIXS*, 11th International Conference on Inelastic X-ray Scattering (IXS2019), Stony Brook, New York, USA, **2019**.

183. Vozárová, N.; Finck, N.; Schild, D.; Geckeis, H.; Schlegel, M., *Corrosion of ductile iron under saline and elevated temperature conditions*, EuroCorr 2019, Seville, Spain, **2019**.

184. Vozárová, N.; Finck, N.; Schild, D.; Geckeis, H.; Schlegel, M., *Studies on Fe corrosion in brine systems*, ABC-Salt (VI) Workshop, Karlsruhe, Germany, **2019**.

185. Weßling, P.; Geist, A.; Panak, P. J., *Aromatische Lösungsmittel zur selektiven Extraktion von Actiniden*, GDCh- Jahrestagung der Fachgruppe Nuklearchemie, Dresden, Germany, **2019**.

186. Wilden, A.; Kowalski, P. M.; Modolo, G.; Geist, A.; Verlinden, B.; Verboom, W., *Application of methylated diglycolamides in the EURO-GANEX process*, 43rd Annual Actinide Separations Conference, Kingsport, USA, **2019**.

187. Zunftmeister, L.; Nie, Z.; Heberling, F.; Marsac, R.; Hanna, K.; Finck, N.; Liu, C.; Lützenkirchen, J., *Selenite and Strontium breakthrough in a column of goethite coated sand: experiments and modelling*, Goldschmidt Conference 2019, Barcelona, Spain, **2019**.

188. Zunftmeister, L.; Nie, Z.; Heberling, F.; Marsac, R.; Hanna, K.; Lützenkirchen, J., *Simulation of Selenite and Strontium breakthrough in a column of goethite coated sand*, EGU General Assembly 2019, Vienna, Austria, **2019**.

Proceedings

189. Altmaier, M.; Montoya, V.; Duro, L.; Valls, A., *Proceedings of the Second Workshop of the HORIZON 2020 CEBAMA Project (KIT Scientific Reports ; 7752)*, KIT Scientific Publishing, Karlsruhe: **2019**.

190. Altmaier, M., *CO_2-Production rates in saline systems. Relevance in the context of Schachtanlage Asse II,* Proceedings of the 10th US/GERMAN Workshop on Salt Repository Research, Design, and Operation, (Eds: S. Buchholz, E. Keffeler, K. Lipp, K. DeVries, F. Hansen), SAND2019-9997 R, TOPICAL REPORT RSI-2948, **2019**.

191. Becker, F.; Suaréz, H. S.; Pang, B.; Metz, V.; Geckeis, H., *Monte Carlo simulations for individual dosimetry of workers in disposal facilities for spent nuclear fuel*, IRPA 2018 Proceedings, **2019**.

192. Brandauer, M.; Friedrich, S.; Gentes, S.; Schilp, S.; Hartung, F.; Johannes, P., *Robotersysteme zur Kartierung von kerntechnischen Anlagen*, 14. Internationales Symposium Konditionierung radioaktiver Betriebs- und Stilllegungsabfälle (KONTEC 2019), Dresden, Germany, **2019**.

193. Dubos, J. L.; Orberger, B.; Milazzo, J. M.; Blancher, S. B.; Lützenkirchen, J., *Physico-chemical characterisation of industrial manganese dusts and sludges and its implication for agglomeration: From ore to metal*, Proceedings of the 29th International Mineral Processing Congress, IMPC 2018, Moscow, Russia, CIM, Montreal: **2019**.

194. Haaf, N.; Schill, E., *Processing of magnetotelluric data for monitoring changes in electric resistivity during drilling operation*, PROCEEDINGS, 44th Workshop on Geothermal Reservoir Engineering, Stanford University, Stanford, California, USA, **2019**.

195. Modolo, G.; Wilden, A.; Kaufholz, P.; Marie, C.; Vanel, V.; Miguirditchian, M.; Bourg, S.; Casnati, A.; Geist, A., *Selective separation of Am(III) from PUREX raffinate with a TODGA-based solvent using innovative hydrophilic complexing agents*, Proceedings of the Internat. Conf. GLOBAL 2019, Seattle, USA, ANS, La Grange Park (IL): **2019**.

196. Montoya, V.; Mouheb, N. A.; Schäfer, T., *Modelling of radionuclides migration in the low pH cement / clay interface*, Proceedings of the Second Workshop of the HORIZON 2020 CEBAMA Project, Altmaier, M.; Montoya, V.; Duro, L.; Valls, A., Eds. KIT Scientific Publishing, Karlsruhe: **2019**; pp 237-240.

197. Mouheb, N. A.; Montoya, V.; Schild, D.; Soballa, E.; Adam, C.; Geyer, F.; Schäfer, T., *Characterization and sorption properties of low pH cements*, Proceedings of the Second Workshop of the HORIZON 2020 CEBAMA Project, Altmaier, M.; Montoya, V.; Duro, L.; Valls, A., Eds. KIT Scientific Publishing, Karlsruhe: **2019**; pp 149-160.

198. Vehmas, T., *Cebama reference mix design for low-pH concrete and paste, preliminary characterisation*, Proceedings of the Second Workshop of the HORIZON 2020 CEBAMA Project, Altmaier, M.; Montoya, V.; Duro, L.; Valls, A., Eds. KIT Scientific Publishing, Karlsruhe: **2019**; pp 149-160.

Reports

199. Becker, F.; Eßer, R.; Hranitzky, C.; Koletzko, G.; Martini, E. *Kurzbericht von der gemeinsamen Sitzung AKD + AKMed*; VERLAG TÜV Media GmbH, TÜV Rheinland Group, 2019; pp 82-84.

200. Becker, F.; Schischke, S.; Eßer, R. *Kurzbericht von der 89. Sitzung des Arbeitskreises Dosimetrie (AKD)*; VERLAG TÜV Media GmbH, TÜV Rheinland Group, 2019; pp 93-94.

Dissertations

201. Rieder, F., *Impact of competing anions on the sorption of trivalent actinides onto clay mineral surfaces.* KIT, **2019**.

Books

202. Altmaier, M.; Gaona, X.; D. Fellhauer, Clark, D.L.; Runde, W.H.; Hobart, D.E., Aqueous Solution and Coordination Chemistry of Plutonium, Plutonium Handbook, Vol. 3, Ch. 22, pp. 1543-1726. In: Plutonium Handbook 2nd Edition, Eds. D. Clark, D. Geeson, R. Hanrahan, American Nuclear Society (**2019**).

203. Geckeis, H.; Zavarin, M.; Salbu, B.; Lind, O. C., Skipperud, L., Environmental Chemistry of Plutonium, Plutonium Handbook, Vol. 4, Ch. 25, pp. 1979-2118. In: Plutonium Handbook 2nd Edition, Eds. D. Clark, D. Geeson, R. Hanrahan, American Nuclear Society (**2019**).

INE Scientific Working Documents
ISSN 2701-262X

www.kit.edu